



**Universidade do Estado do Rio de Janeiro**

Centro de Tecnologia e Ciências

Instituto de Química

Leandro Morais Silva

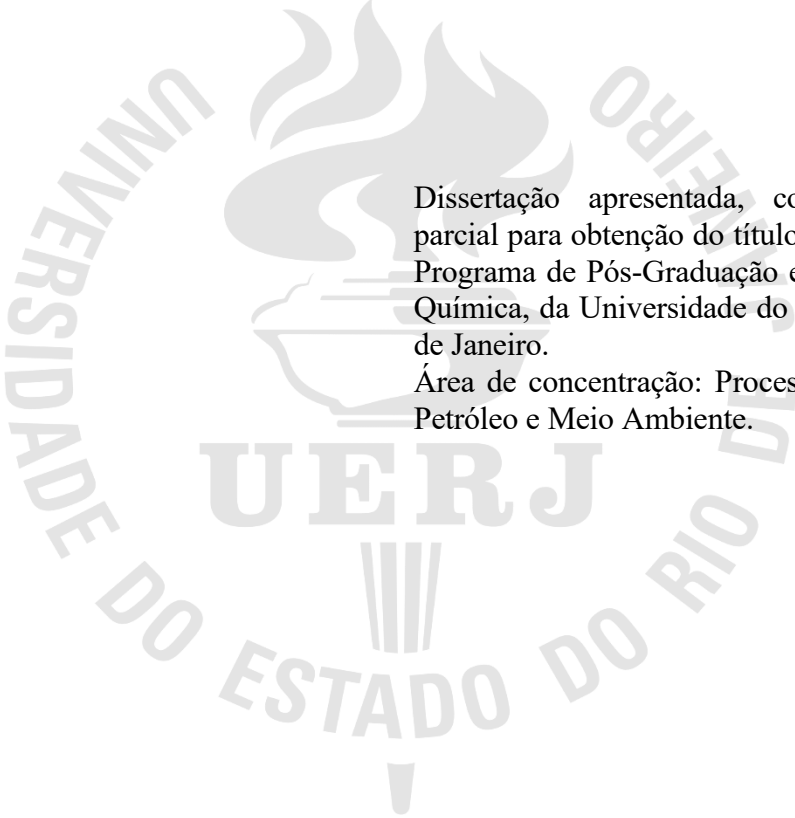
**Modeling and yield profile optimization of a Catalytic Cracking Reactor**

Rio de Janeiro

2023

Leandro Morais Silva

**Modeling and yield profile optimization of a Catalytic Cracking Reactor**



Dissertação apresentada, como requisito parcial para obtenção do título de Mestre, ao Programa de Pós-Graduação em Engenharia Química, da Universidade do Estado do Rio de Janeiro.

Área de concentração: Processos Químicos, Petróleo e Meio Ambiente.

Orientador: Prof. Dr. André Luis Alberton

Rio de Janeiro

2023

CATALOGAÇÃO NA FONTE  
UERJ / REDE SIRIUS / BIBLIOTECA CTC/Q

S586 Silva, Leandro Morais.

Modeling and yield profile optimization of a Catalytic Cracking Reactor.  
– 2023.  
182 f.

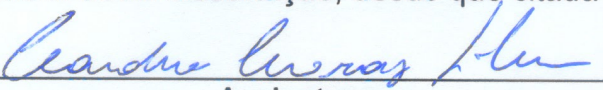
Orientador (a): André Luis Alberton

Dissertação (Mestrado) – Universidade do Estado do Rio de Janeiro.  
Instituto de Química.

1. Craqueamento catalítico – Teses. 2. Modelagem de dados – Teses. I.  
Alberton, André Luis. II. Universidade do Estado do Rio de Janeiro.  
Instituto de Química. III. Título.

CDU 66.092

Autorizo, apenas para fins acadêmicos e científicos, a reprodução total ou parcial desta dissertação, desde que citada a fonte.

  
Assinatura

23/05/2024  
Data

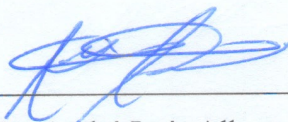
Leandro Morais Silva

**Modeling and yield profile optimization of a Catalytic Cracking Reactor**

Dissertação apresentada, como requisito parcial para obtenção do título de Mestre, ao Programa de Pós-Graduação em Engenharia Química, da Universidade do Estado do Rio de Janeiro.

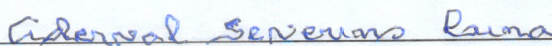
Aprovado em: 14 de setembro de 2023.

Banca Examinadora:



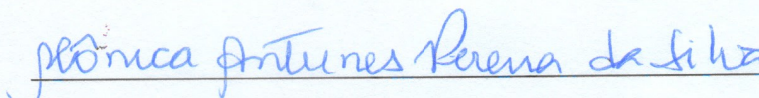
Prof. Dr. André Luís Alberton (Orientador)

Instituto de Química - UERJ



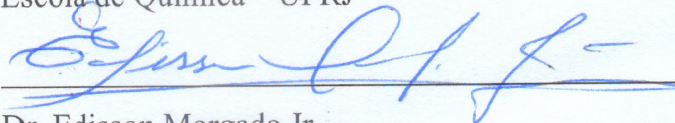
Prof. Dr. Aderval Severino Luna

Instituto de Química - UERJ



Prof. Dr. Mônica Antunes Pereira da Silva

Escola de Química – UFRJ



Dr. Edisson Morgado Jr.

Centro de Pesquisa – PETROBRAS

Rio de Janeiro

2023

## AGRADECIMENTOS

Àquele que conhece o valor verdadeiro de todos os parâmetros, pelo sustento e pelo dom da vida.

A Michelle, Ana Clara, Caio e Yasmin pela compreensão, pelo incentivo e pelos momentos agradáveis de desincentivo.

Aos meus pais por todos os ensinamentos e pelo refúgio no *sprint* final.

Aos amigos do grupo de conversores de FCC da Petrobras pelo apoio em tantos momentos ao longo desta caminhada.

Ao meu estimado orientador professor Alberton pelo impulso por prosseguir e pela confiança.

A todos os professores, pela construção de uma sociedade mais desenvolvida.

À Petrobras, pelo apoio para a realização deste curso e por permitir a utilização dos dados obtidos em projeto de pesquisa e desenvolvimento interno no presente trabalho.

Take the first step in faith. You don't have to see the whole staircase, just take the first step.

*Martin Luther King Jr.*

## RESUMO

SILVA, Leandro M. *Modelagem e otimização do perfil de rendimento de um Reator de Craqueamento Catalítico*. 2023. 182 f. Dissertação (Mestrado em Engenharia Química) – Instituto de Química, Universidade do Estado do Rio de Janeiro, Rio de Janeiro, 2023.

O craqueamento catalítico fluido (FCC) é um processo que permanece relevante para a rentabilidade e para o esquema de produção de refinarias. Por questões de mercado, seria desejável que a unidade de FCC maximizasse a produção de derivados médios (LCO) para o pool de diesel, mas isto requer uma otimização cuidadosa das condições do processo. Neste contexto, o presente trabalho usou uma base de dados de 69 testes, explorando regiões de baixa conversão, obtidos em uma planta piloto de FCC de grande porte. Em uma primeira parte do trabalho (capítulo 1), desenvolveu-se um modelo empírico dos rendimentos em função da temperatura de reação, tempo de reação, relação catalisador óleo e teor de leves na carga, empregando-se seleção progressiva de inclusão dos parâmetros e validação cruzada para a construção do modelo. Após obtido o modelo, os parâmetros foram re-estimados impondo-se a restrição de fechamento do balanço de massa. Obtidos os modelos, efetuou-se a análise e otimização do modo de operação da unidade. O modelo indicou que operar a unidade de FCC em elevada conversão e na máxima temperatura de reação possível permanece mais rentável, particularmente devido ao aumento relativamente pequeno do rendimento de LCO comparado ao grande aumento do rendimento da borra em baixa conversão. Em uma segunda parte do trabalho (capítulo 2), apresenta-se uma discussão acerca do balanço de energia da unidade. Comparou-se o calor de reação obtido pela diferença de entalpia dos produtos e reagentes (para produtos líquidos foram usadas correlações envolvendo a curva de destilação e a densidade) com o calor de reação pelo fechamento do balanço de energia da unidade. Os resultados revelam que as metodologias levam a resultados discrepantes para o calor de reação. À luz da discussão da literatura, salienta-se que a obtenção de uma correlação precisa para o poder calorífico da carga e dos produtos líquidos craqueados ainda não foi alcançada e demanda, portanto, novos desenvolvimentos. Ainda nesta segunda parte do trabalho, foi implementado o ajuste de um modelo empírico capaz de retornar não apenas os rendimentos dos cortes, mas a composição detalhada das correntes de gás e GLP, e a curva de destilação e densidade dos produtos líquidos (nafta, LCO e óleo decantado), o que é um passo importante para a posterior caracterização de uma função de entalpia dos produtos desde que exista uma correlação adequada de predição do poder calorífico para os produtos líquidos.

Palavras-chave: craqueamento catalítico; modelagem; perfil de rendimento.

## ABSTRACT

SILVA, Leandro M. *Modeling and yield profile optimization of a Catalytic Cracking Reactor*. 2023. 182 f. Dissertação (Mestrado em Engenharia Química) – Instituto de Química, Universidade do Estado do Rio de Janeiro, Rio de Janeiro, 2023.

Fluid catalytic cracking (FCC) is a process that remains relevant to the profitability and production scheme of refineries. For market reasons, it would be desirable for the FCC unit to maximize the production of middle distillates (LCO) for the diesel pool, but this requires careful optimization of process conditions. In this context, the present work used a database of 69 tests, exploring regions of low conversion, obtained in a large FCC pilot plant. In a first part of the work (chapter 1), an empirical model for yields prediction was developed as a function of reaction temperature, reaction time, catalyst-to-oil ratio and light content in the feed, using parameter inclusion by forward selection and cross-validation for model construction. After obtaining the model, the parameters were re-estimated by imposing mass balance closure restriction. Once the models were obtained, the unit's operating mode was analyzed and optimized. The model indicated that operating the FCC unit at high conversion and at the maximum possible reaction temperature remains more profitable, particularly due to the relatively small increase in LCO yield compared to the large increase in slurry oil yield at low conversion. In a second part of the work (chapter 2), a discussion about the energy balance of the unit is presented. The heat of reaction obtained by the difference in enthalpy of the products and reactants (for liquid products, correlations involving the distillation curve and the density were used) was compared with the heat of reaction by closing the energy balance of the unit. The results reveal that the methodologies lead to discrepant results for the heat of reaction. In the light of the literature discussion, it should be noted that obtaining a precise correlation for the heating value of the feed and cracked liquid products has not yet been achieved and, therefore, demands new developments. Still in this second part of the work, it was implemented the adjustment of an empirical model capable of returning not only the yields of the cuts, but the detailed composition of the gas and LPG streams, and the distillation curve and density of the liquid products (naphtha, LCO and decanted oil), which is an important step for the subsequent characterization of an enthalpy function of the products, provided that there is an adequate correlation for predicting the heating value for the liquid products.

Keywords: catalytic cracking; modeling; yield profile.

## LIST OF FIGURES

Figure 1 - 7.5 m <sup>3</sup> /d FCC pilot plant general assembly.....	31
Figure 2 - Schematic of empirical model construction procedure .....	34
Figure 3 - Schematic of process simulator calculations to return yield profile and other operational conditions .....	43
Figure 4 - Products yield as a function of Slurry oil yield. Feed “A1” injected in: Nozzle #1 (■); Nozzle #2 (▲); Nozzle #3 (◇); Nozzle #4 (+) .....	45
Figure 5 - Products yield as a function of Catalyst-to-oil ratio. Feed “A1” injected in: Nozzle #1 (■); Nozzle #2 (▲); Nozzle #3 (◇); Nozzle #4 (+).....	46
Figure 6 - LCO yield as a function of light gasoil content in the feed (see Table 1): Feed “A1” (□); Feed “A2” (■); Feed “B” (△); Feed “C” (◇); Feed “D” (+).....	49
Figure 7 - Reaction temperature vs. Catalyst-to-oil ratio .....	49
Figure 8 - Fitting of FCC yield profile empirical modeling – individual cuts.....	56
Figure 9 - Sensitivity analysis of the empirical Dry gas yield model response to normalized values of -1 to 1 as input data .....	57
Figure 10 - Sensitivity analysis of the empirical LPG yield model response to normalized values of -1 to 1 as input data.....	58
Figure 11 - Sensitivity analysis of the empirical Naphtha yield model response to normalized values of -1 to 1 as input data .....	58
Figure 12 - Sensitivity analysis of the empirical LCO yield model response to normalized values of -1 to 1 as input data .....	58
Figure 13 - Sensitivity analysis of the empirical Slurry oil yield model response to normalized values of -1 to 1 as input data .....	59
Figure 14 - Sensitivity analysis of the empirical Coke yield model response to normalized values of -1 to 1 as input data .....	59
Figure 15 - Products yield as a function of Catalyst-to-oil ratio in the ACE FCC pilot plant: Vacuum gasoil reference feed (▲); 21.4 wt.% slurry oil (◇); 35.5 wt.% slurry oil (+). Linear model for vacuum gasoil reference feed data (---).....	63
Figure 16 - Contour plots from screening of the input variables $T_{rx}$ and $T_{feed}$ . $Q_{vgo} = 8000$ m <sup>3</sup> /d, $L_{riser} = 30$ m, $Q_{recycle} = 0$ . (a) LCO yield (wt.%), (b) Slurry oil yield (wt.%), (c) Naphtha yield (wt.%), (d) Profit margin (10 <sup>3</sup> US\$/d), (e) Air rate (10 <sup>3</sup> kg/h).	

(---) minimum experimental CTO, (---) constraints: maximum $T_{reg}$ (1013.15 K) and maximum air rate ( $230.0 \cdot 10^3$ kg/h) .....	70
Figure 17 - Contour plots from screening of the input variables $T_{feed}$ and $L_{riser}$ . $T_{rx} = 823.15$ K, $Q_{vgo} = 8000$ m <sup>3</sup> /d, $Q_{recycle} = 0$ . (a) LCO yield (wt.%), (b) Slurry oil yield (wt.%), (c) Naphtha yield (wt.%), (d) Profit margin ( $10^3$ US\$/d), (e) Air rate ( $10^3$ kg/h). (---) minimum experimental CTO, (---) constraint: maximum $T_{reg}$ (1013.15 K).....	71
Figure 18 - Four lump gasoil cracking reaction model .....	74
Figure 19 – Adjustments made to Chapter 1 empiric model structure to obtain an empiric model able to provide data on liquid product characterization .....	90
Figure 20 - Boxplot of the lower heating values in kJ/kg of liquid product (lp), gas product (gp), coke and VGO at reference conditions. The (*) notation refers to the lower heating value corrected to conditions at the riser outlet.....	96
Figure 21 - Boxplot of the yield-weighted lower heating values in kJ/kg of liquid product (lp), gas product (gp), coke and VGO at reference conditions. The (*) notation refers to the lower heating value corrected to conditions at the riser outlet .....	97
Figure 22 - Boxplot of the resulting heat of reaction and sensible (and latent) heat in kJ/kg of liquid product (lp), gas product (gp), coke and VGO (reference conditions to the riser outlet).....	98
Figure 23 - Boxplot of the resulting heat of reaction and yield-weighted sensible (and latent) heat in kJ/kg of liquid product (lp), gas product (gp), coke and VGO (reference conditions to the riser outlet) .....	98
Figure 24 – Parameters a and b of the logistic function (Eq. 68) estimated for the VGO feed distillation curves at normalized temperatures between -1 and 1 .....	102
Figure 25 - Parameters a and b of the logistic function (Eq. 68) estimated for the VGO feed distillation curves at original temperatures in °C .....	103
Figure 26 - Fitting of the empirical models from Table 21 .....	114
Figure 27 - Fitting of the lumped yields obtained by manipulating the empirical models from Table 21 .....	118

## LIST OF TABLES

Table 1 - Vacuum gasoil properties – 7.5 m <sup>3</sup> /d FCC pilot plant .....	29
Table 2 - Equilibrium catalyst properties – 7.5 m <sup>3</sup> /d FCC pilot plant.....	30
Table 3 - Equilibrium catalyst properties – Testing in ACE fixed fluidized-bed unit .....	37
Table 4 - Feed properties – Testing in ACE fixed fluidized-bed unit.....	37
Table 5 - Correlation matrix of possible input variables .....	48
Table 6 - Empirical model of FCC yield profile – individual cuts and complete product slate. Variables in physical units.....	51
Table 7 - Empirical model of FCC yield profile – individual cuts and complete product slate. Normalized dimensionless variables .....	54
Table 8 - Regression of ACE FCC pilot plant data for reference VGO feed as a function of CTO .....	64
Table 9 - Simplified model for correction factor due to change of feed from fresh VGO to slurry oil recycle.....	65
Table 10 - Numerical example of obtaining the normalized yield profile for Slurry oil recracking for feed “C” (HC <sub>light</sub> = 5.8 %), T <sub>rx</sub> = 808.15 K, CTO = 5.0 and t <sub>c</sub> = 1.5 s .....	66
Table 11 - Range of operating conditions allowed for the FCC unit in the optimization study.....	67
Table 12 - Price basis considered in the optimization study .....	67
Table 13 - Results of the cases run in the optimization.....	68
Table 14 - Thermodynamic data for the reaction components of Eq. 25.....	76
Table 15 - Heat capacities for components of Eq. 25.....	78
Table 16 - Heats of reaction for catalytic cracking reactions estimated by Han, Chung (2001a, 2001b).....	80
Table 17 - Kinetic and thermodynamic parameters estimated in the model of John, Mustafa, Patel and Mutjaba (2019).....	81
Table 18 - Characterization of vacuum gasoil feed to obtain thermodynamic parameters .....	96
Table 19 - Assessment of API correlation for LHV .....	99
Table 20 - Modified version of Table 17 with the proposal to use a single heat of reaction for reactions converting feed into light hydrocarbons.....	101

Table 21 - Empirical models with retrieval of complete characterization of cracking products for heat of reaction estimation .....	106
--	-----

## LIST OF ABBREVIATIONS

ACE	Advanced Cracking Evaluation (fixed fluidized-bed unit)
CTO	Catalyst-to-oil ratio
DAE	Differential-algebraic equation
D86	Distillation ASTM D86
DS	Simulated distillation ASTM D2887
FCC	Fluid Catalytic Cracking
HHV	Higher heating value
LCO	Light cycle oil
LHV	Lower heating value
LPG	Liquefied petroleum gas
MeABP	Mean average boiling point
MW	Molecular weight
ODE	Ordinary differential equation
OLS	Ordinary least squares
RCR	Ramsbottom carbon residue
RLS	Restricted least squares
SSE	Squared sum of errors
VGO	Vacuum gasoil

## SYMBOL LIST

$a, b, c, g, h$	Parameters for a sigmoidal function to express $P_{dist}^{cum}$
$a_0, a_1, \dots$	Coefficients for the polynomial of cumulative distilled mass fraction as a function of temperature in the canonic form
$A_1, A_2, \dots$	Constants for hydrocarbon enthalpy calculation
$A_{p_{ef}}$	Effective interface heat transfer area per unit volume between the catalyst and fluid (gas) phases in the riser ( $m^2/m^3$ )
$A_{riser}$	Cross sectional area of the riser ( $m^2$ )
$API$	Degree API (or API gravity)
$B_1, B_2, \dots$	Constants for hydrocarbon enthalpy calculation
$C_1, C_2, \dots$	Constants for heat capacity calculation
$C_{p_{cat}}$	Heat capacity of the catalyst ( $kJ.kg^{-1}.K^{-1}$ )
$C_{p_{fluid}}$	Heat capacity of the fluid (gas) phase ( $kJ.kg^{-1}.K^{-1}$ )
$C_{p_i}$	Heat capacity of pure component ( $kJ.kmol^{-1}.K^{-1}$ )
$CTO$	Catalyst-to-oil ratio ( $kg/kg$ )
$\overline{CTO}$	$CTO$ in normalized dimensionless form (between -1 and 1)
$d_{20}$	Density at $20^\circ C$ ( $kg/dm^3$ )
$d_{20^\circ C}$	Specific gravity at $20^\circ C$ referred to water at $4^\circ C$
$d_{60^\circ F}$	Specific gravity at $60^\circ F$ referred to water at $60^\circ F$
$Dev_N$	Maximum squared sum of errors of applying model $M_N$ with input data from all partitions $N$
$D_{riser}$	Riser internal diameter (m)
$E_{a_j}$	Activation energy of reaction $j$ ( $kJ/kmol$ ), $j = \{1rs, 2rs, \dots\}$

$Error_{CTO}$	Absolute error of calculated CTO between successive iterations in the FCC process simulator (kg/kg)
$Error_{O_2}$	Absolute error of calculated $O_2$ content in the dry flue gas between successive iterations in the FCC process simulator (mol%)
$Error_{t_c}$	Absolute error of calculated $t_c$ between successive iterations in the FCC process simulator (s)
$Error_{T_{reg}}$	Absolute error of calculated $T_{reg}$ between successive iterations in the FCC process simulator (K)
$\vec{F}_i$	Vector of experimental correction factors accounting for the effect of changing the feed quality from fresh vacuum gasoil to recycled slurry oil to component i yield
$\overrightarrow{F_{calc,i}}$	Vector of calculated (regressed) correction factors accounting for the effect of changing the feed quality from fresh vacuum gasoil to recycled slurry oil to component i yield
$F_{rx}$	Volumetric flow rate of reaction mixture at the Riser outlet ( $m^3/s$ )
$h_{liq,T_{feed}}$	Enthalpy of the liquid feed vaporized at $T_{feed}$ (kJ/kg)
$h_p$	Interface heat transfer coefficient between the catalyst and fluid (gas) phases in the riser, ( $kJ.m^{-2}.s^{-1}.K^{-1}$ )
$h_{vap,T_{rx}}$	Enthalpy of the feed vaporized at $T_{rx}$ (kJ/kg)
$h_{T_{air}}^{air}$	Enthalpy of air at $T_{air}$ (kJ/kg)
$h_{T_{ref}}^{air}$	Enthalpy of air at $T_{ref}$ (kJ/kg)
$h_{T_{dil}}^{flue}$	Enthalpy of flue gas at $T_{dil}$ (kJ/kg)
$h_{T_{ref}}^{flue}$	Enthalpy of flue gas at $T_{ref}$ (kJ/kg)
$h_{T_{rx}}^{st}$	Enthalpy of steam at $T_{rx}$ (kJ/kg)

$h_{Tst}^{st}$	Enthalpy of steam at steam header temperature (kJ/kg)
$H_{(l)}$	Enthalpy of petroleum fraction at the liquid phase, (btu/lb)
$H_{(v)}$	Enthalpy of petroleum fraction at the vapor phase, (btu/lb)
$H_f$	Enthalpy of formation, (kJ/kmol)
$HC_{light}$	Light hydrocarbons content (mass content with a distillation point below 343°C) in the feed (wt.%)
$\overline{HC_{light}}$	$HC_{light}$ in normalized dimensionless form (between -1 and 1)
$i$	Counter; component index
$j$	Counter; index
$k$	Counter; index
$k_j$	Reaction rate coefficient for reaction j ( $s^{-1}$ ), $j = \{1rs, 2rs, \dots\}$
$k_{j_0}$	Frequency factor in the Arrhenius expression for Reaction rate coefficient for reaction j ( $s^{-1}$ ), $j = \{1rs, 2rs, \dots\}$
$K_{factor}$	Characterization factor of the FCC feed
$K_w$	Watson's characterization factor of petroleum fraction
$L$	Matrix of restriction coefficients for $\vec{\beta}$ in a RLS model
$L_{i(x)}$	i-th Lagrange interpolating polynomial
$L_{riser}$	Riser length from feed injection nozzle to the outlet (m)
$LHV_i^{T_{ref}}$	Lower heating value for component i at $T_{ref}$ (kJ/kmol)
$m_C$	Weight fraction of Carbon on coke
$m_H$	Weight fraction of Hydrogen on coke
$m_O$	Weight fraction of Oxygen on coke
$M_N$	Model selected in partition N
$M_{N,i}$	Candidate model i in partition N

$MW_i$	Molecular weight of component i
$n$	Counter; degree of a polynomial
$n_d$	Number of experimental points of the distillation curve
$N$	Random partition in training set
$N'$	Random partition in test set
$N_{bas}$	Basic Nitrogen content in the feed (mg/kg)
$p$	Counter of nodal points for $P_{dist}^{cum}$ as a function of temperature in Lagrange form
$p_{best}$	Variable (parameter) which resulted in a $M_{N,i}$ with greatest increase in $R_{adj}^2$ during forward model generation
$P_{dist}^{cum}$	Experimental cumulative distilled mass fraction
$P_{dist}^{cum,calc}$	Calculated cumulative distilled mass fraction
$\vec{P}_{dist}^{cum,calc}$	Calculated cumulative distilled mass fraction (vectorial notation)
$\vec{P}_{dist}^{cum,exp}$	Experimental cumulative distilled mass fraction (vectorial notation)
$P_{rx}$	Absolute pressure at the Riser outlet (kPa)
$Q_i$	Flow rate of component i produced in the Riser (m <sup>3</sup> /d)
$Q_{recycle}$	Flow rate of Slurry oil recycle feed to the Riser (m <sup>3</sup> /d)
$Q_{rx}$	Rate of heat generation (or removal) due reactions (kJ.kg <sup>-1</sup> .s <sup>-1</sup> )
$Q_{vgo}$	Flow rate of VGO feed to the Riser (m <sup>3</sup> /d)
$\vec{r}$	Vector of restriction values in a RLS model
$r_i$	Reaction rate for component i (s <sup>-1</sup> )
$R_{ideal}$	Ideal gas constant, 8.31446 kJ/(kmol.K)
$R_{adj}^2$	Coefficient of determination of the regression adjusted for the number of regressors in the model

$R_{CR}$	Ramsbottom carbon residue of the feed (wt.%)
$SSE_{N,N'}$	Squared sum of errors of applying model $M_N$ with input data from partition $N'$
$t_c$	Contact time between the feed and catalyst along the Riser for cracking reactions (s)
$\bar{t}_c$	$t_c$ in normalized dimensionless form (between -1 and 1)
$T$	Temperature (K)
$T_{0\%}, T_{10\%}, \dots$	Points of the distillation curve at the percentage vaporized indicated ( $^{\circ}\text{C}$ )
$T_{air}$	Temperature of air upstream of the Regenerator (K)
$T_b$	Mean average boiling point (R)
$T_{cat}$	Temperature of the catalyst (K)
$T_{dil}$	Temperature of the dilute phase of the Regenerator (K)
$T_{feed}$	Temperature of the feed to the Riser (K)
$T_{fluid}$	Temperature of the fluid phase i.e., hydrocarbons and steam in the gas phase (K)
$T_{inlet_{reg}}$	Temperature of the circulating catalyst at the Regenerator inlet (K)
$T_k$	Experimental (temperature) point of the distillation curve ( $^{\circ}\text{C}$ )
$T_p$	Temperature nodal points for $P_{dist}^{cum}$ in Lagrange form ( $^{\circ}\text{C}$ )
$T_{pc}$	Pseudocritical temperature (R)
$T_r$	Reduced temperature
$T_{ref}$	Reference temperature for tabulated enthalpy data on pure species involved in combustion of coke (K)
$T_{reg}$	Temperature of the dense bed phase of the Regenerator (K)
$T_{rx}$	Reaction temperature in the outlet of the Riser (K)

$\overline{T_{rx}}$	$T_{rx}$ in normalized dimensionless form (between -1 and 1)
$Tol_{CTO}$	Tolerance for CTO convergence in the FCC process simulator (kg/kg)
$Tol_{O_2}$	Tolerance for O <sub>2</sub> content in the dry flue gas convergence in the FCC process simulator (mol%)
$Tol_{t_c}$	Tolerance for $t_c$ convergence in the FCC process simulator (s)
$Tol_{T_{reg}}$	Tolerance for $T_{reg}$ convergence in the FCC process simulator (K)
$w_{air}$	Mass flow rate of air to the Regenerator (kg/s)
$w_{cat}$	Mass flow rate of the catalyst (kg/s)
$w_{ck}$	Weight fraction of coke in the Riser outlet
$w_{coke}$	Mass flow rate of coke to the Regenerator (kg/s)
$w_{conv}$	Mass flow rate of converted feed (100% - LCO wt.% yield - slurry oil wt.% yield of $w_{feed}$ ) in the outlet of the Riser (kg/s)
$w_{feed}$	Mass flow rate of feed to the Riser (kg/s)
$w_{flue}$	Mass flow rate of flue gas exiting the Regenerator (kg/s)
$w_{fluid}$	Mass flow rate of the fluid phase i.e., hydrocarbons and steam in the gas phase (kg/s)
$w_{gp}$	Weight fraction of gaseous products (Dry gas and LPG) in the Riser outlet
$w_i$	Mass flow rate of component i produced in the Riser (kg/h)
$w_{k,i}$	Weighting factor for $P_{dist}^{cum,calc}$ associated with polynomial $L_i$ integrated until point $T_k$
$w_{lp}$	Weight fraction of liquid products (Naphtha, LCO and Slurry oil) in the Riser outlet
$w_{st}$	Mass flow rate of steam to the Riser (kg/s)
<b>W</b>	Matrix of weighting factors $w_{k,i}$ for $P_{dist}^{cum,calc}$

$x$	Riser length (m)
$\mathbf{X}$	Matrix of explanatory variables
$X_{model\_slurry}$	Set of input variables to the Slurry oil cracking model in the FCC process simulator
$X_{model\_VGO}$	Set of input variables to the VGO cracking model in the FCC process simulator
$X_{opt}$	Set of input variables to the FCC process simulator
$\mathbf{X}^{full}$	Matrix of explanatory variables with all terms initially available
$\mathbf{X}_N^{sel}$	Matrix of explanatory variables selected for the model in partition N
$\mathbf{X}_{N'}^{sel}$	Matrix of explanatory variables selected for the model in partition N'
$\vec{y}, \overrightarrow{y_{exp}}$	Vector of experimental output variables
$y(x)$	Generic polynomial y as a function of x
$y_{calc}$	Vector of calculated output variables
$y_{calc,N\_N'}$	Vector of calculated output variables using model $M_N$ with input data from partition N'
$y_i$	Weight fraction of component i
$z$	Modified form of $P_{dist}^{cum}$ when linearizing the sigmoidal function with two parameters

Greek letters:

$\beta, \vec{\beta}$	Vector of estimated coefficients in a regression
$\beta_N$	Vector of estimated coefficients for parameters in model $M_N$
$\overrightarrow{\beta}_{OLS}$	Vector of estimated coefficients in an ordinary least squares regression

$\vec{\beta}_{RLS}$	Vector of estimated coefficients in a restricted least squares regression
$\gamma_i$	Weight fraction or mass yield of component i
$\Delta h_{comb_{coke}} \Big ^{T_{ref}}$	Combustion enthalpy of coke at $T_{ref}$ (kJ/kg)
$\Delta H_{cat_{reg}}$	Heat demanded for heating the circulating catalyst from $T_{inlet_{reg}}$ to $T_{reg}$ in the Regenerator (kJ/s)
$\Delta H_{cat_{rx}}$	Heat supplied by the hot circulating catalyst to the Riser (kJ/s)
$\Delta H_{coke}$	Heat supplied by the combustion of coke in the Regenerator (kJ/s)
$\Delta H_{feed}$	Heat demanded to vaporize the liquid feed and to heat it up to the reaction temperature (kJ/s)
$\Delta H_{flue_{air}}$	Heat differential between hot flue gas exiting and relative cold air injected into the Regenerator (kJ/s)
$\Delta H_i$	Sensible heat variation for component i (kJ/kmol)
$\Delta H_j$	Heat of reaction for reaction j (kJ/kg), $j = \{1rs, 2rs, \dots\}$
$\Delta H_{loss_{reg}}$	Heat loss to the environment in the Regenerator (kJ/s)
$\Delta H_{loss_{rx}}$	Heat loss to the environment in the Riser (kJ/s)
$\Delta H_{rx}$	Heat of reaction (kJ/kg)
$\Delta H_{steam}$	Heat demanded for heating steam from steam header temperature to $T_{rx}$ (kJ/s)
$\Delta H_{rx}^{calorimetry}$	Heat of reaction obtained from the calorimetry of the products (kJ/kg)
$\Delta H_{rx}^{energy\ bal.}$	Heat of reaction obtained from the energy balance of the FCC unit (kJ/kg)
$\Delta H_{coke}^{sens}$	Sensible heat of coke from $T_{ref}$ to $T_{rx}$ (kJ/kg)
$\Delta H_{gp}^{sens}$	Sensible heat of gaseous products (Dry gas and LPG) from $T_{ref}$ to $T_{rx}$ (kJ/kg)

$\Delta H_{lp}^{sens}$	Sensible (and latent) heat of liquid products (Naphtha, LCO and Slurry oil) from $T_{ref}$ to $T_{rx}$ (kJ/kg)
$\Delta H_{vgo}^{sens}$	Sensible (and latent) heat of VGO feed from $T_{ref}$ to $T_{rx}$ (kJ/kg)
$\vec{\varepsilon}$	Vector of error between experimental output variables and calculated output variables
$\varepsilon_{cat}$	Volume fraction of catalyst
$\zeta_i, \zeta_k$	Stoichiometric index for components i, k
$\vec{\theta}$	Vector of densities of probability of $P_{dist}^{cum}$ at temperatures $T_p$
$\theta_i$	Density of probability of $P_{dist}^{cum}$ at a temperature T equals to the i-th nodal point $T_p$
$\rho_{cat}$	Catalyst density (kg/m <sup>3</sup> )
$\phi_{cat}$	Catalyst deactivation function

## SUMMARY

<b>INTRODUCTION</b> .....	25
<b>1 EMPIRICAL MODELING AND YIELD PROFILE OPTIMIZATION OF A CATALYTIC CRACKING REACTOR</b> .....	26
<b>1.1 Introduction</b> .....	26
<b>1.2 Methodology</b> .....	27
1.2.1 <u>Experimental section – cracking of vacuum gasoil</u> .....	28
1.2.2 <u>Empirical modeling – individual products</u> .....	32
1.2.3 <u>Empirical modeling – complete product slate</u> .....	34
1.2.4 <u>Experimental section and simplified empirical modeling – cracking of slurry oil</u> .....	36
1.2.5 <u>Optimization of FCC unit product slate</u> .....	39
<b>1.3 Results and discussion</b> .....	44
1.3.1 <u>Empirical modeling – individual products</u> .....	47
1.3.2 <u>Empirical modeling – complete product slate</u> .....	60
1.3.3 <u>Simplified empirical modeling of slurry oil cracking</u> .....	61
1.3.4 <u>Optimization of FCC unit product slate</u> .....	66
<b>1.4 Conclusion</b> .....	72
<b>2 CONSIDERATIONS ON THE ENERGY BALANCE OF CRACKING REACTIONS</b> .....	74
<b>2.1 Introduction</b> .....	74
<b>2.2 Methodology</b> .....	83
2.2.1 <u>Heat of reaction by estimated calorimetry of feed and products</u> .....	83
2.2.2 <u>Empirical modeling with retrieval of liquid product distillation curve</u> .....	89
<b>2.3 Results and discussion</b> .....	96
2.3.1 <u>Heat of reaction by estimated calorimetry of feed and products</u> .....	96
2.3.2 <u>Empirical modeling with retrieval of liquid product distillation curve</u> .....	101
<b>2.4 Conclusion</b> .....	119
<b>CONCLUSION</b> .....	121
<b>REFERENCES</b> .....	123

<b>ANNEX 1</b> – Experimental conditions of the tests performed at the 7.5 m <sup>3</sup> /d FCC pilot plant	128
<b>ANNEX 2</b> – Experimental yields (wt. %) obtained at the 7.5 m <sup>3</sup> /d FCC pilot plant .....	129
<b>ANNEX 3</b> – Characterization of the liquid products to obtain thermodynamic parameters ....	131
<b>ANNEX 4</b> – Composition of the gaseous products.....	137
<b>ANNEX 5</b> – Distillation curves of the VGO batches.....	139
<b>ANNEX 6</b> – Distillation curves of the liquid products .....	141

## INTRODUCTION

The fluid catalytic cracking is a process in which residual feeds are cracked, in a fluidized reactor with catalyst particles, into lighter and more noble hydrocarbons (notably naphtha and LPG). It was initially developed in the early 1940's and remains playing a central role in the profitability of a refinery (Sadeghbeigi, 2020).

There is currently internal and global trend of reducing the demand of gasoline (EPE, 2018); although, to this day, an extreme event of deep reducing of throughput or even shutdown of FCC units has not yet been consummated in the Brazilian refining scheme. This scenario is expected to become considerably more challenging for the FCC with the starting operation of hydrocracking units (Petrobras, 2022), which competes for the same feedstock with the FCC unit and produces a large yield of high quality diesel (Stanislaus; Marafi; Rana, 2010).

In this scenario of uncertainties on the horizon of the FCC process, alternatives for adapting the process are being studied. A possible demand is the operation of the FCC at low conversion, in order to increase the production of a medium distilled cut, called LCO (light cycle oil); which can be sent to the diesel hydrotreater unit in order to be incorporated in the diesel pool. However, a known drawback of operating the FCC unit at low conversion is that this is accompanied by an increase in the production of a low-value unconverted product, slurry oil (Benoit, 2015; Corma; Sauvinaud, 2007; Gilbert; Baptista; Pinho, 2007; Gilbert; Morgado Jr; de Abreu; de la Puente; Passamonti; Sedran, 2011; Ma; Hu; Langan; Hunt; Cheng, 2010; Niccum, 2013; Sadeghbeigi, 2020).

The objective of this work was to study the FCC for middle distillates mode of operation and evaluate its attractiveness potential compared to the conventional route of gasoline maximization. A quite amount of experimental data was produced during the course of this study. Through a statistical treatment of these data, it was possible to build an empirical model that assisted in the performance evaluation of the FCC unit at maximum middle distillates (i.e. low conversion) mode. Chapter 1 presents the empirical model building procedure, the model thus obtained and the results of its application in optimal yield profile studies carried out.

Although it has not been fulfilled in the scope of the present work, the path to obtaining a kinetic model with a phenomenological basis was better paved with studies on the energy balance of cracking reactions, which must be included in the differential kinetic model of the cracking reactions along the riser. Chapter 2 discusses this subject. Each one of Chapters 1 and 2 contains inner introductions that further contextualize the topics under study.

# 1 EMPIRICAL MODELING AND YIELD PROFILE OPTIMIZATION OF A CATALYTIC CRACKING REACTOR

## 1.1 Introduction

The natural vocation of the catalytic cracking process is the production of gasoline and LPG. In this latter, usually the emphasis relies upon the light olefins content such as propene (an important feedstock to the petrochemical industry). The reaction mechanism favored by acid catalysts used in the catalytic cracking process directs toward the concentration of hydrocarbon species in the range of LPG (with a high concentration of olefins) and cracked naphtha (with high concentration of aromatics and olefins) (Corma; Sauvanaud, 2007; Gilbert; Baptista; Pinho, 2007; Vogt; Weckhuysen, 2015).

Due to trends in Brazilian fuel market of increased demand of diesel, which is yet exacerbated because of freight transport logistics heavily based on the road modal, and stagnation or even decline of gasoline demand due to several factors (including: increased efficiency of Otto cycle engines, changes in urban mobility, competition with other Otto cycle fuels such as ethanol and vehicular natural gas, Diesel cycle engines for light fleets and advent of electric vehicles) (EPE, 2018), in recent years the FCC process has experienced strong pressure to adapt product slate to meet such market demand.

Possible paths to adjust the ordinary operating mode of the FCC unit include: (a) maximizing middle distillates yield (Benoit, 2015; Corma; Sauvanaud, 2007; Gilbert; Morgado Jr; de Abreu; de la Puente; Passamonti; Sedran, 2011; Ma; Hu; Langan; Hunt; Cheng, 2010; Niccum, 2013), i.e. the light cycle oil (LCO) cut, and (b) maximizing light olefins (especially propene) yield (Akah; Al-Ghrami, 2015; Alabdullah; Gomez; Vittenet; Sedjerari; Xu; Abba; Gascon, 2020; Corma; Melo; Sauvanaud; Ortega, 2004; Gholami; Gholami; Tisler; Tomas; Vakili, 2021).

It is interesting to note that these two routes conflict with each other (Gilbert; Baptista; Pinho, 2007). Maximizing LCO yield implies reducing the conversion typically practiced in FCC unit, with a consequent reduction in the yields of cracked naphtha and LPG. However, this comes with the disadvantage of an increased yield of slurry oil (or unconverted feedstock), which impairs the process economics. An option that can be employed to partially mitigate excessive bottoms production is the re cracking of a portion of the slurry oil stream to the FCC Riser (Lan; Xu; Wang; Gao, 2009; Niccum, 2013; Sadeghbeigi, 2020), recovering some conversion and thus lowering the overall slurry oil yield.

On the other hand, maximizing propene yield implies increasing the reaction severity, thus increasing the unit conversion and also generally resulting in a slight to moderate reduction of cracked naphtha as it is overcracked to produce LPG. Despite this conflict, some licensors have developed processes aimed at the production of propene that simultaneously seek to maximize the production of middle distillate (LCO), usually requiring two or more risers (or two or more distinct reaction zones), where each riser has the flexibility to operate at independent severity levels (Khande; Dasila; Majumder; Maity; Thota, 2021).

Both for a FCC unit that has the flexibility to increase middle distillate and light olefins at the same time, but even more relevant in the case of a unit that does not possess such flexibility, it is beneficial to map the operating window for maximizing LCO yield in order to reduce the drawbacks that come along, mainly the increased throughput of slurry oil, especially if a region has already been reached where additional steps towards lower conversions do not increase further LCO yield or quality (Corma; Sauvanaud, 2007).

Thus, one purpose of the present study was to statistically treat data from experiments that had been conducted to explore the LCO yield maximization region to better enlighten the optimal operating conditions for this low conversion production mode. Additional experiments were included in which slurry oil samples of selected runs in low severity operation were cracked on a smaller scale FCC pilot plant, in order to investigate the alternative of slurry oil re cracking.

Yet another purpose of the study was to evaluate which operation mode, among conventional high conversion (cracked naphtha maximization) and low conversion (middle distillate maximization), offers the highest operating profit margin for a typical price basis of refining products in Brazilian market.

## **1.2 Methodology**

This section describes the tests performed in the FCC pilot plants and the statistical approach for the construction of an empirical model of the riser cracking yield profile.

### 1.2.1 Experimental section – cracking of vacuum gasoil

The tests were carried out in a large scale, 7.5 m<sup>3</sup>/d capacity, FCC pilot plant located in São Mateus do Sul/PR research site (Mello; Gobbo; Moure; Miracca, 2013; Pinho; Almeida; Mendes; Casavechia; Talmadge; Kinchin; Chum, 2017). Tests investigating the middle distillate maximization route were run at different periods between 2009 and 2016. All data made available were from tests that used vacuum gasoil from a commercial FCC unit as feed, at 200 kg/h rate. Due to the extensive time span, the tests were carried out with different batches of vacuum gasoil (see Table 1) and this led to the need of taking into account, in the yield profile modeling, slight differences in gasoil quality, which was not a main explanatory variable designed for the study. In Table 1, light gasoil content is reported, in a simplified way, as the mass content of feed with a distillation point below 343°C (based on the simulated distillation curve provided). Also, the Characterization Factor reported is a simplified version of Watson's Characterization Factor that uses an average boiling point estimated directly from simulated distillation data and density at 20°C (instead of the specific gravity 60°F/60°F) as Eq. 1:

$$K_{factor} = \frac{\sqrt[3]{1.8 * \left( \frac{T_{10\%} + T_{30\%} + T_{50\%} + T_{70\%} + T_{90\%}}{5} + 273.15 \right)}}{d_{20}} \quad \text{Eq. 1}$$

Table 1 - Vacuum gasoil properties – 7.5 m<sup>3</sup>/d FCC pilot plant

Property	Value				
	A1	A2	B	C	D
Feed					
Density, kg/dm <sup>3</sup> (20°C)	0.9424	0.9448	0.9376	0.9382	0.9345
Sulfur, wt.%	0.53	0.64	0.61	0.58	0.40
Total nitrogen, wt.%	0.26	0.29	0.36	0.36	0.26
Basic nitrogen, mg/kg	1059	1267	1197	1304	829
Aniline point, °C	76.2	74.2	82.1	83.2	77.9
Ramsbottom carbon residue, wt.%	1.1	0.98	0.82	2.04	1.3
Characterization factor	11.57	11.55	11.67	11.74	11.62
<i>Simulated distillation (mass recovery, °C)</i>					
5%	319.2	323.6	344.6	336.4	255.4
10%	350.0	355.6	372.8	366.2	297.0
30%	412.2	415.6	421.8	424.8	392.8
50%	444.6	448.8	452.0	462.0	435.8
70%	486.4	488.0	487.6	507.6	478.0
90%	540.4	537.8	540.4	587.4	584.2
95%	564.0	560.2	565.8	655.4	649.0
Light gasoil content, wt.%	8.8	7.9	4.8	5.8	16.9

Source: The author, 2023.

The equilibrium catalyst used in the tests performed at FCC pilot plant (see Table 2) is from a developmental project of middle distillate maximization catalysts sampled during a commercial trial in an industrial unit (Gilbert; Baptista; Pinho, 2007).

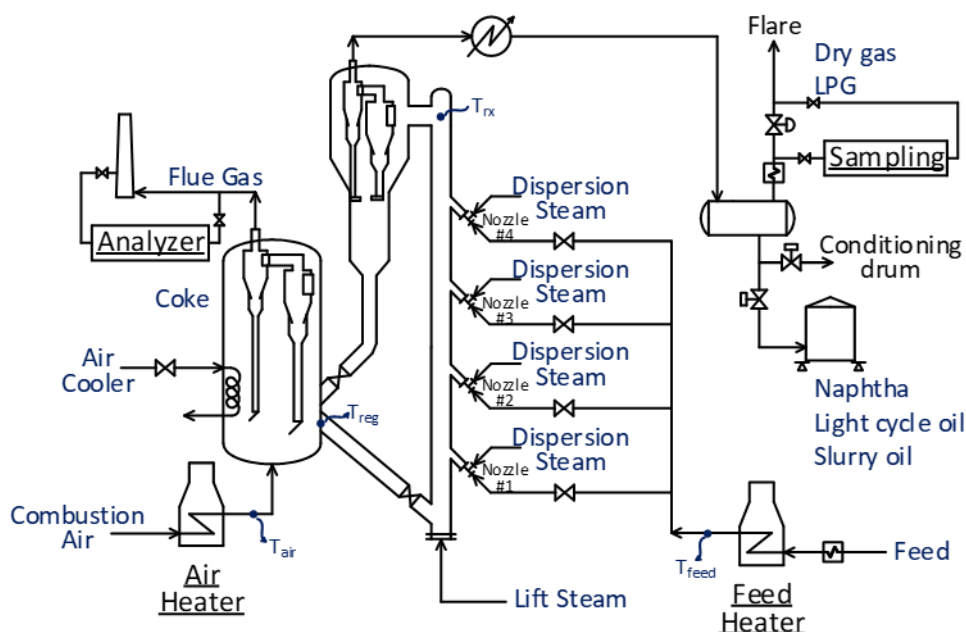
Table 2 - Equilibrium catalyst properties – 7.5 m<sup>3</sup>/d FCC pilot plant

Property	Value
Surface area, m <sup>2</sup> /g	128
Mesopore area, m <sup>2</sup> /g	74
Micropore volume, cm <sup>3</sup> /g	0.025
Al <sub>2</sub> O <sub>3</sub> content, wt. %	55.1
Rare earth oxides content, wt. %	2.1
V content, mg/kg	1324
Ni content, mg/kg	1946
Combustion promoter content, mg/kg	0.5

Source: The author, 2023.

The study was mainly focused on the effect of operating variables associated with the reaction severity level employed in the Riser: reaction temperature ( $T_{rx}$ ), catalyst-to-oil mass ratio (CTO) and contact time between the feed and catalyst in the Riser reactor ( $t_c$ ), this last one a variable usually not explored in commercial units.

In the pilot plant where the tests were carried out, the contact time between feed and catalyst (or reaction time) was adjusted by selecting the feed injection point, as the unit is assembled with four injections points in different elevations along the length of the Riser, as shown in Figure 1.

Figure 1 - 7.5 m<sup>3</sup>/d FCC pilot plant general assembly

Source: The author, 2023.

Tests were carried with a 3-hour run length. Mass balances obtained were within a range of 97 – 103 wt.%, which was deemed acceptable. In all tests, the coke yield was taken from the mass balance in the Regenerator section by the typical approach using the flue gas composition measured by an online analyzer (Sadeghbeigi, 2020). The coke yield calculated in this way was maintained for the complete normalized yield profile, thus the deviations in mass balance closure were addressed through normalization of the mass flow rate of the gas product stream (which is sampled hourly for a subsequently chromatographic analysis in the laboratory) and the mass inventory of the liquid product accumulated in the test storage tank.

Products considered in the study were the typical cuts of commercial FCC units: dry gas (C<sub>1</sub>, C<sub>2</sub> hydrocarbons, and hydrogen), LPG (C<sub>3</sub>, C<sub>4</sub> hydrocarbons), naphtha (C<sub>5</sub> – 221°C simulated distillation boiling range), LCO (221 – 343°C simulated distillation boiling range), slurry oil (343°C+ simulated distillation boiling range) and coke.

Catalyst-to-oil ratio (CTO) was calculated from the energy balance of the Regenerator. In general, riser outlet reaction temperature ( $T_{rx}$ ) and CTO are directly correlated, as a typical control scheme for the FCC unit manipulates the reaction temperature by adjusting the regenerated catalyst valve opening, thus modifying the catalyst circulation rate (and CTO) accordingly.

In order to introduce some level of independence between  $T_{rx}$  and CTO, a number of tests were performed with feed temperature ( $T_{feed}$ ) or dense phase regenerator temperature ( $T_{reg}$ )

adjusted so that CTO could vary aside from reaction temperature. When executed, manipulation of  $T_{\text{reg}}$  was done by adjusting combustion air inlet temperature ( $T_{\text{air}}$ ) through the air heater or by using the cooling coil with ambient air. In all tests  $T_{\text{reg}}$  was maintained in the 670 – 730°C range.

The cracking reactions taking place in the riser are mainly endothermic, along with some secondary exothermic reactions such as cyclization, aromatic rings condensation and coke formation (Pekediz; Kraemer; Blasetti; de Lasa, 1997; Sadeghbeigi, 2020). The overall heat of reaction (at the reaction temperature) was calculated from the energy balance of the riser envelope. The experimental values thus obtained were reported in basis of kJ per kg of feed and in kJ per kg of converted feed, as it is common practice in the industry (Pekediz; Kraemer; Blasetti; de Lasa, 1997). Although the light cycle oil is a product of interest for the purpose of this study, conversion is considered 100 wt.% of feed discounted of LCO and slurry oil yields, as usually applied (Pekediz; Kraemer; Blasetti; de Lasa, 1997; Sadeghbeigi, 2020).

### 1.2.2 Empirical modeling – individual products

The experimental data available from the 7.5 m<sup>3</sup>/d FCC pilot plant was statistically treated to obtain empirical models useful for product slate prediction.

One of the challenges in modeling catalytic cracking yield profile is that it is highly specific for a particular catalyst system employed in the process since different properties and distribution of active sites in the porous structure of the catalyst favors certain reaction pathways that alters the product slate (Hiramatsu; Aita; Umeki, 2012; Mahgoub; Al-Khattaf, 2005). Thus, it should be considered that the empirical model developed is applicable specifically to the equilibrium catalyst used in the tests (Table 2), which was previously selected for its reported higher LCO / slurry oil ratio for a given conversion level (Gilbert; Baptista; Pinho, 2007).

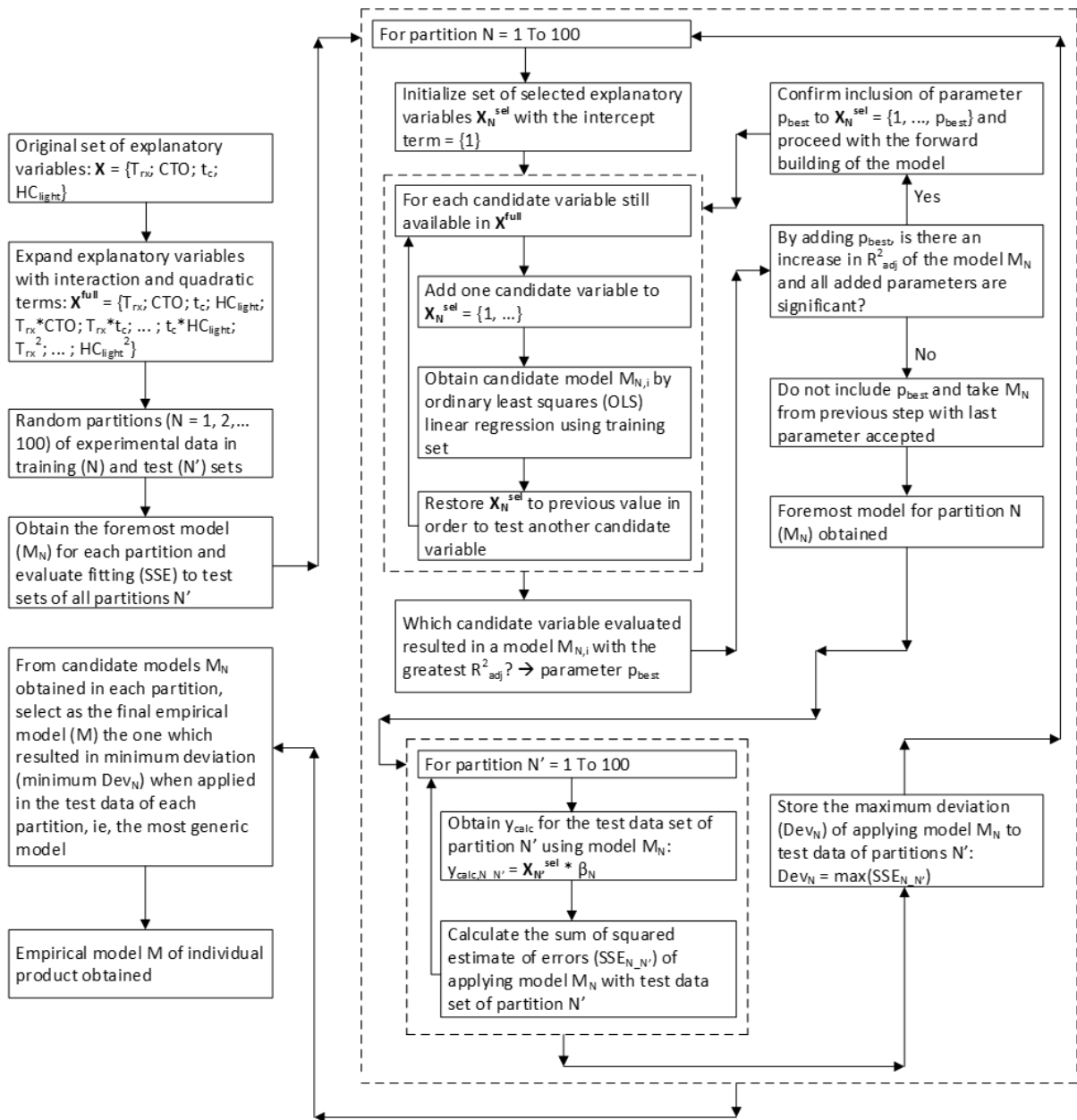
The explanatory variables for the model included the following process variables: reaction temperature ( $T_{\text{rx}}$ ), catalyst-to-oil ratio (CTO) and contact time between the feed and catalyst in the Riser ( $t_c$ ); and, to account for slight variations in feed quality of gasoil batches, it was investigated, with the aid of techniques such as principal components analysis and data correlation analysis, which set of explanatory variables should be included in the empirical model related to feed characterization: modified Watson's characterization factor ( $K_{\text{factor}}$ ), carbon residue content (RCR), basic nitrogen content ( $N_{\text{bas}}$ ) and light gasoil content ( $HC_{\text{light}}$ ), the latter defined, in a simplified way, as the mass content of feed with a distillation point below 343°C (based on the

simulated distillation curve provided). It was eventually selected the light gasoil content ( $HC_{light}$ ) as the explanatory variable related to feed characterization.

The empirical model for each individual product (dry gas, LPG, cracked naphtha, LCO, slurry oil and coke) was developed with structures formulated by forward regression of the original candidate variables plus quadratic and two-way interaction terms, a methodology in which the next explanatory variable to be included in the model is selected as the one that provides the greatest increase in the coefficient of determination. The stop criteria in the forward selection of new variables to the model was the interruption of model's  $R^2$  increase or the addition of a non-significant term. The procedure for estimating the coefficients of the variables in the models was the conventional least squares linear regression, i.e., maximum likelihood estimator.

Ultimately, a single representative empirical model, one such that avoids overfitting the model to the database on which it was trained, was obtained by cross-validation via Monte Carlo with 100 random partitions of the data between training and test sets, being selected the model with the lowest SSE (squared sum of errors) of all test sets of the random partitions. Figure 2 illustrates the procedure used in building the model.

Figure 2 - Schematic of empirical model construction procedure



Source: The author, 2023.

### 1.2.3 Empirical modeling – complete product slate

In addition to specific models for each individual cut, a model was developed that returns the complete yields profile, guaranteeing the closure of the mass balance by applying linear regression with restricted least squares (RLS).

Restricted least squares regression implies solving (Eq. 2) for the coefficients of the independent variables ( $\vec{\beta}$ ):

$$\vec{y} = \mathbf{X} \cdot \vec{\beta} + \vec{\varepsilon} \quad \text{Eq. 2}$$

However, the coefficients  $\vec{\beta}$  are subjected to a constraint (Eq. 3):

$$\mathbf{L} \cdot \vec{\beta} = \vec{r} \quad \text{Eq. 3}$$

The solution for  $\vec{\beta}$  in a restricted least squares regression ( $\vec{\beta}_{RLS}$ ) is given by Eq. 4 (Guilkey; Price, 1981):

$$\vec{\beta}_{RLS} = \vec{\beta}_{OLS} - (\mathbf{X}^T \cdot \mathbf{X})^{-1} \cdot \mathbf{L}^T \cdot (\mathbf{L} \cdot (\mathbf{X}^T \cdot \mathbf{X})^{-1} \cdot \mathbf{L}^T)^{-1} \cdot (\mathbf{L} \cdot \vec{\beta}_{OLS} - \vec{r}) \quad \text{Eq. 4}$$

Whereas the ordinary least squares coefficients ( $\vec{\beta}_{OLS}$ ) are obtained as usual (Eq. 5):

$$\vec{\beta}_{OLS} = (\mathbf{X}^T \cdot \mathbf{X})^{-1} \cdot \mathbf{X}^T \cdot \vec{y} \quad \text{Eq. 5}$$

To apply this method in the present case it is first required to select one of the cracking products as the mass balance closing cut, so it is treated as additional parameters  $\vec{\beta}$  in assembling the calculation. Then, stacking all the cuts at once ( $i$  = dry gas, LPG, cracked naphtha, LCO, slurry oil and coke, being one of them the  $i^{\text{th}}$  selected to close the material balance), the matrix calculation can be written as Eq. 6:

$$\begin{pmatrix} \vec{y}_1 \\ \vec{y}_2 \\ \vdots \\ \vec{y}_{i-1} \\ \vec{y}_i \end{pmatrix} = \begin{pmatrix} \mathbf{X}_1 & \mathbf{0} & \dots & \mathbf{0} & \mathbf{0} \\ \mathbf{0} & \mathbf{X}_2 & \dots & \mathbf{0} & \mathbf{0} \\ \vdots & \vdots & \ddots & \mathbf{0} & \mathbf{0} \\ \mathbf{0} & \mathbf{0} & \dots & \mathbf{X}_{i-1} & \mathbf{0} \\ \mathbf{0} & \mathbf{0} & \dots & \mathbf{0} & \mathbf{I} \end{pmatrix} \cdot \begin{pmatrix} \vec{\beta}_1 \\ \vec{\beta}_2 \\ \vdots \\ \vec{\beta}_{i-1} \\ \vec{\beta}_i \end{pmatrix} + \begin{pmatrix} \vec{\varepsilon}_1 \\ \vec{\varepsilon}_2 \\ \vdots \\ \vec{\varepsilon}_{i-1} \\ \vec{\varepsilon}_i \end{pmatrix} \quad \text{Eq. 6}$$

Constrained to a material balance in which the sum of product yields of each run must be 100% (Eq. 7):

$$(\mathbf{X}_1 \quad \mathbf{X}_2 \quad \dots \quad \mathbf{X}_{i-1} \quad \mathbf{I}) \cdot \begin{pmatrix} \vec{\beta}_1 \\ \vec{\beta}_2 \\ \vdots \\ \vec{\beta}_{i-1} \\ \vec{\beta}_i \end{pmatrix} = \begin{pmatrix} \vec{1} \\ \vec{1} \\ \vdots \\ \vec{1} \\ \vec{1} \end{pmatrix} \quad \text{Eq. 7}$$

In this approach, the explanatory variables for each cracking product were initially taken from the empirical models that were built earlier with the forward selection method for the individual cuts. Subsequently, the parameters were retested for statistical significance and the parameters that eventually ceased to be significant were removed from the final RLS model.

#### 1.2.4 Experimental section and simplified empirical modeling – cracking of slurry oil

Samples of recovered liquid hydrocarbon products from two test runs obtained in the large scale 7.5 m<sup>3</sup>/d FCC pilot plant (one at a higher conversion level and the other at a lower conversion level) were distilled on a true boiling point column in order to isolate the slurry oil cut. These recovered slurry oil samples, along with a standard vacuum gasoil as reference feed, were catalytically cracked on a fixed fluidized-bed ACE (Advanced Cracking Evaluation) unit (Passamonti; de la Puente; Gilbert; Morgado Jr; Sedran, 2012) located at Petrobras Research and Development Center (CENPES) in Rio de Janeiro/RJ.

In each experiment, 9 g of a typical equilibrium catalyst (Table 3) was loaded into the reactor at 535°C. Slurry oil samples or vacuum gasoil reference feed (Table 4) were injected at a constant flow rate of 0.02 g/s. CTO ratios (between 4.0 and 8.0) were varied by adjusting feed injection time between 56 and 112 s. The coke yield was obtained through the spent catalyst analysis on a LECO<sup>®</sup> instrument. Both gaseous and liquid effluents were collected and subsequently submitted to gas chromatography analysis to determine the yields profile.

Table 3 - Equilibrium catalyst properties – Testing in ACE fixed fluidized-bed unit

Property	Value
Surface area, m <sup>2</sup> /g	148
Mesopore area, m <sup>2</sup> /g	51
Micropore volume, cm <sup>3</sup> /g	0.046
Al <sub>2</sub> O <sub>3</sub> content, wt. %	47.0
Rare earth oxides content, wt. %	2.8
V content, mg/kg	1414
Ni content, mg/kg	978

Source: The author, 2023.

Table 4 - Feed properties – Testing in ACE fixed fluidized-bed unit

Property	Value		
	Reference vacuum gasoil	Slurry oil (low conversion run)	Slurry oil (high conversion run)
Feed			
Slurry oil yield wt.% ( $\gamma_{Slurry}$ ) from the 7.5 m <sup>3</sup> /d FCC pilot plant run	---	35.5	21.4
Density, kg/dm <sup>3</sup> (20°C)	0.9497	0.9592	1.0014
Sulfur, wt. %	0.70	0.39	0.58
Basic nitrogen, mg/kg	1254	204	320
Aniline point, °C	75.2	69.2	54.6
SFC – saturated hydrocarbons, wt. %	48.3	54.9	41.8
SFC – monoaromatics, wt. %	19.0	12.2	12.8
SFC – diaromatics, wt. %	19.7	14.7	12.6
SFC – triaromatics, wt. %	8.2	11.9	8.3
SFC – polyaromatics, wt. %	4.8	6.3	24.5

Table 4 - Feed properties – Testing in ACE fixed fluidized-bed unit (cont.)

Property	Value		
	Reference vacuum gasoil	Slurry oil (low conversion run)	Slurry oil (high conversion run)
Feed			
<i>Simulated distillation (mass recovery,</i> °C)			
0%	316	311	312
10%	388	345	339
30%	433	382	369
50%	462	417	399
70%	494	449	433
90%	535	505	487
100%	596	618	617

Source: The author, 2023.

Subsequently, results of these ACE tests were used to generate a simplified model for predicting the impact of changing feed quality from vacuum gasoil to slurry oil on the yields profile, as a function of the conversion level (slurry oil yield) at which the slurry oil feed was obtained, and of the CTO. This was performed by carrying out the following steps, for each individual product ( $i$  = Dry gas, LPG, cracked naphtha, LCO, slurry oil and coke):

1 - Linear regression of reference vacuum gasoil feed experimental yield data as a function of CTO (Eq. 8).

$$\vec{y}_{calc,i,VGO} = (\vec{1} \quad \overline{CTO}) \cdot \vec{\beta}_{i,VGO} \quad \text{Eq. 8}$$

2 - Obtaining a multiplicative correction factor for the yield  $F$  that accounts for the effect of changing the feed quality from fresh vacuum gasoil to recycled slurry oil by element wise ( $\odot$ ) dividing experimental yield of component  $i$  with slurry oil feed by the calculated yield of component  $i$  with vacuum gasoil at the same CTO (Eq. 9).

$$\vec{F}_i = \vec{y}_{exp,i,Slurry} \odot \vec{y}_{calc,i,VGO} \quad \text{Eq. 9}$$

3 - Linear regression of the multiplicative correction factor for the yield  $F$  (effect of changing vacuum gasoil to recycled slurry oil) as a function of CTO and original yield of slurry oil ( $\gamma_{slurry}$ ) for the recycled slurry oil feed (Eq. 10).

$$\vec{F}_{calc_i} = \left( \vec{1} \quad \overrightarrow{CTO} \quad \overrightarrow{\gamma_{slurry}} \right) \cdot \vec{\beta}_{i,slurry} \quad \text{Eq. 10}$$

This yield correction factor  $F = f(CTO, \gamma_{slurry})$  is later employed in the optimization study (section 1.2.5) in order to estimate the yields profile of a recycled slurry oil stream to the FCC riser as a correction from the yields profile given by the empirical models of sections 1.2.2 and 1.2.3 for vacuum gasoil cracking<sup>1</sup>.

### 1.2.5 Optimization of FCC unit product slate

A model that allows predicting the yields profile for a specific set of catalyst and vacuum gasoil quality as a function of operational variables of the Riser may be used to support the economic decision on which mode of operation to run (maximum conversion or maximum middle distillate) and to optimize process conditions of the FCC unit accordingly. In maximum middle distillate mode, the availability of such a model is particularly useful to minimize the drawback of an excessive slurry oil throughput.

Although the empirical model's predictor variables include CTO and  $t_c$ , both associated with kinetics of cracking reactions in the Riser, these are not process variables directly manipulable in unit operation. A simplified process simulator was then developed in which the input variables are those that can be manipulated operationally (or defined in a design) such as: reaction temperature, feed throughput, feed temperature and Riser geometry (length of Riser above feed injection nozzle). The slurry oil recycle throughput was included as one of the input variables in the process simulator so as to evaluate, with the simplified model developed according to section 1.2.4, any potential benefit of re cracking this stream in the process.

---

<sup>1</sup> In section 1.2.5, since there is no restriction forcing a mass balance closure for the estimated slurry oil recycle stream yields profile, the yields of all cuts are subsequently normalized to sum up 100%.

The FCC process simulator basically solves the energy balance of the conversion section, according to:

1 - Energy balance of the Riser (Eq. 11): the enthalpy provided by the hot catalyst from the Regenerator ( $\Delta H_{cat\_rx}$ ) must supply the required energy to compensate for the following heat demands: i. vaporization of the liquid feed and heating up to the reaction temperature at the end of the Riser ( $\Delta H_{feed}$ ); ii. endothermic heat of cracking reactions ( $w_{conv} \cdot \Delta H_{rx}$ ); iii. heating of steam streams injected in the Riser ( $\Delta H_{steam}$ ); iv. thermal losses to the environment ( $\Delta H_{loss\_rx}$ ).

$$\Delta H_{cat\_rx} = \Delta H_{feed} + (w_{conv} \cdot \Delta H_{rx}) + \Delta H_{steam} + \Delta H_{loss\_rx} \quad \text{Eq. 11}$$

Which can be further expanded to Eq. 12:

$$\begin{aligned} w_{cat} \cdot c_{p\_cat} \cdot (T_{reg} - T_{rx}) & \quad \text{Eq. 12} \\ & = w_{feed} \cdot (h_{vap,T_{rx}} - h_{liq,T_{feed}}) + (w_{conv} \cdot \Delta H_{rx}) + w_{st} \\ & \cdot (h_{T_{rx}}^{st} - h_{T_{st}}^{st}) + \Delta H_{loss\_rx} \end{aligned}$$

2 - Energy balance of the Regenerator (Eq. 13): the enthalpy provided by burning the adsorbed coke on the spent catalyst ( $\Delta H_{coke}$ ) must supply the required energy quantities of: i. enthalpy differential ( $\Delta H_{flue\_air}$ ) between hot flue gas exiting and relative cold air injected into the Regenerator; ii. heating of circulating catalyst up to Regenerator's temperature ( $\Delta H_{cat\_reg}$ ); iii. thermal losses to the environment ( $\Delta H_{loss\_reg}$ ).

$$\Delta H_{coke} = \Delta H_{flue\_air} + \Delta H_{cat\_reg} + \Delta H_{loss\_reg} \quad \text{Eq. 13}$$

Which can be further expanded to Eq. 14:

$$\begin{aligned} w_{coke} * \Delta h_{comb\_coke} \Big|^{T_{ref}} & \quad \text{Eq. 14} \\ & = w_{air} \cdot (h_{T_{ref}}^{air} - h_{T_{air}}^{air}) + w_{flue} \cdot (h_{T_{dil}}^{flue} - h_{T_{ref}}^{flue}) + w_{cat} \cdot c_{p\_cat} \\ & \cdot (T_{reg} - T_{inlet\_reg}) + \Delta H_{loss\_reg} \end{aligned}$$

It should be noted that, if the catalyst inlet temperature to the Regenerator ( $T_{\text{inlet\_reg}}$ ) is equal to the reaction temperature at the end of the Riser ( $T_{\text{rx}}$ ), then  $\Delta H_{\text{cat\_rx}}$  equals  $\Delta H_{\text{cat\_reg}}$ . Also, this clearly shows that the catalyst circulation rate is the link for the simultaneous energy balance closing of the Riser and Regenerator envelopes. As this was a simplified process simulator useful for the purpose of the present study, the stripping section was not included. As  $T_{\text{inlet\_reg}}$  tends to be slightly lower than  $T_{\text{rx}}$  due to thermal exchange with injected stripping steam and thermal losses in the Stripper, the temperature differential between  $T_{\text{inlet\_reg}}$  and  $T_{\text{rx}}$  (which is usually in the range of 5 to 15°C) was included as an inlet parameter to be informed to the process simulator.

Sadeghbeigi (2020) mentions a heat loss in the Regenerator plus Stripper section up to 4% of the coke combustion enthalpy and a heat loss in the Riser section up to 1.2% of the coke combustion enthalpy, which totals an environment heat loss of up to 5.2% of the coke combustion enthalpy. In the present study, since the effect of catalyst temperature reduction between the Riser outlet and the Regenerator inlet was computed separately, and adopting usual values of the large scale FCC pilot plant from previous studies that resulted in consistent energy balance parameters, the total environment heat loss ( $\Delta H_{\text{loss\_rx}} + \Delta H_{\text{loss\_reg}}$ ) was considered as 2.7% of the coke combustion enthalpy.

The endothermic heat of reaction ( $\Delta H_{\text{rx}}$ ) is an important and relevant portion of the FCC energy balance (Pekediz; Kraemer; Blasetti; de Lasa, 1997; Sadeghbeigi, 2020). It was considered as a constant value of 580 kJ/kg of converted feed in the present study. Heat of catalytic cracking reactions will be further discussed in Chapter 2. When reported per unit of converted feed (or per unit of gas, LPG, naphtha and coke produced) the heat of reaction tends to fluctuate around a fairly constant value, thus eliminating dependency with conversion level.  $\Delta H_{\text{feed}}$ ,  $\Delta H_{\text{steam}}$ ,  $\Delta H_{\text{coke}}$  and  $\Delta H_{\text{flue\_air}}$  were calculated with hydrocarbon fractions correlations (API, 1997; Sadeghbeigi, 2020) ( $\Delta H_{\text{feed}}$ ) and with tabulated thermodynamic data (Green; Southard, 2019) for pure species (other quantities).

The Regenerator combustion regime considered was complete burning of coke to  $\text{CO}_2$ , and the dry basis  $\text{O}_2$  content in the flue gas (excess  $\text{O}_2$ ) was one of the inlet parameters to be informed to the simulator and was used to calculate the air rate required. Afterburning extent, i.e., temperature differential between the dilute phase ( $T_{\text{dil}}$ ) and the dense bed ( $T_{\text{reg}}$ ) of the regenerator, was another inlet parameter to the simulator. In a simplified way,  $\Delta H_{\text{cat\_rx}}$  and  $\Delta H_{\text{cat\_reg}}$  were calculated considering a constant catalyst  $C_p$  of 1.15 kJ/(kg\*K).

Contact time between catalyst and hydrocarbon vapors along the Riser (Eq. 16) was calculated considering ideal gas assumption and the yield profile and conditions ( $T_{\text{rx}}$  and  $P_{\text{rx}}$ ) at the end of the Riser, as usually done in the industry (Eq. 15):

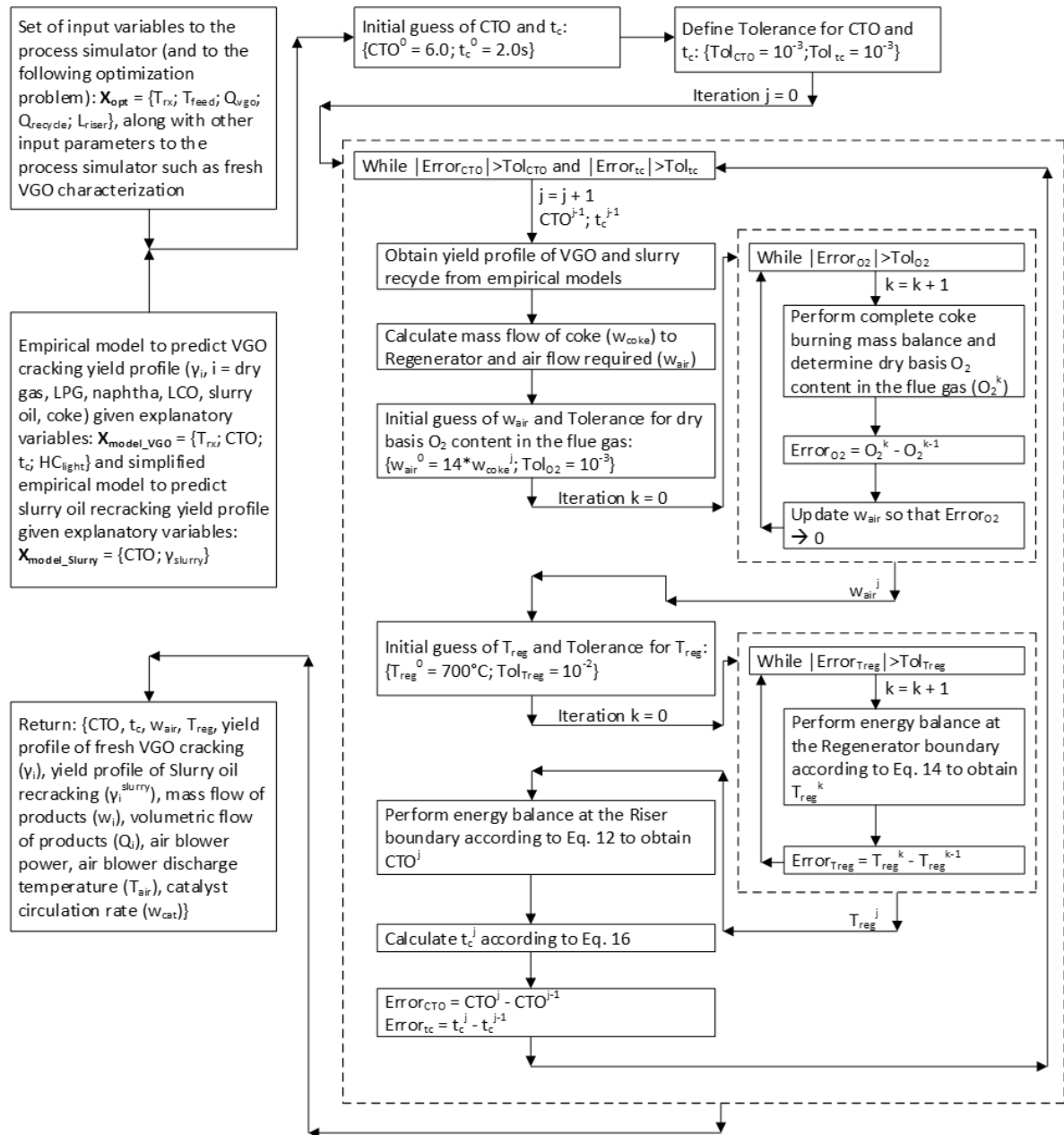
$$F_{rx} = \frac{R_{ideal} \cdot T_{rx} \cdot \left[ \frac{w_{st}}{18.02} + \left( w_{feed} * \sum_i \frac{\gamma_i}{100 * MW_i} \right) \right]}{P_{rx}} \quad \text{Eq. 15}$$

$$t_c = \frac{\pi \cdot \frac{D_{riser}^2}{4} \cdot L_{riser}}{F_{rx}} \quad \text{Eq. 16}$$

In Eq. 15:  $i = \{\text{Dry gas, LPG, Naphtha, LCO, Slurry oil}\}$ , i.e., products of cracking reactions at vapor phase under Riser conditions;  $MW_i$  (kg/kmol) was assumed to be, respectively:  $MW = \{20, 50, 100, 200, 300\}$ .

Performing the iterative calculations to obtain the input variables CTO and  $t_c$  and using the previously developed empirical models, the process simulator returns the catalytic cracking yield profile. Figure 3 schematically summarizes the calculations performed by the process simulator.

Figure 3 - Schematic of process simulator calculations to return yield profile and other operational conditions



Source: The author, 2023.

The process simulator was subsequently coupled with a non-linear optimization tool (using a sequential least squares quadratic programming routine (Kraft, 1988) with a maximum profit objective function in order to obtain the optimized response of input process variables ( $T_{rx}$ ,  $T_{feed}$ , fresh VGO feed rate, slurry oil recycle rate and length of Riser) subjected to operational constraints such as design temperature of the Regenerator, air blower capacity and a maximum catalyst circulation rate that would be associated with a limitation in the unit's pressure balance.

### 1.3 Results and discussion

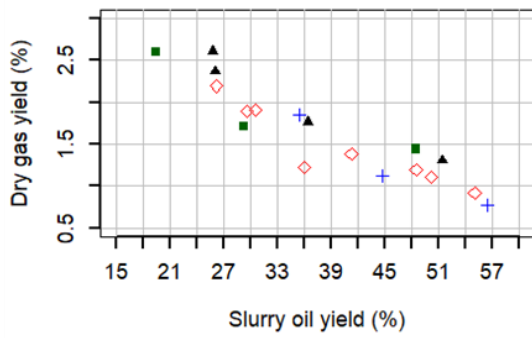
The experimental data from the tests carried out in the large scale FCC pilot plant are presented in Annex 1 (input variables) and Annex 2 (resulting yield profile).

Initially, a qualitative graphical inspection of the results was performed in order to verify the general consistency with expected trends. A set of experimental points with the same feed quality, feed “A1”, was selected for this analysis. Figures 4-5 graphically show products yields obtained with feed “A1”. In Figure 4, each product yield is plotted against Slurry oil yield, which is inversely proportional to the conversion level. In Figure 5, products yields are plotted against CTO, a variable that expresses the level of severity employed.

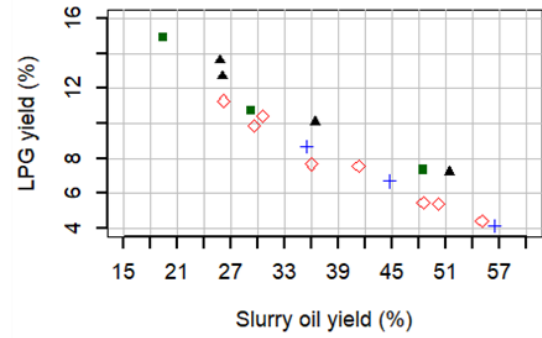
In general, the expected behavior of the catalytic cracking process can be observed, such as the increase in naphtha and LPG yields with the increase in CTO or conversion (expressed in terms of the slurry oil yield obtained).

It is also possible to observe some relevant aspects in the graphs of Figures 4-5. In Figure 4.d and Figure 5.d it can be seen the intermediate product character of LCO (Corma; Sauvanaud, 2007): at low conversions, there is apparently a low cracking rate of gasoil to LCO, while at high conversions the cracking rate of LCO towards lighter derivatives increases, thus leading to a region of maximum LCO yield (which may vary for different catalysts or set of operating conditions). Moreover, comparing the scale of Figure 4.d with those of Figures 4.b (LPG), 4.c (Naphtha) and 4.e (Slurry oil), it is possible to verify that the range of variation in the yield of LCO is much lower than that of the other products.

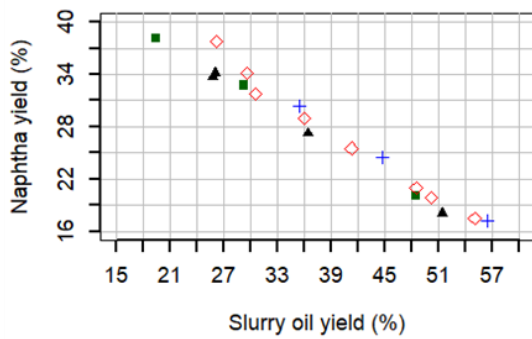
Figure 4 - Products yield as a function of Slurry oil yield. Feed “A1” injected in: Nozzle #1 (■); Nozzle #2 (▲); Nozzle #3 (◇); Nozzle #4 (+)



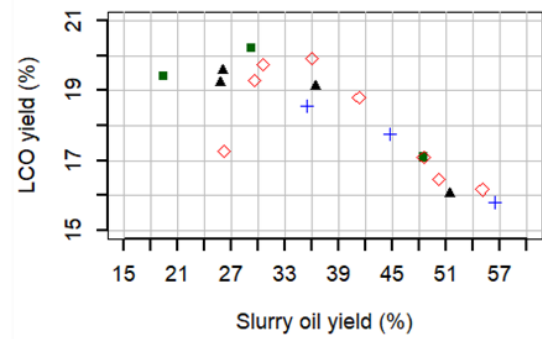
(a)



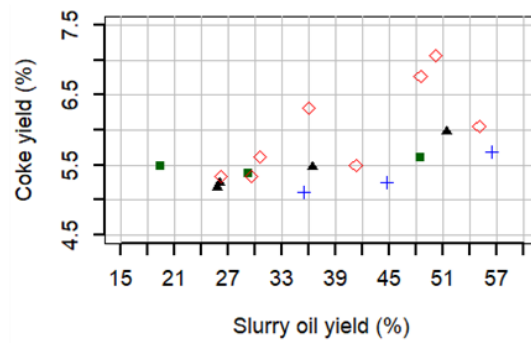
(b)



(c)



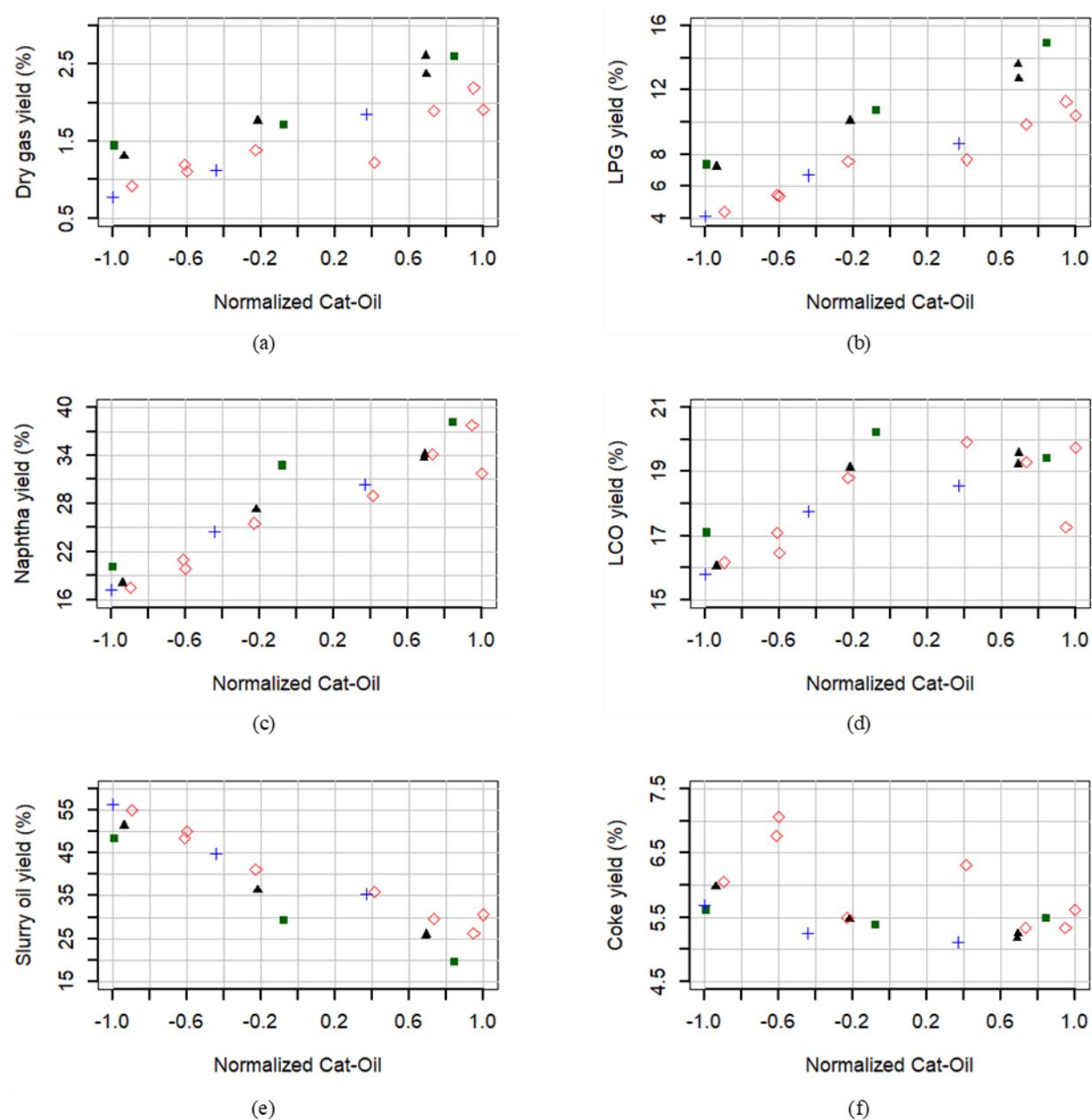
(d)



(e)

Source: The author, 2023.

Figure 5 - Products yield as a function of Catalyst-to-oil ratio. Feed “A1” injected in: Nozzle #1 (■); Nozzle #2 (▲); Nozzle #3 (◇); Nozzle #4 (+)



Source: The author, 2023.

While the yield of cracked naphtha or slurry oil, for example, vary by up to 20wt.% or more between conversion levels extremes, the range of variation for LCO is less than 5wt.%. Although this intermediate product characteristic of LCO has been earlier mentioned (Benoit, 2015; Corma; Sauvanaud, 2007; Gilbert; Baptista; Pinho, 2007), this very narrow range of variation for the LCO yield, which does not follow in the same extent the increase of slurry oil in the regions of low conversion, is somewhat remarkable. Despite this, the investigation and

economic assessment of the region of maximum LCO yield remains valid and perhaps even more necessary (in order to avoid operating in a low conversion region with high yield of slurry oil and decreasingly yield of LCO), especially in conjunctural cases in which the FCC unit is pressured to reduce the production of cracked naphtha.

Figures 4-5 also show some effects of the contact time between feed and catalyst ( $t_c$ ): as can be seen in Figures 5.b, 5.c and 5.e, for the same CTO, tests performed with feed injection at the base of the Riser (nozzle #1), and slightly above (nozzle #2) tended to provide a higher conversion degree (i.e. higher LPG and cracked naphtha yields and lower slurry oil yield) than those with elevated (nozzles #3 and #4) feed injection. This confirms that  $t_c$  adds another degree of freedom to manipulate the process severity. In Figure 4.c, where the naphtha yield is plotted against a conversion flag in slurry oil yield, the feed injection point becomes somewhat indifferent, i.e. it does not appear to alter the naphtha yield for a given conversion threshold, though it must be noted that in order to achieve an equivalent naphtha yield a test run with reduced  $t_c$  (i.e. feed injected in upper nozzles such as #3 or #4 nozzles) must have used a higher  $T_{rx}$  or CTO. In this sense, to exploit the flexibility of injecting the feed in an elevated nozzle (if available in the unit's hardware) while sustaining a relatively high  $T_{rx}$  may be a useful tool to overcome some common inconveniences in middle distillate operation mode such as Stripper efficiency degradation (Gilbert; Baptista; Pinho, 2007), which could lead to Regenerator temperature restrictions.

### 1.3.1 Empirical modeling – individual products

Initially, it was intended to obtain an empirical model with only process variables as input:  $T_{rx}$  (range: 752.7 – 847.2 K), CTO (range: 3.74 – 11.04 m/m) and  $t_c$  (range: 0.41 – 2.23s). However, as the tests were carried out in different moments across a relatively long time span and thus it was necessary to use other gasoil batches, it was noticed that the modeling of some cuts required the inclusion of explanatory variables related to feed characterization, in order to account for some variation in quality of these batches.

It was evaluated the correlation and the independent information content between the possible input data: process variables ( $T_{rx}$ , CTO and  $t_c$ ) along with the possible variables listed to represent feed quality ( $K_{factor}$ , RCR,  $N_{bas}$  and  $HC_{light}$ ). Table 5 presents the correlation matrix of the input variables available.

Table 5 - Correlation matrix of possible input variables

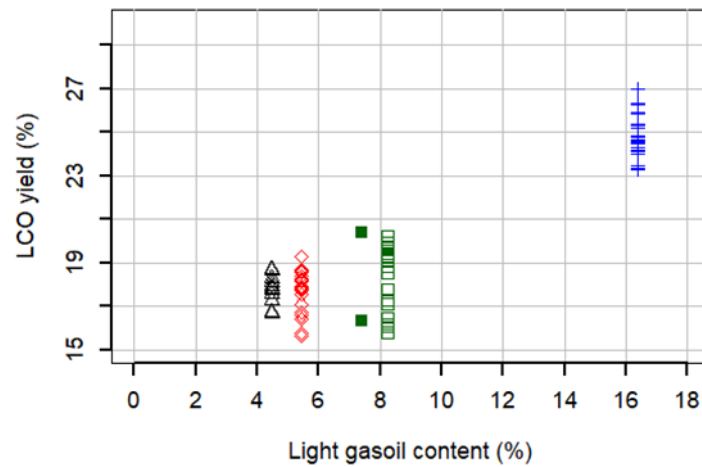
	T <sub>rx</sub>	CTO	t <sub>c</sub>	K <sub>factor</sub>	RCR	N <sub>bas</sub>	HC <sub>light</sub>
T <sub>rx</sub>		<b>0.77</b>	-0.17	0.53	0.27	0.41	-0.34
CTO	<b>0.77</b>		-0.13	0.08	-0.05	0.31	-0.34
t <sub>c</sub>	-0.17	-0.13		0.07	-0.01	0.31	-0.29
K <sub>factor</sub>	0.53	0.08	0.07		<b>0.84</b>	0.46	-0.26
RCR	0.27	-0.05	-0.01	<b>0.84</b>		0.23	0.00
N <sub>bas</sub>	0.41	0.31	0.31	0.46	0.23		<b>-0.96</b>
HC <sub>light</sub>	-0.34	-0.34	-0.29	-0.26	0.00	<b>-0.96</b>	

Source: The author, 2023.

According to Table 5, the process variables are not correlated to the feed characterization variables, as expected. There are two strong correlations between variables related to feed quality: (i) carbon residue content (RCR) and modified Watson's characterization factor (K<sub>factor</sub>) share a correlation coefficient of 0.84; (ii) basic Nitrogen content (N<sub>bas</sub>) and light gasoil content (HC<sub>light</sub>) share a negative correlation of -0.96. This is in line with the fact that feed quality was not initially designed as an input variable to the present study, and those correlations were arisen casually in a small sample of 5 different vacuum gasoil batches.

This collinearity presented among feed characterization variables, in addition to independent information content obtained through QR matrix decomposition, indicated that only one variable related to feed quality should be included as a predictor in the model. Initially K<sub>factor</sub> was selected as a single variable that embodies intrinsic characteristics of the gasoil, but later it was noticed that the range of input data for this variable was too tight (11.55 to 11.74, see Table 1) and this would cause deviations in the subsequent applicability of the model whenever extrapolation for diverse gasoil data was required. At the same time, it was perceived a substantial correlation between HC<sub>light</sub> and LCO yield (Figure 6), what is quite consistent with the fact that a feed that has a higher light content (mass fraction with simulated distillation temperature lower than 343°C) already contains inherently a higher LCO yield in the unconverted feed. For this reason, HC<sub>light</sub> was the feed characterization variable chosen to be included as input variable. In spite of this, it should be remarked that regarding the overall diesel production balance of the refinery, it is not advisable to degrade diesel to the vacuum distillation unite because, although it would raise LCO yield in the FCC unit, a large portion of the diesel content in the feed would be cracked to LPG and naphtha, thus reducing the total diesel throughput in the refinery.

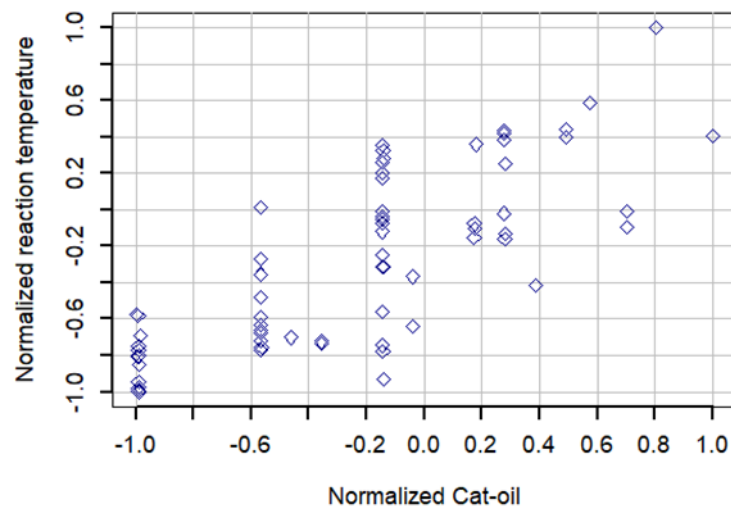
Figure 6 - LCO yield as a function of light gasoil content in the feed (see Table 1): Feed “A1” ( $\square$ ); Feed “A2” ( $\blacksquare$ ); Feed “B” ( $\triangle$ ); Feed “C” ( $\diamond$ ); Feed “D” ( $+$ )



Source: The author, 2023.

Another sizable correlation shown in Table 5 is that between reaction temperature ( $T_{rx}$ ) and catalyst-to-oil ratio (CTO), with a correlation coefficient of 0.77. If no further action is taken,  $T_{rx}$  and CTO are directly associated with each other, as discussed previously. Figure 7 displays a plot of  $T_{rx}$  vs. CTO for all runs.

Figure 7 - Reaction temperature vs. Catalyst-to-oil ratio



Source: The author, 2023.

It can be observed in Figure 7 that the adjustment of other energy balance variables (such as feed temperature, combustion air temperature) allowed introducing a satisfactory degree of

independency between  $T_{rx}$  and CTO at the middling severity region, but at the extremes of low and high severities this same degree of independency could not be achieved. In brief, it can be stated that it was not possible to obtain experimental points coupling a low CTO with a high  $T_{rx}$  or coupling a high CTO with a low  $T_{rx}$ , thus reflecting the overall correlation coefficient of 0.77. The correlation between  $T_{rx}$  and CTO after filtering for  $-0.6 < \text{Normalized CTO} < 0.8$  would reduce to 0.59. An aspect to be pointed out is that it is highly unpractical (perhaps inviable) for a commercial FCC unit to operate at these regions (high  $T_{rx}$  – low CTO or low  $T_{rx}$  – high CTO) not explored experimentally, so it is believed that for all practical purposes the developed empirical model included roughly independent variables in  $T_{rx}$  and CTO as input data.

After defining the input variables, the empirical model of each individual cut was built following the forward selection of the candidate variables (which included quadratic and two-way interaction terms). Tables 6-7, and Figure 8 present the individual models and the fit to experimental data obtained. In Table 7 the parameters are given in the normalized dimensionless form (between -1 and 1) according to Eq. 17 through Eq. 20. Table 7 is presented because a few parameters in physical units in Table 6 seem not significant as the 95% level confidence interval passes through zero; but this is a mere consequence of the transformation of the parameters originally estimated as normalized terms back to the physical units representation, situation in which the interaction parameters between two normalized terms carry coefficients for the intercept and the expanded individual variables in physical units. In Table 7, applying the 95% level confidence interval, there is no intersection through zero for any estimated parameter. Also, in Table 7 some terms are not included in the model because these terms only appeared in Table 6 after the variables were expanded from their normalized dimensionless state to its correspondent in physical unit.

$$\overline{T_{rx}} = \frac{2 * T_{rx} - 1599.89}{94.41} \quad \text{Eq. 17}$$

$$\overline{CTO} = \frac{2 * CTO - 14.78}{7.3} \quad \text{Eq. 18}$$

$$\overline{t_c} = \frac{2 * t_c - 2.64}{1.82} \quad \text{Eq. 19}$$

$$\overline{HC_{light}} = \frac{2 * HC_{light} - 20.87}{11.89} \quad \text{Eq. 20}$$

Table 6 - Empirical model of FCC yield profile – individual cuts and complete product slate.  
Variables in physical units

Product	Ordinary least squares			Restricted least squares	
	Variables	Coefficients	95% level CI	Coefficients	95% level CI
Dry gas	Intercept	$4.416 \cdot 10^{-1}$	$\pm 8.063 \cdot 10^{-1}$	1.178	$\pm 4.289 \cdot 10^{-1}$
	$T_{rx}$ (K)	$-1.430 \cdot 10^{-3}$	$\pm 1.839 \cdot 10^{-3}$	$-3.134 \cdot 10^{-3}$	$\pm 1.045 \cdot 10^{-3}$
	$t_c$ (s)	$-8.069 \cdot 10^{-2}$	$\pm 3.809 \cdot 10^{-2}$	$-9.473 \cdot 10^{-2}$	$\pm 2.834 \cdot 10^{-2}$
	CTO (m/m)	$-1.428 \cdot 10^{-3}$	$\pm 1.337 \cdot 10^{-3}$	---	---
	$HC_{light}$ (%)	$1.451 \cdot 10^{-2}$	$\pm 1.100 \cdot 10^{-2}$	$1.488 \cdot 10^{-3}$	$\pm 7.451 \cdot 10^{-4}$
	$T_{rx} \cdot t_c$	$1.068 \cdot 10^{-4}$	$\pm 4.975 \cdot 10^{-5}$	$1.262 \cdot 10^{-4}$	$\pm 3.688 \cdot 10^{-5}$
	$T_{rx} \cdot HC_{light}$	$-1.669 \cdot 10^{-5}$	$\pm 1.116 \cdot 10^{-5}$	---	---
	$CTO \cdot HC_{light}$	$1.369 \cdot 10^{-4}$	$\pm 1.281 \cdot 10^{-4}$	---	---
	$T_{rx}^2$	$1.128 \cdot 10^{-6}$	$\pm 1.061 \cdot 10^{-6}$	$2.091 \cdot 10^{-6}$	$\pm 6.405 \cdot 10^{-7}$
	$HC_{light}^2$	$-1.170 \cdot 10^{-4}$	$\pm 6.303 \cdot 10^{-5}$	$-8.100 \cdot 10^{-5}$	$\pm 4.161 \cdot 10^{-5}$
Coeff. of determination ( $R^2$ )	0.947	---	0.949	---	
LPG	Intercept	$-5.112 \cdot 10^{-1}$	$\pm 7.469 \cdot 10^{-2}$	LPG yield obtained as to close the mass balance	
	$T_{rx}$ (K)	$6.571 \cdot 10^{-4}$	$\pm 6.666 \cdot 10^{-5}$		
	$t_c$ (s)	$-7.606 \cdot 10^{-3}$	$\pm 3.030 \cdot 10^{-2}$		
	CTO (m/m)	$6.533 \cdot 10^{-3}$	$\pm 1.310 \cdot 10^{-3}$		
	$HC_{light}$ (%)	$3.028 \cdot 10^{-2}$	$\pm 2.167 \cdot 10^{-2}$		
	$T_{rx} \cdot HC_{light}$	$-3.563 \cdot 10^{-5}$	$\pm 2.498 \cdot 10^{-5}$		
	$t_c \cdot CTO$	$6.049 \cdot 10^{-3}$	$\pm 3.306 \cdot 10^{-3}$		
	$t_c \cdot HC_{light}$	$-1.347 \cdot 10^{-3}$	$\pm 1.279 \cdot 10^{-3}$		
Coeff. of determination ( $R^2$ )	0.902	---	0.895	---	

Table 6 - Empirical model of FCC yield profile – individual cuts and complete product slate.  
Variables in physical units (cont.)

Product	Ordinary least squares			Restricted least squares	
	Variables	Coefficients	95% level CI	Coefficients	95% level CI
Naphtha	Intercept	$-7.027 \times 10^{-1}$	$\pm 5.783 \times 10^{-1}$	$-7.517 \times 10^{-1}$	$\pm 3.726 \times 10^{-1}$
	$T_{rx}$ (K)	$7.675 \times 10^{-4}$	$\pm 6.672 \times 10^{-4}$	$8.084 \times 10^{-4}$	$\pm 4.276 \times 10^{-4}$
	$t_c$ (s)	$-5.155 \times 10^{-1}$	$\pm 3.136 \times 10^{-1}$	$-4.976 \times 10^{-1}$	$\pm 1.945 \times 10^{-1}$
	CTO (m/m)	$7.368 \times 10^{-2}$	$\pm 1.916 \times 10^{-2}$	$7.793 \times 10^{-2}$	$\pm 1.262 \times 10^{-2}$
	$HC_{light}$ (%)	$3.817 \times 10^{-2}$	$\pm 3.561 \times 10^{-2}$	$4.467 \times 10^{-2}$	$\pm 2.344 \times 10^{-2}$
	$T_{rx} * t_c$	$7.105 \times 10^{-4}$	$\pm 4.076 \times 10^{-4}$	$6.880 \times 10^{-4}$	$\pm 2.525 \times 10^{-4}$
	$T_{rx} * HC_{light}$	$-4.771 \times 10^{-5}$	$\pm 4.452 \times 10^{-5}$	$-5.584 \times 10^{-5}$	$\pm 2.930 \times 10^{-5}$
	$CTO^2$	$-3.335 \times 10^{-3}$	$\pm 1.606 \times 10^{-3}$	$-3.610 \times 10^{-3}$	$\pm 1.052 \times 10^{-3}$
Coeff. of determination ( $R^2$ )	0.968	---	0.968	---	
LCO	Intercept	-1.764	$\pm 6.151 \times 10^{-1}$	-1.201	$\pm 2.971 \times 10^{-1}$
	$T_{rx}$ (K)	$2.428 \times 10^{-3}$	$\pm 7.649 \times 10^{-4}$	$1.715 \times 10^{-3}$	$\pm 3.577 \times 10^{-4}$
	$t_c$ (s)	$1.972 \times 10^{-1}$	$\pm 1.234 \times 10^{-1}$	$8.914 \times 10^{-3}$	$\pm 2.713 \times 10^{-3}$
	CTO (m/m)	$1.537 \times 10^{-1}$	$\pm 3.488 \times 10^{-2}$	$1.271 \times 10^{-1}$	$\pm 2.229 \times 10^{-2}$
	$HC_{light}$ (%)	$5.207 \times 10^{-2}$	$\pm 1.992 \times 10^{-2}$	$3.973 \times 10^{-2}$	$\pm 1.402 \times 10^{-2}$
	$T_{rx} * t_c$	$-2.399 \times 10^{-4}$	$\pm 1.602 \times 10^{-4}$	---	---
	$T_{rx} * CTO$	$-1.944 \times 10^{-4}$	$\pm 4.526 \times 10^{-5}$	$-1.588 \times 10^{-4}$	$\pm 2.786 \times 10^{-5}$
	$T_{rx} * HC_{light}$	$-6.466 \times 10^{-5}$	$\pm 2.098 \times 10^{-5}$	$-5.186 \times 10^{-5}$	$\pm 1.454 \times 10^{-5}$
$HC_{light}^2$	$2.805 \times 10^{-4}$	$\pm 1.700 \times 10^{-4}$	$3.769 \times 10^{-4}$	$\pm 1.298 \times 10^{-4}$	
Coeff. of determination ( $R^2$ )	0.968	---	0.969	---	

Table 6 - Empirical model of FCC yield profile – individual cuts and complete product slate.  
Variables in physical units (cont.)

Product	Ordinary least squares			Restricted least squares	
	Variables	Coefficients	95% level CI	Coefficients	95% level CI
Slurry oil	Intercept	3.853	$\pm 2.058$	2.244	$\pm 4.901 \cdot 10^{-1}$
	$T_{rx}$ (K)	$-3.660 \cdot 10^{-3}$	$\pm 2.461 \cdot 10^{-3}$	$-1.556 \cdot 10^{-3}$	$\pm 5.762 \cdot 10^{-4}$
	$t_c$ (s)	$6.523 \cdot 10^{-1}$	$\pm 3.788 \cdot 10^{-1}$	$8.641 \cdot 10^{-1}$	$\pm 2.576 \cdot 10^{-1}$
	CTO (m/m)	$-2.801 \cdot 10^{-1}$	$\pm 2.142 \cdot 10^{-1}$	$-1.135 \cdot 10^{-1}$	$\pm 1.658 \cdot 10^{-2}$
	$HC_{light}$ (%)	$-1.305 \cdot 10^{-1}$	$\pm 4.803 \cdot 10^{-2}$	$-9.655 \cdot 10^{-2}$	$\pm 3.138 \cdot 10^{-2}$
	$T_{rx} \cdot t_c$	$-9.243 \cdot 10^{-4}$	$\pm 4.902 \cdot 10^{-4}$	$-1.192 \cdot 10^{-3}$	$\pm 3.351 \cdot 10^{-4}$
	$T_{rx} \cdot CTO$	$2.316 \cdot 10^{-4}$	$\pm 2.234 \cdot 10^{-4}$	---	---
	$T_{rx} \cdot HC_{light}$	$1.559 \cdot 10^{-4}$	$\pm 6.167 \cdot 10^{-5}$	$1.124 \cdot 10^{-4}$	$\pm 4.046 \cdot 10^{-5}$
	$CTO^2$	$3.775 \cdot 10^{-3}$	$\pm 2.746 \cdot 10^{-3}$	$5.173 \cdot 10^{-3}$	$\pm 1.382 \cdot 10^{-3}$
Coeff. of determination ( $R^2$ )	0.974	---	0.973	---	
Coke	Intercept	2.268	$\pm 7.386 \cdot 10^{-1}$	2.246	$\pm 4.615 \cdot 10^{-1}$
	$T_{rx}$ (K)	$-5.370 \cdot 10^{-3}$	$\pm 1.887 \cdot 10^{-3}$	$-5.302 \cdot 10^{-3}$	$\pm 1.181 \cdot 10^{-3}$
	CTO (m/m)	$1.165 \cdot 10^{-3}$	$\pm 1.676 \cdot 10^{-4}$	$1.344 \cdot 10^{-3}$	$\pm 1.071 \cdot 10^{-4}$
	$HC_{light}$ (%)	$9.073 \cdot 10^{-4}$	$\pm 2.424 \cdot 10^{-3}$	$2.845 \cdot 10^{-4}$	$\pm 1.448 \cdot 10^{-3}$
	$CTO \cdot HC_{light}$	$1.860 \cdot 10^{-4}$	$\pm 9.523 \cdot 10^{-5}$	$1.727 \cdot 10^{-4}$	$\pm 5.956 \cdot 10^{-5}$
	$T_{rx}^2$	$3.220 \cdot 10^{-6}$	$\pm 1.223 \cdot 10^{-6}$	$3.172 \cdot 10^{-6}$	$\pm 7.657 \cdot 10^{-7}$
	$HC_{light}^2$	$-1.222 \cdot 10^{-4}$	$\pm 9.268 \cdot 10^{-5}$	$-9.010 \cdot 10^{-5}$	$\pm 5.526 \cdot 10^{-5}$
Coeff. of determination ( $R^2$ )	0.884	---	0.886	---	

Source: The author, 2023.

Table 7 - Empirical model of FCC yield profile – individual cuts and complete product slate.  
Normalized dimensionless variables

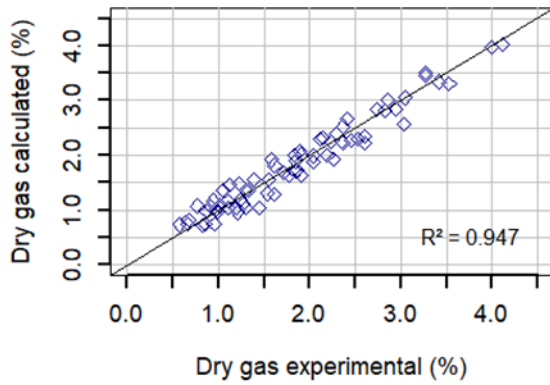
Product	Ordinary least squares			Restricted least squares	
	Variables	Coefficients	95% level CI	Coefficients	95% level CI
Dry gas	Intercept	$2.488 \cdot 10^{-2}$	$\pm 1.914 \cdot 10^{-3}$	$2.434 \cdot 10^{-2}$	$\pm 1.354 \cdot 10^{-3}$
	$\overline{T_{rx}}$	$1.610 \cdot 10^{-2}$	$\pm 1.942 \cdot 10^{-3}$	$1.785 \cdot 10^{-2}$	$\pm 1.357 \cdot 10^{-3}$
	$\overline{t_c}$	$4.338 \cdot 10^{-3}$	$\pm 1.550 \cdot 10^{-3}$	$5.692 \cdot 10^{-3}$	$\pm 1.059 \cdot 10^{-3}$
	$\overline{CTO}$	---	---	---	---
	$\overline{HC_{light}}$	$-1.607 \cdot 10^{-3}$	$\pm 1.142 \cdot 10^{-3}$	$-1.203 \cdot 10^{-3}$	$\pm 7.332 \cdot 10^{-4}$
	$\overline{T_{rx}} \cdot \overline{t_c}$	$4.589 \cdot 10^{-3}$	$\pm 2.137 \cdot 10^{-3}$	$5.423 \cdot 10^{-3}$	$\pm 1.584 \cdot 10^{-3}$
	$\overline{T_{rx}} \cdot \overline{HC_{light}}$	$-4.683 \cdot 10^{-3}$	$\pm 3.133 \cdot 10^{-3}$	---	---
	$\overline{CTO} \cdot \overline{HC_{light}}$	$2.970 \cdot 10^{-3}$	$\pm 2.780 \cdot 10^{-3}$	---	---
	$\overline{T_{rx}}^2$	$2.513 \cdot 10^{-3}$	$\pm 2.365 \cdot 10^{-3}$	$4.659 \cdot 10^{-3}$	$\pm 1.427 \cdot 10^{-3}$
	$\overline{HC_{light}}^2$	$-4.137 \cdot 10^{-3}$	$\pm 2.228 \cdot 10^{-3}$	$-2.863 \cdot 10^{-3}$	$\pm 1.471 \cdot 10^{-3}$
LPG	Intercept	$1.117 \cdot 10^{-1}$	$\pm 3.932 \cdot 10^{-3}$	LPG yield	
	$\overline{T_{rx}}$	$1.347 \cdot 10^{-2}$	$\pm 9.159 \cdot 10^{-3}$	obtained as to	
	$\overline{t_c}$	$2.096 \cdot 10^{-2}$	$\pm 6.801 \cdot 10^{-3}$	close the	
	$\overline{CTO}$	$5.299 \cdot 10^{-2}$	$\pm 1.115 \cdot 10^{-2}$	mass balance	
	$\overline{HC_{light}}$	---	---		
	$\overline{T_{rx}} \cdot \overline{HC_{light}}$	$-9.998 \cdot 10^{-3}$	$\pm 7.011 \cdot 10^{-3}$		
	$\overline{t_c} \cdot \overline{CTO}$	$2.009 \cdot 10^{-2}$	$\pm 1.098 \cdot 10^{-2}$		
	$\overline{t_c} \cdot \overline{HC_{light}}$	$-7.289 \cdot 10^{-3}$	$\pm 6.917 \cdot 10^{-3}$		
Naphtha	Intercept	$3.433 \cdot 10^{-1}$	$\pm 7.141 \cdot 10^{-3}$	$3.433 \cdot 10^{-1}$	$\pm 4.512 \cdot 10^{-3}$
	$\overline{T_{rx}}$	$5.700 \cdot 10^{-2}$	$\pm 1.583 \cdot 10^{-2}$	$5.352 \cdot 10^{-2}$	$\pm 9.978 \cdot 10^{-3}$
	$\overline{t_c}$	$4.804 \cdot 10^{-2}$	$\pm 1.133 \cdot 10^{-2}$	$4.805 \cdot 10^{-2}$	$\pm 6.802 \cdot 10^{-3}$
	$\overline{CTO}$	$8.902 \cdot 10^{-2}$	$\pm 1.673 \cdot 10^{-2}$	$8.969 \cdot 10^{-2}$	$\pm 1.067 \cdot 10^{-2}$
	$\overline{HC_{light}}$	---	---	---	---
	$\overline{T_{rx}} \cdot \overline{t_c}$	$3.052 \cdot 10^{-2}$	$\pm 1.751 \cdot 10^{-2}$	$2.955 \cdot 10^{-2}$	$\pm 1.085 \cdot 10^{-2}$
	$\overline{T_{rx}} \cdot \overline{HC_{light}}$	$-1.339 \cdot 10^{-2}$	$\pm 1.249 \cdot 10^{-2}$	$-1.567 \cdot 10^{-2}$	$\pm 8.222 \cdot 10^{-3}$
	$\overline{CTO}^2$	$-4.443 \cdot 10^{-2}$	$\pm 2.140 \cdot 10^{-2}$	$-4.809 \cdot 10^{-2}$	$\pm 1.402 \cdot 10^{-2}$

Table 7 - Empirical model of FCC yield profile – individual cuts and complete product slate.  
Normalized dimensionless variables (cont.)

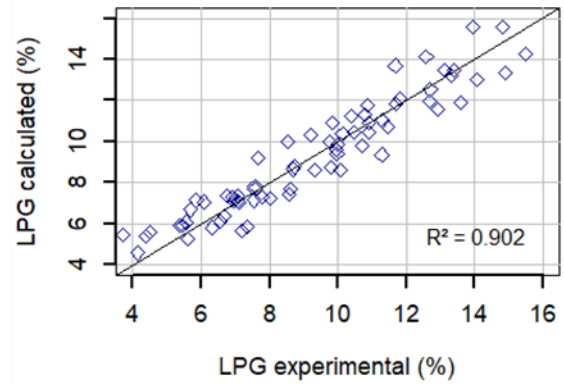
Product	Ordinary least squares			Restricted least squares	
	Variables	Coefficients	95% level CI	Coefficients	95% level CI
LCO	Intercept	$2.059 \cdot 10^{-1}$	$\pm 5.104 \cdot 10^{-3}$	$2.051 \cdot 10^{-1}$	$\pm 3.822 \cdot 10^{-3}$
	$\overline{T_{rx}}$	---	---	---	---
	$\overline{t_c}$	$4.803 \cdot 10^{-3}$	$\pm 4.360 \cdot 10^{-3}$	$8.112 \cdot 10^{-3}$	$\pm 2.469 \cdot 10^{-3}$
	$\overline{CTO}$	$-6.471 \cdot 10^{-1}$	$\pm 4.821 \cdot 10^{-3}$	---	---
	$\overline{HC_{light}}$	$3.686 \cdot 10^{-2}$	$\pm 2.464 \cdot 10^{-3}$	$3.632 \cdot 10^{-2}$	$\pm 1.929 \cdot 10^{-3}$
	$\overline{T_{rx}} \cdot \overline{t_c}$	$-1.030 \cdot 10^{-2}$	$\pm 6.883 \cdot 10^{-3}$	---	---
	$\overline{T_{rx}} \cdot \overline{CTO}$	$-3.350 \cdot 10^{-2}$	$\pm 7.798 \cdot 10^{-3}$	$-2.737 \cdot 10^{-2}$	$\pm 4.800 \cdot 10^{-3}$
	$\overline{T_{rx}} \cdot \overline{HC_{light}}$	$-1.815 \cdot 10^{-2}$	$\pm 5.887 \cdot 10^{-3}$	$-1.455 \cdot 10^{-2}$	$\pm 4.082 \cdot 10^{-3}$
Slurry oil	$\overline{HC_{light}}^2$	$9.914 \cdot 10^{-3}$	$\pm 6.009 \cdot 10^{-3}$	$1.332 \cdot 10^{-2}$	$\pm 4.588 \cdot 10^{-3}$
	Intercept	$2.558 \cdot 10^{-1}$	$\pm 8.575 \cdot 10^{-3}$	$2.558 \cdot 10^{-1}$	$\pm 6.234 \cdot 10^{-3}$
	$\overline{T_{rx}}$	$-7.277 \cdot 10^{-2}$	$\pm 2.268 \cdot 10^{-2}$	$-9.237 \cdot 10^{-2}$	$\pm 1.361 \cdot 10^{-2}$
	$\overline{t_c}$	$-7.929 \cdot 10^{-2}$	$\pm 1.210 \cdot 10^{-2}$	$-8.142 \cdot 10^{-2}$	$\pm 9.564 \cdot 10^{-3}$
	$\overline{CTO}$	$-1.424 \cdot 10^{-1}$	$\pm 1.872 \cdot 10^{-2}$	$-1.353 \cdot 10^{-1}$	$\pm 1.405 \cdot 10^{-2}$
	$\overline{HC_{light}}$	$-3.410 \cdot 10^{-2}$	$\pm 7.731 \cdot 10^{-3}$	$-3.943 \cdot 10^{-2}$	$\pm 5.817 \cdot 10^{-3}$
	$\overline{T_{rx}} \cdot \overline{t_c}$	$-3.971 \cdot 10^{-2}$	$\pm 2.106 \cdot 10^{-2}$	$-5.121 \cdot 10^{-2}$	$\pm 1.440 \cdot 10^{-2}$
	$\overline{T_{rx}} \cdot \overline{CTO}$	$3.990 \cdot 10^{-2}$	$\pm 3.850 \cdot 10^{-2}$	----	---
Coke	$\overline{T_{rx}} \cdot \overline{HC_{light}}$	$4.376 \cdot 10^{-2}$	$\pm 1.731 \cdot 10^{-2}$	$3.154 \cdot 10^{-2}$	$\pm 1.135 \cdot 10^{-2}$
	$\overline{CTO}^2$	$5.029 \cdot 10^{-2}$	$\pm 3.659 \cdot 10^{-2}$	$6.892 \cdot 10^{-2}$	$\pm 1.842 \cdot 10^{-2}$
	Intercept	$5.159 \cdot 10^{-2}$	$\pm 2.793 \cdot 10^{-3}$	$5.064 \cdot 10^{-2}$	$\pm 1.600 \cdot 10^{-3}$
	$\overline{T_{rx}}$	$-1.032 \cdot 10^{-2}$	$\pm 3.301 \cdot 10^{-3}$	$-1.071 \cdot 10^{-2}$	$\pm 2.090 \cdot 10^{-3}$
	$\overline{CTO}$	$1.134 \cdot 10^{-2}$	$\pm 3.015 \cdot 10^{-3}$	$1.148 \cdot 10^{-2}$	$\pm 1.878 \cdot 10^{-3}$
	$\overline{HC_{light}}$	$-1.600 \cdot 10^{-3}$	$\pm 1.274 \cdot 10^{-3}$	$-1.900 \cdot 10^{-3}$	$\pm 8.648 \cdot 10^{-4}$
	$\overline{CTO} \cdot \overline{HC_{light}}$	$4.036 \cdot 10^{-3}$	$\pm 2.066 \cdot 10^{-3}$	$3.745 \cdot 10^{-3}$	$\pm 1.292 \cdot 10^{-3}$
Coke	$\overline{T_{rx}}^2$	$7.175 \cdot 10^{-3}$	$\pm 2.725 \cdot 10^{-3}$	$7.069 \cdot 10^{-3}$	$\pm 1.706 \cdot 10^{-3}$
	$\overline{HC_{light}}^2$	$-4.320 \cdot 10^{-3}$	$\pm 3.275 \cdot 10^{-3}$	$-3.184 \cdot 10^{-3}$	$\pm 1.953 \cdot 10^{-3}$

Source: The author, 2023.

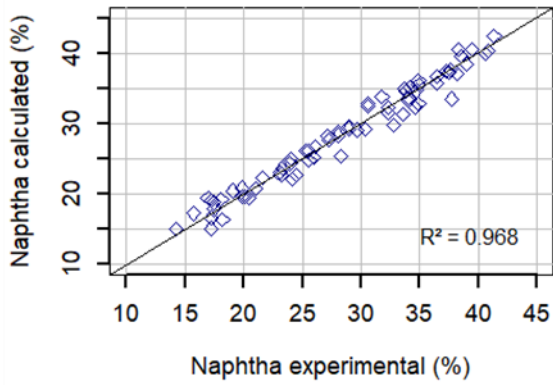
Figure 8 - Fitting of FCC yield profile empirical modeling – individual cuts



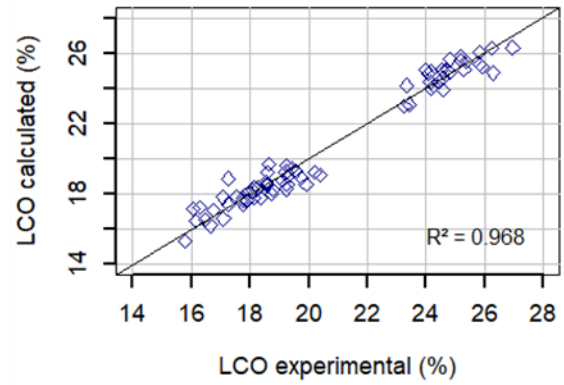
(a)



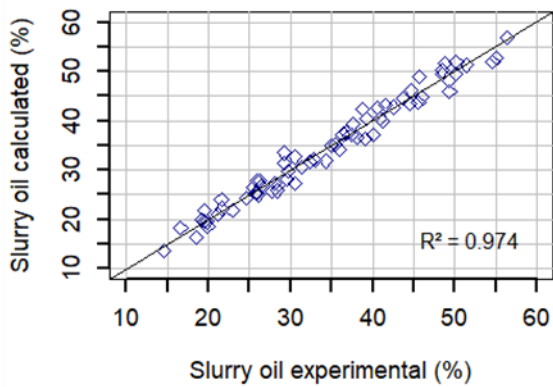
(b)



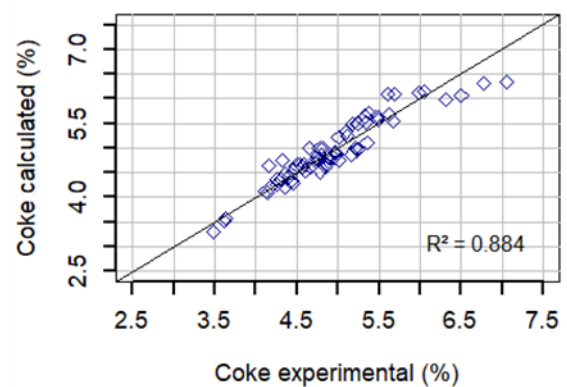
(c)



(d)



(e)



(f)

Source: The author, 2023.

Figure 8 depicts a reasonable to good fitting of models to experimental data. Fitting is greater for naphtha, LCO and slurry oil yields, and a lower tier for LPG and coke, specially at higher yields for the later. Coke yield is a particular important quantity as errors in its assessment would be further propagated as it is involved in the computation of CTO, which in turn is an input

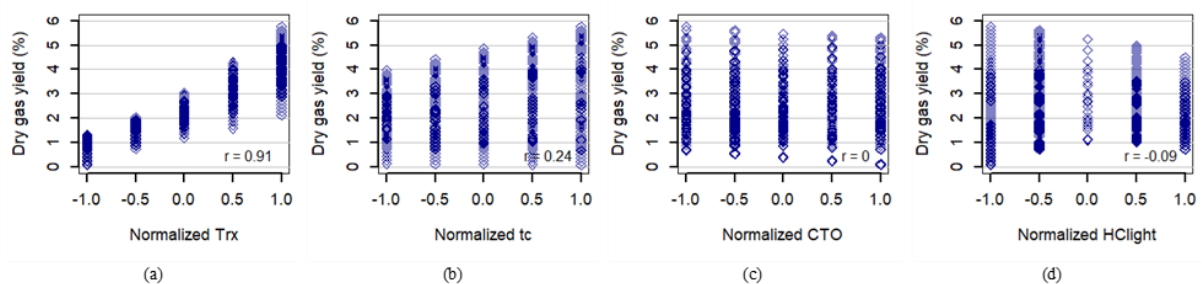
for yield profile estimation. Obtaining a model for coke yield is challenging because coke seems to be more influenced by feed quality (even similar assays may lead to noticeable different coke yields) and because the stripper, an equipment located upstream of the Riser, also plays a major role in effectively establishing the overall coke yield that will be experimentally measured (as a sum of adsorbed coke in the catalyst's pores and entrained hydrocarbons to the Regenerator).

Figure 8.d shows that it was obtained a relatively well-adjusted empirical model for LCO cut, and it exhibits the importance of including  $HC_{light}$  as one of the input variables, especially for LCO as the trend clearly exposes two separate regions: one at higher LCO yields for runs made with feed "D" (higher  $HC_{light}$ ) and another region with lower LCO yields for runs with other feeds.

As can be seen in Table 6, the built models, although straightforward, generally presented many terms. Overfitting was avoided by cross-validating all available experimental data through training (48 data) and test (21 data) sets at random partitions generated via Monte Carlo. Thus,  $R^2$  reported in Table 4 is calculated using all 69 experimental points.

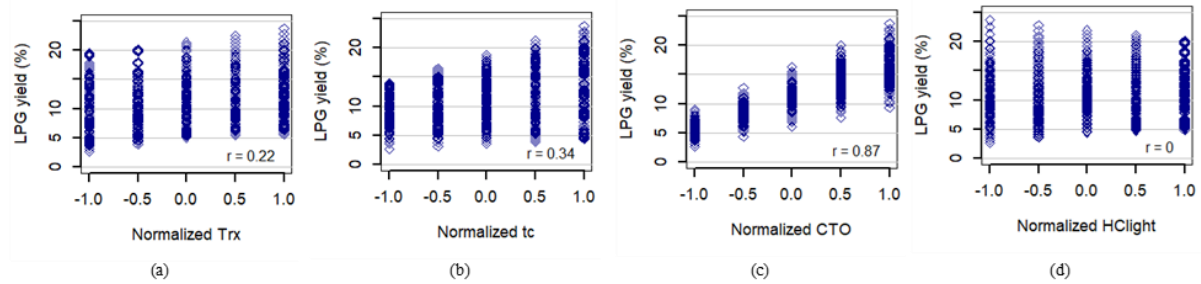
To further evaluate the generalist feature of the models developed, it was performed a sensitivity analysis employing a complete factorial survey with normalized values of -1 (low level), -0.5, 0, 0.5 (center and intermediate levels) and 1 (high level) as input data. This included the regions unexplored experimentally of high CTO – low  $T_{rx}$  and low CTO – high  $T_{rx}$ . Figures 9-14 graphically present results from this analysis for each cut and isolating one independent variable in each trend.

Figure 9 - Sensitivity analysis of the empirical Dry gas yield model response to normalized values of -1 to 1 as input data



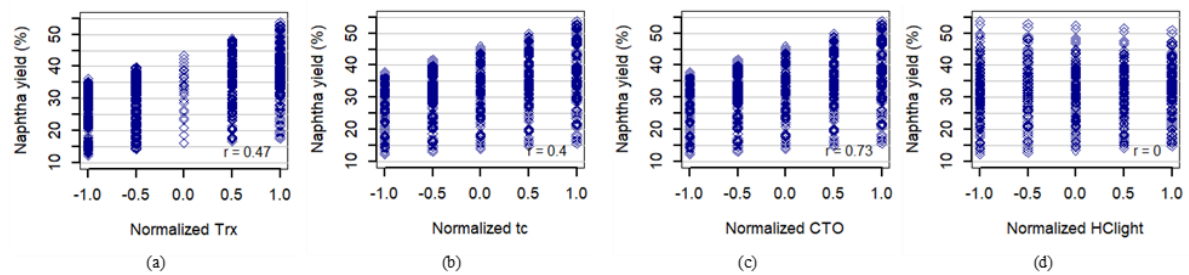
Source: The author, 2023.

Figure 10 - Sensitivity analysis of the empirical LPG yield model response to normalized values of -1 to 1 as input data



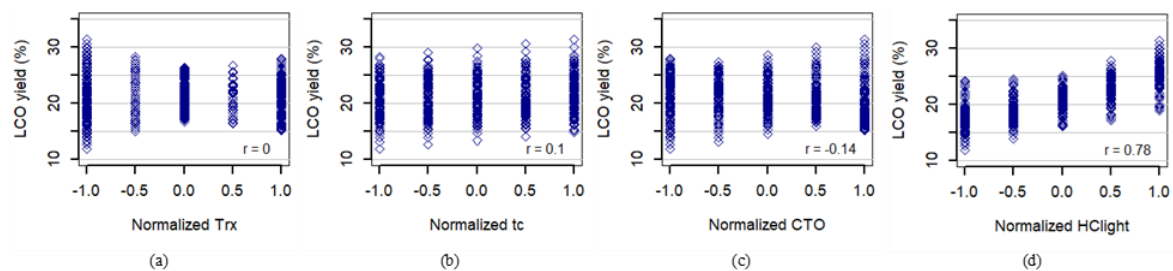
Source: The author, 2023.

Figure 11 - Sensitivity analysis of the empirical Naphtha yield model response to normalized values of -1 to 1 as input data



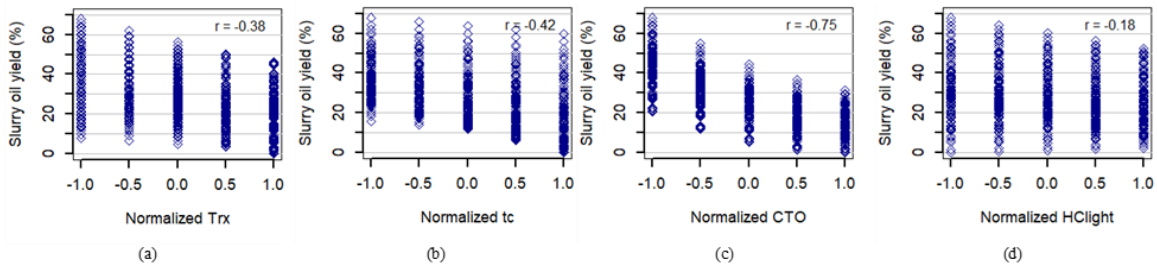
Source: The author, 2023.

Figure 12 - Sensitivity analysis of the empirical LCO yield model response to normalized values of -1 to 1 as input data



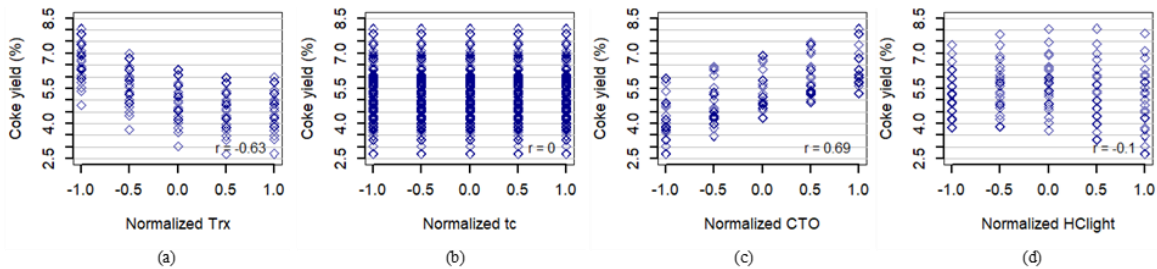
Source: The author, 2023.

Figure 13 - Sensitivity analysis of the empirical Slurry oil yield model response to normalized values of -1 to 1 as input data



Source: The author, 2023.

Figure 14 - Sensitivity analysis of the empirical Coke yield model response to normalized values of -1 to 1 as input data



Source: The author, 2023.

Overall, graphs from Figures 9-14 reveal that no spurious or inconsistent yield estimates (such as negative values or far above typical yields of each cut) were produced by the empirical models. Some interesting aspects can be noted through these graphs. Figure 9.a shows that the one single independent variable that is better correlated to Dry gas yield is  $T_{rx}$ , with a correlation value of 0.91. Even with other input variables being altered simultaneously, it can be seen a clear interdependence between  $T_{rx}$  and Dry gas yield in Figure 9.a. This is in agreement with the known fact that light components in Dry gas are produced primarily by thermal cracking, so higher  $T_{rx}$  leads to higher Dry gas yield.

For LPG (Figure 10), Naphtha (Figure 11) and Slurry oil (Figure 13), trends are similar: the greatest correlation occurs to CTO ( $r = 0.87$  for LPG,  $r = 0.73$  for Naphtha and  $r = -0.75$  for Slurry oil), from which it follows that, among process variables, CTO is the one that has a greater impact on FCC unit conversion. For these cuts, there is very little to no correlation at all between  $HC_{light}$  and the product yield.

Regarding LCO yield (Figure 12), on the other hand, it is interesting to note that no correlation arises individually for process variables. The intermediate characteristic of LCO (in

which both in low and high severity LCO yield is minimized) may play a part in this behavior. The only singular independent variable that displays a high correlation level with LCO yield is the light gasoil content ( $r = 0.78$ ), which was expected (see Figure 6).

Coke yield (Figure 14) exhibits a high correlation with both  $T_{rx}$  and CTO. Interesting enough, these correlations are opposite: with  $T_{rx}$  a negative correlation of -0.63, and with CTO a positive correlation of 0.69. The positive correlation with CTO is plainer, in the sense that coke yield, as a conversion product, is expected to increase with a higher severity level. The negative correlation with  $T_{rx}$ , contrariwise, is not so straightforward: this behavior is probably related to higher hydrocarbon entrainment from a low efficiency stripper operating with reduced  $T_{rx}$  to the regenerator (Gilbert; Baptista; Pinho, 2007), which settles the FCC unit to a relatively high coke yield regime. Figure 14.a shows that after some point, the negative correlation of  $T_{rx}$  with coke yield tends to stabilize, which may indicate a turning point in terms of the effect of  $T_{rx}$  in the stripper efficiency.

An interesting observation that arises in Figure 14.b is the lack of correlation between coke yield and  $t_c$ . This agrees with the established theory in which coke buildup in FCC catalyst particles occurs very rapidly in the first meters of the Riser above feed injection, and then tends to stabilize (Chen; Wang; Zhao; Zhang, 2022; Den Hollander; Makkee; Moulijn, 2001; Selalame; Patel; Mujtaba; John, 2022; Souza; Vargas; Von Meien; Martignoni; Amico, 2006). In this way, coke yield becomes indifferent to the isolated change of feed injection nozzle along the Riser, hence the absence of correlation with  $t_c$ .

Figure 14.d also shows no correlation between coke yield and  $HC_{light}$ , which may indicate that this particular feed quality variable did not quite express the usually relevant effect of feedstock in coke yield (Dahl; Tangstad; Mostad, 1996; Sadeghbeigi, 2020), or that aside one specific feed (feed “D”) with a higher diesel content, there were no major differences between feed batches used throughout the study.

### 1.3.2 Empirical modeling – complete product slate

Previous section discussed individual yield models that have a slight caveat: adding all yields does not necessarily total to 100 wt.%, i.e., the mass balance closing is not guaranteed. For all 69 experimental points available, calculated yields using the empirical models for individual

products added to a mean mass balance of 99.96 wt.%, with a minimum value of 98.47 wt.% and a maximum value of 101.61 wt.%.

Typical solutions to correct this issue include: (a) defining *a priori* a specific component to be obtained as a goal seek to mass balance closure, i.e. the yield for this component will not be estimated as it will be taken as 100 wt.% less the other products; (b) to normalize all yields to 100 wt.% sum; (c) a variation of (b) in which one or some of the products (usually coke yield) are kept unaltered, and the other are normalized to obtain a 100 wt.% sum. All these options are prone to subjective considerations.

An envisaged alternative used in the present study was to force the mass balance closure directly in the parameter estimation process of model building by using restricted least squares. LPG, that had presented one of the lowest coefficients of determination in the individual cut empirical model ( $R^2 = 0.902$ ), was the cut selected as the mass balance closure key in this methodology. This should not be confused to one of the mentioned conventional methods to deal with the issue of mass balance closing in estimating FCC yield profile of defining *a priori* a given component just as a mass balance closer. In the case of restricted regression, experimental LPG yield data were effectively being utilized in the model building process, as the error in estimating LPG yield was also being considered in order to estimate the coefficients for other cuts.

A detail to be mentioned is that because all products were stacked into the same matrix structure, squared errors minimization had to consider a normalization by the mean yield value of each cut. Otherwise, the model would tend to prioritize error minimization only for the highest yielding cuts (such as Slurry oil and Naphtha). Due to difficulties of this type, it was opted out of generating a new model by forward selection from scratch, being preferred the utilization of the same model structure previously obtained in the individual cuts modeling. Models with mass balance closure embedded are displayed in Table 6.

Remarks and graphical analysis of the complete product slate empirical modeling are analogous to the ones presented for the individual cuts in the previous section and will not be further discussed.

### 1.3.3 Simplified empirical modeling of slurry oil cracking

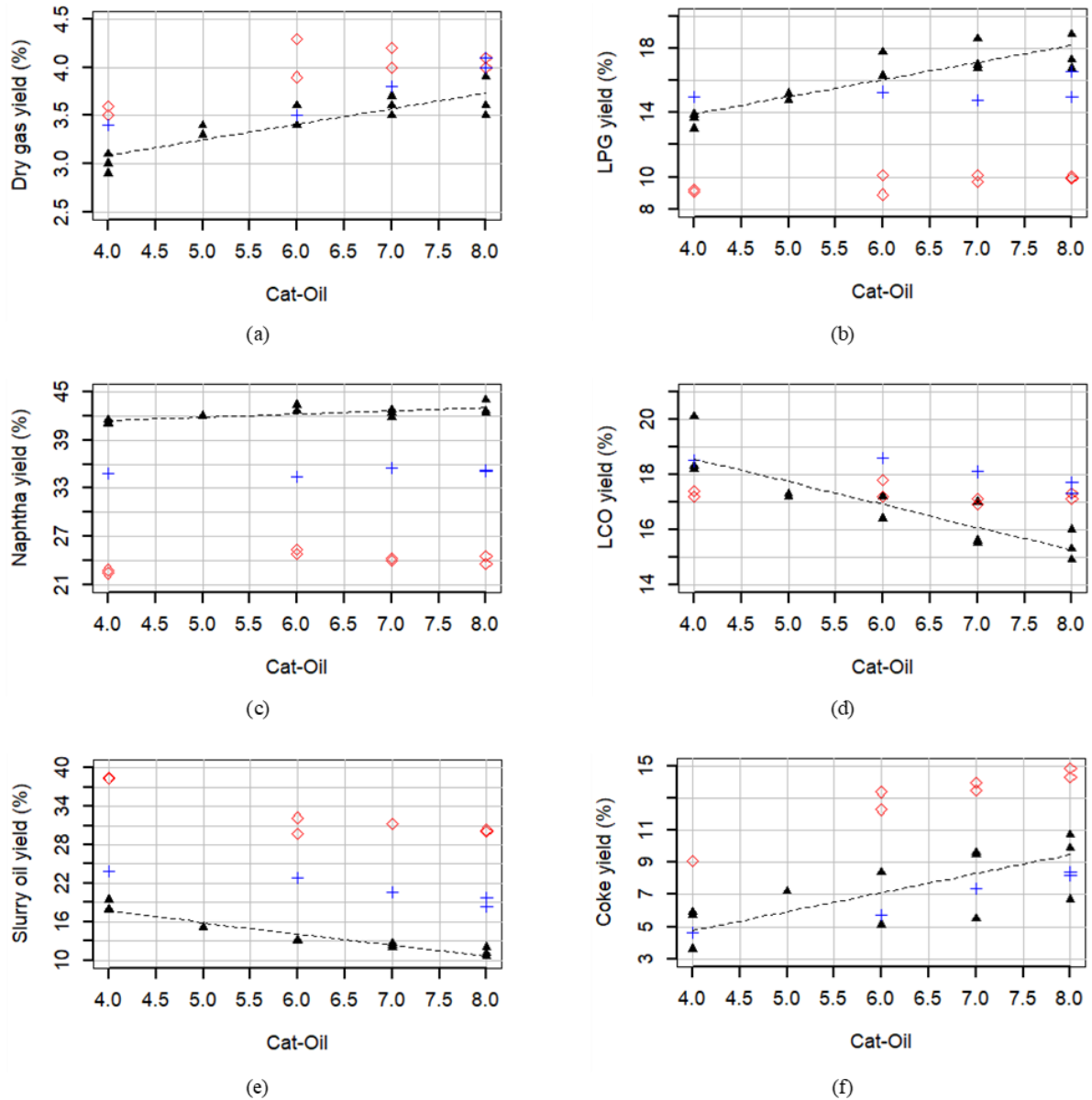
Compared to the fresh vacuum gasoil feed, the slurry oil has already gone through a catalytic conversion process, so a lower amount of lighter noble products would be expected from

a new catalytic cracking step for the slurry oil. Figure 15 shows that this is the case for a more deeply converted slurry oil (obtained from a prior test with a slurry oil yield of 21.4 wt.%). But for the slurry oil coming from a lower conversion run (with a slurry oil yield of 35.5 wt.%), although it is still noticeable a lower conversion tier than that of vacuum gasoil, there is a greater similarity with typical conversion thresholds of unconverted direct distillation heavy feeds.

Figures 15.b, 15.c and 15.d show that the 35.5 wt.% slurry oil feed presents an intermediate conversion profile between that of fresh vacuum gasoil and the 21.4 wt.% slurry oil. For the latter, the extent of cyclization reactions and aromatics formation with increased conversion from the original cracking step is higher (as can be seen in the feed characterization analysis in Table 4), so that there is less conversion potential remaining and higher tendency of coke formation (Figure 15.f).

This feature in which slurry oil obtained from a catalytic cracking step at low conversion remains with considerable conversion potential can be useful for enhancing the economic margin of a FCC unit operating towards middle distillate maximization. Reducing the level of reaction severity, i.e. using a lower  $T_{rx}$  and CTO (or lower  $t_c$  or a less active catalyst), inherently tends to debottleneck some equipment such as the Air Blower, which makes room for the slurry oil recycle, which in turn still possesses a reasonable crackability, with the potential to recover some LPG and naphtha production (along with some extra LCO), in addition to minimizing the drawback of excessive slurry oil production. It should be noted that this route competes with the alternative of increasing fresh vacuum gasoil processing, as long as additional gasoil is available to the FCC unit, as it also competes with the maximum conversion mode without an increased feed throughput.

Figure 15 - Products yield as a function of Catalyst-to-oil ratio in the ACE FCC pilot plant: Vacuum gasoil reference feed ( $\blacktriangle$ ); 21.4 wt.% slurry oil ( $\diamond$ ); 35.5 wt.% slurry oil ( $+$ ). Linear model for vacuum gasoil reference feed data (---)



Source: The author, 2023.

To evaluate the route of slurry oil re cracking, these experiments with slurry oil in the ACE FCC pilot plant were included in the study and a simplified model was developed in which the output is a correction factor of the yield profile predicted by the main empiric model (developed for vacuum gasoil cracking) to account for the difference in crackability between VGO and the slurry oil recycle stream.

The first step was to perform a linear regression of the experimental data for the reference vacuum gasoil (see Table 8). As can be seen in Figures 15.a-15.f, there was a certain degree of scattering of the experimental data for the reference VGO in the ACE pilot plant unit, so it was necessary to estimate a baseline of predicted yields for the reference VGO. The dispersion of experimental data was responsible for the relative high degree of experimental error (low  $R^2$ ) for the simplified models of Table 8, nonetheless these models were considered admissible for the purpose of a simplified assessment of the slurry oil recycle route. In Table 8, the coefficient for the intercept from the coke regression is not shown because it was statistically not significant.

Table 8 - Regression of ACE FCC pilot plant data for reference VGO feed as a function of CTO

Coefficients	Products					
	Dry gas	LPG	Naphtha	LCO	Slurry oil	Coke
<i>Intercept</i>	2.440	9.640	39.874	21.898	24.526	---
<i>CTO (m/m)</i>	0.162	1.073	0.398	-0.831	-1.732	1.187
Coefficient of determination ( $R^2$ )	0.77	0.78	0.53	0.78	0.91	0.42

Source: The author, 2023.

The next step was to calculate the ratio between the experimental yield data for the slurry oil streams and the estimated data for the reference vacuum gasoil at the same CTO. Later this ratio was regressed as a function of CTO and original yield of slurry oil ( $\gamma_{\text{slurry}}$ ) for the slurry oil feed. Table 9 presents the coefficients of the linear regression thus obtained. Although the ACE unit's reference vacuum gasoil (Table 4) does not have the exact same characterization as the feeds used in the large scale FCC plant (Table 1), it was considered that the correction factor obtained from the simplified model in Table 9 could be applied to correct the yield profile estimated by the empirical models developed from the experimental data of the large FCC plant (i.e. models from Table 6) due to change of feed from fresh VGO to slurry oil recycle. In Table 9, coefficients that are not shown were statistically not significant.

Table 9 - Simplified model for correction factor due to change of feed from fresh VGO to slurry oil recycle

Coefficients	Products					
	Dry gas	LPG	Naphtha	LCO	Slurry oil	Coke
<i>Intercept</i>	1.259	0.301	0.171	0.691	2.834	3.384
$\gamma_{slurry}$ (wt.%)	-0.526	2.453	1.841	0.358	-5.937	-5.851
<i>CTO</i> (m/m)	---	-0.0373	---	0.0432	0.138	-0.0647
Coefficient of determination ( $R^2$ )	0.39	0.96	0.98	0.95	0.93	0.97

Source: The author, 2023.

To illustrate the use of the model presented in Table 9 to estimate the yield profile of the FCC unit in a case containing slurry oil recycle, a numerical example will be provided:

Assuming a feed quality of feed “C” from Table 1 ( $HC_{light} = 5.8\%$ ) and the following operating conditions for the Riser:

- $T_{rx} = 808.15$  K;  $CTO = 5.0$ ;  $t_c = 1.5$  s

Applying the restricted least squares model from Table 6 and the simplified model to correct for a different feed in the case of slurry oil recycling from Table 9, the following values are obtained (Table 10):

Table 10 - Numerical example of obtaining the normalized yield profile for Slurry oil re cracking for feed “C” ( $HC_{light} = 5.8 \%$ ),  $T_{rx} = 808.15 \text{ K}$ ,  $CTO = 5.0$  and  $t_c = 1.5 \text{ s}$

Product	Yield profile (wt.%) for VGO cracking with empirical RLS model (Table 6)	Correction factors for Slurry oil ( $\gamma_{slurry} = 0.3665$ ) recycling (Table 9)	Raw yield profile for Slurry oil re cracking applying the correction factors	Normalized yield profile for Slurry oil re cracking
Dry gas	2.81	1.066	2.99	2.74
LPG	8.50	1.013	8.61	7.89
Naphtha	28.59	0.846	24.19	22.17
LCO	19.15	1.039	19.89	18.23
Slurry oil	36.65	1.350	49.50	45.36
Coke	4.29	0.916	3.93	3.61

Source: The author, 2023.

#### 1.3.4 Optimization of FCC unit product slate

As an example of the scenario evaluation possibilities, a case was run in which a FCC unit with  $D_{riser} = 1.3 \text{ m}$  was supplied with feed “C” (Table 1) and could operate constrained to conditions and ranges shown in Table 11. Variation in contact time ( $t_c$ ) was limited to the range of experimental data to avoid extrapolation of this parameter. The constraint of a maximum dense phase regenerator temperature ( $T_{reg}$ ) corresponds to metallurgical limits of the equipment’s internals. Restriction of a maximum catalyst circulation rate ( $w_{cat}$ ) was included to represent a limit in the unit pressure balance at which the riser pressure drop can increase to such an extent that there is no longer any pressure differential to the catalyst valves, which is an impediment to unit operation. A maximum value for combustion air flow to the regenerator ( $w_{air}$ ) was included since the air blower capacity is a common restraint for the converter section of the FCC unit.

Table 11 - Range of operating conditions allowed for the FCC unit in the optimization study

Variable	Minimum value	Maximum value
$T_{rx}$ (K)	788.15	833.15
$T_{feed}$ (K)	483.15	613.15
$Q_{vgo}$ (m <sup>3</sup> /d)	5000	8800
$L_{riser}$ (m)	10	30
$Q_{recycle}$ (m <sup>3</sup> /d)	0	800
$t_c$ (s)	0.4	2.2
$T_{reg}$ (K)	---	1013.15
$w_{cat}$ (t/min)	---	53
$w_{air}$ (t/h)	---	230

Source: The author, 2023.

Optimization was sought aiming at maximum FCC unit operating margin. Costs of feed and products have a very high variability. The costs considered in the present optimization study are shown in Table 12. Evidently the price basis is one of the most influential factors in this analysis. In a simplified way, it was assumed that the intermediate streams of cracked naphtha, LCO and slurry oil would constitute the finished pool of gasoline, diesel and fuel oil, respectively.

Table 12 - Price basis considered in the optimization study

Product	Cost (US\$/m <sup>3</sup> )
Vacuum gasoil	580
LPG	420
Gasoline	640
Diesel	750
Fuel oil	510

Source: The author, 2023.

Results are presented in Table 13. In Case 1, the optimization used only the constraints reported in Table 11. As it can be seen, the optimized result associated a higher profitability with operating the FCC unit at high conversion. It appears that the slight increase of LCO yield and

the large increase of slurry oil yield in maximum middle distillate mode are both hard drawbacks to supplant the option for the maximum conversion mode in the FCC unit. It can be noted that in Case 1, the maximum air rate constraint has been reached.

Table 13 - Results of the cases run in the optimization

Variable	Case 1 – optimum production mode (maximum profitability)	Case 2 – forced minimum production of LCO	Case 3 – forced minimum production of LCO and slurry oil recycle disallowed
Optimized input variables			
$T_{rx}$ (K)	833.15	833.15	833.15
$T_{feed}$ (K)	501.45	538.25	569.25
$Q_{vgo}$ ( $m^3/d$ )	8169	8800	8800
$L_{riser}$ (m)	30	30	30
$Q_{recycle}$ ( $m^3/d$ )	0	342	0
Other variables			
$t_c$ (s)	1.73	1.56	1.59
$T_{reg}$ (K)	955.45	985.61	1004.55
$W_{cat}$ (t/min)	52.55	41.66	31.85
$W_{air}$ (t/h)	230.0	230.0	199.5
CTO (m/m)	9.87	6.98	5.55
$Q_{LPG}$ ( $m^3/d$ )	2388	1990	1567
$Q_{naphtha}$ ( $m^3/d$ )	4632	4393	3833
$Q_{LCO}$ ( $m^3/d$ )	1495	1800	1800
$Q_{slurry}$ ( $m^3/d$ )	674	1368	2125
Unit margin ( $10^3 \cdot US\$/d$ )	694.1	591.1	441.3

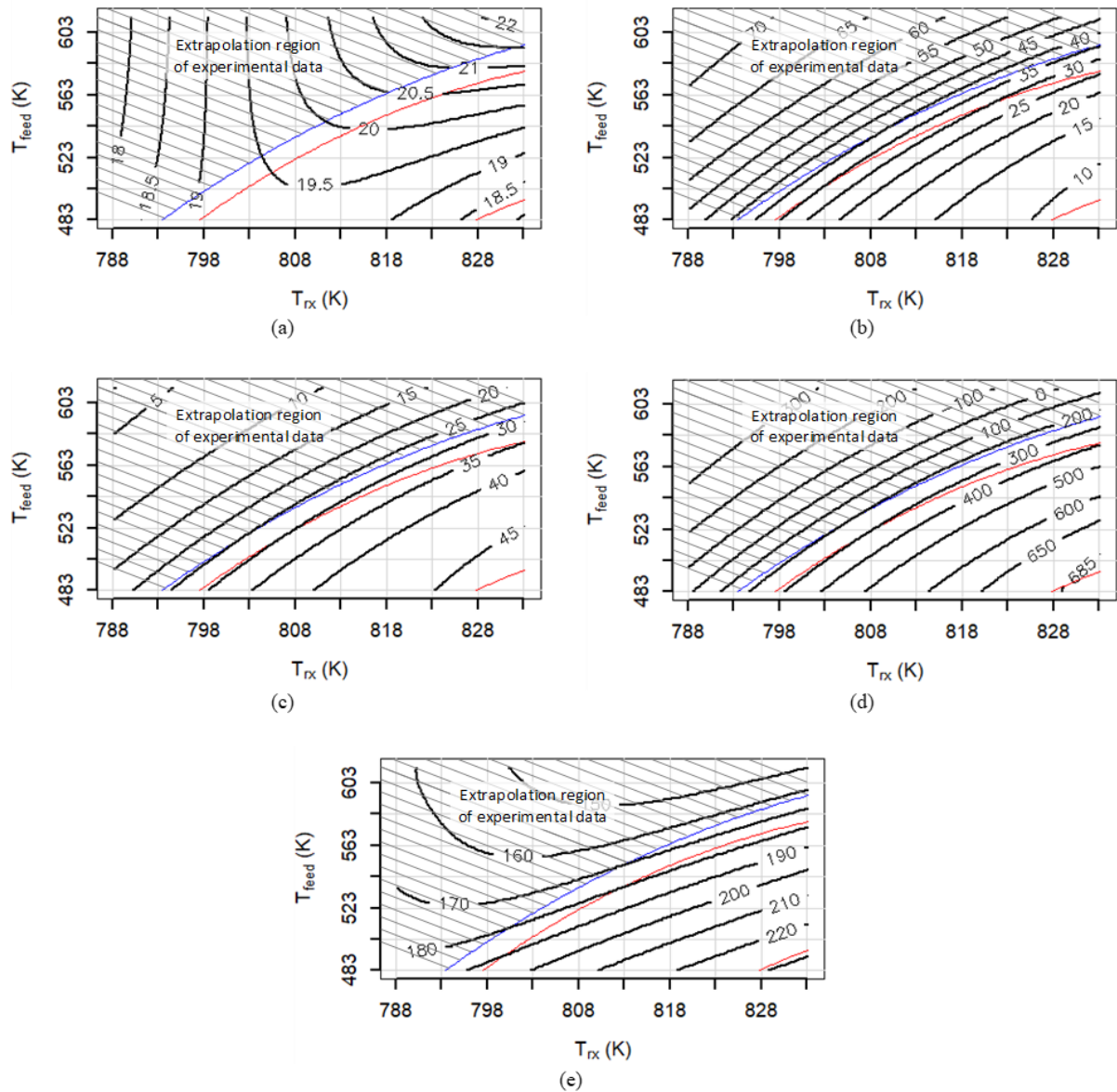
Source: The author, 2023.

In Case 2 of Table 13, it was forced a minimum production of 1800  $m^3/d$  of LCO, maintaining the previous constraints reported in Table 11. Case 2 shows a clear drop in the unit profit margin. It also shows two interesting moves when the FCC unit is directed towards a low conversion region: feed throughput is increased (in this case to the constrained maximum value) and recycling of slurry oil becomes useful. It is worth noting that the maximum air rate is still at

the constrained maximum value, showing that the operating room in the air blower provided by the conversion level reduction is consumed by the increase in feed rate (fresh VGO and slurry oil recycle) to the riser. In Case 3, it was again forced a minimum production of 1800 m<sup>3</sup>/d of LCO as in Case 2, but the option of slurry oil re cracking was not allowed. It can be observed a steep drop of margin when the option of slurry oil re cracking is not available. The unit is forced to maintain the highest throughput of fresh vacuum gasoil (8800 m<sup>3</sup>/d), although the air blower is now at reduced capacity, and to carry out a more pronounced adjustment of yields profile in the low severity region. Hence the increase in slurry oil production (without the possibility of recycling some portion to the riser) harms the unit profitability.

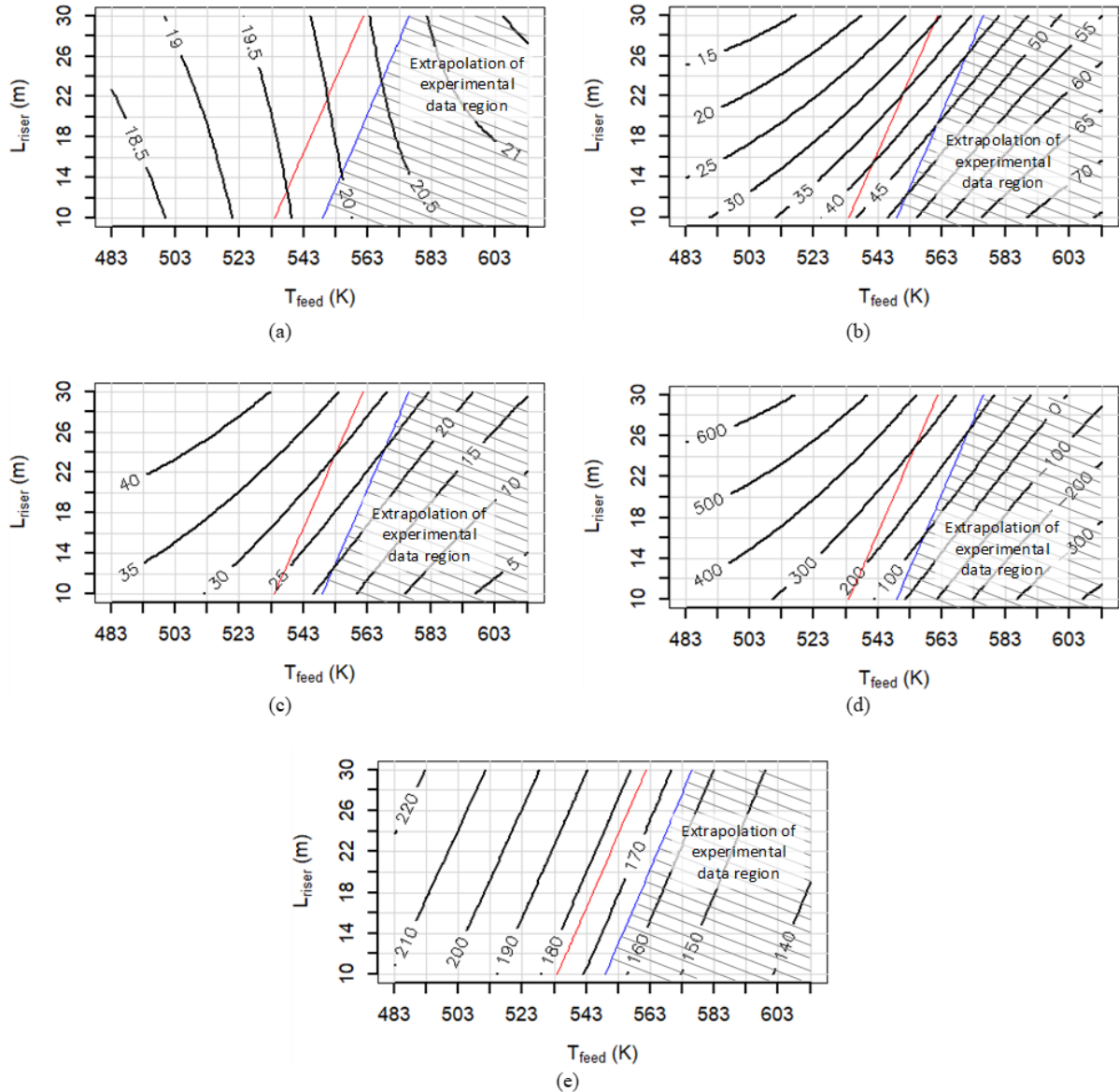
An aspect that draws attention in the optimized results obtained in Table 13 is that in all cases, even when a reduction in the conversion level was forced in order to achieve the minimum production of 1800 m<sup>3</sup>/d of LCO, the selected  $T_{rx}$  was the maximum value allowed (833.15 K). This is probably due to the previous result discussed for Figure 14.a, in which it was observed a negative correlation between coke yield with  $T_{rx}$ , which seems somewhat counterintuitive, but it is most likely related to an effect of improved stripper efficiency (and also possibly an improvement in feed vaporization at the base of the riser), so that the FCC unit tends to balance itself with a lesser  $T_{reg}$  and a slightly lower coke yield, which in turn frees up some required air blower capacity (at the constrained maximum value in Cases 1 and 2). The path selected for reducing conversion in Cases 2 and 3 was to increase  $T_{feed}$  (sustaining a high  $T_{rx}$ ), thus reducing CTO. Figures 16-17 present a screening exercise of two of the input variables aiming at visualizing the effect of selected variables. In Figure 16, the screening variables are  $T_{rx}$  and  $T_{feed}$ .  $Q_{vgo}$ ,  $L_{riser}$  and  $Q_{recycle}$  are set to 8000 m<sup>3</sup>/d, 30 m and 0, respectively. In Figure 17, the screening variables are  $T_{feed}$  and  $L_{riser}$ .  $T_{rx}$ ,  $Q_{vgo}$  and  $Q_{recycle}$  are set to 823.15 K, 8000 m<sup>3</sup>/d and 0, respectively.

Figure 16 - Contour plots from screening of the input variables  $T_{rx}$  and  $T_{feed}$ .  $Q_{vgo} = 8000 \text{ m}^3/\text{d}$ ,  $L_{riser} = 30 \text{ m}$ ,  $Q_{recycle} = 0$ . (a) LCO yield (wt.%), (b) Slurry oil yield (wt.%), (c) Naphtha yield (wt.%), (d) Profit margin ( $10^3 \text{ US}\$/\text{d}$ ), (e) Air rate ( $10^3 \text{ kg/h}$ ). (---) minimum experimental CTO, (---) constraints: maximum  $T_{reg}$  (1013.15 K) and maximum air rate ( $230.0 \cdot 10^3 \text{ kg/h}$ )



Source: The author, 2023.

Figure 17 - Contour plots from screening of the input variables  $T_{\text{feed}}$  and  $L_{\text{riser}}$ .  $T_{\text{rx}} = 823.15 \text{ K}$ ,  $Q_{\text{vgo}} = 8000 \text{ m}^3/\text{d}$ ,  $Q_{\text{recycle}} = 0$ . (a) LCO yield (wt.%), (b) Slurry oil yield (wt.%), (c) Naphtha yield (wt.%), (d) Profit margin ( $10^3 \text{ US}\$/\text{d}$ ), (e) Air rate ( $10^3 \text{ kg/h}$ ). (---) minimum experimental CTO, (---) constraint: maximum  $T_{\text{reg}}$  (1013.15 K)



Source: The author, 2023.

Figure 16 clearly confirms that the highest profit margin occurs at the high conversion region, i.e. at elevated  $T_{\text{rx}}$  and low  $T_{\text{feed}}$ , which results in high catalyst circulation to the riser. Even though there is a higher yield of LCO in a region with higher  $T_{\text{feed}}$  (thus lower CTO), the resulting exchange of cracked naphtha for slurry oil cut down the unit margin.

Figure 17 aids graphically exploring the difference between reducing conversion via lowering CTO (thus raising  $T_{\text{feed}}$ ) and via lowering  $t_c$  (thus reducing the riser height above the

feed nozzle). If there is a LCO yield target to be achieved (e.g. 19 wt.%), this can be obtained with  $L_{\text{riser}} = 30$  m (resulting in a higher  $t_c$ ) and lesser  $T_{\text{feed}}$ , or with  $L_{\text{riser}} = 10$  m and a slightly higher  $T_{\text{feed}}$ . In the first case, while the LCO target is achieved, the slurry oil yield is lower and the naphtha yield is higher, thus in Figure 17.d the profit margin increases in this direction of increasingly  $t_c$ . This indicates that low contact time should not be a tool of first choice to reduce the FCC unit's conversion to a maximum middle distillate operation mode.

It should be remarked that the present economic analysis, in which the preference for the high conversion operation mode was demonstrated, is quite simplified, in that its boundary is restricted to the FCC unit. This should be in line with the case of refineries where there is only one FCC unit and this is the main or only conversion unit present; but if there are two or more FCC units or a more complex refining scheme with other conversion units, the analysis should include an overall economic optimization of the entire refinery, and the option for one of the FCC units to operate at low conversion may prove itself attractive in this global balance.

## 1.4 Conclusion

Empirical models were built to predict yield profile of the FCC unit, considering a specific grade of catalyst designed for maximizing middle distillate. Two approaches were employed in constructing the models: individual cuts, where each product was modeled separately by ordinary least squares; and complete product slate, in which all products are modeled simultaneously by restricted least squares, guarantying mass balance closing.

Regarding LCO yield, the single independent variable that presented the strongest correlation with was feed light gasoil content ( $HC_{\text{light}}$ ). In the present study the intermediate character of LCO could be displayed: at low conversions, the cracking rate of gasoil is reduced, thus LCO production rate is kept relatively low. At high conversions, despite a more pronounced gasoil cracking rate (and higher LCO production from gasoil cracking), cracking rate of LCO itself to lighter products (mainly LPG and Naphtha) also increase, thus reducing again LCO yield. There is a maximum in LCO yield that occurs in a moderate conversion level, but the range of LCO yield, across a quite large range of conversion level, was very narrow, which reduces the economic attractiveness of the middle distillate maximization route in the FCC.

Applying a FCC unit process simulator, an optimization tool and the empirical models developed, it is possible to optimize process conditions to maximize the unit's profit margin. In

this regard, empirical models can also be useful in assisting economic analysis and planning of FCC unit operation mode, i.e. defining whether it is advantageous or not to proceed with a maximum middle distillate operation mode in FCC, and to what extent, considering the relevant associated drawback of increased production of Slurry oil.

A simplified analysis of this type was carried out, considering the boundary of a single FCC unit. Preference for high conversion mode, i.e. naphtha maximization, was confirmed. Increase of slurry oil throughput in a maximum middle distillate mode was seen as too much of a hurdle to overcome. A possibility to mitigate some of this deleterious effect is to recycle a portion of the slurry oil to the riser, as a reduced conversion in the FCC unit tends to open up room for a total feed throughput increase. It was verified that when a constraint of minimum production of LCO is included, the slurry oil re-cracking option is used and results in less loss of margin than if this option is disabled. The maximum middle distillate route may prove to be more attractive in the case of a refinery with more conversion units and with more possibilities for exchanging intermediate streams between process units. In this case, the assessment must consider the boundary of the entire refinery.

This work included innovative experimental investigation of the effect of contact time in the Riser ( $t_c$ ) on the LCO/slurry oil ratio, taking advantage of the flexibility of feed injection at different elevations of the large FCC pilot plant used in the study (Figure 1). It was found that reducing contact time did not bring any benefit in increasing the LCO/slurry oil ratio. The LCO yield curve as a function of conversion remained practically unchanged with variation in  $t_c$ .

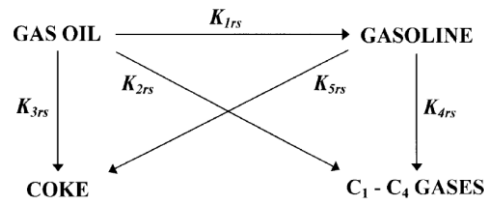
If it is necessary to carry out a low conversion operation in the FCC, the empirical model obtained showed that an ideal path to reduce the conversion would be to keep  $T_{rx}$  (generally limited by the design temperature of the reaction section of the FCC unit, among other known bottlenecks such as air blower capacity) and  $t_c$  (i.e. to maintain feed injection at the base of the riser) at the maximum allowed values, and to lower severity through reducing CTO (i.e. by increasing  $T_{feed}$ ).

## 2 CONSIDERATIONS ON THE ENERGY BALANCE OF CRACKING REACTIONS

### 2.1 Introduction

To develop the phenomenological modeling of catalytic cracking reactions in the riser, it is necessary to consider the differential energy balance along the length of the riser. Most phenomenological models of catalytic cracking reactions with some kind of lumping technic found in literature (Fernandes; Verstraete; Pinheiro; Oliveira; Ribeiro, 2007; Han; Chung, 2001a; Han; Chung, 2001b; John; Mustafa; Patel; Mutjaba, 2019; Olafadehan; Sunmola; Jaiyeola; Efeovbokhan; Abatan, 2018) have a structure that involves the simultaneous resolution of a system of differential equations that accounts for: product formation rate balance, hydrodynamic and pressure balance, and energy balance along the riser. Taking the structure proposed by Han, Chung (2001a, 2001b) as an example, Eq. 21, Eq. 22 and Eq. 23 present the reactional mass and energy balance for a four-lump gasoil cracking reaction model shown in Figure 18.

Figure 18 - Four lump gasoil cracking reaction model



Source: Han; Chung, 2001a

$$\frac{d\gamma_i}{dx} = \frac{\rho_{cat} \cdot \varepsilon_{cat} \cdot A_{riser} \cdot \phi_{cat}}{w_{fluid}} \cdot r_i \quad i = VGO, naphtha, gas (C1 - C4), coke \quad \text{Eq. 21}$$

Where, according to the symbology and reaction pathway shown in Figure 18:

$$r_{VGO} = -(k_{1rs} + k_{2rs} + k_{3rs}) \cdot \gamma_{VGO}^2 \quad \text{Eq. 21b}$$

$$r_{naphtha} = k_{1rs} \cdot \gamma_{VGO}^2 - k_{4rs} \cdot \gamma_{naphtha} - k_{5rs} \cdot \gamma_{naphtha} \quad \text{Eq. 21c}$$

$$r_{gas} = k_{2rs} \cdot \gamma_{VGO}^2 + k_{4rs} \cdot \gamma_{naphtha} \quad \text{Eq. 21d}$$

$$r_{coke} = k_{3rs} \cdot \gamma_{VGO}^2 + k_{5rs} \cdot \gamma_{naphtha} \quad \text{Eq. 21e}$$

$$\frac{dT_{cat}}{dx} = \frac{A_{riser} \cdot h_p \cdot A_{p_{ef}}}{w_{cat} \cdot C_{p_{cat}}} \cdot (T_{fluid} - T_{cat}) \quad \text{Eq. 22}$$

$$\frac{dT_{fluid}}{dx} = \frac{A_{riser}}{w_{fluid} \cdot C_{p_{fluid}}} \cdot \left[ h_p \cdot A_{p_{ef}} \cdot (T_{cat} - T_{fluid}) - \rho_{cat} \cdot \varepsilon_{cat} \cdot Q_{rx} \right] \quad \text{Eq. 23}$$

Where  $Q_{rx}$  is obtained as a sum of the enthalpies of each reaction involved:

$$Q_{rx} = (\Delta H_{rx1} \cdot k_{1rs} \cdot \gamma_{VGO}^2 + \Delta H_{rx2} \cdot k_{2rs} \cdot \gamma_{VGO}^2 + \Delta H_{rx3} \cdot k_{3rs} \cdot \gamma_{VGO}^2 + \Delta H_{rx4} \cdot k_{4rs} \cdot \gamma_{naphtha} + \Delta H_{rx5} \cdot k_{5rs} \cdot \gamma_{naphtha}) \cdot \phi_{cat} \quad \text{Eq. 23b}$$

Given adequate boundary conditions and solving numerically the system of Eq. 21 through Eq. 23 along with hydrodynamic and pressure balance differential equations, it is possible to obtain the estimated conditions such as gasoil conversion, yields of products, temperature and pressure not only at the riser outlet, but a complete profile along the riser becomes available.

Strictly speaking, the system of equations to be solved is a differential algebraic system of equations (DAE) (Olafadehan; Sunmola; Jaiyeola; Efevbokhan; Abatan, 2018) because some of the parameters vary with the independent variable length of riser ( $x$ ), but do not appear as derivative terms in the differential equations. One such example is the reaction rate coefficient  $k_j$ , that is related to temperature (which, in turn, varies along the length of riser) through an Arrhenius relationship presented in Eq. 24. However, this is an index 1 semi-explicit DAE that could be easily converted in a set of ordinary differential equations (ODE) by proper substitution of the pure algebraic parameters in the existent differential equations, but can also be solved directly by most ODE numerical solvers (Shampine; Reichelt; Kierzenka, 1999).

$$k_j = k_{j_0} \cdot \exp\left(\frac{-E_{aj}}{R_{ideal} \cdot T_{fluid}}\right) \quad \text{Eq. 24}$$

It is evident that in order to calculate the energy balance in the riser prior, knowledge of the heats of cracking reactions and of the heat capacities of the lumps is necessary. This is very simple for reactions involving only pure species.

Knowing the thermodynamic properties of the components involved in the chemical reaction, it is possible to calculate the enthalpy change due to the reaction, or heat of reaction. Taking for example the dehydrogenation reaction of propane to propylene (Eq. 25):



Table 14 presents thermodynamic data for the components involved in the reaction. From these data it is possible to calculate the heat of reaction of Eq. 25.

Table 14 - Thermodynamic data for the reaction components of Eq. 25

Component	Molar mass (kg/kmol)	Ideal gas enthalpy of formation at T = 298.15 K (kJ/kmol x 10 <sup>-4</sup> )	Lower heating value at T = 298.15 K (kJ/kmol x 10 <sup>-6</sup> )
Propane	44.097	-10.4680	2.0431
Propylene	42.081	1.9710	1.9257
Hydrogen	2.016	0	0.2418

Source: Green; Southard, 2019

Through the enthalpies of formation (Eq. 26):

$$\Delta H_{rx}^{T=298.15K} = \sum H_{f,products}^{T=298.15K} - \sum H_{f,reagents}^{T=298.15K} \quad \text{Eq. 26}$$

$$\Delta H_{rx,Eq.25}^{T=298.15K} = H_{f,C_3H_6}^{T=298.15K} + H_{f,H_2}^{T=298.15K} - H_{f,C_3H_8}^{T=298.15K} \quad \text{Eq. 26b}$$

$$\Delta H_{rx,Eq.25}^{T=298.15K} = 1.9710 \cdot 10^4 + 0 - (-10.4680 \cdot 10^4) = 12.439 \cdot 10^4 \text{ kJ/kmol} \quad \text{Eq. 26c}$$

The lower heating values are the positive values of the enthalpies of combustion, which are mostly highly exothermic reactions. Thus, when using the lower calorific value, the heat of reaction is also obtained by the difference between the LHV of the reactants and the LHV of the products (Eq. 27):

$$\Delta H_{rx}^{T=298.15K} = \sum LHV_{products}^{T=298.15K} - \sum LHV_{reagents}^{T=298.15K} \quad \text{Eq. 27}$$

$$\Delta H_{rx,Eq.25}^{T=298.15K} = LHV_{C_3H_6}^{T=298.15K} + LHV_{H_2}^{T=298.15K} - LHV_{C_3H_8}^{T=298.15K} \quad \text{Eq. 27b}$$

$$\begin{aligned} \Delta H_{rx,Eq.25}^{T=298.15K} &= 1.9257 \cdot 10^6 + 0.2418 \cdot 10^6 - (2.0431 \cdot 10^6) = 0.1244 \cdot 10^6 \quad \text{Eq. 27c} \\ &= 12.44 \cdot 10^4 \text{ kJ/kmol} \end{aligned}$$

Both by the enthalpy of formation and by the lower heating value, the same value of an endothermic heat of reaction of  $1.244 \cdot 10^5$  kJ/kmol is reached, as it should be. In fact, Eq. 26 and Eq. 27 already demonstrate a tendency, albeit quite subtle, of loss of information when using lower heating values path to calculate the heat of reaction: there is a subtle loss of significant digit when using Eq. 27 (lower heating values) compared to using enthalpies of formation in Eq. 26. This is associated with the relative high content of energy released in the combustion of these components (on the order of  $10^6$  kJ/kmol as expressed in Table 14), while the reaction enthalpy obtained by the difference of lower heating values is orders of magnitude lower (in this case, of  $10^5$  kJ/kmol). However, the most available experimental method to determine reaction enthalpies is through the calorimetry of the components involved in the reaction, the heat of reaction being obtained according to Eq. 27 (Dart; Oblad, 1949).

Nonetheless, it is important to emphasize this fact: even for this highly endothermic reaction, the heat of reaction amounts to only 6.1% of the LHV of propane. In other words, if there were an error of 6.1% (admittedly a large error) on the tabulated LHV of propane in Table 14, then this would result in a 100% error in the estimated value for propane dehydrogenation heat of reaction, i.e. it would be estimated an erroneous value of 0 kJ/kmol. This is a known predicament when estimating heats of reaction by the difference between large quantities like the LHV of the reactional components (Dart; Oblad, 1949; Moura; Pinho; Fusco, 2006).

When it comes to fluid catalytic cracking, it is more convenient to express the heat of reaction in units of mass. So, the dehydrogenation of propane, which is a cracking reaction, has a

heat of reaction of 2821 kJ/kg. This is, however, the heat of reaction at a reference temperature, in this case at 298 K. If the reaction takes place at different temperature levels, then it is necessary to account for enthalpy variations of the reaction components due to temperature changes.

Assuming no phase change and neglecting any variation due to mixing (Fogler, 2016), the effect of temperature on the enthalpy variation of a component  $i$  can be expressed by Eq. 28:

$$\Delta H_i^{(T_1 \rightarrow T_2)} = \int_{T_1}^{T_2} C_{p_i(T)} \cdot dT \quad \text{Eq. 28}$$

Thus the heat of reaction at a temperature  $T_1$  may be obtained through the reference LHV by Eq. 29:

$$\Delta H_{rx}^{T_1} = \sum_i \zeta_i \cdot \left( LHV_{product_i}^{T=298.15K} + \int_{298.15K}^{T_1} C_{p_i(T)} \cdot dT \right) - \sum_k \zeta_k \cdot \left( LHV_{reagent_k}^{T=298.15K} + \int_{298.15K}^{T_1} C_{p_k(T)} \cdot dT \right) \quad \text{Eq. 29}$$

Table 15 presents heat capacity data for the components involved in the reaction of Eq. 25. Constants displayed in Table 15 must be used in the  $C_p$  function presented in Eq. 30 (Green; Southard, 2019).

Table 15 - Heat capacities for components of Eq. 25

Component	Constant C1 x 10 <sup>-5</sup>	Constant C2 x 10 <sup>-5</sup>	Constant C3 x 10 <sup>-3</sup>	Constant C4 x 10 <sup>-5</sup>	Constant C5
Propane	0.5192	1.9245	1.6265	1.1680	723.6
Propylene	0.4339	1.5200	1.4250	0.7860	623.9
Hydrogen	0.2762	0.0956	2.4660	0.0376	567.6

Source: Green; Southard, 2019

$$C_p \left( \frac{J}{kmol \cdot K} \right) = C1 + C2 \cdot \left[ \frac{\frac{C3}{T(K)}}{\sinh\left(\frac{C3}{T(K)}\right)} \right]^2 + C4 \cdot \left[ \frac{\frac{C5}{T(K)}}{\cosh\left(\frac{C5}{T(K)}\right)} \right]^2 \quad \text{Eq. 30}$$

The integration of Eq. 28 with the Cp function of Eq. 30 results in Eq. 31:

$$\begin{aligned} \Delta H_i^{(T_1 \rightarrow T_2)} = & C1_i \cdot (T_2 - T_1) + C2 \cdot C3 \cdot \left[ \coth\left(\frac{C3}{T_2}\right) - \coth\left(\frac{C3}{T_1}\right) \right] \\ & - C4 \cdot C5 \cdot \left[ \tanh\left(\frac{C5}{T_2}\right) - \tanh\left(\frac{C5}{T_1}\right) \right] \end{aligned} \quad \text{Eq. 31}$$

Using Eq. 29 and Eq. 31, and data from Tables 14-15, it is possible to obtain, for example, the heat of dehydrogenation of propane at 873.15K (Eq. 32) of  $1.298 \cdot 10^5$  kJ/kmol, or 2944 kJ/kg of propane. This represents an increase of 4.4% in the heat of reaction that would have been ignored if the enthalpy correction term due to temperature change (Eq. 28) was not considered.

$$\begin{aligned} \Delta H_{rx, \text{Eq. 25}}^{T=873.15K} = & \left( \sum LHV_{products}^{T=298.15K} - \sum LHV_{reagents}^{T=298.15K} \right) \\ & + \left( \int_{298.15K}^{873.15K} C_{p_{Propylene}(T)} \cdot dT + \int_{298.15K}^{873.15K} C_{p_{H_2}(T)} \cdot dT \right. \\ & \left. - \int_{298.15K}^{873.15K} C_{p_{Propane}(T)} \cdot dT \right) \end{aligned} \quad \text{Eq. 32}$$

$$\begin{aligned} \Delta H_{rx, \text{Eq. 25}}^{T=873.15K} = & (1.244 \cdot 10^5) + (6.1123 \cdot 10^4 + 1.6962 \cdot 10^4 - 7.2376 \cdot 10^4) \\ = & 1.301 \cdot 10^5 \text{ kJ/kmol} \end{aligned} \quad \text{Eq. 32b}$$

Unfortunately, catalytic cracking of high boiling point hydrocarbons does not revolve around pure components for which there are plenty of thermodynamic available data. Only for dry gas and LPG, which are comprised of well-defined light hydrocarbons, it is possible to use available thermodynamic data for individual components; this could also apply, to some extent, to coke. However, for the vacuum gasoil feed and the liquid products, it becomes necessary to use correlations developed for petroleum fractions (API, 1997), both for lower heating values and for heat capacities.

Even using available correlations for the thermodynamic properties of hydrocarbon fractions, a difficulty remains for liquid products. Rigorously, a lump like naphtha contains some lighter C5 – C6 hydrocarbons and also some heavier C8 – C11 hydrocarbons; in addition, it contains saturated species, along with olefinic and aromatic components, each with different

enthalpies of formation (or LHV). The difficulty stems from the fact that if the thermodynamic properties is the same for the entire lump, then one fails to capture the effect of lump's composition (and therefore properties) variation with conversion along the riser. As a variation in the composition of the lump is expected in a similar way to the variation in the yield profile of the bulk lumped clusters along the riser, neglecting the former could lead to deviations in the heat of reaction estimated, and consequently in the estimated outlet temperature  $T_{rx}$ , which could certainly impact the kinetics of the phenomenological model.

In the literature there are different ways to manage the thermodynamic parameters involved in the riser energy balance in phenomenological modeling. Ahmed, Maulud, Ramasamy and Lau (2014) calculated thermodynamic properties for the lumps using correlations developed for petroleum fractions. Similarly, Olafadehan, Sunmola, Jaiyeola, Efevbokhan and Abatan (2018) select to assign a pure component to represent the entire lump; for example, it was selected n-octahexacontane ( $C_{68}H_{138}$ , for which the properties were estimated by group theory for linear alkanes) to represent vacuum residue and n-heptacosane ( $C_{27}H_{56}$ ) to represent VGO. It seems an odd choice to select a linear alkane to represent the vacuum residue feed when at the same time Olafadehan, Sunmola, Jaiyeola, Efevbokhan and Abatan (2018) report an 89 wt.% aromatic content for the feed.

Han, Chung (2001a, 2001b) report a trial and error attempt to estimate heats of reactions in order to minimize deviations in the energy balance of the FCC unit from experimental data. Values estimated by Han, Chung (2001a, 2001b) are presented in Table 16.

Table 16 - Heats of reaction for catalytic cracking reactions estimated by Han, Chung (2001a, 2001b)

Four lump cracking reaction	Heat of reaction (kJ/kg)
Gasoil to naphtha	195
Gasoil to C1 – C4 gases	670
Gasoil to coke	745
Naphtha to C1 – C4 gases	530
Naphtha to coke	690

Source: Han; Chung, 2001a, 2001b

John, Mustafa, Patel and Mutjaba (2019) included the estimation of thermodynamic parameters together with the estimation of kinetic parameters of the model. One of the disadvantages of this path is that the number of parameters to be estimated increases excessively. Table 17 shows all parameters estimated in the six lump phenomenological model of John, Mustafa, Patel and Mutjaba (2019). Including heats of reaction, the total number of parameters to be estimated amount to 45. If such a structure were to be used in the present work the number of experimental data would have to be much higher than the 69 runs available, in order to reasonably estimate the parameters and to account for the model validation (even using cross-validation technique).

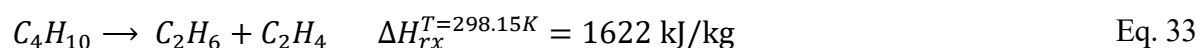
Table 17 - Kinetic and thermodynamic parameters estimated in the model of John, Mustafa, Patel and Mutjaba (2019)

Six lump cracking reaction	Frequency factor (s <sup>-1</sup> )	Activation energy (kJ/kmol)	Heat of reaction (kJ/kg) <sup>a</sup>
Gasoil to LCO	7957.29	53927.7	190.709
Gasoil to naphtha	14433.4	57186.6	128.45
Gasoil to coke	40.253	32433.6	458.345
Gasoil to LPG	2337.1	51308.6	209.192
Gasoil to dry gas	449.917	48620.4	44.543
LCO to coke	75.282	61159.4	305.925
LCO to naphtha	197.933	48114.5	513.568
LCO to LPG	3.506	67792.9	90.894
LCO to dry gas	3.395	64266.6	204.381
Naphtha to LPG	2.189	56194.4	225.082
Naphtha to dry gas	1.658	63319.1	19.667
Naphtha to coke	2.031	61785.1	117.212
LPG to dry gas	3.411	55513.0	17.618
LPG to coke	0.601	52548.2	11.839
Dry gas to coke	2.196	53046.0	52.863

<sup>a</sup> – This data is reported by John, Mustafa, Patel and Mutjaba (2019) as being in kJ/kmol, but it is very suggestive of a typo.

Source: John; Mustafa; Patel; Mutjaba, 2019.

Two curiosities drew attention in the model described by John, Mustafa, Patel and Mutjaba (2019). One is related to some values obtained for the heat of reaction in Table 17. For the reaction of LPG cracking into dry gas, for example, it was estimated a heat of reaction of 17.6 kJ/kg. To illustrate, applying the same procedure demonstrated for the dehydrogenation of propane to the cracking of n-butane to yield ethane and ethylene (Eq. 33), it is obtained a heat of reaction of 1622 kJ/kg of n-butane at a reference temperature of 298.15K, and a heat of reaction of 1550 kJ/kg at a typical catalytic cracking reaction temperature of 813.15K. In other words, if all parameters were estimated simultaneously with insufficient data, the set of parameters thus obtained may contain values that are not adherent to reality.



Another curiosity was that John, Mustafa, Patel and Mutjaba (2019) report a deviation of 37.9 K in the riser outlet temperature ( $T_{rx}$ ) estimated by the model (735.3 K) compared to an industrial data of 773.2 K. This is reported as an 5.15% difference, but it draws some attention that this difference in the absolute value of  $T_{rx}$  would have repercussions on the estimated value of CTO and consequently on the entire balance of the unit, including the yield profile. Also, while it seems reasonable a  $T_{rx}$  of 773.2 K (500°C) for highly crackable paraffinic feedstocks, the estimated  $T_{rx}$  of 735.3 K (462°C), on the other hand, seems unlikely for conventional gasoil feedstocks.

It is apparent that there is still room for improvement in the characterization of the energy balance of catalytic cracking reactions, even if it is in a direction of oversimplification focusing more on an empirical reproducibility of experimental data than a rigorous chemically consistent representation of the enthalpies of reactions involved.

Although the development of phenomenological modeling of catalytic cracking reactions has not entered the scope of the present work, adequate and consistent characterization of the heats of reaction and enthalpies as function of temperature for the lumps participating in the catalytic cracking reaction scheme is an important prerequisite to such a model. The discussions that follow were evolved amidst a pursuit of a better representation of the energy balance of catalytic cracking reaction along the riser.

Two evaluations were conducted in this regard. In one of them, an attempt was made to estimate the heat of reaction that would be obtained by the method of Eq. 29 for all test runs (i.e. using experimental yield data as an input to the analysis), using correlations (API, 1997) to estimate thermodynamic parameters for the VGO and liquid products. Experimental heats of

reaction obtained in this way shall be compared to the experimental values obtained by energy balance in the riser boundary. Possible differences for the estimated value of heat of reaction between these two experimental routes should be associated with an erroneous assessment of the energy balance for the tests in the large scale FCC pilot plant or errors when using the correlations (API, 1997) to estimate the calorific properties of the feed and liquid products.

In the other evaluation, the procedure for building an empirical model from Chapter 1 was repeated, this time substituting  $HC_{light}$  as an input variable related to feed quality for parameters able to reproduce the complete distillation curve of the VGO, as well as detailing the pure species composition of dry gas and LPG and substituting the single yield value of each lump of the liquid fraction (naphtha, LCO and slurry oil) for parameters able to reproduce the complete distillation curve of the liquid product as output variables. This model may be a useful tool to further explore possibilities towards a better characterization of the energy balance of catalytic cracking reaction along the riser.

## 2.2 Methodology

This section describes the enthalpy calculation procedure by calorimetry of feed and products for comparison with the value obtained by the energy balance of the riser envelope in the tests and also describes the statistical approach for building an empirical model fed with information from the distillation curves of the feed and liquid products.

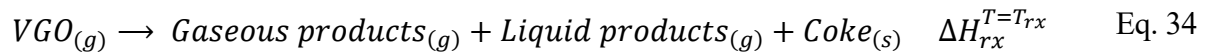
### 2.2.1 Heat of reaction by estimated calorimetry of feed and products

In the FCC, the experimental heat of reaction arises from the energy balance of the unit, being the unknown variable in the riser envelope. The experimental value obtained in this way is often used to assess the consistency of the overall energy balance of the unit.

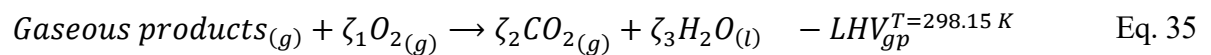
Another way to retrieve the experimental heat of reaction would be to estimate it as a difference between the lower heating values of products and feed, as described in the classical work of Dart, Oblad (1949) and introduced in section 2.1.

Experiments carried out in the large FCC pilot plant as described in section 1.2.1 were used in this evaluation. The feed characterization, the simulated distillation and density of the liquid product (comprising naphtha, LCO and slurry oil) and the complete composition of the gaseous products (dry gas and LPG) are available for the tests and these data were used to estimate the heat of reaction of each test by the calorimetric method.

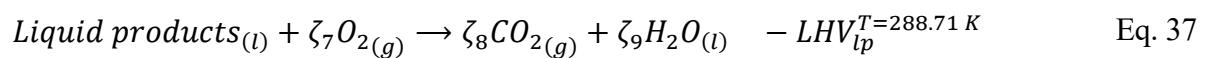
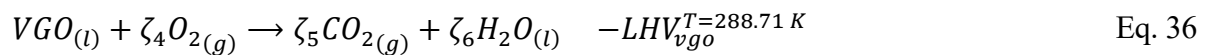
The catalytic cracking heat of reaction is usually referenced at the riser outlet temperature, i.e., at  $T_{rx}$ . In this way, as depicted in Eq. 34, all products (and feed) enthalpies are considered at the vaporized state, as they are in these conditions, except for coke that is formed on the catalyst at the solid state along the riser. Effect of pressure is neglected, as typically the operating gauge pressure is lower than 245 kPa.



Lower heating values, however, either for tabulated values (gaseous products) or taken from correlations for petroleum fractions (feed and liquid products) are obtained for the physical state in which the product is found at a given reference temperature. For gaseous products, the reference temperature is 298.15 K (Green; Southard, 2019) (Eq. 35). It must be remarked that, in Eq. 35, the enthalpy of this reaction equals the negative of the lower heating value since LHV are, by definition, positive values and combustion of hydrocarbons are exothermic reactions. The same applies for other products.



For feed and total liquid product lower heating values (Eq. 36 and Eq. 37, respectively) estimation, it was used the correlation of Eq. 38 presented by API (1997), which is referenced at 288.71 K (60°F) and is a function of API gravity of the liquid (defined by Eq. 39).



$$LHV \left( \frac{btu}{lb} \right) = 16796 + 54.5 \cdot API - 0.217 \cdot API^2 - 0.0019 \cdot API^3 \quad \text{Eq. 38}$$

$$API = \frac{141.5}{d_{60^\circ F}} - 131.5 \quad \text{Eq. 39}$$

As experimental specific gravities were measured at a temperature of 20°C ( $d_{20^\circ C}$ ), the conversion to  $d_{60^\circ F}$  was performed according to the correlation presented by Brasil (2004) in Eq. 40:

$$\text{for } 0.639 \leq d_{20^\circ C} \leq 0.931: \quad \text{Eq. 40}$$

$$d_{60^\circ F} = 0.0156 \cdot (d_{20^\circ C})^2 + 0.9706 \cdot d_{20^\circ C} + 0.0175$$

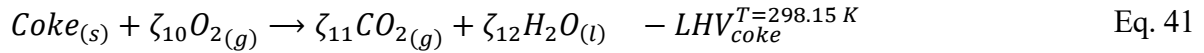
$$\text{for } 0.931 < d_{20^\circ C} \leq 1.055: \quad \text{Eq. 40b}$$

$$d_{60^\circ F} = 0.0638 \cdot (d_{20^\circ C})^2 + 0.8769 \cdot d_{20^\circ C} + 0.0628$$

Unfortunately, API (1997) reports an average deviation of 205 btu/lb of fuel (476.5 kJ/kg) for the correlation of LHV of Eq. 38, which seems little relevant for the case of combustion systems design, but it is in the order of magnitude of the heat of catalytic cracking reactions. Other correlations for LHV (Lima; Silva; Alberton, 2023) require the fuel's elementary composition of carbon and hydrogen of the fuel, which was not available. It would be necessary to estimate carbon and hydrogen contents through other correlations, which was considered not to provide better accuracy than the correlation of API (1997).

In regards of the lower heating value of coke (Eq. 41), it could be considered as graphite carbon, for which there is a tabulated data (Green; Southard, 2019) of  $3.9351 \cdot 10^5$  kJ/kmol (or  $3.2762 \cdot 10^4$  kJ/kg). However, strictly speaking, coke is a carbonaceous material that has some hydrogen content, both from condensed polyaromatic adsorbed on the catalyst (sometimes called “hard coke”) and from light hydrocarbons entrained to the regenerator (sometimes called “soft coke”, as it will also be accounted for as coke) (Sadeghbeigi, 2020). The typical range of hydrogen content in coke is 5.0 – 7.0 wt.% (Sadeghbeigi, 2020). Dart, Oblad (1949) presented an interesting way to account for the effect of this hydrogen content in coke lower heating value. They collected data on the enthalpy of combustion (and melting for liquid compounds) for aromatic hydrocarbons (and some non-aromatic as well) and proposed a graphical correlation between the enthalpy of combustion and the hydrogen content of the material. But they used the higher heating

value (HHV) basis, so it would demand a correction for water enthalpy of vaporization to use this correlation in the present work. Instead, Hosokai, Matsuoka, Kuramoto and Suzuki (2016) studied a large database of organic compounds including a database of 770 coals and they took into account the heat of fusion in the case of solid fuels to propose the following correlation of Eq. 42 to estimate the lower heating value (referenced at  $T = 298.15$  K) of solid fuels:



$$LHV \left( \frac{kJ}{g} \right) = 38.2 \cdot m_C + 84.9 \cdot (m_H - m_O/8) - (0.5 + 0.12) \quad \text{Eq. 42}$$

So, considering a hydrogen content in the coke of 0.06 (weight fraction), the LHV of coke would be 40.4 kJ/g ( $4.04 \cdot 10^4$  kJ/kg).

It is still necessary to correct the lower heating values from the reference condition in which it is measured to the condition of the component at the riser outlet. Eq. 43 through Eq. 46 bring about the enthalpy variations involved in this correction.

$$Gaseous\ products_{(g)}^{T=298.15K} \rightarrow Gaseous\ products_{(g)}^{T=T_{rx}} \quad \Delta H_{gp}^{298.15 K \rightarrow T_{rx}} \quad \text{Eq. 43}$$

$$VGO_{(l)}^{T=288.71K} \rightarrow VGO_{(g)}^{T=T_{rx}} \quad \Delta H_{vgo}^{288.71 K \rightarrow T_{rx}} \quad \text{Eq. 44}$$

$$Liquid\ products_{(l)}^{T=288.71K} \rightarrow Liquid\ products_{(g)}^{T=T_{rx}} \quad \Delta H_{lp}^{288.71 K \rightarrow T_{rx}} \quad \text{Eq. 45}$$

$$Coke_{(s)}^{T=298.15K} \rightarrow Coke_{(s)}^{T=T_{rx}} \quad \Delta H_{coke}^{298.15 K \rightarrow T_{rx}} \quad \text{Eq. 46}$$

$\Delta H_{gp}^{298.15 K \rightarrow T_{rx}}$  and  $\Delta H_{coke}^{298.15 K \rightarrow T_{rx}}$  can be estimated using API (1997) data for heat capacities of pure species and Eq. 28.

For VGO feed and total liquid product (naphtha + LCO + slurry oil), it is necessary to use a petroleum fraction correlation for enthalpy as a function of temperature and physical state. API (1997) also presents such correlation. The enthalpy of the liquid phase with a reduced temperature  $T_r \leq 0.8$  is estimated by Eq. 47:

$$H_{(l)}^{(T)} \left( \frac{btu}{lb} \right) = A_1 \cdot (T(R) - 259.7) + A_2 \cdot (T(R)^2 - 259.7^2) + A_3 \cdot (T(R)^3 - 259.7^3) \quad \text{Eq. 47}$$

Where:

$$A_1 = 10^{-3} \cdot \left[ -1171.26 + (23.722 + 24.907 \cdot d_{60^\circ F}) \cdot K_w + \frac{1149.82 - 46.535 \cdot K_w}{d_{60^\circ F}} \right] \quad \text{Eq. 47b}$$

$$A_2 = 10^{-6} \cdot (1.0 + 0.82463 \cdot K_w) \cdot \left( 56.086 - \frac{13.817}{d_{60^\circ F}} \right) \quad \text{Eq. 47c}$$

$$A_3 = -10^{-9} \cdot (1.0 + 0.82463 \cdot K_w) \cdot \left( 9.6757 - \frac{2.3653}{d_{60^\circ F}} \right) \quad \text{Eq. 47d}$$

Reduced temperature ( $T_r$ ) is defined as the ratio between absolute operating temperature ( $T$ , in Rankine in the case of API (1997)) and pseudocritical temperature ( $T_{pc}$ ) as shown in Eq. 48:

$$T_r = \frac{T}{T_{pc}} \quad \text{Eq. 48}$$

And  $T_{pc}$ , in turn, is obtained by the correlation shown in Eq. 49:

$$T_{pc}(R) = 10.6443 \cdot T_b^{0.81067} \cdot d_{60^\circ F}^{0.53691} \cdot \exp(-5.1747 \cdot 10^{-4} \cdot T_b - 0.54444 \cdot d_{60^\circ F} + 3.5995 \cdot 10^{-4} \cdot T_b \cdot d_{60^\circ F}) \quad \text{Eq. 49}$$

In Eq. 49, the mean average boiling point ( $T_b$ ) of the liquid stream is in degrees Rankine.

The enthalpy of the vapor phase (or liquid phase with  $T_r > 0.8$ ), neglecting the effect of pressure, is estimated by Eq. 50, with  $T_{pc}$  in Rankine:

$$H_{(v)}^{(T)} \left( \frac{btu}{lb} \right) = H_{(l)}^{(T=0.8 \cdot T_{pc})} + B_1 \cdot (T(R) - 0.8 \cdot T_{pc}) + B_2 \cdot (T(R)^2 - 0.64 \cdot T_{pc}^2) + B_3 \cdot (T(R)^3 - 0.512 \cdot T_{pc}^3) \quad \text{Eq. 50}$$

Where:

$$B_1 = 10^{-3} \cdot \left[ -356.44 + 29.72 \cdot K_w + B_4 \cdot \left( 295.02 - \frac{248.46}{d_{60^\circ F}} \right) \right] \quad \text{Eq. 50b}$$

$$B_2 = 10^{-6} \cdot \left[ -146.24 + (77.62 - 2.772 \cdot K_w) \cdot K_w - B_4 \cdot \left( 301.42 - \frac{253.87}{d_{60^\circ F}} \right) \right] \quad \text{Eq. 50c}$$

$$B_3 = 10^{-9} \cdot (-56.487 - 2.95 \cdot B_4) \quad \text{Eq. 50d}$$

For  $10.0 < K_w < 12.8$  and  $0.70 < d_{60^\circ F} < 0.885$ : Eq. 50e

$$B_4 = \left[ \left( \frac{12.8}{K_w} - 1.0 \right) \cdot \left( 1.0 - \frac{10.0}{K_w} \right) \cdot (d_{60^\circ F} - 0.885) \cdot (d_{60^\circ F} - 0.70) \cdot 10^4 \right]^2$$

For all other cases: Eq. 50f

$$B_4 = 0$$

Finally, considering the fact that the quantities of O<sub>2</sub>, CO<sub>2</sub> and H<sub>2</sub>O will cancel out, the heat of reaction of catalytic cracking at T<sub>rx</sub>, as defined in Eq. 34, can be calculated by combining the LHV terms of Eq. 35 (gaseous products), Eq. 36 (VGO feed), Eq. 37 (liquid products), Eq. 42 (coke) and sensible and/or latent heat terms of Eq. 43 (gaseous products), Eq. 44 (VGO feed), Eq. 45 (liquid products), Eq. 46 (coke) as shown in Eq. 51:

$$\begin{aligned} \Delta H_{rx}^{T=T_{rx}} = & w_{gp} \cdot (\Delta H_{gp}^{298.15 K \rightarrow T_{rx}} + LHV_{gp}^{T=298.15 K}) + w_{lp} \\ & \cdot (\Delta H_{lp}^{288.57 K \rightarrow T_{rx}} + LHV_{lp}^{T=288.57 K}) + w_{ck} \\ & \cdot (\Delta H_{ck}^{298.15 K \rightarrow T_{rx}} + LHV_{coke}^{T=298.15 K}) \\ & - (\Delta H_{vgo}^{288.57 K \rightarrow T_{rx}} + LHV_{vgo}^{T=288.57 K}) \end{aligned} \quad \text{Eq. 51}$$

The heat of reaction calculated in such manner, which resembles the form presented in Eq. 29 (as it should), shall be compared with the value that comes from the riser envelope energy balance.

### 2.2.2 Empirical modeling with retrieval of liquid product distillation curve

Carrying on the discussion on enthalpies involved in catalytic cracking reaction, it was proposed the formulation of an empirical model capable of returning the necessary data for the calculation of the enthalpy of reaction by the calorimetry method approach discussed in section 2.2.1. Experimental data raised in the large scale FCC pilot plant (section 1.2.1) were once more employed to obtain this model. The same general structure and building strategy of the empirical model for individual lumps dry gas, LPG, naphtha, LCO, slurry oil and coke (according to section 1.2.2) were used for this purpose, although with some required adjustments.

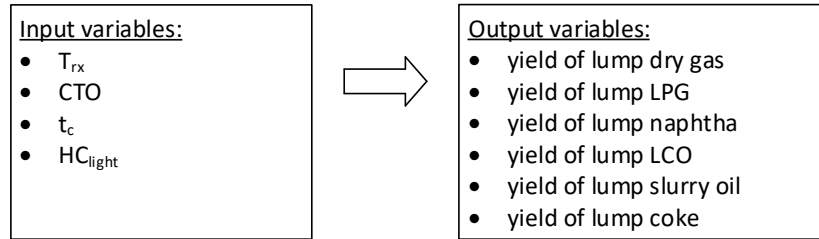
Complete composition of gaseous products (dry gas and LPG) was available, so for these products the modification consisted of a direct substitution of the grouped lumps for the corresponding individual components as outputs to the model. For coke there is no adjustment to be made. The greatest scope of modifications in the model was for vacuum gasoil feed and liquid products.

Both for VGO (Table 1) and the total liquid products, simulated distillation and density data were available. Simulated distillation of the liquid product accumulated in the pilot plant test storage tank (Figure 1) for each run is carried out precisely to allow discrimination of naphtha, LCO and slurry oil yields, since fractionation to obtain individual cuts is not a facility available in the routine operation of the pilot plant unit. Coupled with the density information, these data could be used to obtain thermodynamic properties (LHV and enthalpies as function of temperature) using correlations for petroleum fractions described in section 2.2.1. In this regard, yields of the lumps were replaced by density and distillation curve information of the liquid product as model responses.

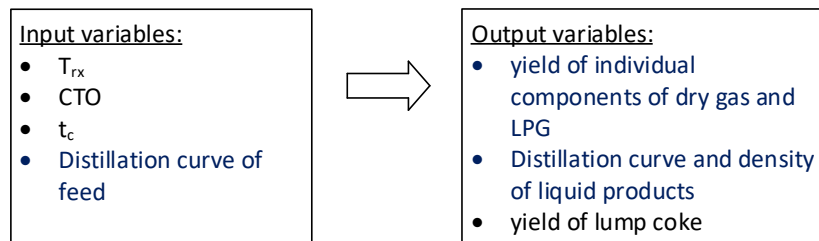
Figure 19 summarizes the adjustments made to Chapter 1 empiric model structure to obtain an empiric model able to provide data on liquid product characterization.

Figure 19 – Adjustments made to Chapter 1 empiric model structure to obtain an empiric model able to provide data on liquid product characterization

Empiric model of Chapter 1



Empiric model of Chapter 2



Source: The author, 2023.

At this point, the question remains of how to translate the complete distillation curve of the feed and products so that the model uses or predicts this information. As a matter of fact, the replacement of the explanatory variable  $HC_{light}$  for the complete distillation curve of the feed was not mandatory for the objective of obtaining a model capable of recovering the distillation curve of the products as a response. However, it was thought that this would be an improvement in the sense that the information contained in the feed distillation curve is more complete than a cut of the fraction with distillation point below  $343^{\circ}\text{C}$  of variable  $HC_{light}$ , although it was verified that the latter served perfectly well the purpose of explaining the higher LCO yield of feed “D” in section 1.3.1.

To translate the information contained in the distillation curves into the model, the experimental curves were expressed as polynomials, whose coefficients were estimated. It was selected a four degree polynomial to represent the experimental distillation curves. The polynomial of cumulative distilled mass fraction as a function of temperature could be written in the canonic form (Eq. 52):

$$P_{dist}^{cum}(T) = a_4 \cdot (T^4) + a_3 \cdot (T^3) + a_2 \cdot (T^2) + a_1 \cdot (T) + a_0 \quad \text{Eq. 52}$$

However, it was found more convenient to express the distillation curve by a Lagrange polynomial. Generically, Lagrange polynomials are interpolation polynomials with the format of Eq. 53, being  $n = 4$  for a four degree polynomial:

$$y(x) = \sum_{i=0}^n L_{i(x)} \cdot y_{(x_i)} \quad , L_{i(x)} = \begin{cases} 1, & \text{if } x = x_i \\ 0, & \text{if } x \neq x_i \end{cases} \quad \text{Eq. 53}$$

Where  $L_{i(x)}$  is itself a polynomial of order  $n$  defined by (Eq. 54):

$$L_{i(x)} = \prod_{\substack{j=0 \\ j \neq i}}^n \frac{x - x_j}{x_i - x_j} \quad \text{Eq. 54}$$

It is interesting to note that to obtain the polynomials  $L_{i(x)}$  (Eq. 54) no information is needed about the dependency between  $y$  and  $x$ , as these polynomials  $L_{i(x)}$  serve as weighting factors to recover the value of  $y$  for any given value of  $x$  ( $y_{(x)}$ ) previously knowing values of the dependent variable  $y$  for specific points (nodal points) from  $x$  in Eq. 53. For this reason, Lagrange polynomials are extensively used as an interpolation method in numerical calculus (Chapra; Canale, 2010).

At present case, given five nodal points  $T_p$  with  $p = 4$  and  $i = \{0; 1; 2; 3; 4\}$ , Eq. 52 can be written in Lagrange form as (Eq. 55):

$$P_{dist(T)}^{cum} = \sum_{i=0}^p L_{i(T)} \cdot P_{dist(T_{p_i})}^{cum} \quad , L_{i(T)} = \begin{cases} 1, & \text{if } T = T_{p_i} \\ 0, & \text{if } T \neq T_{p_i} \end{cases} \quad \text{Eq. 55}$$

Whereas  $L_{i(T)}$  is given by Eq. 56:

$$L_{i(T)} = \prod_{\substack{j=0 \\ j \neq i}}^n \frac{T - T_{p_j}}{T_{p_i} - T_{p_j}} \quad \text{Eq. 56}$$

As the number of nodal points  $T_p$  is (much) smaller than the number ( $n_d$ ) of experimental points ( $T_k$ ) of the distillation curve ( $n_d = 101$ ), this should not be treated as an interpolation by Lagrange polynomials, but as a regression that requires minimizing the error between the experimental curve and the estimated curve. It is one that uses the format and properties of the Lagrange polynomial for this purpose.

For every normalized (between 0 and 1) experimental point  $T_k$  of the distillation curve, Eq. 55 can be rewritten as Eq. 57:

$$P_{dist}^{cum,calc}(T_k) = \int_0^{T_k} \left( \sum_{i=0}^p \theta_i \cdot L_{i(T)} \right) dT \quad , \quad \begin{array}{l} i = 0, 1, \dots, p \\ k = 0, 1, 2, 3, \dots, 100 \end{array} \quad \text{Eq. 57}$$

Where now there are two weighting factors:  $L_{i(T)}$  as already mentioned, and  $\theta_i$ , which is the density of probability of  $P_{dist}^{cum}$  at  $T = T_{p_i}$ . It should be noted that  $P_{dist}^{cum}$  is a cumulative distribution since the maximum admissible value of  $P_{dist}^{cum}$  is 100% (Eq. 58):

$$\theta_i = \left. \frac{dP_{dist}^{cum}}{dT} \right|_{T=T_{p_i}} \quad \text{Eq. 58}$$

Since the sum  $\sum_{i=0}^p \theta_i \cdot L_{i(T)}$  is an integral, the order integral – sum can be inverted. Also, as the integral do not depend on the index  $i$ ,  $\theta_i$  can be removed from inside the integral. This way, Eq. 57 can be rearranged to Eq. 59:

$$P_{dist}^{cum,calc}(T_k) = \sum_{i=0}^p \theta_i \cdot \int_0^{T_k} L_{i(T)} dT \quad , \quad \begin{array}{l} i = 0, 1, \dots, p \\ k = 0, 1, 2, 3, \dots, 100 \end{array} \quad \text{Eq. 59}$$

Each integral part  $\int_0^{T_k} L_{i(T)} dT$  can be previously calculated. By defining it as a weighting factor  $w_{k,i}$  associated with polynomial  $L_{i(T)}$  integrated until point  $T_k$  (Eq. 60):

$$w_{k,i} = \int_0^{T_k} L_{i(T)} dT \quad , \quad \begin{array}{l} i = 0, 1, \dots, p \\ k = 0, 1, 2, 3, \dots, 100 \end{array} \quad \text{Eq. 60}$$

Thus, Eq. 59 can be rewritten as Eq. 61:

$$P_{dist}^{cum,calc}(T_k) = \sum_{i=0}^p \theta_i \cdot w_{k,i} \quad , \quad \begin{matrix} i = 0, 1, \dots, p \\ k = 0, 1, 2, 3, \dots, 100 \end{matrix} \quad \text{Eq. 61}$$

Eq. 61 can be written vectorially as Eq. 62:

$$\left\{ \begin{array}{l} P_{dist}^{cum,calc}(T_{k=0}) = \sum_{i=0}^p \theta_i \cdot w_{0,i} \\ P_{dist}^{cum,calc}(T_{k=1}) = \sum_{i=0}^p \theta_i \cdot w_{1,i} \\ \dots \\ P_{dist}^{cum,calc}(T_{k=100}) = \sum_{i=0}^p \theta_i \cdot w_{100,i} \end{array} \right. \quad , \quad i = 0, 1, \dots, p \quad \text{Eq. 62}$$

$$\begin{pmatrix} P_{dist}^{cum,calc}(T_{k=0}) \\ P_{dist}^{cum,calc}(T_{k=1}) \\ \dots \\ P_{dist}^{cum,calc}(T_{k=100}) \end{pmatrix} = \begin{pmatrix} w_{0,0} & w_{0,1} & \dots & w_{0,p} \\ w_{1,0} & w_{1,1} & \dots & w_{1,p} \\ \dots & \dots & \dots & \dots \\ w_{n_d-1,0} & w_{n_d-1,1} & \dots & w_{n_d-1,p} \end{pmatrix} \cdot \begin{pmatrix} \theta_0 \\ \theta_1 \\ \dots \\ \theta_p \end{pmatrix} \quad \text{Eq. 62b}$$

Since the cumulative probability for the first experimental point ( $T_{k=0}$ ) is zero, the first equation can be excluded, i.e., in the matrix of  $w_{k,i}$  elements, the first row is all zeros, the first column can be eliminated and  $\theta_0$  is deemed equal to zero and removed from the vector of parameters. Thus, Eq. 62b becomes Eq. 63:

$$\begin{pmatrix} P_{dist}^{cum,calc}(T_{k=0}) \\ P_{dist}^{cum,calc}(T_{k=1}) \\ \dots \\ P_{dist}^{cum,calc}(T_{k=100}) \end{pmatrix} = \begin{pmatrix} 0 & \dots & 0 \\ w_{1,1} & \dots & w_{1,p} \\ \dots & \dots & \dots \\ w_{100,1} & \dots & w_{100,p} \end{pmatrix} \cdot \begin{pmatrix} \theta_1 \\ \dots \\ \theta_p \end{pmatrix} \quad \text{Eq. 63}$$

$$\vec{P}_{dist}^{cum,calc} = \mathbf{W} \cdot \vec{\theta} \quad \text{Eq. 63b}$$

Now, it can be employed least squares between experimental and calculated cumulative distillation points to estimate the parameters  $\theta$  (Eq. 64):

$$\hat{\theta} = \arg \min (\vec{P}_{dist}^{cum,calc} - \vec{P}_{dist}^{cum,exp})^T \cdot (\vec{P}_{dist}^{cum,calc} - \vec{P}_{dist}^{cum,exp}) \quad \text{Eq. 64}$$

Thereby, the parameter estimation becomes (Eq. 65):

$$\hat{\theta} = (\mathbf{W}^T \cdot \mathbf{W})^{-1} \cdot \mathbf{W}^T \cdot \vec{P}_{dist}^{cum,exp} \quad \text{Eq. 65}$$

And the calculated cumulative distillation point is obtained by Eq. 66:

$$\vec{P}_{dist}^{cum,calc} = \mathbf{W} \cdot \hat{\theta} \quad \text{Eq. 66}$$

The nodal points  $T_p$  for the Lagrange polynomials were taken as the extreme points (initial and final distillations points), along with three evenly distributed center points. It was observed that, in comparison with multiple linear regression in the canonical polynomial format, expressing the least squares regression with this structure of Lagrange polynomials resulted in a monotonic form for the cumulative distillation curve (i.e. mass fraction distilled increasing continuously) near the end of the curve, which is more consistent.

However, the form of Eq. 66 is still not useful for handling the parameters in the empirical model, since the matrix  $\mathbf{W}$  is specific for each test due to the fact that the extreme points of the distillation curves ( $T_{k=0}$  and  $T_{k=100}$ ) are not the same for all runs. Only the three center nodal points are the same in all runs. At the same time, the initial boiling point of naphtha and the final boiling point of slurry oil are not relevant for yield estimation or characterization of these products, so there is no need to pursue an unlikely precise estimation for these extreme points. This way, the individual extreme nodal points ( $T_{k=0}$  and  $T_{k=100}$ ) for each run were replaced by extreme nodal points common to all distillation curves. The initial common nodal point was taken as the maximum initial boiling point found in all tests, and the final common nodal point was taken as the minimum initial boiling point found in all tests. Then, the densities of probability ( $\hat{\theta}$ ) for these common extreme nodal points were obtained by interpolation using previous nodal points for each test (Eq. 53 and Eq. 54).

Finally, retrieval of calculated distillation curve was performed using a slightly modified version of Eq. 57 that filters out any negative estimated value of density of probability of  $P_{dist}^{cum}$  at temperatures below the common initial nodal point (Eq. 67):

$$P_{dist}^{cum,calc}(T) = \int_0^T \left[ \max \left( 0; \sum_{i=0}^p \hat{\theta}_i \cdot \prod_{\substack{j=0 \\ j \neq i}}^n \frac{T - T_{p_j}}{T_{p_i} - T_{p_j}} \right) \right] dT \quad \text{Eq. 67}$$

Later, it was found that a sigmoidal function such as the logistic function expressed in Eq. 68 could be an alternative to the four degree polynomial representation of the dependence of  $P_{dist}^{cum}$  with temperature for the VGO feed distillation curve. The advantage of using a sigmoidal curve like Eq. 68 is that the distillation curve can be adequately represented using only two parameters (a and b).

$$P_{dist}^{cum}(T) = \frac{1}{1 + e^{-(aT+b)}} \quad \text{Eq. 68}$$

Eq. 68 can be conveniently linearized as Eq. 69. Thus, parameters a and b can be obtained through a simple linear regression of the modified experimental variable z function expressed in Eq. 69c.

$$\frac{1 - P_{dist}^{cum}(T)}{P_{dist}^{cum}(T)} = e^{-(aT+b)} \quad \text{Eq. 69}$$

$$\underbrace{\ln \left( \frac{1 - P_{dist}^{cum}(T)}{P_{dist}^{cum}(T)} \right)}_z = -aT - b \quad \text{Eq. 69b}$$

$$z = -aT - b \quad \text{Eq. 69c}$$

Subsequently, obtaining the empirical model with liquid products distillation curve as one of the responses (Figure 19) was achieved in a completely analogous way to the procedure described in Figure 2.

## 2.3 Results and discussion

### 2.3.1 Heat of reaction by estimated calorimetry of feed and products

Table 18 presents the characterization of the VGO feed necessary for estimating the heat of reaction using the enthalpy difference between products and reactants method.

Table 18 - Characterization of vaccum gasoil feed to obtain thermodynamic parameters

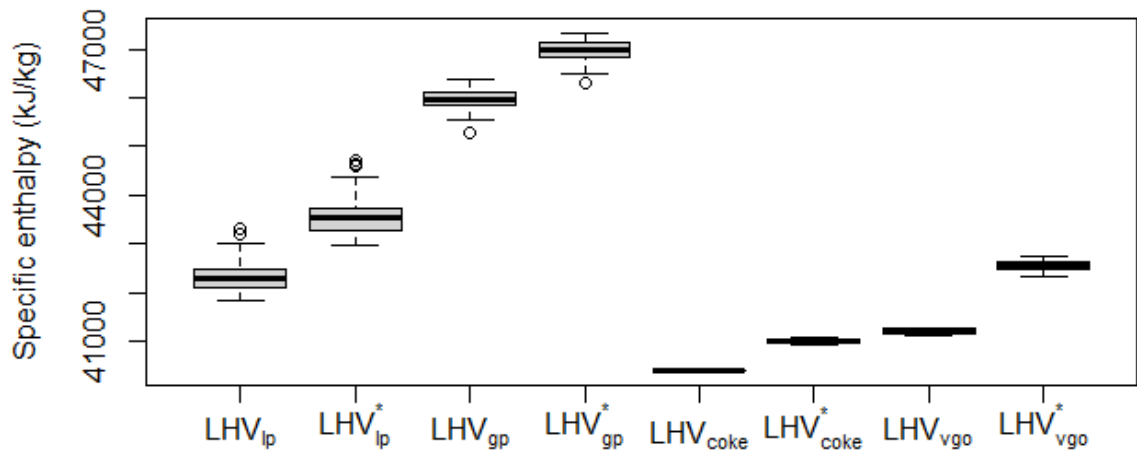
Feed	A1	A2	B	C	D
d <sub>20</sub> °C	0.9424	0.9448	0.9376	0.9382	0.9345
DS_0 wt.% (°C)	249.8	255.8	247.2	254.2	216.6
DS_10 wt.% (°C)	350	355.6	372.8	366.2	297
DS_30 wt.% (°C)	412.2	415.6	421.8	424.8	392.8
DS_50 wt.% (°C)	444.6	448.8	452	462	435.8
DS_70 wt.% (°C)	486.4	488	487.6	507.6	478
DS_90 wt.% (°C)	540.4	537.8	540.4	587.4	584.2
DS_100 wt.% (°C)	621.8	619.2	632	737.6	734.2
D86_0v.% (°C)	325.0	331.1	331.3	333.7	275.8
D86_10v.% (°C)	383.7	389.5	407.0	400.3	321.6
D86_30v.% (°C)	427.1	430.6	437.3	439.9	405.2
D86_50v.% (°C)	450.2	454.6	458.0	468.5	440.9
D86_70v.% (°C)	489.8	490.7	489.5	513.3	481.1
D86_90v.% (°C)	538.3	534.7	536.7	591.9	592.9
D86_100v.% (°C)	577.1	573.5	578.6	650.1	651.0
MeABP (°F)	839.0	844.6	857.2	877.8	795.2
d <sub>60</sub> °F	0.9459	0.9482	0.9411	0.9417	0.9380
K <sub>w</sub>	11.53	11.52	11.65	11.70	11.50
T <sub>pc</sub> (R)	1639.4	1645.4	1648.7	1664.0	1600.8
°API	18.1	17.7	18.9	18.8	19.4
LHV (kJ/kg)	41142	41103	41221	41211	41272

Source: The author, 2023.

For clarity, estimated thermodynamic properties for liquid products from tests performed at the FCC pilot plant (section 1.2.1) are presented in Annex 3.

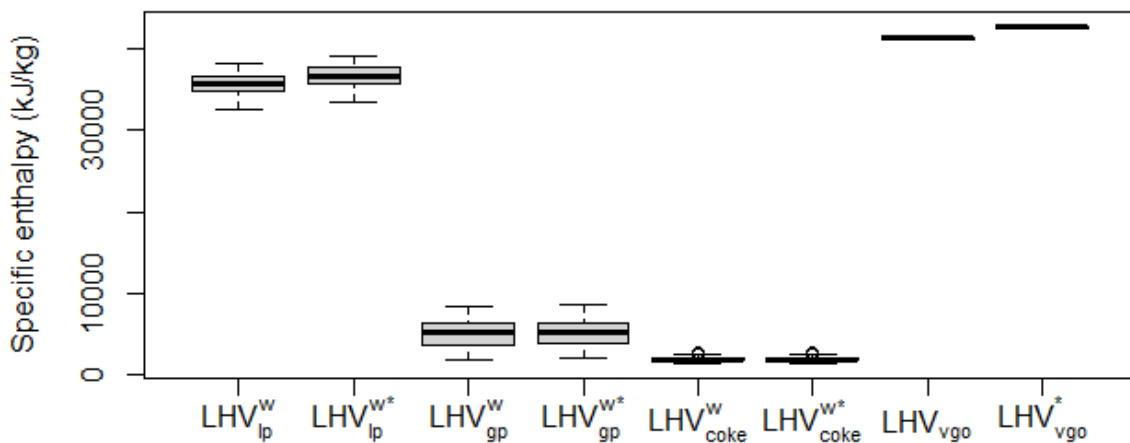
Figures 20-23 summarize in boxplot presentation the result of the intermediate calculations described in section 2.2.1 applied to the experimental data to obtain the estimated heat of catalytic cracking reactions by the calorimetric method.

Figure 20 - Boxplot of the lower heating values in kJ/kg of liquid product (lp), gas product (gp), coke and VGO at reference conditions. The (\*) notation refers to the lower heating value corrected to conditions at the riser outlet



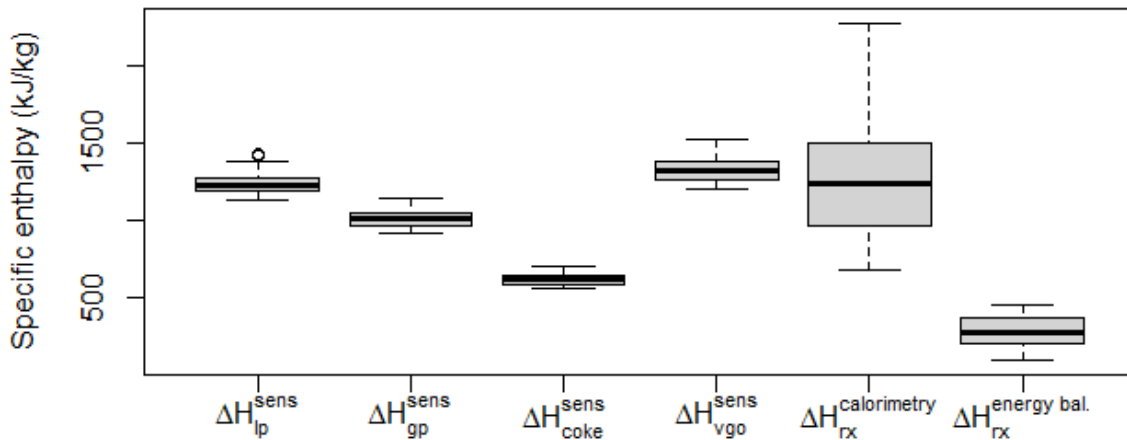
Source: The author, 2023.

Figure 21 - Boxplot of the yield-weighted lower heating values in kJ/kg of liquid product (lp), gas product (gp), coke and VGO at reference conditions. The (\*) notation refers to the lower heating value corrected to conditions at the riser outlet



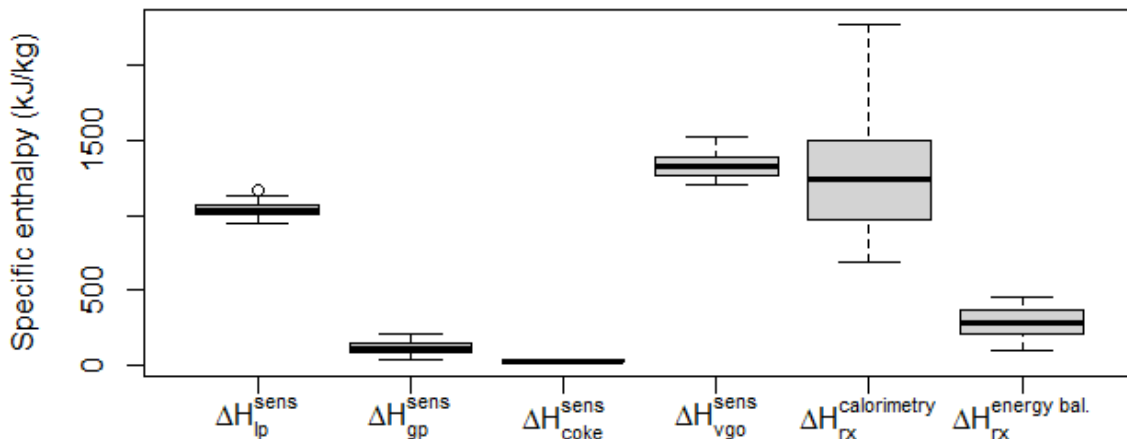
Source: The author, 2023.

Figure 22 - Boxplot of the resulting heat of reaction and sensible (and latent) heat in kJ/kg of liquid product (lp), gas product (gp), coke and VGO (reference conditions to the riser outlet)



Source: The author, 2023.

Figure 23 - Boxplot of the resulting heat of reaction and yield-weighted sensible (and latent) heat in kJ/kg of liquid product (lp), gas product (gp), coke and VGO (reference conditions to the riser outlet)



Source: The author, 2023.

The heat of reaction estimated by the calorimetric method is not presented in Figures 20-21 because the magnitude of the heat of reaction is considerably different from the lower heating values involved. In Figure 21 the lower heating values are weighted by the yields of the cracking products, thus the LHV for VGO feed is not altered. What draws attention is that even for the yield-weighted LHV of coke (varied between 1427 and 2889 kJ/kg when accounting for the sensible heat) any uncertainty in estimating such lower heating value could impact the estimated heat of reaction by this method, which varied between 684 and 2276 kJ/kg (Figures 22-23).

The heat of reaction obtained by the energy balance in the riser envelope in the pilot plant tests (varied between 96 and 454 kJ/kg) is considerably lower than the value estimated by the calorimetric method, being clearly at different levels in the boxplots of Figures 22-23.

The main hypothesis for this difference is in the estimation of the LHV of the liquid products (feed and cracked products) since the data for pure dry gas and LPG components are quite consolidated. Without disregarding the possibility of error in obtaining the heat of reaction by the energy balance of the riser, since in this methodology the heat of reaction is also obtained from calculations involving other considerable enthalpies such as that of coke combustion in the regenerator and it is a parameter that will carry all unit instrumentation errors, the estimation of LHV poses as the main suspect, as the LHV correlation already reports an average deviation of 205 btu/lb (477 kJ/kg).

To illustrate this further, Table 19 presents a survey of the experimental LHV reported by API (1997) for some components and the LHV that is obtained by correlation from the same author. In reality, it all indicates that the correlation of Eq. 38 was developed for heavy fuel oils, but even this reinforces the distrust for the applicability of this correlation to the case of products of cracking reactions.

Table 19 - Assessment of API correlation for LHV

Component	Exp. LHV (btu/lb) (Note 1)	$d_{20^{\circ}\text{C}}$ (Note 2)	$^{\circ}\text{API}$	Eq. 38 LHV (btu/lb) (Note 1)	Absolute error (btu/lb)	Absolute error (kJ/kg)	Relative error (%)
Benzene	17254	0.879	28.80	18140	886	2060	5.1
Toluene	17419	0.866	31.19	18227	808	1879	4.6
Ethylbenzene	17591	0.867	31.01	18221	630	1463	3.6
Cyclohexane	18672	0.779	49.20	18726	54	125	0.3
Methylcyclohexane	18632	0.769	51.53	18768	136	316	0.7
n-Hexane	19229	0.659	81.63	18765	-464	-1078	-2.4
2,2-Dimethylbutane	19159	0.649	84.86	18697	-462	-1074	-2.4
n-Heptane	19153	0.684	73.96	18871	-282	-655	-1.5
2,4-Dimethylpentane	19107	0.675	76.66	18843	-264	-614	-1.4

Note 1: Source: API, 1997; Note 2: Source: Green; Southard, 2019.

Source: The author, 2023.

Table 19 shows that the correlation for LHV of Eq. 38 (API, 1997), when applied to light hydrocarbons that are present in cracked naphtha, results in relative errors of up to 5% (an absolute error of 2060 kJ/kg, quite above the experimental range of heat of reaction obtained by

energy balance of the riser) for the aromatic compounds. It is interesting to note that the error changes direction: for aromatics, the correlation estimates a higher LHV than the experimental value; for saturated hydrocarbons, the correlation estimates a lower LHV. So, it appears that the correlation does not capture well the effect of chemical composition on the LHV, which is absolutely required when coping with cracked products at different conversion levels.

Without an in-depth experimental investigation to obtain correlations that best represent the LHV of feed and cracked products, any attempt to further develop a function for heat of reaction and enthalpy of the products in the riser seems questionable. In this scenario, an envisioned alternative would be to double down on the empiricism and to propose the use of a single heat of reaction for the actual conversion reactions (i.e. those that convert the feed into components other than LCO or slurry oil) coherent with experimental (energy balance of the riser method) data while considering a zero value for other secondary reactions. For example, considering a heat of cracking of 580 kJ per kg of converted feed (like it was considered in section 1.2.5) in this alternative proposal Table 17 would become Table 20.

Whatever reaction mechanism that is taking place in heat generation or absorption along the riser, using a unique value of heat reaction for all reactions related to the conversion of heavy components (i.e. vacuum gasoil, slurry oil and LCO) into lighter hydrocarbons would at least make this approach consistent with the observed value of endothermic heat of reaction by the riser energy balance.

Table 20 - Modified version of Table 17 with the proposal to use a single heat of reaction for reactions converting feed into light hydrocarbons

Six lump cracking reaction	Frequency factor (s <sup>-1</sup> )	Activation energy (kJ/kmol)	Proposed heat of reaction (kJ/kg)
Gasoil to LCO	7957.29	53927.7	0
Gasoil to naphtha	14433.4	57186.6	580
Gasoil to coke	40.253	32433.6	580
Gasoil to LPG	2337.1	51308.6	580
Gasoil to dry gas	449.917	48620.4	580
LCO to coke	75.282	61159.4	580
LCO to naphtha	197.933	48114.5	580
LCO to LPG	3.506	67792.9	580
LCO to dry gas	3.395	64266.6	580
Naphtha to LPG	2.189	56194.4	0
Naphtha to dry gas	1.658	63319.1	0
Naphtha to coke	2.031	61785.1	0
LPG to dry gas	3.411	55513.0	0
LPG to coke	0.601	52548.2	0
Dry gas to coke	2.196	53046.0	0

Source: Adapted from John; Mustafa; Patel; Mutjaba, 2019.

### 2.3.2 Empirical modeling with retrieval of liquid product distillation curve

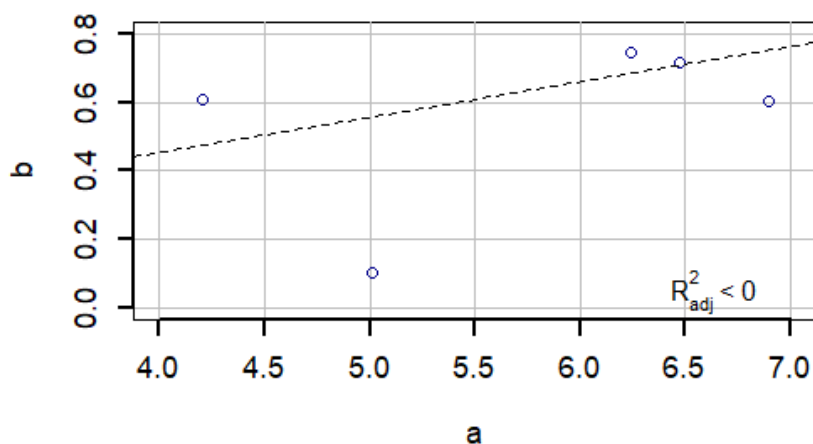
Experimental data on the complete composition of dry gas and LPG lumps are presented in Annex 4. Along with dry gas and LPG yield data of Annex 2, it is possible to calculate individual yields of components of dry gas and LPG. For the sake of concision, n-butane and isobutane were grouped as butanes, and the isomers of C<sub>4</sub>H<sub>8</sub> together with 1,3-butadiene were grouped as butylenes. In several runs there was an issue with the chromatography of the gaseous product for H<sub>2</sub>S (reported value zero), so it was decided to group this component with the H<sub>2</sub> in the dry gas.

For VGO feed, it was opted to characterize the distillation curves by the logistic function of Eq. 69 which only demands two parameters to accomplish this objective. Annex 5 presents the

complete simulated distillation data of the batches of vacuum gasoil employed in the study along with parameters  $a$  and  $b$  obtained both initially with normalized distillation temperatures (between -1 and 1) and in terms of the original distillation temperature in °C through linear regression of Eq. 69c.

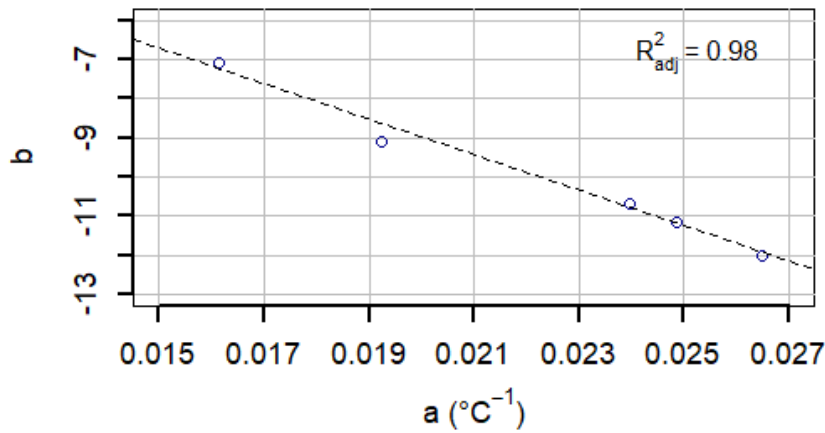
Normalizing experimental data before performing numerical matrix calculations is a good practice, but in this case it assumes even greater importance because power and exponential functions (such as Arrhenius equation frequently used in kinetic models) may present a high correlation among estimated parameters which could cause significant numerical difficulties (Schwaab; Pinto, 2008). Figure 24 shows that, in terms of normalized temperatures, parameters  $a$  and  $b$  are not correlated with each other. On the other hand, in Figure 25 parameters  $a$  and  $b$  exhibit a high degree of linear dependence. Thus, parameters  $a$  and  $b$  of Figure 24 were carried for the construction of the empirical model.

Figure 24 – Parameters  $a$  and  $b$  of the logistic function (Eq. 68) estimated for the VGO feed distillation curves at normalized temperatures between -1 and 1



Source: The author, 2023.

Figure 25 - Parameters a and b of the logistic function (Eq. 68) estimated for the VGO feed distillation curves at original temperatures in °C



Source: The author, 2023.

For total liquid product (naphtha, LCO and slurry oil), characterization of the distillation curves by the logistic function of Eq. 68 was tried, but it was verified that this function did not represent very well the distillation of the cracked product. While for vacuum gasoil an unimodal behavior for the densities of probability curve of  $P_{dist}^{cum}(T)$  with temperature was observed (which is adequately described by the logistic function of Eq. 68), for the cracked product the densities of probability curve of  $P_{dist}^{cum}(T)$  showed a bimodal behavior, for which the logistic function of Eq. 68 is not well suited. It was found that to represent bimodality it would be necessary to use a sigmoidal function with more parameters, such as that of Eq. 70:

$$P_{dist}^{cum}(T) = \frac{c}{1 + e^{-(aT+b)}} + \frac{1-c}{1 + e^{-(gT+h)}} \quad \text{Eq. 70}$$

Eq. 70 cannot be linearized as the simpler logistic function was in Eq. 69, so the parameters must be estimated through an optimization process, which does not impose a difficulty per se. Eq. 70 requires estimating five parameters, just like the procedure described in section 2.2.2 using Lagrange polynomials. Nevertheless, it was opted to proceed with the four degree Lagrange polynomials method (section 2.2.2) to the liquid products.

Annex 6 presents the complete simulated distillation data of the liquid products of each test along with densities of probability ( $\hat{\theta}$ ) of  $P_{dist}^{cum}(T)$  at nodal points: (a) original nodal points set in which the initial and final nodal points are particular for each test as they are taken from the experimental distillation curve of each test, and (b) common nodal points set in which nodal

points are the same for all tests. The distillation curve can be recovered from these densities of probability by using Eq. 67. Annex 6 also contains density data of the liquid products.

A QR decomposition analysis was then performed to determine whether parameters  $\theta_0$ ,  $\theta_1$ ,  $\theta_2$ ,  $\theta_3$ ,  $\theta_4$  were linearly independent. It resulted in that there is a considerable linear dependence of one of the parameters towards the others, i.e.,  $\theta_4$ , for example, could be obtained as a linear function of  $\theta_0$ ,  $\theta_1$ ,  $\theta_2$ ,  $\theta_3$  with relatively little loss of information content. The densities of probability were originally estimated using distillation temperatures normalized between 0 and 1. It was found that this trend of one of the parameters to present a considerable linear dependence with the others is maintained even by normalizing distillation temperatures between -1 and 1, or by subtracting the original temperatures by a reference temperature prior to normalization. As the linear dependence is not thorough and these parameters are outputs of the model, it was opted to proceed with modeling of the complete set of parameters  $\theta_0$ ,  $\theta_1$ ,  $\theta_2$ ,  $\theta_3$ ,  $\theta_4$ .

Another QR decomposition analysis was performed including the liquid product density ( $d_{20}$ ) variable. The tendency of one parameter displaying a considerable linear dependence with the others was not modified, indicating that this linear dependence was already present before inclusion of  $d_{20}$ , and that the liquid density was not involved in this linear dependency. This was later confirmed by trying to obtain a linear model of  $d_{20}$  as a function of the distillation curve parameters  $\theta_0$ ,  $\theta_1$ ,  $\theta_2$ ,  $\theta_3$ ,  $\theta_4$ . It was found upon using all parameters  $\theta_0$ ,  $\theta_1$ ,  $\theta_2$ ,  $\theta_3$ ,  $\theta_4$  that all coefficients, but the intercept, in the linear regression to estimate  $d_{20}$  are statistically not significant and the coefficient of determination ( $R^2$ ) obtained is 0.63. The maximum number of parameters  $\theta_0$ ,  $\theta_1$ ,  $\theta_2$ ,  $\theta_3$ ,  $\theta_4$  to be included in the regression so that all regression coefficients remain significant is two, and the obtained fit remains very poor ( $R^2$  around 0.63). This is an important result, in which the density of the liquid product is not directly linearly obtained by the information of the distillation curve embedded in the parameters  $\theta_0$ ,  $\theta_1$ ,  $\theta_2$ ,  $\theta_3$ ,  $\theta_4$ . This implies that similar distillation curves of cracked products could have somewhat different densities, which means that intrinsic chemical composition of fractions of similar boiling point range is distinct. Thus, another empiric model should be devised to return the density of the liquid product independently of the distillation curve parameters.

After defining the input and output variables (Figure 19), the empirical models were built following the forward selection of the candidate variables (which included quadratic and two-way interaction terms), accordingly to Figure 2. Table 21 and Figure 26 present the models and the fit to experimental data obtained. Table 21 also includes coefficients for the parameters in the normalized dimensionless form (between -1 and 1) as discussed in section 1.3.1.

It was later realized that it was necessary to include the estimation of the yield of  $C_5^+$  (pentanes and other light components of cracked naphtha) in the modeling, in order to eliminate deviation from normality for the calculated reconstituted yield of naphtha (Figure 27c). These components are actually recovered in the sampled gaseous stream before being sent to flare in the pilot plant (Figure 1) and correspond to the naphtha's light fraction that was not condensed in the gas-liquid separation system of the unit's product recovery section. Without taking  $C_5^+$  into account, the calculated reconstituted naphtha yield points were fully below the line of  $y_{calc} = y_{exp}$ . Upon accounting for  $C_5^+$  yield (which is obtained experimentally according to **Erro! Fonte de referência não encontrada.**), this deviation for naphtha was eliminated. So, an empiric model for  $C_5^+$  yield was included in this analysis, although this value is greatly influenced by the efficiency of the condensation system in the product recovery section of the pilot plant. In fact, this light naphtha fraction can be recovered as  $C_5^+$  in the gas stream or as the lower distillation temperature fraction in the liquid product accumulated in the storage tank, so variations in the condensing system can also affect the initial points of the distillation curve of the liquid product. A more dedicated consideration on this issue of how to treat the presence of  $C_5^+$  (for example considering them as pure components and removing them from the distillation curve of the liquid product) would be interesting, but it is not included in the present scope.

$$C_5^+ yield_{(wt.\%)} = \frac{C_5^+ \text{ content in the sampled gas}_{(wt.\%)} \cdot LPG \text{ yield}_{(wt.\%)}}{Total \text{ LPG content in the sampled gas}_{(wt.\%)}} \quad \text{Eq. 71}$$

Table 21 - Empirical models with retrieval of complete characterization of cracking products for heat of reaction estimation

Product (or Output)	Input variables in physical units			Dimensionless normalized input variables	
	Variables	Coefficients	95% level CI	Coefficients	95% level CI
H <sub>2</sub> + H <sub>2</sub> S	Intercept	-1.034	$\pm 3.479 \cdot 10^{-1}$	$2.364 \cdot 10^{-1}$	$\pm 2.973 \cdot 10^{-2}$
	T <sub>rx</sub> (K)	$1.934 \cdot 10^{-3}$	$\pm 8.229 \cdot 10^{-4}$	$9.146 \cdot 10^{-2}$	$\pm 3.884 \cdot 10^{-2}$
	t <sub>c</sub> (s)	$2.745 \cdot 10^{-1}$	$\pm 1.857 \cdot 10^{-1}$	---	---
	a (Figure 24)	$-7.566 \cdot 10^{-2}$	$\pm 3.579 \cdot 10^{-2}$	---	---
	b (Figure 24)	-1.089	$\pm 3.735 \cdot 10^{-1}$	$-3.093 \cdot 10^{-2}$	$\pm 3.087 \cdot 10^{-2}$
	a*b	$1.788 \cdot 10^{-1}$	$\pm 8.456 \cdot 10^{-2}$	$7.742 \cdot 10^{-2}$	$\pm 3.662 \cdot 10^{-2}$
	t <sub>c</sub> <sup>2</sup>	$-1.040 \cdot 10^{-1}$	$\pm 7.033 \cdot 10^{-2}$	$-8.611 \cdot 10^{-2}$	$\pm 5.824 \cdot 10^{-2}$
Coeff. of determination (R <sup>2</sup> )	0.664	---	---	---	
Methane	Intercept	$5.093 \cdot 10^1$	$\pm 2.724 \cdot 10^1$	$7.624 \cdot 10^{-1}$	$\pm 3.563 \cdot 10^{-2}$
	T <sub>rx</sub> (K)	$-1.312 \cdot 10^{-1}$	$\pm 6.680 \cdot 10^{-2}$	$5.672 \cdot 10^{-1}$	$\pm 8.437 \cdot 10^{-2}$
	t <sub>c</sub> (s)	-3.566	$\pm 1.708$	$1.944 \cdot 10^{-1}$	$\pm 5.636 \cdot 10^{-2}$
	CTO (m/m)	$2.312 \cdot 10^{-2}$	$\pm 2.174 \cdot 10^{-2}$	$8.438 \cdot 10^{-2}$	$\pm 7.937 \cdot 10^{-2}$
	a (Figure 24)	$-8.245 \cdot 10^{-2}$	$\pm 4.981 \cdot 10^{-2}$	---	---
	b (Figure 24)	-1.081	$\pm 6.533 \cdot 10^{-1}$	---	---
	T <sub>rx</sub> *t <sub>c</sub>	$4.725 \cdot 10^{-3}$	$\pm 2.213 \cdot 10^{-3}$	$2.030 \cdot 10^{-1}$	$\pm 9.504 \cdot 10^{-2}$
	a*b	$1.948 \cdot 10^{-1}$	$\pm 1.177 \cdot 10^{-1}$	$8.436 \cdot 10^{-2}$	$\pm 5.096 \cdot 10^{-2}$
	T <sub>rx</sub> <sup>2</sup>	$8.562 \cdot 10^{-5}$	$\pm 4.104 \cdot 10^{-5}$	$1.908 \cdot 10^{-1}$	$\pm 9.146 \cdot 10^{-2}$
Coeff. of determination (R <sup>2</sup> )	0.941	---	---	---	

Table 21 - Empirical models with retrieval of complete characterization of cracking products for heat of reaction estimation (cont.)

Product (or Output)	Input variables in physical units			Dimensionless normalized input variables	
	Variables	Coefficients	95% level CI	Coefficients	95% level CI
Ethane	Intercept	-5.620	$\pm 5.032$	$5.464 \cdot 10^{-1}$	$\pm 1.964 \cdot 10^{-2}$
	T <sub>rx</sub> (K)	$7.559 \cdot 10^{-3}$	$\pm 6.240 \cdot 10^{-3}$	$4.296 \cdot 10^{-1}$	$\pm 3.565 \cdot 10^{-2}$
	t <sub>c</sub> (s)	-1.301	$\pm 8.710 \cdot 10^{-1}$	$1.329 \cdot 10^{-1}$	$\pm 2.919 \cdot 10^{-2}$
	CTO (m/m)	$-3.053 \cdot 10^{-2}$	$\pm 1.951 \cdot 10^{-2}$	---	---
	a (Figure 24)	$-6.654 \cdot 10^{-1}$	$\pm 5.591 \cdot 10^{-1}$	$3.688 \cdot 10^{-2}$	$\pm 1.952 \cdot 10^{-2}$
	b (Figure 24)	$1.016 \cdot 10^1$	$\pm 3.220$	---	---
	T <sub>rx</sub> *t <sub>c</sub>	$1.809 \cdot 10^{-3}$	$\pm 1.129 \cdot 10^{-3}$	$7.772 \cdot 10^{-2}$	$\pm 4.850 \cdot 10^{-2}$
	T <sub>rx</sub> *a	$8.661 \cdot 10^{-4}$	$\pm 7.171 \cdot 10^{-4}$	$5.501 \cdot 10^{-2}$	$\pm 4.555 \cdot 10^{-2}$
	T <sub>rx</sub> *b	$-1.336 \cdot 10^{-2}$	$\pm 3.599 \cdot 10^{-3}$	$-2.030 \cdot 10^{-1}$	$\pm 5.469 \cdot 10^{-2}$
	CTO*b	$7.214 \cdot 10^{-2}$	$\pm 4.610 \cdot 10^{-2}$	$8.475 \cdot 10^{-2}$	$\pm 5.416 \cdot 10^{-2}$
Coeff. of determination (R <sup>2</sup> )	0.950	---	---	---	
Ethylene	Intercept	-4.957	5.862	$6.707 \cdot 10^{-1}$	$2.931 \cdot 10^{-2}$
	T <sub>rx</sub> (K)	$7.069 \cdot 10^{-3}$	$7.220 \cdot 10^{-3}$	$5.528 \cdot 10^{-1}$	$6.171 \cdot 10^{-2}$
	t <sub>c</sub> (s)	-2.690	1.165	$1.641 \cdot 10^{-1}$	$4.555 \cdot 10^{-2}$
	CTO (m/m)	$-6.918 \cdot 10^{-1}$	$5.028 \cdot 10^{-1}$	---	---
	a (Figure 24)	$2.964 \cdot 10^{-2}$	$1.862 \cdot 10^{-2}$	$3.987 \cdot 10^{-2}$	$2.505 \cdot 10^{-2}$
	b (Figure 24)	$1.022 \cdot 10^1$	4.618	---	---
	T <sub>rx</sub> *t <sub>c</sub>	$3.588 \cdot 10^{-3}$	$1.520 \cdot 10^{-3}$	$1.541 \cdot 10^{-1}$	$6.527 \cdot 10^{-2}$
	T <sub>rx</sub> *CTO	$7.921 \cdot 10^{-4}$	$5.902 \cdot 10^{-4}$	$1.365 \cdot 10^{-1}$	$1.017 \cdot 10^{-1}$
	T <sub>rx</sub> *b	$-1.405 \cdot 10^{-2}$	$5.102 \cdot 10^{-3}$	$-2.135 \cdot 10^{-1}$	$7.752 \cdot 10^{-2}$
	CTO*b	$1.375 \cdot 10^{-1}$	$7.257 \cdot 10^{-2}$	$1.615 \cdot 10^{-1}$	$8.526 \cdot 10^{-2}$
Coeff. of determination (R <sup>2</sup> )	0.950	---	---	---	

Table 21 - Empirical models with retrieval of complete characterization of cracking products for heat of reaction estimation (cont.)

Product (or Output)	Input variables in physical units			Dimensionless normalized input variables	
	Variables	Coefficients	95% level CI	Coefficients	95% level CI
Propane	Intercept	$1.113 \cdot 10^1$	6.242	$7.571 \cdot 10^{-1}$	$4.810 \cdot 10^{-2}$
	T <sub>rx</sub> (K)	$-1.423 \cdot 10^{-2}$	$6.941 \cdot 10^{-3}$	---	---
	t <sub>c</sub> (s)	$-1.450 \cdot 10^{-1}$	$1.840 \cdot 10^{-1}$	$1.502 \cdot 10^{-1}$	$8.275 \cdot 10^{-2}$
	CTO (m/m)	$1.967 \cdot 10^{-1}$	$1.810 \cdot 10^{-1}$	$2.694 \cdot 10^{-1}$	$8.827 \cdot 10^{-2}$
	a (Figure 24)	-2.051	1.000	---	---
	T <sub>rx</sub> *a	$2.564 \cdot 10^{-3}$	$1.250 \cdot 10^{-3}$	$1.628 \cdot 10^{-1}$	$7.941 \cdot 10^{-2}$
	t <sub>c</sub> *CTO	$4.194 \cdot 10^{-2}$	$3.721 \cdot 10^{-2}$	$1.393 \cdot 10^{-1}$	$1.236 \cdot 10^{-1}$
	CTO <sup>2</sup>	$-1.206 \cdot 10^{-2}$	$1.056 \cdot 10^{-2}$	$-1.607 \cdot 10^{-1}$	$1.406 \cdot 10^{-1}$
Coeff. of determination (R <sup>2</sup> )	0.670	---	---	---	
Propylene	Intercept	$-1.223 \cdot 10^1$	5.440	4.085E	$1.475 \cdot 10^{-1}$
	T <sub>rx</sub> (K)	$1.792 \cdot 10^{-2}$	$7.107 \cdot 10^{-3}$	$8.457 \cdot 10^{-1}$	$3.355 \cdot 10^{-1}$
	t <sub>c</sub> (s)	$-9.739 \cdot 10^{-1}$	$6.535 \cdot 10^{-1}$	$7.546 \cdot 10^{-1}$	$2.866 \cdot 10^{-1}$
	CTO (m/m)	$1.207 \cdot 10^{-1}$	$6.950 \cdot 10^{-2}$	1.616	$3.777 \cdot 10^{-1}$
	t <sub>c</sub> *CTO	$2.440 \cdot 10^{-1}$	$1.311 \cdot 10^{-1}$	$8.104 \cdot 10^{-1}$	$4.353 \cdot 10^{-1}$
	Coeff. of determination (R <sup>2</sup> )	0.905	---	---	---

Table 21 - Empirical models with retrieval of complete characterization of cracking products for heat of reaction estimation (cont.)

Product (or Output)	Input variables in physical units			Dimensionless normalized input variables	
	Variables	Coefficients	95% level CI	Coefficients	95% level CI
Butanes	Intercept	$-6.638 \cdot 10^1$	$5.128 \cdot 10^1$	1.793	$9.389 \cdot 10^{-2}$
	$T_{rx}$ (K)	$1.707 \cdot 10^{-1}$	$1.288 \cdot 10^{-1}$	$-3.189 \cdot 10^{-1}$	$1.644 \cdot 10^{-1}$
	$t_c$ (s)	-1.405	1.014	$3.468 \cdot 10^{-1}$	$1.492 \cdot 10^{-1}$
	CTO (m/m)	$1.341 \cdot 10^{-1}$	$2.888 \cdot 10^{-2}$	1.140	$2.170 \cdot 10^{-1}$
	a (Figure 24)	$2.926 \cdot 10^{-1}$	$1.134 \cdot 10^{-1}$	---	---
	b (Figure 24)	3.838	1.487	---	---
	$t_c \cdot CTO$	$1.351 \cdot 10^{-1}$	$6.693 \cdot 10^{-2}$	$4.487 \cdot 10^{-1}$	$2.223 \cdot 10^{-1}$
	$a \cdot b$	$-6.913 \cdot 10^{-1}$	$2.679 \cdot 10^{-1}$	$-2.994 \cdot 10^{-1}$	$1.160 \cdot 10^{-1}$
	$T_{rx}^2$	$-1.109 \cdot 10^{-4}$	$8.265 \cdot 10^{-5}$	$-2.472 \cdot 10^{-1}$	$1.842 \cdot 10^{-1}$
	$t_c^2$	$2.983 \cdot 10^{-1}$	$2.590 \cdot 10^{-1}$	$2.470 \cdot 10^{-1}$	$2.144 \cdot 10^{-1}$
Coeff. of determination ( $R^2$ )	0.832	---	---	---	
Butylenes	Intercept	$-1.336 \cdot 10^1$	6.838	4.772	$1.580 \cdot 10^{-1}$
	$T_{rx}$ (K)	$2.003 \cdot 10^{-2}$	$7.954 \cdot 10^{-3}$	$9.457 \cdot 10^{-1}$	$3.755 \cdot 10^{-1}$
	$t_c$ (s)	-1.027	$6.501 \cdot 10^{-1}$	1.049	$2.965 \cdot 10^{-1}$
	CTO (m/m)	$1.951 \cdot 10^{-1}$	$5.809 \cdot 10^{-2}$	2.133	$4.242 \cdot 10^{-1}$
	a (Figure 24)	$-1.538 \cdot 10^{-1}$	$1.139 \cdot 10^{-1}$	$-2.069 \cdot 10^{-1}$	$1.533 \cdot 10^{-1}$
	$t_c \cdot CTO$	$2.950 \cdot 10^{-1}$	$1.321 \cdot 10^{-1}$	$9.797 \cdot 10^{-1}$	$4.386 \cdot 10^{-1}$
	Coeff. of determination ( $R^2$ )	0.920	---	---	---

Table 21 - Empirical models with retrieval of complete characterization of cracking products for heat of reaction estimation (cont.)

Product (or Output)	Input variables in physical units			Dimensionless normalized input variables	
	Variables	Coefficients	95% level CI	Coefficients	95% level CI
Coke	Intercept	$3.781 \cdot 10^1$	$1.853 \cdot 10^2$	$1.775 \cdot 10^1$	5.150
	$T_{rx}$ (K)	$-5.539 \cdot 10^{-1}$	$2.312 \cdot 10^{-1}$	-2.072	$4.480 \cdot 10^{-1}$
	CTO (m/m)	$2.008 \cdot 10^{-1}$	$7.788 \cdot 10^{-1}$	1.776	$3.460 \cdot 10^{-1}$
	a (Figure 24)	$7.150 \cdot 10^1$	$2.914 \cdot 10^1$	---	---
	b (Figure 24)	$8.513 \cdot 10^1$	$3.804 \cdot 10^1$	---	---
	$T_{rx} \cdot a$	$-2.005 \cdot 10^{-2}$	$7.278 \cdot 10^{-3}$	-1.273	$4.623 \cdot 10^{-1}$
	CTO $\cdot a$	$1.408 \cdot 10^{-1}$	$8.240 \cdot 10^{-2}$	$6.917 \cdot 10^{-1}$	$4.047 \cdot 10^{-1}$
	a $\cdot b$	$8.496 \cdot 10^{-1}$	$4.017 \cdot 10^{-1}$	$3.680 \cdot 10^{-1}$	$1.740 \cdot 10^{-1}$
	$T_{rx}^2$	$3.883 \cdot 10^{-4}$	$1.252 \cdot 10^{-4}$	$8.653 \cdot 10^{-1}$	$2.789 \cdot 10^{-1}$
	CTO $^2$	$-3.357 \cdot 10^{-2}$	$2.816 \cdot 10^{-2}$	$-4.473 \cdot 10^{-1}$	$3.751 \cdot 10^{-1}$
	a $^2$	-5.122	2.030	-9.272	3.675
	b $^2$	$-1.061 \cdot 10^2$	$4.230 \cdot 10^1$	$-1.100 \cdot 10^1$	4.383
Coeff. of determination ( $R^2$ )	0.918	---	---	---	
$\theta_0$ (Eq. 67)	Intercept	-1.836	$8.765 \cdot 10^{-1}$	$6.556 \cdot 10^{-1}$	$3.785 \cdot 10^{-2}$
	$T_{rx}$ (K)	$3.440 \cdot 10^{-3}$	$1.739 \cdot 10^{-3}$	$1.624 \cdot 10^{-1}$	$8.211 \cdot 10^{-2}$
	$t_c$ (s)	$4.688 \cdot 10^{-2}$	$2.825 \cdot 10^{-1}$	$2.170 \cdot 10^{-1}$	$8.324 \cdot 10^{-2}$
	CTO (m/m)	$2.330 \cdot 10^{-2}$	$1.578 \cdot 10^{-2}$	$3.244 \cdot 10^{-1}$	$9.880 \cdot 10^{-2}$
	a (Figure 24)	$-1.764 \cdot 10^{-1}$	$5.482 \cdot 10^{-2}$	---	---
	b (Figure 24)	-1.767	1.137	---	---
	$t_c \cdot CTO$	$4.967 \cdot 10^{-2}$	$3.246 \cdot 10^{-2}$	$1.650 \cdot 10^{-1}$	$1.078 \cdot 10^{-1}$
	$t_c \cdot b$	$-4.145 \cdot 10^{-1}$	$3.166 \cdot 10^{-1}$	$-1.214 \cdot 10^{-1}$	$9.275 \cdot 10^{-2}$
	a $\cdot b$	$4.167 \cdot 10^{-1}$	$1.295 \cdot 10^{-1}$	$1.805 \cdot 10^{-1}$	$5.609 \cdot 10^{-2}$
	Coeff. of determination ( $R^2$ )	0.907	---	---	---

Table 21 - Empirical models with retrieval of complete characterization of cracking products for heat of reaction estimation (cont.)

Product (or Output)	Input variables in physical units			Dimensionless normalized input variables	
	Variables	Coefficients	95% level CI	Coefficients	95% level CI
$\theta_1$ (Eq. 67)	Intercept	5.696	2.329	1.266	$3.044 \cdot 10^{-2}$
	$T_{rx}$ (K)	$-6.454 \cdot 10^{-3}$	$2.710 \cdot 10^{-3}$	$2.467 \cdot 10^{-1}$	$7.374 \cdot 10^{-2}$
	$t_c$ (s)	$-2.104 \cdot 10^{-1}$	$9.829 \cdot 10^{-2}$	$2.072 \cdot 10^{-1}$	$4.235 \cdot 10^{-2}$
	CTO (m/m)	$1.685 \cdot 10^{-1}$	$9.030 \cdot 10^{-2}$	$4.267 \cdot 10^{-1}$	$7.855 \cdot 10^{-2}$
	a (Figure 24)	-1.757	$5.961 \cdot 10^{-1}$	$-9.981 \cdot 10^{-2}$	$2.613 \cdot 10^{-2}$
	b (Figure 24)	$1.842 \cdot 10^{-1}$	$1.159 \cdot 10^{-1}$	$5.927 \cdot 10^{-2}$	$3.732 \cdot 10^{-2}$
	$T_{rx} \cdot a$	$2.104 \cdot 10^{-3}$	$7.694 \cdot 10^{-4}$	$1.336 \cdot 10^{-1}$	$4.887 \cdot 10^{-2}$
	$t_c \cdot CTO$	$5.929 \cdot 10^{-2}$	$1.960 \cdot 10^{-2}$	$1.969 \cdot 10^{-1}$	$6.509 \cdot 10^{-2}$
	$CTO^2$	$-8.785 \cdot 10^{-3}$	$5.815 \cdot 10^{-3}$	$-1.170 \cdot 10^{-1}$	$7.748 \cdot 10^{-2}$
Coeff. of determination ( $R^2$ )	0.971	---	---	---	
$\theta_2$ (Eq. 67)	Intercept	-5.814	7.011	1.227	$3.958 \cdot 10^{-2}$
	$T_{rx}$ (K)	$6.199 \cdot 10^{-3}$	$8.463 \cdot 10^{-3}$	---	---
	$t_c$ (s)	$9.960 \cdot 10^{-2}$	$2.669 \cdot 10^{-2}$	$9.063 \cdot 10^{-2}$	$2.429 \cdot 10^{-2}$
	CTO (m/m)	1.282	$2.986 \cdot 10^{-1}$	$2.087 \cdot 10^{-1}$	$3.335 \cdot 10^{-2}$
	a (Figure 24)	$-7.570 \cdot 10^{-1}$	$6.140 \cdot 10^{-1}$	---	---
	b (Figure 24)	7.486	4.005	---	---
	$T_{rx} \cdot CTO$	$-1.531 \cdot 10^{-3}$	$3.847 \cdot 10^{-4}$	$-2.637 \cdot 10^{-1}$	$6.628 \cdot 10^{-2}$
	$T_{rx} \cdot a$	$1.335 \cdot 10^{-3}$	$7.228 \cdot 10^{-4}$	$8.476 \cdot 10^{-2}$	$4.591 \cdot 10^{-2}$
	$T_{rx} \cdot b$	$-5.428 \cdot 10^{-3}$	$3.797 \cdot 10^{-3}$	$-8.248 \cdot 10^{-2}$	$5.769 \cdot 10^{-2}$
	$a \cdot b$	$-7.337 \cdot 10^{-1}$	$8.465 \cdot 10^{-2}$	$-3.177 \cdot 10^{-1}$	$3.666 \cdot 10^{-2}$
	$b^2$	1.098	$5.884 \cdot 10^{-1}$	$1.138 \cdot 10^{-1}$	$6.096 \cdot 10^{-2}$
Coeff. of determination ( $R^2$ )	0.939	---	---	---	

Table 21 - Empirical models with retrieval of complete characterization of cracking products for heat of reaction estimation (cont.)

Product (or Output)	Input variables in physical units			Dimensionless normalized input variables	
	Variables	Coefficients	95% level CI	Coefficients	95% level CI
$\theta_3$ (Eq. 67)	Intercept	8.459	2.587	1.265	$3.611 \cdot 10^{-2}$
	$T_{rx}$ (K)	$-9.195 \cdot 10^{-3}$	$2.666 \cdot 10^{-3}$	$-1.121 \cdot 10^{-1}$	$7.629 \cdot 10^{-2}$
	$t_c$ (s)	$2.455 \cdot 10^{-1}$	$1.516 \cdot 10^{-1}$	$-2.131 \cdot 10^{-1}$	$6.059 \cdot 10^{-2}$
	CTO (m/m)	$-7.066 \cdot 10^{-1}$	$5.520 \cdot 10^{-1}$	$-4.983 \cdot 10^{-1}$	$9.259 \cdot 10^{-2}$
	a (Figure 24)	$1.525 \cdot 10^{-1}$	$7.302 \cdot 10^{-2}$	$5.750 \cdot 10^{-2}$	$3.574 \cdot 10^{-2}$
	$T_{rx} \cdot CTO$	$9.228 \cdot 10^{-4}$	$5.795 \cdot 10^{-4}$	$1.590 \cdot 10^{-1}$	$9.985 \cdot 10^{-2}$
	$t_c \cdot CTO$	$-6.491 \cdot 10^{-2}$	$2.952 \cdot 10^{-2}$	$-2.156 \cdot 10^{-1}$	$9.805 \cdot 10^{-2}$
	$CTO \cdot a$	$-1.485 \cdot 10^{-2}$	$1.348 \cdot 10^{-2}$	$-7.294 \cdot 10^{-2}$	$6.618 \cdot 10^{-2}$
Coeff. of determination ( $R^2$ )	0.936	---	---	---	
$\theta_4$ (Eq. 67)	Intercept	-5.143	6.524	$5.611 \cdot 10^{-1}$	$6.416 \cdot 10^{-2}$
	$T_{rx}$ (K)	$1.071 \cdot 10^{-2}$	$6.445 \cdot 10^{-3}$	$-2.453 \cdot 10^{-1}$	$1.021 \cdot 10^{-1}$
	$t_c$ (s)	$6.949 \cdot 10^{-1}$	$5.491 \cdot 10^{-1}$	$-3.563 \cdot 10^{-1}$	$1.013 \cdot 10^{-1}$
	CTO (m/m)	$-4.238 \cdot 10^{-1}$	$1.823 \cdot 10^{-1}$	$-5.402 \cdot 10^{-1}$	$1.447 \cdot 10^{-1}$
	a (Figure 24)	2.120	1.328	---	---
	b (Figure 24)	-2.246	1.153	---	---
	$T_{rx} \cdot a$	$-2.865 \cdot 10^{-3}$	$1.550 \cdot 10^{-3}$	$-1.820 \cdot 10^{-1}$	$9.846 \cdot 10^{-2}$
	$t_c \cdot CTO$	$-8.403 \cdot 10^{-2}$	$4.066 \cdot 10^{-2}$	$-2.791 \cdot 10^{-1}$	$1.351 \cdot 10^{-1}$
	$a \cdot b$	$4.045 \cdot 10^{-1}$	$2.077 \cdot 10^{-1}$	$1.752 \cdot 10^{-1}$	$8.996 \cdot 10^{-2}$
	$t_c^2$	$-1.763 \cdot 10^{-1}$	$1.363 \cdot 10^{-1}$	$-1.460 \cdot 10^{-1}$	$1.129 \cdot 10^{-1}$
	$CTO^2$	$2.616 \cdot 10^{-2}$	$1.138 \cdot 10^{-2}$	$3.486 \cdot 10^{-1}$	$1.517 \cdot 10^{-1}$
Coeff. of determination ( $R^2$ )	0.934	---	---	---	

Table 21 - Empirical models with retrieval of complete characterization of cracking products for heat of reaction estimation (cont.)

Product (or Output)	Input variables in physical units			Dimensionless normalized input variables	
	Variables	Coefficients	95% level CI	Coefficients	95% level CI
d <sub>20</sub> of the liquid product	Intercept	-1.243*10 <sup>-1</sup>	6.099*10 <sup>-1</sup>	8.628*10 <sup>-1</sup>	5.724*10 <sup>-3</sup>
	T <sub>rx</sub> (K)	9.247*10 <sup>-4</sup>	7.359*10 <sup>-4</sup>	-2.072*10 <sup>-2</sup>	1.136*10 <sup>-2</sup>
	t <sub>c</sub> (s)	-8.428*10 <sup>-3</sup>	7.604*10 <sup>-3</sup>	-7.669*10 <sup>-3</sup>	6.919*10 <sup>-3</sup>
	CTO (m/m)	-5.493*10 <sup>-3</sup>	3.385*10 <sup>-3</sup>	-2.005*10 <sup>-2</sup>	1.236*10 <sup>-2</sup>
	a (Figure 24)	2.503*10 <sup>-1</sup>	1.498*10 <sup>-1</sup>	2.025*10 <sup>-2</sup>	1.166*10 <sup>-2</sup>
	b (Figure 24)	5.092*10 <sup>-1</sup>	2.332*10 <sup>-1</sup>	---	---
	T <sub>rx</sub> *a	-2.456*10 <sup>-4</sup>	1.759*10 <sup>-4</sup>	-1.560*10 <sup>-2</sup>	1.117*10 <sup>-2</sup>
	a*b	-9.171*10 <sup>-2</sup>	4.201*10 <sup>-2</sup>	-3.972*10 <sup>-2</sup>	1.819*10 <sup>-2</sup>
Coeff. of determination (R <sup>2</sup> )	0.762	---	---	---	
C <sub>5</sub> <sup>+</sup> yield	Intercept	1.337*10 <sup>1</sup>	6.837	3.695	2.550*10 <sup>-1</sup>
	T <sub>rx</sub> (K)	-1.315*10 <sup>-2</sup>	1.051*10 <sup>-2</sup>	1.139	8.426*10 <sup>-1</sup>
	CTO (m/m)	-3.812	2.880	8.166*10 <sup>-1</sup>	6.925*10 <sup>-1</sup>
	b (Figure 24)	-1.911	9.972*10 <sup>-1</sup>	-6.152*10 <sup>-1</sup>	3.210*10 <sup>-1</sup>
	T <sub>rx</sub> *CTO	5.045*10 <sup>-3</sup>	3.837*10 <sup>-3</sup>	8.693*10 <sup>-1</sup>	6.612*10 <sup>-1</sup>
Coeff. of determination (R <sup>2</sup> )	0.771	---	---	---	

Source: The author, 2023.

Figure 26 - Fitting of the empirical models from Table 21

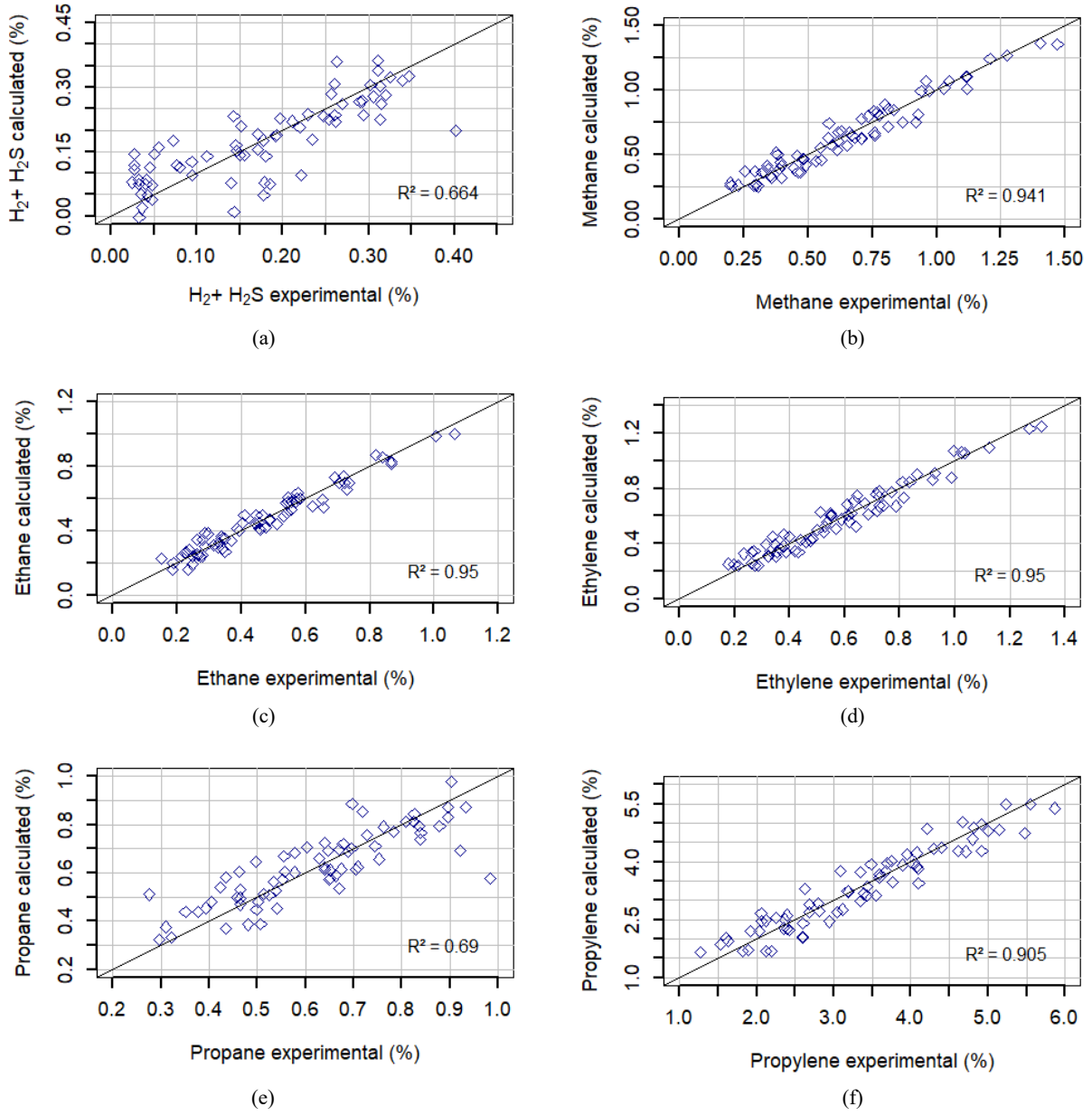


Figure 26 - Fitting of the empirical models from Table 21 (cont.)

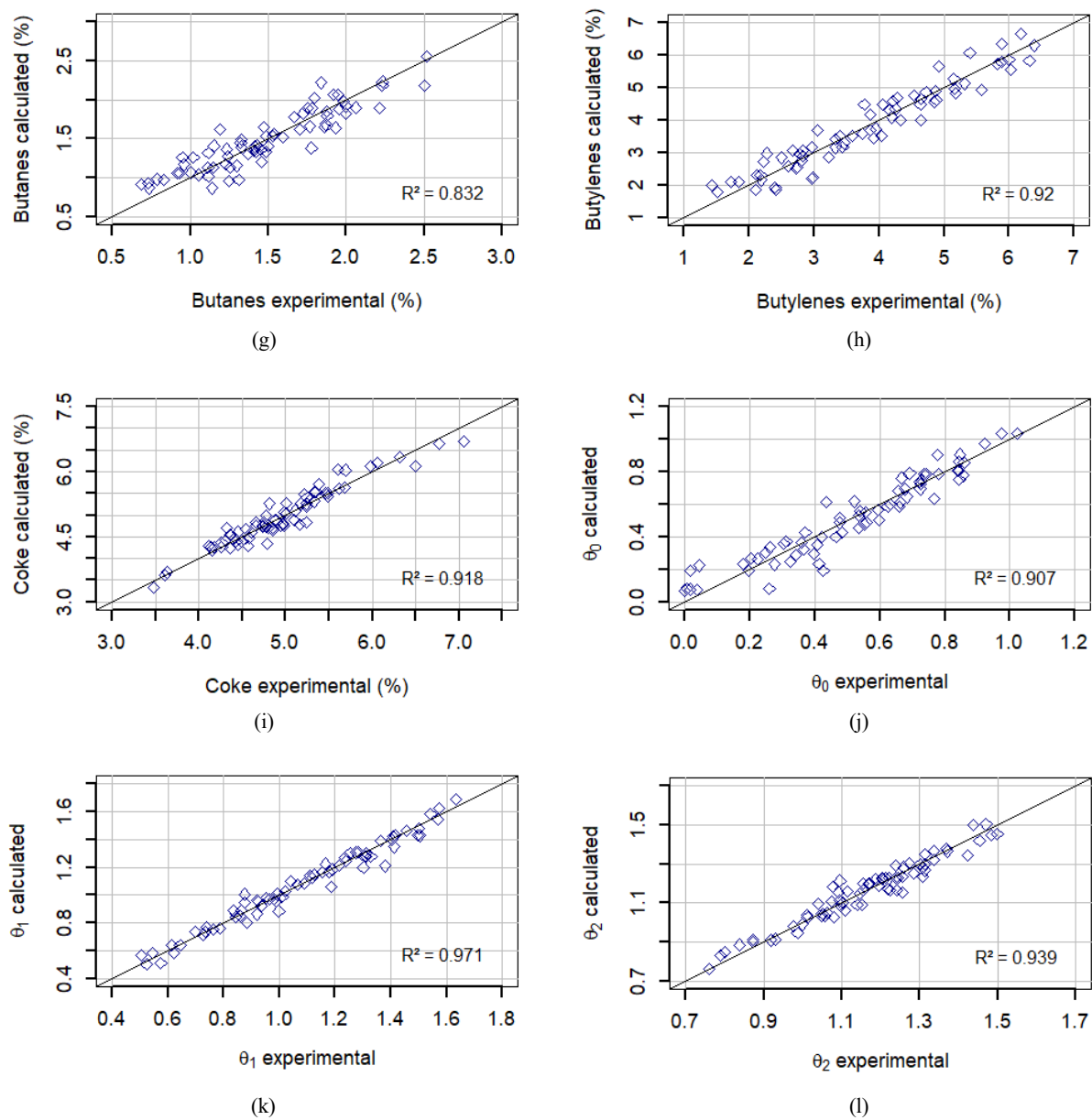
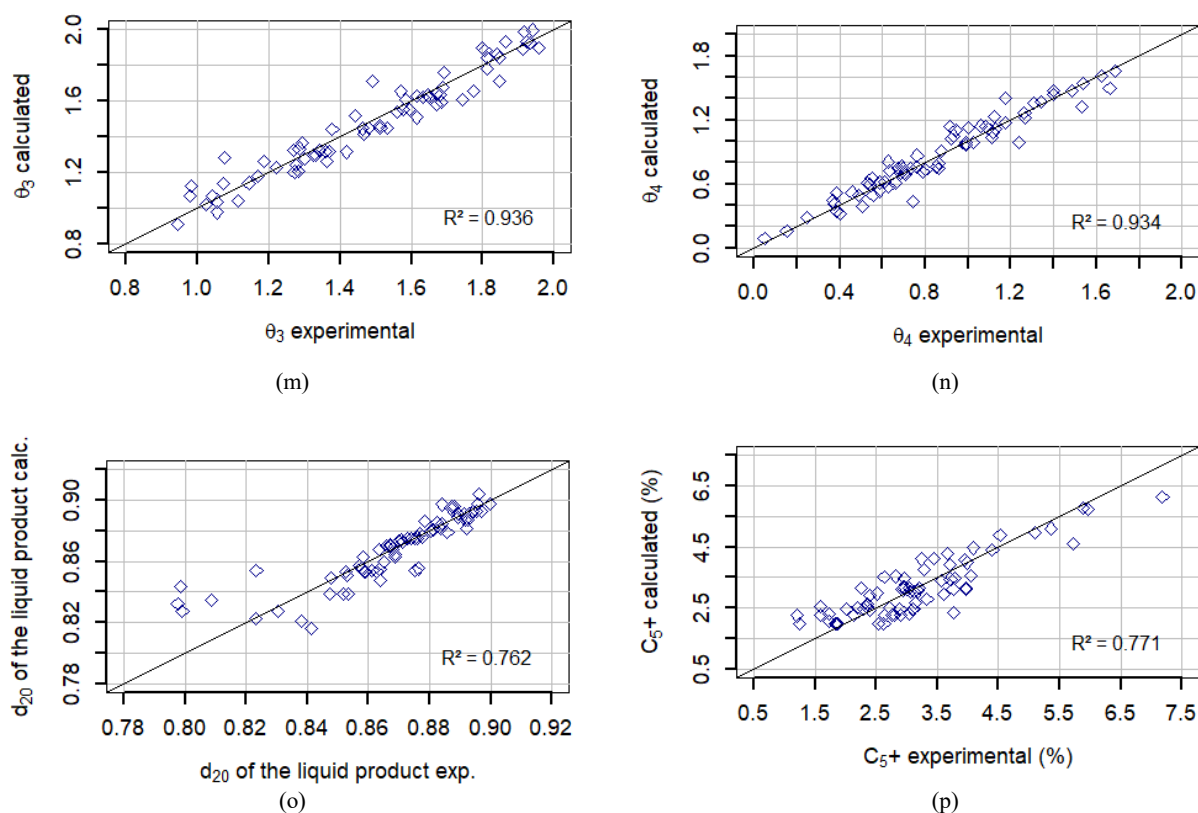


Figure 26 - Fitting of the empirical models from Table 21 (cont.)



Source: The author, 2023.

Results from Table 21 and Figure 26.a show, as expected, a poor fit for combined  $H_2 + H_2S$  yield. This is a consequence of the fact that the sampled gas chromatography showed error (zero value) for the  $H_2S$  component in many of the available experimental runs. Other components of dry gas (Figures 26.b, 26.c and 26.d) presented a good fit, comparable to that of the whole dry gas lump in the empiric models of Chapter 1 (Tables 6-7, Figure 8.a).

For the LPG components, an alluring detail can be noted: the olefinic components (Figures 26.f and 26.h) resulted in better correlated models, while the aliphatic components (Figures 26.e and 26.g) showed greater scattering in the correlation graph, with some points showing considerable deviations. This indicates that, in this case, obtaining greater precision in estimating the LPG yield (Figure 8.b) would require greater attention to the data relating to the saturated components.

Figure 26.i presents the fitting for the coke regression model. For coke, this is essentially the same experimental data that produced the models of Tables 6-7 and Figure 8.f, except for the replacement of a cutoff point of light content in the feed ( $HC_{light}$ ) by parameters a and b that contain the information of the complete distillation curve of the VGO. There is a subtle improvement in the correlation of the coke yield estimation model with this modification.

Figures 26.j-26.n present the results for the densities of probability  $\theta_i$  of the distillation cumulated mass recovered ( $P_{dist}^{cum}$ ) with distilled temperatures normalized between 0 and 1. It is interesting to note that the quality of fitting varied among the parameters  $\theta_i$ . The greater fit ( $R^2 = 0.971$ ) was obtained for  $\theta_1$  (Figure 26.k) at normalized nodal point 0.3241 or 156.05°C, while for  $\theta_0$  (Figure 26.j), at normalized nodal point 0.1204 or 40.0°C, the scatter of estimated values were larger ( $R^2 = 0.907$ ). For  $\theta_2$ ,  $\theta_3$  and  $\theta_4$  (Figures 26.l-26.n) it was obtained what seemed as reasonable fitting ( $0.934 \leq R^2 \leq 0.939$ ).

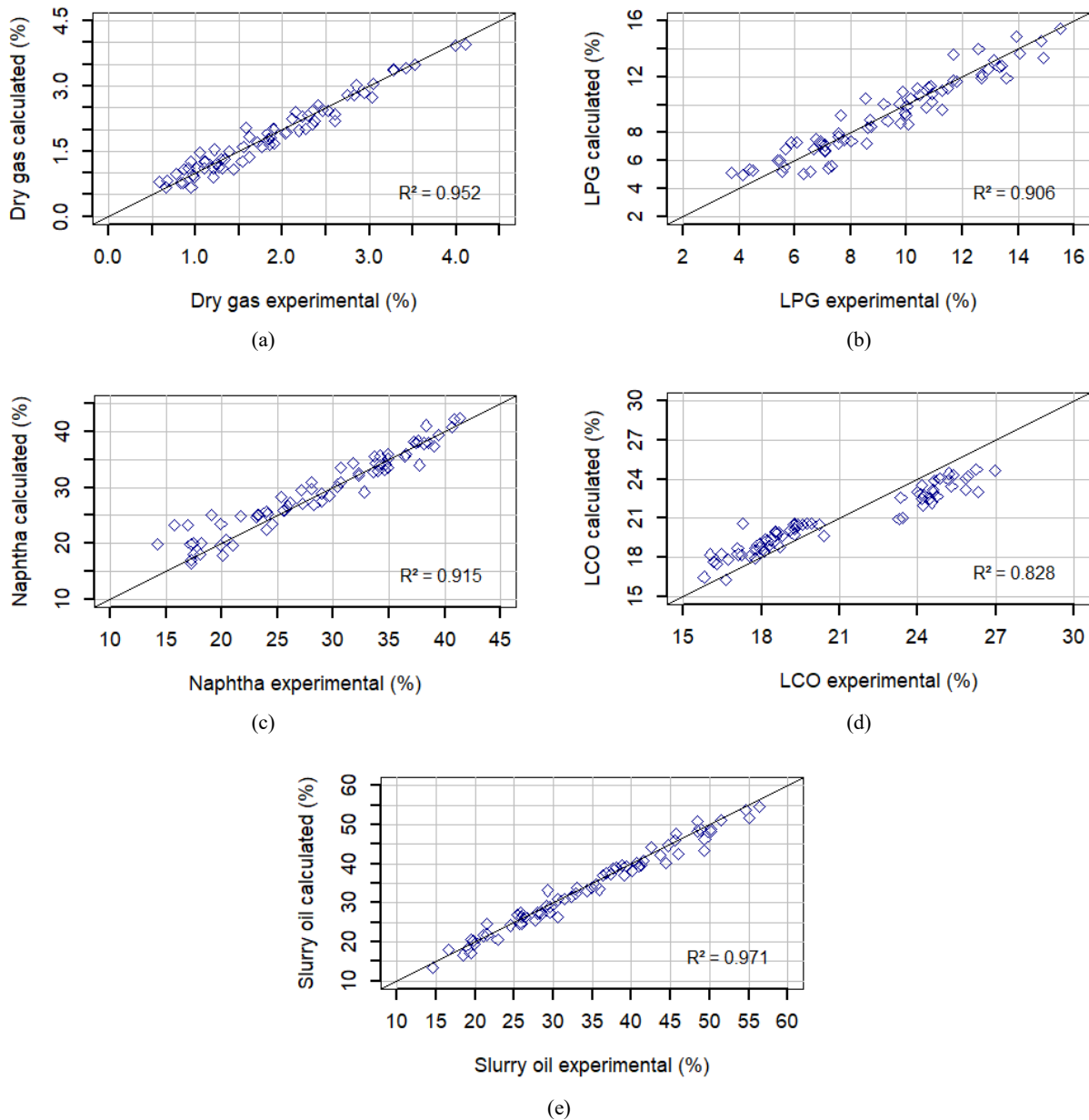
The density  $d_{20}$  of the liquid product was included in the modeling with the objective of allowing a subsequent characterization of the liquid product for the estimation of thermodynamic properties such as the lower heating value to obtain the heat of reaction by the method of calorimetry of the products (section 2.2.1). For example, API (1997) correlation for lower heating value uses density as the sole explanatory variable. However, the obtained model for  $d_{20}$  (Figure 26.o) presented a poor fit. This is yet another factor that compromises the use of this strategy for predicting the heat of reaction by this method.

As it could be expected, the model for  $C_5^+$  yield (Figure 26.p) showed a relatively poor fit as well, which is probably related to variations in the pilot plant gas-liquid separation efficiency in different runs.

In order to verify whether the recovery of the distillation curve of the products from the estimated parameters  $\theta_i$  would return estimates of yield profiles for naphtha, LCO and slurry oil compatible with the yields obtained in section 1.3.1, lump yields estimated using the empirical model in Table 21 were calculated. Coke yield (Figure 26.i) is transported directly from the model. Dry gas yield is obtained by summing the individual components ( $H_2 + H_2S$ , Methane, Ethane and Ethylene) estimated by the model. Similarly, LPG yield is obtained by summing the individual components (Propane, Propylene, Butanes and Butylenes).

There is no model with mass balance restriction like the one discussed in section 1.3.2 because the philosophy of obtaining an estimate of the yield profile of the lumps in the present case, where the information available for the liquid products is the distillation curve, already implies that the total yield of liquid products is obtained by the difference between 100% and the estimated yield of the other lumps (dry gas, LPG and coke), hence the relevance of including  $C_5^+$  as one of the constituents of naphtha yield. The content of naphtha and LCO in the liquid product is calculated through Eq. 67 using estimated  $\theta_i$  parameters (Figures 26.j-26.n). The content of slurry oil in the liquid product is obtained by difference. Figure 27 presents the calculated yields of the lumps obtained in such way.

Figure 27 - Fitting of the lumped yields obtained by manipulating the empirical models from Table 21



Source: The author, 2023.

Figure 27.a (dry gas), 27.b (LPG) and 27.e (slurry oil), along with Figure 26.i for coke, show that a quality of fitting quite comparable to that of Figure 8 was obtained for these lumps. Figure 27.c show that, apparently, the manipulations involved in obtaining the naphtha yield by this strategy, which initially predicts the parameters of the distillation curve of the liquid product, penalized the estimate of the overall yield of the lump.

But the most intriguing result is undoubtedly the behavior of the estimated yield of the LCO lump in Figure 27.d, which clearly display a correlation whose residual errors deviate from

the normal distribution. The impression is that the use of the feed parameters a and b, combined with the indirect method of estimating the LCO yield from parameters  $\theta_i$  of the distillation curve of the liquid product, failed to fully capture the effect of the higher content of a light front in the vacuum gasoil on LCO yield, and the regression eventually minimized the error by estimating higher values of LCO yield for the region of lower  $HC_{\text{light}}$  and lower values of LCO yield for the region of higher  $HC_{\text{light}}$ . The direct estimation of LCO yield with the cutoff variable  $HC_{\text{light}}$  applied in Chapter 1 proved more effective in this regard.

As several obstacles accumulated for an accurate estimation, with the information available at the time, of the heat of reaction by the product calorimetry method (main objective of this model), it was decided not to proceed with the application of the empirical model of Table 21 in the present study. Hereupon, the study of optimization of the operation mode of the FCC unit discussed in section 1.3.4, for example, was developed using the model of section 1.3.1.

In summary, for the purpose of estimating the yield profile of the FCC unit with the aid of a simpler empirical model, it is more advisable to proceed with the models depicted in sections 1.3.1 and 1.3.2.

## 2.4 Conclusion

The estimation of the heat of reaction of catalytic cracking reactions by the product calorimetry method still lacks the availability of more robust correlations for feed and liquid products LHV. The existence of such a correlation would facilitate the proposition of more chemically and experimentally consistent models for representing the energy balance of cracking reactions along the riser.

The empirical model presented in Table 21 was developed with a view to using it to recover the heat of reaction based on the estimated enthalpy difference between products and feed. In order to do so, the model was adapted to return the complete composition of dry gas and LPG, along with distillation (and density) data for the total liquid product. In this strategy, it was verified the need to include the  $C_5^+$  contained in the gaseous stream for the proper accounting of naphtha yield.

In addition, taking advantage of the philosophy of representing the complete distillation curve through parameters that allow the reconstruction of these distillation curves, the variable  $HC_{\text{light}}$  was replaced by parameters a and b of a logistic function (Eq. 68).

Compared to the empirical model developed in Chapter 1, little difference was observed in predicting dry gas, LPG and coke yields. Slurry oil yield also seems to have been little influenced by the new model format. Yet it was noted a worsening in the fitting for the naphtha yield. However, and interesting enough, the LCO yield estimation was clearly upset in this model, as it started to present a deviation from normality for the residual errors between the two regions of LCO yield, indicating that the structure of the previous model, in which the lump LCO yield was directly estimated as an output and the explanatory variable referring to the feed was the cutoff variable  $HC_{\text{light}}$ , was more efficient in capturing the effect of the light front content of the feed on the LCO yield.

In addition to these setbacks, it was noticed that the subsequent characterization of the product to obtain the heat of reaction was deficient, so there was no advantage in continuing the study with this model to the detriment of the models obtained in Chapter 1.

For future phenomenological modeling development, an envisioned alternative to deal with heat of reaction would be to consider a single heat of reaction for the conversion reactions like proposed in Table 20.

## CONCLUSION

By the aid of the empirical model obtained and a process simulator developed within the present work, it was observed that for a single FCC unit envelope and a typical pricing basis, the maximum conversion mode of operation (i.e. maximum cracked naphtha yield) is preferred over the maximum middle distillate mode.

The experimental data produced and used in the present work, which included an innovative investigation of the effect of varying the reaction contact time between feed and catalyst in the Riser ( $t_c$ ) to the LCO/slurry oil ratio, confirmed that the LCO yield does not increase significantly in the low conversion region (and that reduced contact time does not bring any improvement to this trend), while the slurry oil (or unconverted feed) yield experiences a pronounced increase. This combination results in a worsening of the economic attractiveness of the middle distillate maximization route. However, it was found that if there is a juncture that requires a reduction in the throughput of cracked naphtha or an increase in the production of LCO by the FCC unit, then recycling of excessive slurry oil (which is quite more crackable at low conversions) can be an interesting option.

The developed model also pointed to the ideal operating condition in the maximum conversion mode as the one in which the reaction temperature is the maximum possible, and the feed temperature is maintained at a necessary level so that the unit does not reach some operational limit such as the air blower capacity.

In addition to the empirical model developed itself, which is specific to the catalytic system and feed quality employed in the tests at the FCC pilot plant (Figure 1), the model construction procedure (Figure 2) is a tool that can be used whenever sufficient and reliable experimental data for a given unit is available for evaluation and optimization purposes.

In an initial survey regarding the energy balance of cracking reactions in the riser, the description of which is necessary in a phenomenologically based kinetic model, it was found that obtaining a precise correlation for the heating value of the feed and liquid cracked products is still a task that demands further developments. The evaluated correlation results in relative errors of up to 5%, which results in an absolute error that is greater than the magnitude of the heat of reaction estimated through the riser energy balance. Such correlations can be very useful for the design and evaluation of furnaces and boilers, in which a variation in the fuel oil flow rate demand of 5% may not be decisive, but in the case of the representation of the enthalpic content of the

species involved in the catalytic cracking reactions this could make such an assessment completely inconsistent.

Some studies that, if continued, would add relevant contribution to the area of catalytic cracking include:

1 - Reassess the potential of the maximum middle distillate route for cases where there are two FCC units or, within the envelope of the refinery's overall refining scheme, there are other conversion units (such as delayed coking, deasphalting, etc.) that could exchange intermediate streams with the FCC unit.

2 - Study of promising alternatives for the future of the FCC unit, in the face of pressing scenarios that include competition for the vacuum gasoil feed with other destinations (such as the hydrocracking unit) and shifts in production profile demanded for the FCC unit, such as revamps for the production of light olefins (petrochemical FCC), biomass conversion and others.

3 - Conduct in-depth experimental research to survey valid correlations for the heating value of vacuum gas oil and liquid cracking products (cracked naphtha, LCO and decanted oil), in order to enable obtaining the heat of reaction using the product calorimetry method so that it is coherent with the value obtained by the energy balance of the riser.

4 - Develop a model for representing the heat of cracking reactions and the enthalpy dependence of products on temperature that has experimental consistency and is applicable to the construction of a phenomenological kinetic model.

5 - Develop the phenomenological modeling of the catalytic cracking reactions in the riser with the previous model for describing the energy balance parameters of the reaction, and compare it with the simplified proposal in Table 20 (for the heat of reaction). Compare the phenomenological model obtained with the empirical model proposed in this work.

## REFERENCES

- AHMED, A.; MAULUD, A.; RAMASAMY, M.; LAU, K. K.; MAHADZIR, S. 3D CFD modeling and simulation of RFCC riser hydrodynamics and kinetics. **Journal of applied sciences**. 2014, 14, 3172 – 3181. Disponível em: <https://doi.org/10.3923/jas.2014.3172.3181>. Acesso em: 03 nov 2022.
- AKAH, A.; AL-GHRAMI, M. Maximizing propylene production via FCC technology. **Applied Petrochemical Research**. 2015, 5, 377 – 392. Disponível em: <https://doi.org/10.1007/s13203-015-0104-3>. Acesso em: 18 out 2022.
- ALABDULLAH, M. A.; GOMEZ, A. R.; VITTENET, J.; SEDJERARI, A. B.; XU, W.; ABBA, I. A.; GASCON, J. Viewpoint on the Refinery of the Future: Catalyst and Process Challenges. **ACS Catalysis**. 2020, 10 (15), 8131 – 8140. Disponível em: <https://doi.org/10.1021/acscatal.0c02209>. Acesso em: 17 nov 2022.
- API. **Technical Data Book: Petroleum Refining**. 6 ed. American Petroleum Institute: Washington, 1997.
- BENOIT, A. Strategies for maximizing FCC Light Cycle Oil. In: **REFCOMM CONFERENCE**, 2015, Galveston. Disponível em: <https://refiningcommunity.com/wp-content/uploads/2015/05/Strategies-for-Maximizing-FCC-Light-Cycle-Oil-Benoit-GRACE-Shale-Galveston-2015.pdf>. Acesso em: 25 mai 2022
- BRASIL, N. I. **Introdução à engenharia química**. 2 ed. Interciência: Rio de Janeiro, 2004.
- CHAPRA, S. C.; CANALE, R. P. **Numerical methods for engineers**. 6 ed. Mcgraw-Hill: Boston, 2010.
- CHEN, Z.; WANG, G.; ZHAO, S.; ZHANG, L. Prediction of molecular distribution and temperature profile of FCC process through molecular-level kinetic modeling. **Chemical Engineering Science**. 2022, 264, 118189. Disponível em: <https://doi.org/10.1016/j.ces.2022.118189>. Acesso em: 16 mar 2023.
- CORMA, A.; MELO, F. V.; SAUVANAUD, L.; ORTEGA, F. J. Different process schemes for converting light straight run and fluid catalytic cracking naphthas in a FCC unit for maximum propylene production. **Applied Catalysis A: General**. 2004, 265 (2), 195 – 206. Disponível em: <https://doi.org/10.1016/j.apcata.2004.01.020>. Acesso em: 04 nov 2022.
- CORMA, A.; SAUVANAUD, L. Increasing LCO yield and quality in the FCC: cracking pathways analysis. In: OCCELLI, M. L. **Fluid Catalytic Cracking VII: Materials, Methods and Process Innovations**. Amsterdam: Elsevier, 2007. Disponível em: [https://doi.org/10.1016/S0167-2991\(07\)80187-X](https://doi.org/10.1016/S0167-2991(07)80187-X). Acesso em: 17 jun 2022.

DAHL, I. M.; TANGSTAD, E.; MOSTAD, H. B.; ANDERSEN, K. Effect of hydrotreating on catalytic cracking of a VGO. **Energy & Fuels**. 1996, 10 (1), 85 – 90. Disponível em: <https://doi.org/10.1021/ef950086v>. Acesso em: 16 jun 2022.

DART, J. C.; OBLAD, A. G. Heat of cracking and regeneration in catalytic cracking. **Chemical Engineering Progress**. 45, 110 – 118, 1949.

DEN HOLLANDER, M. A.; MAKKEE, M.; MOULIJN, J. A. Development of a kinetic model for FCC valid from ultra-short residence times. **Studies in Surface Science and Catalysis**. 2001, 134, 167 – 185. Disponível em: [https://doi.org/10.1016/S0167-2991\(01\)82318-1](https://doi.org/10.1016/S0167-2991(01)82318-1). Acesso em: 13 mar 2023.

EPE. **Ten-year energy expansion plan 2027 (PDE 2027)**, 2018. Disponível em: [https://www.epe.gov.br/sites-pt/publicacoes-dados-abertos/publicacoes/Documents/PDE%202027\\_aprovado\\_OFICIAL.pdf](https://www.epe.gov.br/sites-pt/publicacoes-dados-abertos/publicacoes/Documents/PDE%202027_aprovado_OFICIAL.pdf). Acesso em: 25 mai 2022.

FERNANDES, J. L.; VERSTRAETE, J. J.; PINHEIRO, C. I. C.; OLIVEIRA, N. M. C.; RIBEIRO, F. R. Dynamic modelling of an industrial R2R FCC unit. **Chemical Engineering Science**. 2007, 62, 1184 – 1198. Disponível em: <https://doi.org/10.1016/j.ces.2006.11.003>. Acesso em: 27 mai 2022.

FOGLER, H. S. **Elements of chemical reaction engineering**. 5 ed. Prentice Hall: Boston, 2016.

GHOLAMI, Z.; GHOLAMI, F.; TISLER, Z.; TOMAS, M.; VAKILI, M. A review on production of light olefins via fluid catalytic cracking. **Energies**. 2021, 14 (4), 1089. Disponível em: <https://doi.org/10.3390/en14041089>. Acesso em: 17 nov 2022.

GILBERT, W. R.; BAPTISTA, C. A.; PINHO, A. R. Exploring FCC flexibility to produce mid-distillates and petrochemicals. Chapter 3 in: OCCELLI, M. L. **Fluid Catalytic Cracking VII: Materials, Methods and Process Innovations**. Amsterdam: Elsevier, 2007. Disponível em: [https://doi.org/10.1016/S0167-2991\(07\)80186-8](https://doi.org/10.1016/S0167-2991(07)80186-8). Acesso em: 25 mai 2022.

GILBERT, W. R.; MORGADO Jr, E.; de ABREU, M. A. S.; de la PUENTE, G.; PASSAMONTI, F.; SEDRAN, U. A novel fluid catalytic cracking approach for producing low aromatic LCO. **Fuel Processing Technology**. 2011, 92 (1), 2235 – 2240. Disponível em: <https://doi.org/10.1016/j.fuproc.2011.07.006>. Acesso em: 27 mai 2022.

GREEN, D. W.; SOUTHARD, M. Z. **Perry's Chemical Engineers' Handbook**. 9 ed. New York: McGraw-Hill Education, 2019. Disponível em: <https://www.accessengineeringlibrary.com/content/book/9780071834087>. Acesso em: 23 mar 2023.

GUILKEY, D. K.; PRICE, J. M. On comparing restricted least squares estimators. **Journal of Econometrics**. 1981, 15 (3), 397 – 404. Disponível em: [https://doi.org/10.1016/0304-4076\(81\)90102-0](https://doi.org/10.1016/0304-4076(81)90102-0). Acesso em: 21 mar 2023.

HAN, I.; CHUNG, C. Dynamic modeling and simulation of a fluidized catalytic cracking process. Part I: Process modeling. **Chemical Engineering Science**. 2001a, 56, 1951 – 1971. Disponível em: [https://doi.org/10.1016/S0009-2509\(00\)00493-0](https://doi.org/10.1016/S0009-2509(00)00493-0). Acesso em: 27 mai 2022.

HAN, I.; CHUNG, C. Dynamic modeling and simulation of a fluidized catalytic cracking process. Part II: Property estimation and simulation. **Chemical Engineering Science**. 2001b, 56, 1973 – 1990. Disponível em: [https://doi.org/10.1016/S0009-2509\(00\)00494-2](https://doi.org/10.1016/S0009-2509(00)00494-2). Acesso em: 27 mai 2022.

HIRAMATSU, Y.; AITA, Y.; UMEKI, T. Effect of Acid Properties of Catalysts on Fluid Catalytic Cracking of Residual Oil. **Journal of the Japan Petroleum Institute**. 2012, 55, 5, 319 – 325. Disponível em: <https://doi.org/10.1627/jpi.55.319>. Acesso em: 23 mar 2023.

HOSOKAI, S.; MATSUOKA, K.; KURAMOTO, K.; SUZUKI, Y. Modification of Dulong's formula to estimate heating value of gas, liquid and solid fuels. **Fuel processing technology**. 2016, 152, 399 – 405. Disponível em: <https://doi.org/10.1016/j.fuproc.2016.06.040>. Acesso em: 23 mar 2023.

JOHN, Y. M.; MUSTAFA, M. A.; PATEL, R.; MUTJABA, I. M. Parameter estimation of a six-lump kinetic model of an industrial fluid catalytic cracking unit. **Fuel**. 2019, 235, 1436 – 1454. Disponível em: <https://doi.org/10.1016/j.fuel.2018.08.033>. Acesso em: 18 nov 2022.

KHANDE, A. R.; DASILA, P. K.; MAJUMDER, S.; MAITY, P.; THOTA, C. Recent developments in FCC process and catalysts. Chapter 3 in: PANT, K. K.; GUPTA, S. K.; AHMAD, E. **Catalysis for Clean Energy and Environmental Sustainability**; 1 ed; Cham: Springer Nature, 2021. Disponível em: [https://doi.org/10.1007/978-3-030-65021-6\\_3](https://doi.org/10.1007/978-3-030-65021-6_3). Acesso em: 21 mar 2023.

KRAFT, D. A software package for sequential quadratic programming. **Institut fuer Dynamik der Flugsysteme**, 1988, Technical report DFVLR-FB 88-28.

LAN, X.; XU, C.; WANG, G.; GAO, J. Reaction performance of FCC slurry catalytic cracking. **Catalysis Today**. 2009, 140 (3 – 4), 174. Disponível em: <https://doi.org/10.1016/j.cattod.2008.10.013>. Acesso em: 23 mar 2023.

LIMA, C.; SILVA, L. M.; ALBERTON, A. L. Comparação de modelos empíricos para a predição do poder calorífico de combustíveis. In: **CONGRESSO BRASILEIRO DE ENGENHARIA QUÍMICA**, 24., 2023, Salvador. Disponível em: [https://proceedings.science/proceedings/100393/\\_papers/170938/download/fulltext\\_file1?lang=pt-br](https://proceedings.science/proceedings/100393/_papers/170938/download/fulltext_file1?lang=pt-br). Acesso em: 19 out 2023.

MA, H.; HU, R.; LANGAN, L.; HUNT, D.; CHENG, W. Maximizing FCC Light Cycle Oil by Heavy Cycle Oil recycle. Chapter 1 in: OCCELLI, M. L. **Advances in Fluid Catalytic Cracking: Testing, Characterization and Environmental Regulations**. Boca Raton: CRC Press, 2010. Disponível em: <https://doi.org/10.1201/b10380>. Acesso em: 06 jul 2022.

MAHGOUB, K. A.; AL-KHATTAF, S. Catalytic Cracking of Hydrocarbons in a Riser Simulator: The Effect of Catalyst Accessibility and Acidity. **Energy & Fuels**. 2005, 19, 2, 329 – 338. Disponível em: <https://doi.org/10.1021/ef049848p>. Acesso em: 22 mar 2023.

MELLO, L. F.; GOBBO, R.; MOURE, G. T.; MIRACCA, I. Oxy-combustion technology development for Fluid Catalytic Crackers (FCC) – Large Pilot Scale Demonstration. **Energy Procedia**. 2013, 37, 7815 – 7824. Disponível em: <https://doi.org/10.1016/j.egypro.2013.06.562>. Acesso em: 30 mar 2022.

MOURA, C. A. D.; PINHO, A. R.; FUSCO, J. M. Heat of Cracking for Naphtha in Risers of Fcc Units. **AIChE Spring Meeting Proceedings**. 2006. Disponível em: <https://www.aiche.org/conferences/aiche-spring-meeting-and-global-congress-on-process-safety/2006/proceeding/paper/56a-heat-cracking-naphtha-risers-fcc-units>. Acesso em: 25 nov 2022.

NICCOM, P. K. Diesel creation in the FCC centered refinery. In: **COKING & CATCRACKING CONFERENCE**, 2013, Galveston. Disponível em: <https://refiningcommunity.com/wp-content/uploads/2017/07/Diesel-Creation-in-the-FCC-Centered-Refinery-Niccum-KBR-FCCU-Galveston-2013.pdf>. Acesso em: 25 mai 2022.

OLAFADEHAN, O. A.; SUNMOLA, O. P.; JAIYEOLA, A.; EFEOVBOKHAN, V.; ABATAN, O. G. Modelling and simulation of an industrial RFCCU-riser reactor for catalytic cracking of vacuum residue. **Applied Petrochemical Research**. 2018, 8, 219 – 237. Disponível em: <https://doi.org/10.1007/s13203-018-0212-y>. Acesso em: 24 nov 2022.

PASSAMONTI, F.; DE LA PUENTE, G.; GILBERT, W. R.; MORGADO JR, E.; SEDRAN, U. Comparison between fixed fluidized bed (FFB) and batch fluidized bed reactors in the evaluation of FCC catalysts. **Chemical Engineering Journal**. 2012, 183, 433 – 447. Disponível em: <https://doi.org/10.1016/j.cej.2011.12.081>. Acesso em: 19 out 2023.

PEKEDIZ, A.; KRAEMER, D.; BLASETTI, A.; de LASA, H. Heats of Catalytic Cracking. Determination in a Riser Simulator Reactor. **Industrial & Engineering Chemistry Research**. 1997, 36, 4516 – 4522. Disponível em: <https://doi.org/10.1021/ie9701229>. Acesso em: 25 nov 2022.

PETROBRAS to proceed with engineering study of GasLub project. **Fuels and Lubes**, December 30, 2022. Disponível em: <https://www.fuelsandlubes.com/petrobras-to-proceed-with-engineering-study-of-gaslub-project/>. Acesso em: 28 ago 2023.

PINHO, A. R.; ALMEIDA, M. B. B.; MENDES, F. L.; CASAVECHIA, L. C.; TALMADGE, M. S.; KINCHIN, C. M.; CHUM, H. L. Fast Pyrolysis Oil from Pinewood Chips co-processing

with Vacuum Gas Oil in an FCC Unit for Second Generation Fuel Production. **Fuel**. 2017, 188, 462 – 473. Disponível em: <https://doi.org/10.1016/j.fuel.2016.10.032>. Acesso em: 25 nov 2022.

SADEGHBEIGI, R. **Fluid Catalytic Cracking Handbook**. 4 ed; Butterworth-Heinemann: Oxford, 2020. Disponível em: <https://doi.org/10.1016/C2016-0-01176-2>. Acesso em: 01 jun 2022.

SCHWAAB, M.; PINTO, J. C. Optimum reparameterization of power function models. **Chemical Engineering Science**. 2008, 63 (18), 4631 – 4635. Disponível em: <https://doi.org/10.1016/j.ces.2008.07.005>. Acesso em: 24 mar 2023.

SELALAME, T. W.; PATEL, R.; MUJTABA, I. M.; JOHN, Y. M. A review of modelling of the FCC Unit – Part I: the Riser. **Energies**. 2022, 15 (1), 308. Disponível em: <https://doi.org/10.3390/en15010308>. Acesso em 22 mar 2023.

SHAMPINE, L. F.; REICHEL, M. W.; KIERZENKA, J. A. Solving index-1 DAEs in MATLAB and Simulink. **SIAM Review**. 1999, 18 (3), 538 – 552. Disponível em: <https://doi.org/10.1137/S003614459933425X>. Acesso em: 04 abr 2023.

SOUZA, J. A.; VARGAS, J. V. C.; VON MEIEN, O. F.; MARTIGNONI, W.; AMICO, S. C. A two-dimensional model for simulation, control and optimization of FCC Risers. **AIChE Journal**. 2006, 52 (5), 1895 – 1905. Disponível em: <https://doi.org/10.1002/aic.10798>. Acesso em: 25 nov 2022.

STANISLAUS, A.; MARAFI, A.; RANA, M. S. Recent advances in the science and technology of ultra low sulfur diesel (ULSD) production. **Catalysis Today**. 2010, 153, 1 – 68. Disponível em: <https://doi.org/10.1016/j.cattod.2010.05.011>. Acesso em: 25 mar 2023.

VOGT, E. T. C.; WECKHUYSSEN, B. M. Fluid catalytic cracking: recent developments on the grand old lady of zeolite catalysis. **Chemical Society Reviews**. 2015, 44, 7342 – 7370. Disponível em: <https://doi.org/10.1039/c5cs00376h>. Acesso em: 29 mar 2022.

ANNEX 1 – Experimental conditions of the tests performed at the 7.5 m<sup>3</sup>/d FCC pilot plant

Test	Feed	Feed nozzle	T <sub>rx</sub>	t <sub>c</sub>	CTO	Test	Feed	Feed nozzle	T <sub>rx</sub>	t <sub>c</sub>	CTO
1	C	1	-0.363	0.604	-0.723	36	B	1	0.161	0.352	-0.077
2	C	1	0.266	0.308	0.255	37	B	1	0.475	0.242	0.444
3	C	1	-0.048	0.440	-0.367	38	B	1	0.160	0.385	-0.151
4	C	1	-0.363	0.582	-0.732	39	B	3	0.168	-0.462	0.359
5	C	1	0.371	0.341	-0.414	40	B	3	-0.153	-0.396	-0.249
6	C	1	0.685	0.198	-0.005	41	B	1	-0.466	0.703	-0.701
7	C	3	-0.049	-0.385	-0.641	42	B	1	-0.151	0.538	-0.315
8	C	3	0.557	-0.527	0.589	43	D	1	-0.991	1.000	-0.945
9	C	3	0.264	-0.451	-0.019	44	D	1	-0.986	0.736	-0.693
10	C	3	0.685	-0.516	-0.093	45	D	1	-0.573	0.747	-0.633
11	C	3	0.979	-0.571	0.405	46	D	1	-0.153	0.495	-0.038
12	A1	1	-0.992	0.835	-0.803	47	D	1	0.265	0.352	0.419
13	A1	1	-0.572	0.571	-0.271	48	D	2	-0.990	0.374	-0.973
14	A1	1	-0.154	0.363	0.263	49	D	2	-0.571	0.198	-0.721
15	A1	4	-0.992	-0.835	-0.805	50	D	2	-0.573	0.176	-0.677
16	A1	4	-0.573	-0.890	-0.482	51	D	2	-0.155	-0.033	-0.071
17	A1	4	-0.154	-0.945	-0.011	52	D	2	0.265	-0.132	0.384
18	A1	3	-1.000	-0.385	-0.575	53	D	3	-0.993	-0.319	-0.981
19	A1	3	-0.574	-0.440	0.011	54	D	3	-0.574	-0.407	-0.660
20	A1	3	-0.155	-0.505	0.353	55	D	3	-0.155	-0.495	-0.011
21	A1	3	-0.155	-0.385	0.200	56	D	3	-0.152	-0.440	-0.781
22	A1	3	-0.574	-0.275	-0.359	57	D	3	0.266	-0.527	-0.132
23	A1	3	-0.991	-0.154	-0.748	58	D	4	-0.989	-0.868	-1.000
24	A1	3	-0.992	-0.374	-0.581	59	D	4	-0.992	-0.923	-0.997
25	A1	3	-0.152	-0.538	0.323	60	D	4	-0.569	-0.934	-0.759
26	A1	2	-0.574	0.187	-0.353	61	D	4	-0.573	-0.901	-0.592
27	A1	2	-0.992	0.363	-0.773	62	D	4	-0.573	-0.923	-0.773
28	A1	2	-0.154	0.044	0.175	63	D	4	-0.155	-0.978	-0.312
29	A1	2	-0.156	0.033	0.173	64	D	4	-0.156	-1.000	-0.049
30	A2	1	-0.990	0.978	-0.849	65	D	4	-0.154	-0.978	-0.121
31	A2	1	-0.151	0.429	0.282	66	D	4	-0.153	-0.945	-0.745
32	B	3	0.785	-0.571	1.000	67	D	4	-0.149	-0.989	-0.932
33	B	3	0.476	-0.527	0.400	68	D	4	0.262	-1.000	0.436
34	B	3	0.162	-0.451	-0.101	69	D	4	0.266	-1.000	-0.162
35	B	1	-0.154	0.538	-0.559						

Note: Normalized data between 0 and 1.

Source: The author, 2023.

ANNEX 2 – Experimental yields (wt. %) obtained at the 7.5 m<sup>3</sup>/d FCC pilot plant

Test	Dry gas	LPG	Naphtha	LCO	Slurry oil	Coke
1	1.83	7.78	28.29	18.15	38.79	5.17
2	2.85	12.58	40.65	19.25	19.42	5.25
3	2.36	9.76	34.58	19.26	29.16	4.88
4	2.03	8.02	25.95	18.37	40.63	4.99
5	3.27	10.90	33.81	19.26	28.50	4.26
6	4.11	13.31	39.44	18.59	19.89	4.66
7	2.35	7.55	25.57	18.21	41.52	4.79
8	3.04	13.12	39.00	17.91	21.57	5.35
9	2.41	10.45	33.95	18.54	29.64	5.01
10	3.27	10.91	34.71	18.65	28.00	4.45
11	3.99	13.40	38.56	18.12	21.12	4.81
12	1.44	7.33	20.08	17.09	48.46	5.6
13	1.71	10.72	32.74	20.20	29.25	5.38
14	2.60	14.90	38.16	19.42	19.43	5.49
15	0.77	4.13	17.21	15.80	56.40	5.69
16	1.12	6.68	24.47	17.76	44.73	5.24
17	1.56	8.76	40.57	17.62	26.40	5.1
18	1.10	5.39	19.86	16.47	50.12	7.06
19	1.22	7.65	28.95	19.91	35.95	6.31
20	1.90	10.39	31.80	19.76	30.53	5.62
21	1.89	9.84	34.14	19.28	29.51	5.34
22	1.39	7.57	25.53	18.80	41.24	5.49
23	0.92	4.37	17.47	16.16	55.02	6.06
24	1.20	5.46	21.02	17.09	48.47	6.77
25	2.19	11.28	37.74	17.27	26.18	5.33
26	1.77	10.07	27.20	19.12	36.38	5.47
27	1.30	7.19	18.08	16.04	51.40	5.98
28	2.37	12.68	34.17	19.57	25.97	5.24
29	2.61	13.59	33.67	19.22	25.74	5.17
30	0.86	4.49	17.21	16.30	54.63	6.5
31	2.15	11.67	37.24	20.39	22.88	5.68
32	3.53	14.82	40.81	16.64	19.09	5.11
33	2.94	12.70	37.46	17.55	24.55	4.8
34	2.29	10.00	32.31	18.07	32.84	4.49

Source: The author, 2023.

Test	Dry gas	LPG	Naphtha	LCO	Slurry oil	Coke
35	2.11	8.73	28.96	17.93	38.12	4.15
36	2.82	11.80	36.50	18.29	26.01	4.58
37	3.42	13.94	41.36	17.77	18.53	4.97
38	2.74	10.86	34.91	18.61	28.31	4.57
39	2.46	11.68	36.44	17.78	26.44	5.21
40	2.04	9.32	29.63	17.26	36.77	4.98
41	1.84	7.06	24.01	16.74	45.57	4.77
42	2.23	9.19	30.61	18.72	34.37	4.88
43	0.83	5.61	20.42	25.83	42.55	4.75
44	0.67	6.93	23.07	26.96	37.36	5.01
45	1.61	8.60	26.12	26.25	33.01	4.42
46	2.27	12.93	34.91	25.20	19.84	4.86
47	3.03	15.49	38.32	23.35	14.57	5.23
48	0.58	3.72	17.41	23.99	49.36	4.95
49	1.10	5.86	23.30	25.17	40.12	4.45
50	0.94	6.74	23.96	24.83	39.10	4.43
51	1.87	11.46	34.91	25.36	21.56	4.85
52	2.52	14.07	37.57	24.26	16.60	4.97
53	0.86	6.30	18.19	24.19	45.72	4.74
54	1.02	8.58	23.16	25.30	37.63	4.3
55	1.55	10.13	32.29	25.92	25.37	4.73
56	1.04	6.08	24.11	25.85	39.30	3.61
57	1.58	8.51	33.61	26.31	25.87	4.12
58	0.66	5.56	17.21	23.43	48.82	4.32
59	0.95	6.56	14.26	23.27	50.19	4.77
60	0.99	7.08	19.91	24.15	43.69	4.17
61	0.97	7.56	21.64	24.57	40.89	4.36
62	1.20	7.09	16.94	24.46	45.96	4.27
63	1.54	9.78	25.31	24.16	34.95	4.27
64	1.30	9.94	28.01	24.83	31.38	4.54
65	1.33	9.97	27.10	24.63	32.37	4.6
66	1.24	6.91	19.03	24.73	44.45	3.72
67	1.26	5.67	15.75	24.55	49.28	3.48
68	1.62	10.79	30.63	24.60	27.70	4.66
69	1.91	11.28	28.04	24.09	30.55	4.14

Source: The author, 2023.

## ANNEX 3 – Characterization of the liquid products to obtain thermodynamic parameters

Test	d20	DS wt.% vap. (°C)						
		DS_0	DS_10	DS_30	DS_50	DS_70	DS_90	DS_100
1	0.8233	-6.4	108.6	221.9	333.6	408.8	470.5	536.7
2	0.7991	-6.4	73.6	145.6	226.2	322.1	426.4	524.3
3	0.7986	-26.9	86.4	177.0	276.2	373.9	451.6	532.2
4	0.8753	3.5	110.3	228.7	340.5	412.3	472.9	537.4
5	0.8516	-6.4	89.2	178.5	275.6	372.5	450.2	531.9
6	0.8305	-28.5	78.3	151.5	230.4	331.3	430.1	525.5
7	0.8764	7.1	114.6	236.8	345.8	415.9	477.4	538.4
8	0.8232	-8.0	79.8	158.1	241.7	341.5	440.3	530.6
9	0.8533	24.3	98.2	186.1	286.6	381.2	457.9	534.8
10	0.8087	4.7	94.8	178.1	275.3	373.5	452.9	533.4
11	0.8381	13.3	88.1	161.1	245.6	342.5	437.6	529.0
12	0.8894	8.2	139.4	278.0	371.8	429.6	483.8	539.0
13	0.8657	-0.4	97.6	187.4	280.0	369.6	449.4	530.6
14	0.8476	-4.4	78.2	152.0	230.2	322.8	423.8	521.6
15	0.896	19.4	152.8	310.2	392.4	441.6	494.0	540.6
16	0.8823	5.6	118.6	246.4	352.8	420.8	480.2	539.0
17	0.8688	-10.4	80.4	188.0	301.2	392.2	465.0	536.2
18	0.8879	8.0	137.8	279.4	376.4	432.6	487.0	539.6
19	0.8711	-10.0	111.8	209.0	309.2	392.6	461.8	534.4
20	0.8612	-2.8	96.0	185.2	281.8	375.2	453.8	532.6
21	0.8576	-1.6	87.8	174.8	273.8	369.8	452.0	532.2
22	0.8769	2.0	110.8	228.2	336.6	409.8	472.0	537.0
23	0.8956	7.0	143.4	302.2	387.8	438.8	491.4	540.4
24	0.8871	2.2	128.8	269.0	368.4	428.6	483.6	539.2
25	0.8636	-1.0	81.4	158.4	249.4	358.8	458.4	538.2
26	0.8728	-4.4	110.2	218.0	320.6	398.4	464.2	534.6
27	0.8871	12.4	144.4	298.4	383.4	436.0	488.8	539.8
28	0.8589	-3.2	87.4	169.2	262.2	356.6	443.4	528.6
29	0.8586	-3.2	86.8	169.2	263.4	357.2	443.6	528.4
30	0.8969	24.4	151.2	303.8	389.0	440.6	492.2	540.0
31	0.8638	-5.4	82.6	162.6	245.6	338.2	433.8	525.4
32	0.8413	2.0	72.8	141.4	223.6	326.5	430.7	523.2
33	0.8472	2.0	78.4	160.4	249.0	356.7	443.9	527.4
34	0.8649	4.5	96.3	188.1	296.9	390.8	458.7	532.2

Source: The author, 2023.

Test	d20	DS wt.% vap. (°C)						
		DS_0	DS_10	DS_30	DS_50	DS_70	DS_90	DS_100
35	0.8700	3.8	99.8	211.0	326.2	405.1	464.9	533.6
36	0.8628	2.0	75.5	162.9	254.5	361.5	444.0	527.1
37	0.7975	1.7	70.6	139.0	217.9	317.2	423.1	519.1
38	0.858	2.0	81.2	169.7	269.5	371.4	447.6	527.8
39	0.8529	2.4	77.6	162.7	254.7	364.6	447.2	528.7
40	0.8708	3.8	97.2	203.2	320.3	403.8	465.4	534.1
41	0.8783	5.6	111.6	248.1	361.8	422.6	475.3	536.4
42	0.8679	4.9	96.8	196.8	303.4	392.3	458.0	531.8
43	0.8919	37.8	138.6	252.0	339.6	407.8	463.2	529.6
44	0.8858	27.6	126.0	237.2	315.6	391.8	454.6	525.8
45	0.8759	16.2	112.2	226.4	298.6	380.8	450.6	525.4
46	0.8581	-1.2	87.6	168.2	248.6	324.0	420.6	511.2
47	0.8524	-4.2	74.6	144.6	227.2	296.0	400.6	504.2
48	0.8924	40.0	157.0	275.2	365.2	428.8	480.8	535.6
49	0.8834	27.8	131.6	245.6	327.6	405.0	467.6	530.8
50	0.8811	-7.8	129.6	244.8	325.2	405.0	469.2	532.2
51	0.8634	-0.6	94.2	175.0	251.4	333.8	425.0	507.0
52	0.8571	-7.0	84.4	160.2	233.4	307.2	409.6	505.0
53	0.8952	39.0	158.0	267.6	357.0	418.8	470.2	533.6
54	0.8839	20.2	125.4	239.4	320.8	398.4	459.6	528.6
55	0.8669	0.4	98.6	189.0	264.8	350.0	435.2	513.0
56	0.8823	27.8	125.8	240.4	322.2	399.8	460.4	529.0
57	0.8670	2.8	97.4	186.4	261.8	348.6	435.6	516.2
58	0.8839	39.6	163.6	276.2	368.0	425.2	474.2	534.2
59	0.8996	19.4	140.0	265.2	358.6	423.0	478.2	538.4
60	0.8914	39.0	143.6	258.6	350.4	415.4	469.0	533.2
61	0.8917	37.6	138.0	249.8	338.4	409.4	465.4	532.0
62	0.8936	6.2	112.8	228.2	313.4	399.2	471.2	538.2
63	0.8804	24.4	118.2	229.2	313.4	394.4	458.6	529.4
64	0.8739	22.2	111.2	221.2	294.8	380.2	451.8	526.2
65	0.8776	17.8	111.0	222.2	296.6	383.8	453.6	527.2
66	0.8894	25.2	134.2	250.0	340.0	411.6	468.0	533.2
67	0.8939	8.6	114.0	238.6	328.6	409.8	475.0	538.6
68	0.8688	10.4	100.8	199.2	273.4	364.6	445.6	523.8
69	0.8751	20.0	110.0	211.4	289.0	378.6	452.2	527.6

Source: The author, 2023.

Test	D86 v.% vap. (°C)							MeABP (°F)
	D86_0	D86_10	D86_30	D86_50	D86_70	D86_90	D86_100	
1	2.5	71.1	178.9	334.0	425.6	482.9	516.7	450.7
2	29.4	74.9	129.1	223.0	352.7	462.1	505.9	367.6
3	1.1	68.5	145.3	274.5	407.7	483.7	522.3	404.4
4	7.5	70.6	185.9	341.2	427.0	482.9	516.2	456.3
5	18.0	73.7	148.9	273.9	405.5	481.5	520.4	410.5
6	17.8	80.9	136.5	227.3	366.8	469.1	512.1	382.0
7	12.9	76.4	197.4	346.7	429.6	486.6	518.7	468.9
8	27.5	78.1	139.6	238.9	376.2	478.5	520.1	386.7
9	38.4	80.1	153.4	285.2	412.4	487.3	524.6	424.5
10	28.6	80.7	148.3	273.5	407.7	485.8	524.3	417.1
11	44.4	86.6	142.0	242.9	374.6	472.1	514.0	398.3
12	29.4	108.9	255.3	373.8	436.8	485.5	515.6	535.1
13	29.2	86.4	162.2	278.4	396.1	474.7	513.4	427.6
14	34.0	81.2	137.5	227.1	350.5	455.6	499.4	378.9
15	40.0	121.1	298.7	395.4	445.4	492.1	519.0	573.2
16	13.4	80.7	210.1	354.0	433.4	488.0	519.3	482.0
17	-10.2	42.4	142.1	300.4	420.7	490.9	526.4	388.9
18	24.0	102.6	253.9	378.7	439.1	488.1	517.2	531.3
19	18.9	92.0	177.5	308.7	414.9	480.8	516.8	456.8
20	23.4	81.2	156.3	280.3	405.2	482.3	520.3	423.0
21	19.3	71.0	143.2	272.0	401.9	483.4	521.8	402.9
22	10.8	75.3	189.1	337.1	425.3	483.1	516.5	459.8
23	24.5	107.6	287.6	390.6	443.2	490.2	517.9	554.6
24	15.3	91.7	240.7	370.3	437.0	486.6	516.8	512.3
25	26.6	73.7	133.7	246.8	403.4	506.7	545.0	386.8
26	16.1	84.4	184.4	320.5	416.7	478.6	513.9	457.9
27	32.2	112.3	284.1	386.0	441.0	488.2	516.7	555.1
28	24.9	77.3	143.0	260.0	386.8	474.0	514.0	400.6
29	23.4	75.5	142.0	261.3	386.9	473.6	513.5	399.0
30	43.6	120.2	289.6	391.8	445.3	491.2	518.5	567.7
31	30.4	81.1	144.7	242.9	366.3	464.5	506.5	392.3
32	33.5	73.2	123.6	220.3	363.8	473.0	515.2	364.7
33	28.6	71.8	137.9	246.4	399.5	487.2	526.6	389.8
34	15.4	68.6	147.0	295.9	421.8	486.1	522.4	418.5

Source: The author, 2023.

Test	D86 v.% vap. (°C)							MeABP (°F)
	D86_0	D86_10	D86_30	D86_50	D86_70	D86_90	D86_100	
35	2.9	58.9	163.7	326.3	424.5	479.5	514.2	429.7
36	23.7	65.1	137.8	252.1	403.8	485.6	525.0	387.1
37	35.0	73.5	123.7	214.5	350.8	462.2	505.5	359.9
38	18.0	63.0	137.2	267.6	409.0	483.2	521.7	393.5
39	24.9	67.4	137.2	252.3	409.9	491.9	530.7	390.2
40	1.7	56.0	153.4	320.2	426.6	483.7	518.4	420.1
41	-1.6	61.0	204.0	363.4	431.0	478.1	510.2	465.0
42	15.8	69.1	158.3	302.6	419.0	480.8	517.2	426.3
43	66.5	125.6	233.6	340.3	420.0	470.0	504.0	523.7
44	63.0	120.5	225.4	315.3	408.7	467.2	502.7	502.7
45	53.3	109.3	218.4	297.7	401.7	468.3	505.0	480.8
46	36.9	88.2	152.5	246.0	338.0	437.5	479.1	396.3
47	29.8	74.6	126.6	224.0	304.7	414.5	460.0	355.8
48	70.8	140.7	255.7	367.0	439.1	485.4	515.3	561.0
49	61.4	122.5	231.4	327.8	423.3	481.5	514.3	515.7
50	37.4	121.2	231.8	325.3	425.0	485.1	517.9	514.0
51	42.7	97.9	162.5	248.9	353.3	446.0	485.0	414.7
52	37.9	90.9	149.4	230.4	319.6	426.5	469.6	385.7
53	74.5	145.8	248.3	358.4	427.6	473.3	506.2	555.4
54	54.5	116.6	225.4	320.7	416.5	473.2	508.0	503.8
55	43.4	100.8	177.3	262.7	372.2	457.4	495.1	434.1
56	59.2	116.4	226.1	322.2	418.0	474.0	508.6	505.0
57	45.1	100.2	174.9	259.6	372.1	459.5	498.1	431.1
58	73.8	148.4	255.2	369.9	431.9	474.9	506.6	566.0
59	44.5	116.8	242.3	360.1	433.5	483.4	515.2	530.9
60	64.9	126.6	236.9	351.5	425.9	474.0	507.2	532.0
61	65.9	124.8	230.4	339.0	423.4	474.2	508.2	522.3
62	36.9	99.9	210.8	313.0	423.6	492.9	527.0	480.1
63	53.6	108.1	212.6	313.0	414.9	475.0	510.4	487.7
64	57.6	109.0	212.1	293.7	403.6	472.4	508.9	476.9
65	53.7	107.8	212.6	295.6	408.8	475.4	511.7	478.3
66	53.4	118.0	229.5	340.7	426.1	477.3	510.8	517.4
67	30.9	93.0	217.6	328.8	431.1	492.3	525.3	485.3
68	49.6	101.9	188.9	271.6	392.3	472.3	510.1	448.7
69	56.0	108.1	199.2	287.7	405.4	476.5	513.4	468.9

Source: The author, 2023.

Test	d60	Kw	Tpc (R)	API	LHV (kJ/kg)
1	0.8272	11.7	1257.1	39.6	42990
2	0.8031	11.7	1172.9	44.7	43301
3	0.8026	11.9	1204.6	44.8	43307
4	0.8790	11.0	1289.2	29.5	42223
5	0.8554	11.2	1236.7	33.9	42585
6	0.8343	11.3	1201.1	38.1	42890
7	0.8801	11.1	1300.8	29.3	42206
8	0.8271	11.4	1201.7	39.6	42991
9	0.8571	11.2	1250.1	33.6	42560
10	0.8126	11.8	1220.8	42.6	43182
11	0.8419	11.3	1219.3	36.6	42783
12	0.8931	11.2	1364.8	26.9	42001
13	0.8694	11.1	1259.0	31.2	42372
14	0.8514	11.1	1206.3	34.7	42644
15	0.8997	11.2	1400.5	25.8	41895
16	0.8860	11.1	1315.4	28.2	42113
17	0.8725	10.9	1225.3	30.7	42324
18	0.8916	11.2	1360.7	27.2	42025
19	0.8748	11.1	1287.5	30.2	42289
20	0.8650	11.1	1252.7	32.1	42441
21	0.8614	11.1	1232.9	32.8	42495
22	0.8806	11.0	1293.1	29.2	42198
23	0.8993	11.2	1384.8	25.8	41902
24	0.8908	11.1	1344.2	27.3	42037
25	0.8673	10.9	1221.0	31.6	42404
26	0.8765	11.1	1289.4	29.9	42262
27	0.8908	11.3	1380.3	27.3	42037
28	0.8627	11.0	1231.4	32.5	42476
29	0.8624	11.0	1229.8	32.6	42480
30	0.9006	11.2	1396.5	25.6	41881
31	0.8675	10.9	1226.1	31.6	42401
32	0.8451	11.1	1190.4	35.9	42737
33	0.8510	11.1	1216.1	34.8	42650
34	0.8686	11.0	1250.5	31.4	42384

Source: The author, 2023.

Test	d60	Kw	Tpc (R)	API	LHV (kJ/kg)
35	0.8737	11.0	1263.0	30.4	42306
36	0.8665	10.9	1220.9	31.8	42416
37	0.8015	11.7	1165.4	45.0	43320
38	0.8618	11.0	1224.5	32.7	42489
39	0.8567	11.1	1219.1	33.7	42566
40	0.8745	11.0	1254.7	30.3	42293
41	0.8820	11.0	1298.4	28.9	42176
42	0.8716	11.0	1258.8	30.8	42338
43	0.8956	11.1	1356.5	26.5	41961
44	0.8895	11.1	1335.2	27.6	42058
45	0.8796	11.1	1311.0	29.4	42214
46	0.8619	11.0	1227.1	32.7	42488
47	0.8562	10.9	1187.3	33.8	42573
48	0.8961	11.2	1388.2	26.4	41953
49	0.8871	11.2	1345.0	28.0	42096
50	0.8848	11.2	1342.2	28.4	42132
51	0.8671	11.0	1246.3	31.7	42407
52	0.8609	11.0	1217.0	32.9	42503
53	0.8989	11.2	1385.2	25.9	41908
54	0.8876	11.1	1335.1	27.9	42088
55	0.8706	11.1	1265.3	31.0	42353
56	0.8860	11.2	1335.2	28.2	42113
57	0.8707	11.1	1262.7	31.0	42352
58	0.8876	11.4	1387.4	27.9	42088
59	0.9033	11.0	1367.0	25.2	41838
60	0.8951	11.1	1363.3	26.6	41969
61	0.8954	11.1	1355.2	26.5	41964
62	0.8973	10.9	1319.6	26.2	41934
63	0.8841	11.1	1319.3	28.5	42143
64	0.8776	11.1	1306.5	29.7	42245
65	0.8813	11.1	1309.7	29.1	42187
66	0.8931	11.1	1349.8	26.9	42001
67	0.8976	10.9	1324.4	26.1	41929
68	0.8725	11.1	1279.2	30.7	42324
69	0.8788	11.1	1300.2	29.5	42226

Source: The author, 2023.

## ANNEX 4 – Composition of the gaseous products

Test	Dry gas composition (wt.%)				Dry gas composition (wt.%)			
	H <sub>2</sub> +H <sub>2</sub> S	Methane	Ethane	Ethylene	Propane	Propylene	Butanes	Butylenes
1	14.2	31.5	24.3	30.0	6.0	36.2	13.6	44.3
2	11.9	33.6	24.3	30.2	5.7	37.1	14.2	42.9
3	12.9	32.6	24.2	30.3	5.9	36.9	13.6	43.6
4	11.3	33.6	25.1	30.0	6.7	37.9	13.9	41.5
5	9.9	34.0	25.7	30.4	6.5	37.5	11.5	44.5
6	6.4	35.8	25.9	31.9	6.3	38.7	11.3	43.7
7	13.6	32.4	23.1	30.9	6.1	37.0	11.0	45.9
8	11.4	34.5	23.6	30.5	5.3	36.7	13.1	44.8
9	12.5	33.6	23.9	30.0	5.3	35.3	12.7	46.7
10	9.5	34.2	25.0	31.3	5.9	36.2	10.5	47.4
11	7.8	35.2	25.2	31.8	5.6	36.7	10.5	47.1
12	15.4	31.9	23.7	29.1	6.9	35.4	17.0	40.7
13	8.5	34.8	25.8	30.9	6.4	35.1	18.0	40.4
14	8.1	35.6	25.1	31.2	6.0	36.8	16.8	40.4
15	12.3	33.0	24.4	30.4	7.2	36.9	19.1	36.8
16	8.4	35.1	25.7	30.8	7.0	35.5	18.6	39.0
17	9.3	35.3	24.7	30.7	6.7	36.6	17.6	39.1
18	14.1	31.2	22.5	32.2	6.5	35.7	17.3	40.5
19	14.5	30.8	23.5	31.1	6.5	34.4	19.2	39.9
20	8.0	34.8	24.4	32.9	6.5	36.1	16.9	40.5
21	13.9	33.4	23.7	29.1	6.5	35.4	17.0	41.2
22	13.8	33.0	24.5	28.7	7.1	35.5	18.2	39.3
23	16.0	31.9	23.4	28.7	7.1	36.8	16.8	39.3
24	12.5	32.4	22.9	32.2	6.9	37.2	16.9	39.0
25	10.0	34.5	24.2	31.2	6.6	35.7	16.6	41.1
26	9.7	34.7	26.0	29.6	7.0	35.2	17.7	40.1
27	3.9	36.0	26.9	33.2	6.7	36.1	15.8	41.3
28	6.0	36.6	26.2	31.2	6.6	36.4	16.2	40.8
29	9.5	35.2	25.2	30.1	6.5	36.2	16.3	41.0
30	3.7	37.3	27.6	31.5	7.2	36.4	15.3	41.2
31	9.2	35.3	25.5	30.1	6.0	36.1	15.8	42.2
32	7.4	36.2	24.6	31.9	6.0	37.5	13.4	43.1
33	8.7	35.0	25.0	31.3	6.4	37.8	13.9	41.9
34	11.8	34.0	24.8	29.5	6.7	36.8	14.5	42.0

Source: The author, 2023.

Test	Dry gas composition (wt.%)				Dry gas composition (wt.%)			
	H <sub>2</sub> +H <sub>2</sub> S	Methane	Ethane	Ethylene	Propane	Propylene	Butanes	Butylenes
35	12.0	33.6	25.6	28.8	7.4	36.6	14.9	41.1
36	10.4	34.4	25.6	29.6	7.0	37.3	14.4	41.3
37	9.2	35.3	25.3	30.3	6.5	37.5	13.7	42.3
38	10.6	34.3	25.7	29.5	7.0	37.5	13.7	41.8
39	12.8	33.9	23.8	29.5	6.7	36.8	16.1	40.5
40	14.4	32.9	24.0	28.8	7.0	36.8	15.9	40.3
41	12.7	33.5	24.8	29.0	7.6	37.9	14.3	40.2
42	14.1	32.9	24.5	28.5	7.0	36.4	14.5	42.1
43	4.0	36.8	27.5	31.7	7.5	33.7	19.8	38.9
44	7.2	29.4	33.7	29.7	13.3	34.0	16.6	36.2
45	11.5	34.1	24.4	30.0	7.3	36.2	17.7	38.8
46	8.0	35.8	24.5	31.7	6.4	36.5	17.3	39.9
47	6.4	36.9	24.1	32.6	6.0	37.9	16.2	39.9
48	8.4	34.7	26.0	30.9	7.4	34.3	19.7	38.6
49	6.9	36.1	25.3	31.6	7.4	36.3	17.4	38.9
50	2.8	35.9	27.8	33.4	8.3	33.3	16.5	41.9
51	3.0	38.0	26.0	33.0	6.4	35.7	17.4	40.5
52	15.9	31.6	22.0	30.5	6.0	35.5	15.9	42.6
53	3.8	33.8	29.0	33.4	7.4	33.6	20.8	38.2
54	2.6	32.4	32.3	32.7	11.5	34.3	16.6	37.6
55	7.2	35.4	25.0	32.4	5.9	35.4	17.6	41.1
56	2.5	36.6	28.4	32.4	6.5	33.8	15.7	43.9
57	4.6	36.9	26.0	32.6	5.4	36.2	14.0	44.3
58	5.4	34.4	28.1	32.1	7.3	32.8	22.1	37.9
59	15.1	31.4	24.6	28.9	7.6	33.4	22.2	36.8
60	4.3	36.2	26.8	32.7	7.3	33.7	20.2	38.8
61	3.6	36.4	26.9	33.1	7.3	34.4	21.1	37.2
62	14.8	32.9	23.3	29.1	7.4	34.2	19.9	38.4
63	11.6	34.5	24.0	29.9	6.7	34.2	19.1	40.1
64	3.1	36.9	26.2	33.7	6.4	34.1	19.7	39.8
65	1.8	36.4	26.2	35.6	6.8	34.5	20.0	38.8
66	3.3	39.5	26.6	30.5	7.2	34.6	17.8	40.3
67	11.1	35.2	24.8	28.9	7.7	36.4	16.8	39.1
68	2.8	38.2	24.9	34.1	6.1	36.1	18.0	39.7
69	4.2	37.2	24.9	33.7	5.9	36.4	16.5	41.2

Source: The author, 2023.

## ANNEX 5 – Distillation curves of the VGO batches

wt.% vap.	A1	A2	B	C	D	wt.% vap.	A1	A2	B	C	D
0	249.8	255.8	247.2	254.2	216.6	36	421.2	424.2	430.2	435.6	408
1	266.0	272.8	277.6	274.8	221.8	37	422.6	425.6	431.6	437.2	410
2	288.2	293.8	308.6	300.6	233.2	38	424	426.8	433.4	439.2	412.2
3	300.6	306	325	315.4	241.4	39	425.2	428.2	435	441	414.6
4	310.4	316	335.6	327.4	246	40	426.4	429.6	436.6	442.8	416.6
5	319.2	323.6	344.6	336.4	255.4	41	427.8	430.8	438	444.6	418.8
6	325.8	331.4	352.4	344.4	262.6	42	429.2	432.6	439.6	446.4	420.4
7	333.2	337.6	358.2	351.2	270	43	430.6	434.6	441	448.4	422.4
8	338.6	343.6	364	356.6	279	44	432.2	436.4	442.6	450.2	424.4
9	344.2	350	368.6	361.6	288.4	45	434.2	438.6	444.2	452.2	426.4
10	350.0	355.6	372.8	366.2	297	46	436	440.6	445.8	454.2	428.4
11	355.4	361.2	376.2	370.6	305.4	47	438.2	442.4	447.2	456	430
12	360.6	365.6	379.6	375.2	312.8	48	440.4	444.6	448.8	458.2	432
13	365.0	370.2	382.8	379.2	319.4	49	442.4	446.6	450.2	460	433.8
14	369.4	373.4	385.8	383.4	326.6	50	444.6	448.8	452	462	435.8
15	372.6	376.4	388.8	387.4	331.6	51	446.6	450.6	453.6	464.2	437.8
16	375.6	379.2	391.2	390.8	338	52	449	452.6	455.2	466.4	439.6
17	378.0	382.2	394.2	394	343.2	53	450.8	454.4	456.8	468.4	441.4
18	380.8	385	397	397.2	348.4	54	452.8	456.2	458.4	470.4	443.4
19	383.6	387.4	399.8	400.4	353.2	55	454.8	458.2	460	472.6	445.4
20	385.8	390.2	402	402.8	357.6	56	456.8	460.2	461.6	474.6	447.6
21	388.4	393.2	404.6	405.6	362.2	57	458.8	462.2	463.4	476.8	449.4
22	390.8	396.2	407.2	408.4	366.4	58	461	464.2	465.2	479	451.4
23	394.0	399.2	409.4	411	370	59	463	466.2	466.8	481.2	453.6
24	396.6	402.2	411.8	413	373.8	60	465.2	468	468.6	483.6	455.6
25	399.4	405.2	413.4	415.4	377.4	61	467.4	470	470.4	486	457.6
26	402.4	408	415.2	417.4	380.4	62	469.4	471.8	472.2	488.4	459.6
27	405.2	410.4	417	419.4	383.8	63	471.4	473.8	474	490.8	462
28	408	412.4	418.6	421.4	387	64	473.4	475.8	475.8	493.2	464.2
29	410	414	420.4	423	389.8	65	475.4	477.6	477.6	495.8	466.4
30	412.2	415.6	421.8	424.8	392.8	66	477.6	479.6	479.6	498	468.6
31	413.8	417.2	423.2	426.6	395.6	67	479.8	481.6	481.4	500.4	470.8
32	415.4	418.6	424.6	428.4	398.4	68	482	483.8	483.4	502.6	473
33	417	420	426	430.2	400.6	69	484.2	485.8	485.6	505.2	475.4
34	418.2	421.6	427.4	431.8	403.2	70	486.4	488	487.6	507.6	478
35	419.6	423	429	433.8	405.6	71	488.8	490	489.6	510.2	480.4

Note: Distillation temperature in °C.

Source: The author, 2023.

wt.% vap.	A1	A2	B	C	D	wt.% vap.	A1	A2	B	C	D
72	491	492.2	491.8	512.8	483.2	87	530.0	528	529.8	567.6	557.6
73	493.4	494.4	494	515.6	486	88	533.4	531.2	533	573.2	565.8
74	495.8	496.6	496.4	518.4	489	89	536.8	534.4	536.6	579.8	574.2
75	498	498.6	498.4	521.4	492.4	90	540.4	537.8	540.4	587.4	584.2
76	500.4	500.8	500.6	524.2	495.8	91	544.2	541.4	544.4	596.2	594.4
77	502.6	502.8	502.8	527.2	499.2	92	548.6	545.2	549	607.4	606.4
78	505.0	505	505	530.2	503.2	93	553.2	549.8	554	621	619.2
79	507.4	507.2	507.4	533.4	507.4	94	558.4	554.8	559.6	637.6	633.2
80	509.8	509.6	509.8	536.8	512.2	95	564.0	560.2	565.8	655.4	649
81	512.4	511.8	512.4	540.4	517.6	96	570.2	566.6	572.8	672.4	666
82	515.2	514.4	515	544	523.4	97	578.0	574	581.6	687.6	683.8
83	518.0	516.8	517.8	548.2	529.6	98	588.4	584.8	593.6	705.2	702.4
84	520.8	519.6	520.6	552.6	536	99	605.8	602.4	614.4	726.8	722.2
85	523.8	522.2	523.4	557.4	542.6	100	621.8	619.2	632	737.6	734.2
86	526.8	525	526.4	562.2	549.8						
Parameters of the logistic function in terms of normalized temperatures between -1 and 1											
	A1	A2	B	C	D						
a	6.24429	6.47546	4.20636	6.89738	5.01550						
b	0.74514	0.71467	0.60905	0.60409	0.10138						
Parameters of the logistic function in terms of original temperatures in °C											
	A1	A2	B	C	D						
a	$2.39704 \cdot 10^{-2}$	$2.48578 \cdot 10^{-2}$	$1.61473 \cdot 10^{-2}$	$2.64775 \cdot 10^{-2}$	$1.92534 \cdot 10^{-2}$						
b	-10.69113	-11.14498	-7.09481	-12.02831	-9.08440						
R <sup>2</sup> of the regression of experimental distillation curve											
	A1	A2	B	C	D						
	0.994	0.994	0.986	0.998	0.982						

Source: The author, 2023.

## ANNEX 6 – Distillation curves of the liquid products

wt.% vap.	Run					wt.% vap.	Run				
	1	2	3	4	5		1	2	3	4	5
0	-6.4	-6.4	-26.9	3.5	-6.4	36	254.2	167.7	206.4	266.5	206.6
1	26.8	5.9	5.9	35.3	21.8	37	261.7	172.5	210.3	271.6	210.7
2	40	32.9	36.7	41.5	38.4	38	267.7	177.7	217.4	277.3	217.7
3	55.1	38.6	39.8	61.1	42.9	39	272.8	181.9	222.4	283.6	222.4
4	69.4	40.6	51.8	70.1	56.9	40	278.4	185.9	225.8	290.7	225.7
5	72.1	53	61.1	74.2	68.3	41	284.8	189.3	228.7	295.6	228.7
6	79.6	59	69.4	81.3	70.3	42	291.8	194.7	235.4	300.9	235.3
7	86.8	67.4	71.1	92.1	73	43	296.5	198.6	242.6	306.4	242.3
8	96	69.8	74.2	98.2	78.9	44	301.8	201.6	246.5	312	246.4
9	99.4	71.2	79.9	104.4	82.1	45	307.6	205.3	249.5	317	249.3
10	108.6	73.6	86.4	110.3	89.2	46	313.1	208.5	254.3	321.3	253.8
11	110.9	79	93.5	114.9	95.9	47	318.1	214.7	261.3	326.6	260.6
12	115.9	80.9	97.5	124.2	98.5	48	322.5	219.7	266.6	332.1	266.1
13	124.2	86.9	99.8	129.4	101.5	49	328.1	224.1	271.1	336.8	270.7
14	128.5	91.2	108.6	136.8	109.6	50	333.6	226.2	276.2	340.5	275.6
15	136.1	96.2	110.3	138.8	110.8	51	337.9	228.6	281.5	345.2	280.6
16	138.2	98.5	113	143.6	114.6	52	342	234.7	287.5	350.1	286.5
17	142.6	100.4	119.5	152.1	122.3	53	346.7	241.7	293.7	354	292.9
18	149.3	107.9	124.8	159.7	125.9	54	351.5	245.8	297.8	357.8	296.9
19	158.2	110.2	128.5	164.7	131.4	55	355.5	248.5	302.6	361.9	301.8
20	161.9	111.2	135.3	167.8	136.4	56	359.4	251.4	308.8	365.7	307.8
21	166.8	114.9	137.6	174.3	138	57	363.4	256.9	313.9	369.5	312.8
22	172.1	120.2	139.6	182.5	141.3	58	367.5	263.2	318.4	373.4	317.6
23	179.7	124.4	143.2	187.9	144.2	59	371.2	267.6	322.8	376.8	321.6
24	185.6	127	149.3	195.8	150.5	60	375	271.7	328.7	380.1	327.1
25	192.2	133.6	156.8	200.6	158.2	61	378.5	276.4	334.2	383.5	332.8
26	198.1	136.5	160.3	206.7	160.7	62	381.8	281.3	338	387.2	337.2
27	203.1	137.9	164	212.9	165.2	63	385.6	287.1	342.5	390.5	340.9
28	208.2	139.1	167	220.2	167.3	64	389.2	293.3	347.6	393.6	345.9
29	215.5	142.6	171.8	225.2	172.3	65	392.4	297.1	352.2	397	351
30	221.9	145.6	177	228.7	178.5	66	395.8	301.9	356.4	400.1	355.1
31	226.2	151.1	182.5	236.5	183.4	67	399.1	308.2	360.8	403	359.4
32	230.9	158.3	186.7	244.1	187	68	402.2	313.2	365	406.3	363.5
33	238.5	160.3	193.3	248.3	193.8	69	405.4	318.1	369.5	409.5	368.1
34	245.4	162.9	197.9	252.8	198.2	70	408.8	322.1	373.9	412.3	372.5
35	249.2	166.4	201.6	260.2	202	71	411.8	328.3	377.8	415.1	376.4

Note: Distillation temperature in °C.

Source: The author, 2023.

wt.% vap.	Run					wt.% vap.	Run				
	1	2	3	4	5		1	2	3	4	5
72	414.5	334.3	381.6	418.2	380.2	87	459	410.4	439.6	461.4	438.2
73	417.7	338.1	386	421.2	384.4	88	462.6	415.2	443.4	465	442
74	420.9	342.8	390.2	423.8	388.7	89	466.5	421	447.3	468.7	445.9
75	423.5	348.8	393.9	426.6	392.3	90	470.5	426.4	451.6	472.9	450.2
76	426.5	353.5	397.9	429.4	396.5	91	474.9	432	456.3	477.1	454.8
77	429.4	358.2	401.7	432	400.3	92	479.6	438.1	461.6	481.7	460
78	432	363.2	405.7	434.6	403.9	93	484.7	444.3	467.2	486.8	465.7
79	434.7	368.7	409.9	437.5	408.3	94	490.2	451.3	473.4	492.3	471.9
80	437.7	374.2	413.1	440.3	411.9	95	496.2	459.3	480.4	498.1	478.9
81	440.6	378.7	417.1	443	415.5	96	502.8	468.5	488.4	504.5	487
82	443.4	383.9	421	445.6	419.6	97	510.3	479.3	497.7	511.9	496.4
83	446.1	389.4	424.6	448.6	423.1	98	519.2	492.9	508.6	520.6	507.6
84	449.2	394.5	428.4	451.5	426.9	99	530	511.2	522.9	530.9	522.3
85	452.2	399.4	431.8	454.5	430.6	100	536.7	524.3	532.2	537.4	531.9
86	455.5	404.8	435.6	457.8	434.1						
(a) Particular nodal points. Densities of probability ( $\theta_i$ ) expressed for normalized temperatures (between 0 and 1)											
i	Run:	1	2	3	4	5					
0	$T_0$ (°C)	-6.4	-6.4	-26.9	3.5	-6.4					
	$T_{0,norm}$	0.0388	0.0388	0.0028	0.0562	0.0388					
	$\theta_0$	0.0000	0.0000	0.0000	0.0000	0.0000					
1	$T_1$ (°C)	156.05	156.05	156.05	156.05	156.05					
	$T_{1,norm}$	0.3243	0.3243	0.3243	0.3243	0.3243					
	$\theta_1$	0.8590	1.5011	1.1179	0.8429	1.1789					
2	$T_2$ (°C)	272.1	272.1	272.1	272.1	272.1					
	$T_{2,norm}$	0.5282	0.5282	0.5282	0.5282	0.5282					
	$\theta_2$	1.0478	1.2389	1.2190	1.0125	1.1855					
3	$T_3$ (°C)	388.15	388.15	388.15	388.15	388.15					
	$T_{3,norm}$	0.7321	0.7321	0.7321	0.7321	0.7321					
	$\theta_3$	1.6153	1.0249	1.2952	1.6815	1.3421					
4	$T_4$ (°C)	536.7	524.3	532.2	537.4	531.9					
	$T_{4,norm}$	0.9931	0.9714	0.9852	0.9944	0.9847					
	$\theta_4$	0.3386	0.1428	0.5587	0.1584	0.1833					

Source: The author, 2023.

(b) Common nodal points. Densities of probability ( $\theta_i$ ) expressed for normalized temperatures (between 0 and 1)						
i	Run:	1	2	3	4	5
0	$T_0$ (°C)	40.0	40.0	40.0	40.0	40.0
	$T_{0,norm}$	0.1204	0.1204	0.1204	0.1204	0.1204
	$\theta_0$	0.5944	0.9221	0.7251	0.5403	0.7297
1	$T_1$ (°C)	156.05	156.05	156.05	156.05	156.05
	$T_{1,norm}$	0.3243	0.3243	0.3243	0.3243	0.3243
	$\theta_1$	0.8590	1.5011	1.1179	0.8429	1.1789
2	$T_2$ (°C)	272.1	272.1	272.1	272.1	272.1
	$T_{2,norm}$	0.5282	0.5282	0.5282	0.5282	0.5282
	$\theta_2$	1.0478	1.2389	1.2190	1.0125	1.1855
3	$T_3$ (°C)	388.15	388.15	388.15	388.15	388.15
	$T_{3,norm}$	0.7321	0.7321	0.7321	0.7321	0.7321
	$\theta_3$	1.6153	1.0249	1.2952	1.6815	1.3421
4	$T_4$ (°C)	504.2	504.2	504.2	504.2	504.2
	$T_{4,norm}$	0.9360	0.9360	0.9360	0.9360	0.9360
	$\theta_4$	1.0942	0.4038	0.8618	1.0853	0.6981
Coefficient of determination ( $R^2$ ) of the Lagrange polynomial regression						
	Run:	1	2	3	4	5
		0.9988	0.9995	0.9984	0.9992	0.9992
Density ( $d_{20}$ ) of the liquid product						
	Run:	1	2	3	4	5
		0.8233	0.7991	0.7986	0.8753	0.8516

Source: The author, 2023.

wt.% vap.	Run					wt.% vap.	Run				
	6	7	8	9	10		6	7	8	9	10
0	-28.5	7.1	-8	24.3	4.7	36	173	272.2	179.1	215.9	206
1	8.4	38.6	18.2	38.4	35.3	37	179.1	277.8	182.6	221.3	209.9
2	36.3	57.6	37.8	52.6	40.7	38	182.6	284.2	186.3	225.2	216.8
3	39.2	70.3	40.7	65.8	57.3	39	186.3	291.2	192.1	228	221.8
4	46.2	75.3	54.7	70.1	68.5	40	191.5	296.1	196.5	234.2	225.4
5	55.5	81.8	62.7	72.8	70.4	41	196	301.4	199.5	241.6	228.2
6	64.1	92.9	69.3	78.6	73	42	199.1	307.1	203.4	245.9	234.7
7	69.5	98.4	70.5	81.8	78.7	43	202.8	312.5	207.2	249	241.8
8	70.8	105.1	72.7	88.7	80.9	44	206.6	317.5	212	253.4	246
9	73.1	110.4	76.3	95.4	87.5	45	209.9	321.9	218.5	260.3	249
10	78.3	114.6	79.8	98.2	94.8	46	216.5	327.4	223	265.8	253.4
11	80.1	124	85.2	100.8	97.7	47	221.2	332.7	225.6	270.4	260.3
12	85.8	129.1	89.3	109.2	99.8	48	225	337.2	228.2	275.5	265.8
13	90.3	136.8	94.9	110.5	107.8	49	226.9	341.3	234.4	280.6	270.4
14	95.8	138.8	97.5	113.7	110.1	50	230.4	345.8	241.7	286.6	275.3
15	98.1	143.5	99.4	121	111.8	51	237.3	350.6	245.8	293	280.4
16	99.9	151.1	104.2	125.3	117	52	243.7	354.5	248.6	297.1	286.3
17	106.2	159.5	109.6	129.2	123.7	53	246.8	358.4	252	302	292.8
18	109.9	164.1	110.6	135.6	126.6	54	249.3	362.3	258.5	308.3	296.9
19	110.9	167.7	113	137.7	133.5	55	253.2	366.2	264.2	313.3	301.7
20	113.7	174	117.7	139.7	136.8	56	259.9	370	268.8	318	307.8
21	119.7	182	123.5	143.1	138.2	57	265	373.8	273.2	322.2	313
22	124.4	187.6	126.3	149.1	141.8	58	269.6	377.2	278	328.1	317.7
23	126.9	195.3	132.2	156.5	145.1	59	273.8	380.6	283.7	333.7	321.9
24	133.6	200.4	136	160.1	150.8	60	278.3	384.1	290.9	337.6	327.5
25	136.5	206.6	137.6	163.4	158.5	61	284	387.7	295.2	341.9	333.2
26	137.9	212.8	138.8	166.8	160.7	62	291.1	391	300.1	347.1	337.4
27	139.1	220.1	142.3	171.2	165.2	63	295.2	394.2	305.5	351.9	341.5
28	142.7	225.3	145	175	167.2	64	299.8	397.6	311.3	356	346.7
29	146	229.1	150.6	181.6	172.2	65	304.5	400.6	316.6	360.5	351.6
30	151.5	236.8	158.1	186.1	178.1	66	310.7	403.7	320.7	364.6	355.7
31	158.7	244.3	160.2	192.2	182.8	67	316	407	326.3	369.2	360.2
32	160.5	248.6	162.9	196.9	186.8	68	320	410.2	332.8	373.6	364.4
33	163.3	253.4	166.4	200.4	193.4	69	325.1	412.9	337.2	377.4	369
34	166.6	260.7	167.8	205.1	197.7	70	331.3	415.9	341.5	381.2	373.5
35	168.1	266.9	172.8	209	201.2	71	336.4	419	347.4	385.7	377.4

Source: The author, 2023

wt.% vap.	Run					wt.% vap.	Run				
	6	7	8	9	10		6	7	8	9	10
72	339.8	421.9	352.5	389.7	381.3	87	414.3	465.8	425.5	445.3	440.5
73	345.3	424.7	357.1	393.4	385.9	88	419.9	469.5	430.3	449.3	444.4
74	351.1	427.5	362	397.5	390	89	424.8	473.3	435	453.3	448.5
75	355.5	430.3	367.4	401.2	393.9	90	430.1	477.4	440.3	457.9	452.9
76	360.5	432.8	372.6	405	398	91	435.3	481.8	445.3	462.8	457.8
77	365	435.6	377	409.2	401.8	92	441.2	486.5	451.1	468	463.1
78	370.6	438.4	381.7	412.5	405.9	93	447.1	491.4	457.3	473.7	468.8
79	375.5	441.2	387.2	416.2	410.1	94	453.9	496.7	464.3	479.9	475.2
80	379.7	443.9	391.8	420.2	413.4	95	461.8	502.3	472.2	486.9	482.3
81	385.1	446.6	396.8	423.6	417.5	96	470.7	508.4	481.1	494.6	490.4
82	390.1	449.5	401.3	427.2	421.5	97	481.3	515.3	491.6	503.4	499.6
83	395.1	452.4	406.4	430.8	425.2	98	494.7	523.3	504	513.8	510.6
84	399.6	455.5	411.1	434.2	429	99	512.7	532.7	520.2	526.7	524.6
85	404.7	458.8	415.7	438.1	432.5	100	525.5	538.4	530.6	534.8	533.4
86	410	462.2	420.8	441.7	436.5						
(a) Particular nodal points. Densities of probability ( $\theta_i$ ) expressed for normalized temperatures (between 0 and 1)											
i	Run:	6	7	8	9	10					
0	$T_0$ (°C)	-28.5	7.1	-8	24.3	4.7					
	$T_{0,norm}$	0.0000	0.0626	0.0360	0.0928	0.0583					
	$\theta_0$	0.0000	0.0000	0.0000	0.0000	0.0000					
1	$T_1$ (°C)	156.05	156.05	156.05	156.05	156.05					
	$T_{1,norm}$	0.3243	0.3243	0.3243	0.3243	0.3243					
	$\theta_1$	1.4084	0.8342	1.4048	1.3008	1.2376					
2	$T_2$ (°C)	272.1	272.1	272.1	272.1	272.1					
	$T_{2,norm}$	0.5282	0.5282	0.5282	0.5282	0.5282					
	$\theta_2$	1.3138	1.011	1.2131	1.0771	1.1544					
3	$T_3$ (°C)	388.15	388.15	388.15	388.15	388.15					
	$T_{3,norm}$	0.7321	0.7321	0.7321	0.7321	0.7321					
	$\theta_3$	0.9839	1.6711	1.073	1.4171	1.3322					
4	$T_4$ (°C)	525.5	538.4	530.6	534.8	533.4					
	$T_{4,norm}$	0.9735	0.9961	0.9824	0.9898	0.9873					
	$\theta_4$	0.7271	0.2876	0.3539	-0.3191	0.073					

Source: The author, 2023

(b) Common nodal points. Densities of probability ( $\theta_i$ ) expressed for normalized temperatures (between 0 and 1)						
i	Run:	6	7	8	9	10
0	$T_0$ (°C)	40.0	40.0	40.0	40.0	40.0
	$T_{0,norm}$	0.1204	0.1204	0.1204	0.1204	0.1204
	$\theta_0$	0.8464	0.4838	0.8579	0.4345	0.6824
1	$T_1$ (°C)	156.05	156.05	156.05	156.05	156.05
	$T_{1,norm}$	0.3243	0.3243	0.3243	0.3243	0.3243
	$\theta_1$	1.4084	0.8342	1.4048	1.3008	1.2376
2	$T_2$ (°C)	272.1	272.1	272.1	272.1	272.1
	$T_{2,norm}$	0.5282	0.5282	0.5282	0.5282	0.5282
	$\theta_2$	1.3138	1.011	1.2131	1.0771	1.1544
3	$T_3$ (°C)	388.15	388.15	388.15	388.15	388.15
	$T_{3,norm}$	0.7321	0.7321	0.7321	0.7321	0.7321
	$\theta_3$	0.9839	1.6711	1.073	1.4171	1.3322
4	$T_4$ (°C)	504.2	504.2	504.2	504.2	504.2
	$T_{4,norm}$	0.9360	0.9360	0.9360	0.9360	0.9360
	$\theta_4$	0.7424	1.1723	0.6296	0.631	0.6849
Coefficient of determination ( $R^2$ ) of the Lagrange polynomial regression						
Run:	6	7	8	9	10	
	0.9980	0.9992	0.9989	0.9999	0.9994	
Density ( $d_{20}$ ) of the liquid product						
Run:	6	7	8	9	10	
	0.8305	0.8764	0.8232	0.8533	0.8087	

Source: The author, 2023

wt.% vap.	11	12	Run			wt.% vap.	11	12	Run		
			13	14	15				13	14	15
0	13.3	8.2	-0.4	-4.4	19.4	36	184.9	312.6	214	174	341.8
1	36.3	36.4	18.8	3.6	39	37	187.3	317.6	220.4	177.4	345.4
2	41.1	59.6	37	26	69.6	38	193.7	322.6	225.6	183	350.4
3	58.4	73.4	42.8	38.8	82	39	197.6	327.2	228.6	187.6	355
4	68.3	85.6	59.2	42.4	97.2	40	200.2	331.8	231.4	189.6	358.2
5	70.2	97.8	70.6	57.2	108.4	41	204	337.4	237	196.2	362.4
6	72.4	106.6	72.8	63.2	115	42	207.8	341.6	244	200.2	366.2
7	75.8	112.8	78.2	70.4	126.8	43	213.7	344.8	248.8	202.6	369.6
8	79.5	122.6	84.4	71.8	138.6	44	219.2	349.4	251.8	206.6	373.4
9	83.7	130.4	91.6	75.2	143.4	45	223.4	353.8	255.2	209.8	377
10	88.1	139.4	97.6	78.2	152.8	46	225.7	357.2	261	214	380.2
11	94.1	143.8	100.4	82.8	163	47	228.3	361.2	266.6	220.2	383
12	96.9	151.2	107	88.6	169.2	48	234.6	365	271	224.4	386.4
13	98.8	161.6	112.4	92.4	179.8	49	241.7	368.4	275.4	228.2	389.8
14	101.6	167.8	113.8	97.6	188.6	50	245.6	371.8	280	230.2	392.4
15	109.1	173.6	118.8	99.8	199.2	51	248.5	375.6	284.8	233.8	395.4
16	110.2	182.4	125.4	102.6	206.2	52	251.6	379	290	239.6	398.4
17	111.5	189.4	129.2	111.2	214.6	53	257.5	381.6	296	246.4	401.4
18	115.6	199	136.6	112.6	224.4	54	263.4	385	300	249.6	403.6
19	122.1	205	139.8	113.2	230.4	55	267.8	388.4	304.2	252.2	406.4
20	125.3	210.8	140.6	116.6	239.4	56	272	391.6	309.2	255.2	409.2
21	128.5	219.8	144.8	121.8	248.6	57	276.7	394.2	314.2	260.8	412
22	134.8	227.2	148.8	125.8	254	58	281.9	397.4	318.6	266.6	414.2
23	137.1	231.2	156	129	262.6	59	287.8	400.6	323	270.8	416.8
24	138.2	239.4	161.8	135.8	270.4	60	293.6	402.8	327	274.6	419.4
25	141	247.6	164.4	139.2	276.8	61	297.5	405.6	331.6	279.2	421.8
26	143.2	252.2	168.6	140.2	284	62	302.2	408.6	337.2	283.6	424
27	148.5	258	170.6	141	291.8	63	308.6	411.6	341.2	288.4	426.4
28	154.5	266	176	144.6	298.4	64	313.7	414	344.6	295.2	428.8
29	159.4	271.8	182.4	146.8	303.8	65	318.2	416.6	349.2	299	431.2
30	161.1	278	187.4	152	310.2	66	322.3	419.4	353.8	303.2	433
31	165.2	284	191.8	159.6	316.2	67	328.5	422	357.4	308	435.2
32	167	290.2	197	162.2	321.6	68	334.3	424.4	361.8	313.6	437.4
33	171.2	296.8	201.6	164.6	326.4	69	337.8	427	366	318.2	439.4
34	174.2	302	205.8	168.6	331.6	70	342.5	429.6	369.6	322.8	441.6
35	180.5	306.8	209.4	169.6	337.4	71	348.2	432	374.2	326.8	443.6

Source: The author, 2023

wt.% vap.	Run					wt.% vap.	Run				
	11	12	13	14	15		11	12	13	14	15
72	352.9	434.2	378.4	332.2	445.8	87	423.1	473	437	407	483.6
73	357.2	436.4	381.8	338.2	448	88	427.8	476.4	441	412.8	487
74	362	439	386	342	450	89	432.4	480.2	445.2	418	490.4
75	367	441.2	390.4	345.8	452	90	437.6	483.8	449.4	423.8	494
76	372.2	443.4	393.8	351.8	454.4	91	442.7	488	454	429.6	497.6
77	376.5	446	398	356.4	456.6	92	448.1	492.2	458.8	435.6	501.4
78	380.7	448.4	401.8	361	458.6	93	454.2	496.8	464.6	441.8	505.4
79	386	450.6	405.4	366	461	94	461.2	501.4	470.6	448.8	509.6
80	390.6	453	409.8	370.6	463.8	95	468.8	506.6	477.4	456.4	514.2
81	395.3	455.8	413.6	376.6	466.4	96	477.6	512	485.4	465.4	519
82	399.7	458	417.4	380.8	468.8	97	488.2	518.4	494.6	475.8	524.4
83	404.3	460.8	421.4	386	471.6	98	501	525.4	505.8	489.4	530.2
84	409.5	463.8	425.2	391.6	474.4	99	517.7	534	520.6	507.8	536.8
85	413.3	466.8	429.4	396.6	477.4	100	529	539	530.6	521.6	540.6
86	418.4	469.8	433	401.8	480.4						

(a) Particular nodal points. Densities of probability ( $\theta_i$ ) expressed for normalized temperatures (between 0 and 1)

i	Run:	11	12	13	14	15
0	$T_0$ (°C)	13.3	8.2	-0.4	-4.4	19.4
	$T_{0,norm}$	0.0734	0.0645	0.0494	0.0423	0.0842
	$\theta_0$	0.0000	0.0000	0.0000	0.0000	0.0000
1	$T_1$ (°C)	156.05	156.05	156.05	156.05	156.05
	$T_{1,norm}$	0.3243	0.3243	0.3243	0.3243	0.3243
	$\theta_1$	1.4973	0.6213	1.1862	1.5047	0.5226
2	$T_2$ (°C)	272.1	272.1	272.1	272.1	272.1
	$T_{2,norm}$	0.5282	0.5282	0.5282	0.5282	0.5282
	$\theta_2$	1.196	0.9294	1.2545	1.3086	0.7594
3	$T_3$ (°C)	388.15	388.15	388.15	388.15	388.15
	$T_{3,norm}$	0.7321	0.7321	0.7321	0.7321	0.7321
	$\theta_3$	1.1708	1.8649	1.3786	1.0432	1.9391
4	$T_4$ (°C)	529	539	530.6	521.6	540.6
	$T_{4,norm}$	0.9796	0.9972	0.9824	0.9666	1.0000
	$\theta_4$	-0.165	0.3684	0.1165	0.1665	0.5033

Source: The author, 2023

(b) Common nodal points. Densities of probability ( $\theta_i$ ) expressed for normalized temperatures (between 0 and 1)						
i	Run:	11	12	13	14	15
0	$T_0$ (°C)	40.0	40.0	40.0	40.0	40.0
	$T_{0,norm}$	0.1204	0.1204	0.1204	0.1204	0.1204
	$\theta_0$	0.6925	0.3971	0.6324	0.8439	0.3053
1	$T_1$ (°C)	156.05	156.05	156.05	156.05	156.05
	$T_{1,norm}$	0.3243	0.3243	0.3243	0.3243	0.3243
	$\theta_1$	1.4973	0.6213	1.1862	1.5047	0.5226
2	$T_2$ (°C)	272.1	272.1	272.1	272.1	272.1
	$T_{2,norm}$	0.5282	0.5282	0.5282	0.5282	0.5282
	$\theta_2$	1.196	0.9294	1.2545	1.3086	0.7594
3	$T_3$ (°C)	388.15	388.15	388.15	388.15	388.15
	$T_{3,norm}$	0.7321	0.7321	0.7321	0.7321	0.7321
	$\theta_3$	1.1708	1.8649	1.3786	1.0432	1.9391
4	$T_4$ (°C)	504.2	504.2	504.2	504.2	504.2
	$T_{4,norm}$	0.9360	0.9360	0.9360	0.9360	0.9360
	$\theta_4$	0.3861	1.4004	0.6286	0.3762	1.688
Coefficient of determination ( $R^2$ ) of the Lagrange polynomial regression						
	Run:	11	12	13	14	15
		0.9996	0.9990	0.9996	0.9995	0.9988
Density ( $d_{20}$ ) of the liquid product						
	Run:	11	12	13	14	15
		0.8381	0.8894	0.8657	0.8476	0.8960

Source: The author, 2023

wt.% vap.	Run					wt.% vap.	Run				
	16	17	18	19	20		16	17	18	19	20
0	5.6	-10.4	8	-10	-2.8	36	280.4	223.8	316	238	213
1	31	-5.4	35.4	38.8	7.2	37	286.6	228	321.4	244.6	220
2	50	20.6	58.2	50.6	33.2	38	294	231.6	325.8	251.4	225
3	69.2	30.4	71.4	68.4	40.6	39	299	239.2	331	255.2	228.4
4	74.6	37.8	82	76.2	56.6	40	304	246.6	336.6	258.2	231.2
5	82.4	40.4	96.4	81.6	68.2	41	309.8	250.8	341.2	263.6	237.2
6	93.2	55.6	102	87.8	70.8	42	315.4	254.2	344.6	270	244.6
7	99.4	63.2	112	96.4	75.2	43	320.4	261.2	349.4	274.4	249
8	109.6	69.4	118.2	102.8	81.6	44	325	267.4	354	279.2	252
9	112.4	73.2	127.2	108.2	89.2	45	330	272.6	357.4	284	255.6
10	118.6	80.4	137.8	111.8	96	46	335.2	278.2	361.6	289.4	262.2
11	126.6	87.2	140.6	121.2	98.6	47	340.2	283.8	365.6	295.8	267.8
12	135.6	95.4	147.6	122.2	105	48	343.8	289.8	369	300.6	272.4
13	139.6	98.4	159	126.8	111.2	49	348	296.4	372.6	304.8	277.2
14	143.4	105.8	164.6	133.6	112	50	352.8	301.2	376.4	309.2	281.8
15	149	111	169.6	137.8	116.6	51	356.6	305.8	379.8	315	287.2
16	159	113.8	179.2	145.2	123.6	52	360.6	312	382.6	319.4	294
17	163.2	121.2	187.6	147.8	127.2	53	364.8	317	386	324.2	298.4
18	168.4	126.2	196	149.8	134.8	54	368.4	322.2	389.4	328.2	302.6
19	173.8	134.6	202.4	153.2	138.8	55	372	326.6	392.2	332.8	307.4
20	181.6	138.6	209.2	159.2	139.6	56	376	331.8	395.2	338.4	313
21	188	139.6	217.8	167.2	143.4	57	379.8	337.8	398.4	342.6	317.6
22	195.6	144.2	226	170	146.4	58	382.6	341.6	401.4	345.8	322.4
23	201.2	150.2	230.6	174.8	152.6	59	386.4	345.6	403.8	350.2	326.4
24	206.8	159.2	238.8	176.6	160.4	60	390	351	406.8	354.8	331.2
25	212.4	162.2	247.4	182.6	162.8	61	392.8	355.6	409.8	358.4	337
26	220.8	167.4	252	189	167.4	62	396.4	359.4	412.6	362.6	341
27	227.2	170	258.8	194.2	168.8	63	399.8	364.2	415	366.6	344.4
28	230.8	176	266.8	199.8	173.8	64	402.6	368.2	417.6	370.2	349.4
29	238	183	273	205.2	180.2	65	405.6	372.4	420.4	374.4	354.4
30	246.4	188	279.4	209	185.2	66	408.8	376.8	422.8	378.2	357.8
31	251.2	195.4	285.8	214	188.6	67	412	380.4	425.4	381.6	362.2
32	255.2	200.8	293.6	218.4	195.6	68	414.6	384.4	428	385.2	366.6
33	263	205.6	299.2	225.8	200.4	69	417.6	388.6	430.4	389.2	370.4
34	269.6	210.2	304.2	231.2	204.2	70	420.8	392.2	432.6	392.6	375.2
35	274.8	217.4	310.4	234	208.6	71	423.4	396.2	434.8	396.2	379.4

Source: The author, 2023

wt.% vap.	Run					wt.% vap.	Run				
	16	17	18	19	20		16	17	18	19	20
72	426.2	400.2	437.2	400	382.8	87	468.6	452.6	476	450.2	441.6
73	429.2	403.4	439.4	403	387.2	88	472.2	456.4	479.6	453.8	445.8
74	431.8	407.4	441.8	406.6	391.2	89	476	460.4	483.2	457.6	449.6
75	434.2	411.2	444	410.4	395	90	480.2	465	487	461.8	453.8
76	437	414.6	446.6	413.6	399.4	91	484.4	469.6	491	466.2	458.4
77	439.6	418.2	448.8	417	402.8	92	489.2	474.6	495.2	471.2	463.6
78	442	421.8	450.8	420.6	406.8	93	494	480.2	499.4	476.4	469
79	445	425.4	453.4	423.8	411.2	94	499	486.2	504	482.4	475
80	447.6	428.8	456	427.2	414.8	95	504.6	492.8	509	489	482
81	450	432	458.2	430.6	418.6	96	510.6	500	514.4	496.2	489.8
82	452.8	435.4	460.8	433.6	422.4	97	517.2	508	520.4	504.6	498.8
83	455.8	438.8	463.8	436.8	426.4	98	524.8	517.6	527.2	514.8	509.6
84	458.6	442	466.6	440.2	430.4	99	533.6	529.2	535	527	523.6
85	461.8	445.8	469.6	443.4	434	100	539	536.2	539.6	534.4	532.6
86	465.4	449	472.8	447	437.8						

(a) Particular nodal points. Densities of probability ( $\theta_i$ ) expressed for normalized temperatures (between 0 and 1)						
i	Run:	16	17	18	19	20
0	$T_0$ (°C)	5.6	-10.4	8	-10	-2.8
	$T_{0,norm}$	0.0599	0.0318	0.0641	0.0325	0.0452
	$\theta_0$	0.0000	0.0000	0.0000	0.0000	0.0000
1	$T_1$ (°C)	156.05	156.05	156.05	156.05	156.05
	$T_{1,norm}$	0.3243	0.3243	0.3243	0.3243	0.3243
	$\theta_1$	0.7852	1.0190	0.6137	0.9909	1.1651
2	$T_2$ (°C)	272.1	272.1	272.1	272.1	272.1
	$T_{2,norm}$	0.5282	0.5282	0.5282	0.5282	0.5282
	$\theta_2$	0.9864	1.0397	0.8734	1.2402	1.2043
3	$T_3$ (°C)	388.15	388.15	388.15	388.15	388.15
	$T_{3,norm}$	0.7321	0.7321	0.7321	0.7321	0.7321
	$\theta_3$	1.6924	1.4433	1.8462	1.4814	1.3630
4	$T_4$ (°C)	539	536.2	539.6	534.4	532.6
	$T_{4,norm}$	0.9972	0.9923	0.9982	0.9891	0.9859
	$\theta_4$	0.3907	0.1474	0.4546	0.5540	0.2124

Source: The author, 2023

(b) Common nodal points. Densities of probability ( $\theta_i$ ) expressed for normalized temperatures (between 0 and 1)						
i	Run:	16	17	18	19	20
0	$T_0$ (°C)	40.0	40.0	40.0	40.0	40.0
	$T_{0,norm}$	0.1204	0.1204	0.1204	0.1204	0.1204
	$\theta_0$	0.4758	0.7658	0.4215	0.5227	0.6659
1	$T_1$ (°C)	156.05	156.05	156.05	156.05	156.05
	$T_{1,norm}$	0.3243	0.3243	0.3243	0.3243	0.3243
	$\theta_1$	0.7852	1.0190	0.6137	0.9909	1.1651
2	$T_2$ (°C)	272.1	272.1	272.1	272.1	272.1
	$T_{2,norm}$	0.5282	0.5282	0.5282	0.5282	0.5282
	$\theta_2$	0.9864	1.0397	0.8734	1.2402	1.2043
3	$T_3$ (°C)	388.15	388.15	388.15	388.15	388.15
	$T_{3,norm}$	0.7321	0.7321	0.7321	0.7321	0.7321
	$\theta_3$	1.6924	1.4433	1.8462	1.4814	1.3630
4	$T_4$ (°C)	504.2	504.2	504.2	504.2	504.2
	$T_{4,norm}$	0.9360	0.9360	0.9360	0.9360	0.9360
	$\theta_4$	1.2633	0.8727	1.4842	0.9874	0.7297
Coefficient of determination ( $R^2$ ) of the Lagrange polynomial regression						
	Run:	16	17	18	19	20
		0.9991	0.9997	0.9988	0.9984	0.9995
Density ( $d_{20}$ ) of the liquid product						
	Run:	16	17	18	19	20
		0.8823	0.8688	0.8879	0.8711	0.8612

Source: The author, 2023

wt.% vap.	Run					wt.% vap.	Run				
	21	22	23	24	25		21	22	23	24	25
0	-1.6	2	7	2.2	-1	36	205.4	262.8	335	305	180.6
1	15.6	22.8	34.4	24.6	7.8	37	209.2	269	339.8	311.2	185.2
2	33.4	39.6	57.4	41	32.6	38	214.6	273.8	343.6	316.4	188.8
3	40.6	56.2	71.2	68	40.2	39	221.2	279.4	348	321.6	195
4	56	68.4	83.6	74.2	50.4	40	226.6	285.2	352.6	326	199.6
5	63.2	72.8	96.8	87	60.2	41	228.8	291.6	356.4	330.8	203.6
6	69.6	80.2	110.2	97	68.4	42	232.6	297.2	360.2	336.6	208
7	71.8	88.6	115.2	106.8	70.2	43	239.2	301.8	364.2	340.8	212.4
8	76.4	96.4	126.6	111.4	73.4	44	246.4	306.4	367.8	344.4	218.4
9	81.4	101.4	138.4	121	78.2	45	250.2	312.4	371	349	223.8
10	87.8	110.8	143.4	128.8	81.4	46	252.6	317	374.8	353.6	228
11	95.4	114	153.8	138.2	87	47	257.4	322	378.4	357	232
12	98.2	123	162.6	141	91.6	48	264.4	326.2	381	361	238
13	101.6	129	168.6	147.8	96.4	49	269.6	331	384.4	365	244.4
14	110.8	137.2	180	159	98.6	50	273.8	336.6	387.8	368.4	249.4
15	111.8	139.2	188.2	164	101.6	51	279	340.8	391	372	253.2
16	114.4	143.8	199	168.6	109.2	52	284.2	344.2	393.4	376	258.4
17	121.4	150.4	206	176.8	111.2	53	289.6	348.6	396.6	379.4	264.8
18	125.8	160	214.6	186.2	112.4	54	296	353.2	399.8	382.2	270.2
19	131.4	163.4	224.2	194.4	115.6	55	300.4	356.8	402.2	385.6	275.2
20	137.2	168	230	200.8	120.8	56	305	360.8	404.8	389.2	280.6
21	139.4	173.2	238.8	207.4	124.8	57	310.6	365	407.6	392	286.2
22	140.4	181	248	214.6	128.2	58	315.8	368.4	410.6	395	292.6
23	144.4	187	253.2	223	134	59	320.8	372.2	413	398.4	298.2
24	148.8	194.2	261.2	228.2	138	60	324.8	376.2	415.4	401.4	303.4
25	156.2	200.2	269.2	234.4	139.2	61	329.6	379.8	418.2	403.8	309.2
26	161.2	205.2	275.6	243.6	141.4	62	335.2	382.8	420.6	406.8	315
27	163.8	209.8	282.2	249.8	144.2	63	340	386.8	423	410	320.6
28	168	217.4	289.6	254.2	147.6	64	343.4	390.4	425.4	412.6	325.8
29	169.4	224	296.8	261.8	152.2	65	348	393.2	427.8	415.2	331.6
30	174.8	228.2	302.2	269	158.4	66	353	396.8	430.2	418	337.8
31	181.4	233	308	274.8	161.4	67	357	400.4	432.4	420.8	342.8
32	186.6	240.4	314.2	280.8	164.6	68	361.4	403	434.4	423.2	348.2
33	190.4	247.4	319.4	287.2	167.8	69	366	406.4	436.6	426	353.8
34	196.4	251.4	324.6	294.8	170.6	70	369.8	409.8	438.8	428.6	358.8
35	201	255.6	329.6	300.2	175	71	374.8	412.8	441	431.2	364.2

Source: The author, 2023

wt.% vap.	Run					wt.% vap.	Run				
	21	22	23	24	25		21	22	23	24	25
72	379.2	415.8	443	433.2	369.2	87	439.6	460.4	481	472.6	443
73	382.6	419	445.2	435.8	374.6	88	443.6	464.4	484.4	476.2	448
74	387.2	422	447.6	438	379.8	89	448	467.8	487.8	479.8	453
75	391.4	425	449.6	440.4	384.6	90	452	472	491.4	483.6	458.4
76	395.4	428.2	451.6	442.8	390	91	456.8	476.4	495.4	487.8	464.4
77	399.8	431	454	445.4	394.6	92	461.8	481.2	499.2	492.2	470.6
78	403.2	433.6	456.4	447.8	399.8	93	467.4	486.2	503.4	496.8	477.4
79	407.6	436.4	458.4	450	404.4	94	473.6	491.8	507.8	501.6	484.8
80	412	439.4	460.8	452.4	409.4	95	480.6	497.6	512.4	506.6	492.8
81	415.6	442	463.6	455.2	414.2	96	488.6	504.2	517.6	512.2	501.4
82	419.8	445.2	466.4	457.6	419	97	497.8	511.4	523	518.6	510.6
83	423.6	448.2	468.8	460.2	423.8	98	508.6	520.2	529.2	525.8	520.8
84	427.8	450.8	471.8	463.4	428.6	99	522.8	530.6	536.4	534.2	532
85	431.6	454	474.6	466.4	433.4	100	532.2	537	540.4	539.2	538.2
86	435.6	457	477.8	469.4	438.2						

(a) Particular nodal points. Densities of probability ( $\theta_i$ ) expressed for normalized temperatures (between 0 and 1)						
i	Run:	21	22	23	24	25
0	$T_0$ (°C)	-1.6	2	7	2.2	-1
	$T_{0,norm}$	0.0473	0.0536	0.0624	0.0539	0.0483
	$\theta_0$	0.0000	0.0000	0.0000	0.0000	0.0000
1	$T_1$ (°C)	156.05	156.05	156.05	156.05	156.05
	$T_{1,norm}$	0.3243	0.3243	0.3243	0.3243	0.3243
	$\theta_1$	1.2146	0.8644	0.5059	0.6436	1.3783
2	$T_2$ (°C)	272.1	272.1	272.1	272.1	272.1
	$T_{2,norm}$	0.5282	0.5282	0.5282	0.5282	0.5282
	$\theta_2$	1.1729	1.0497	0.8003	0.9194	1.0955
3	$T_3$ (°C)	388.15	388.15	388.15	388.15	388.15
	$T_{3,norm}$	0.7321	0.7321	0.7321	0.7321	0.7321
	$\theta_3$	1.3246	1.6493	1.9226	1.8124	1.0761
4	$T_4$ (°C)	532.2	537	540.4	539.2	538.2
	$T_{4,norm}$	0.9852	0.9937	0.9996	0.9975	0.9958
	$\theta_4$	0.1281	0.2148	0.5104	0.4208	0.3339

Source: The author, 2023

(b) Common nodal points. Densities of probability ( $\theta_i$ ) expressed for normalized temperatures (between 0 and 1)						
i	Run:	21	22	23	24	25
0	$T_0$ (°C)	40.0	40.0	40.0	40.0	40.0
	$T_{0,norm}$	0.1204	0.1204	0.1204	0.1204	0.1204
	$\theta_0$	0.7225	0.5356	0.4083	0.4648	0.8444
1	$T_1$ (°C)	156.05	156.05	156.05	156.05	156.05
	$T_{1,norm}$	0.3243	0.3243	0.3243	0.3243	0.3243
	$\theta_1$	1.2146	0.8644	0.5059	0.6436	1.3783
2	$T_2$ (°C)	272.1	272.1	272.1	272.1	272.1
	$T_{2,norm}$	0.5282	0.5282	0.5282	0.5282	0.5282
	$\theta_2$	1.1729	1.0497	0.8003	0.9194	1.0955
3	$T_3$ (°C)	388.15	388.15	388.15	388.15	388.15
	$T_{3,norm}$	0.7321	0.7321	0.7321	0.7321	0.7321
	$\theta_3$	1.3246	1.6493	1.9226	1.8124	1.0761
4	$T_4$ (°C)	504.2	504.2	504.2	504.2	504.2
	$T_{4,norm}$	0.9360	0.9360	0.9360	0.9360	0.9360
	$\theta_4$	0.6732	1.0614	1.6245	1.3969	0.7596
Coefficient of determination ( $R^2$ ) of the Lagrange polynomial regression						
Run:	21	22	23	24	25	
	0.9996	0.9994	0.9988	0.9989	0.9993	
Density ( $d_{20}$ ) of the liquid product						
Run:	21	22	23	24	25	
	0.8576	0.8769	0.8956	0.8871	0.8636	

Source: The author, 2023

wt.% vap.	Run					wt.% vap.	Run				
	26	27	28	29	30		26	27	28	29	30
0	-4.4	12.4	-3.2	-3.2	24.4	36	250.2	329.8	199.4	199.8	336.4
1	19.8	37	6.6	6.6	41	37	253.4	334.8	202.6	203	341
2	37	62.8	32.2	32	69.8	38	259	339.8	206.8	207.4	344.6
3	53.8	74.4	40	39.8	81.4	39	265.6	343.4	210.6	211	349.2
4	67	89.6	52	50.2	96.8	40	270.4	347.4	216.6	217.4	353.6
5	70.8	99	61.6	61	107	41	275.4	352	222.4	223	357.2
6	79.8	111	69.4	69.2	114.6	42	280.4	356	227	227.4	361.2
7	87	119.4	71	70.8	126.2	43	285.8	359.4	229.2	229.8	365
8	95.8	129.6	74.8	74.4	137.4	44	292	363.4	232.8	233.8	368.6
9	99.8	138.8	81.4	81.2	142.4	45	297.2	367	239	240	372.2
10	110.2	144.4	87.4	86.8	151.2	46	301.4	370	245.8	246.6	375.8
11	111.4	155.8	92.8	91.8	161.8	47	305.6	374	249.4	250	379.2
12	117.6	163.8	97.2	96.8	168.6	48	311.2	377.4	252.2	252.6	382.2
13	125.2	170	100	99.4	176.6	49	315.8	380.4	256	256.8	385.4
14	132.8	180.6	107	105.6	187.4	50	320.6	383.4	262.2	263.4	389
15	138.2	188.2	111.4	111.2	196.4	51	324.6	386.8	267.6	268.6	391.8
16	139.6	198.6	112.2	112	203.8	52	329.2	390	272	272.8	394.8
17	144.2	205.6	116.8	116	211	53	334	392.4	276.4	277.4	398
18	150.6	213	123.4	122.6	220.8	54	338.8	395.6	281.2	281.8	401
19	159.4	222.6	126.8	126.4	228	55	342.4	398.6	286.2	287	403.4
20	162.6	228.6	133.4	132.4	234.4	56	346	401.6	292.4	293.8	406.4
21	167.6	235.6	138	137.4	243.8	57	350.8	403.8	297.4	298.2	409.2
22	171.8	245.6	139.4	139.4	250.8	58	355	406.6	301.6	302.2	412
23	178.4	251.2	141.2	140.8	256.2	59	358.2	409.6	305.8	306.4	414.6
24	184.8	257	144.6	144.6	264.8	60	362.4	412.2	311.4	312.2	417.2
25	189.4	265.6	149.4	149	271.4	61	366.2	414.6	316	316.6	419.8
26	196.4	271.8	156.2	155.8	278.4	62	369.6	417.2	321	321.8	422.2
27	201.2	278.4	161.2	161.2	285	63	373.8	419.8	324.8	325.4	424.6
28	206.2	285.2	163.6	163.4	292.6	64	377.6	422.2	329.6	330.2	427.2
29	210.8	292.4	168	168	298.6	65	380.6	424.6	334.8	335.8	429.6
30	218	298.4	169.2	169.2	303.8	66	384.2	427	339.6	340.4	431.8
31	224	303.4	174.2	174.2	310	67	388	429.4	343	343.6	434
32	228	309.2	180.4	180.6	315.8	68	391.4	431.6	347.4	348.2	436.2
33	231.8	315	184.8	185.4	321.2	69	394.8	433.8	352.6	353.4	438.2
34	238.6	320	188.4	188.6	325.8	70	398.4	436	356.6	357.2	440.6
35	245.8	324.8	195	195.4	330.8	71	401.6	438.2	360.8	361.6	442.6

Source: The author, 2023

wt.% vap.	Run					wt.% vap.	Run				
	26	27	28	29	30		26	27	28	29	30
72	404.6	440.4	365.4	366	444.8	87	452.6	478.2	430.2	430.4	482
73	408.2	442.6	369.2	369.8	447	88	456.2	481.6	434.4	434.4	485.2
74	411.8	444.8	374.4	375	449.2	89	459.8	485	438.8	439	488.6
75	414.8	447.2	378.8	379.2	450.8	90	464.2	488.8	443.4	443.6	492.2
76	418	449.2	382.4	382.8	453.2	91	468.4	492.6	448.2	448.4	495.8
77	421.4	451.2	387	387.6	455.6	92	473	496.6	453	453.2	499.6
78	424.4	453.6	391.4	391.8	457.6	93	478.2	501	458.6	458.6	503.4
79	427.6	456	395.4	396	459.8	94	483.8	505.4	465	465.2	507.6
80	430.8	458.2	400.2	400.6	462.4	95	490.2	510.2	472	471.8	512.2
81	433.6	460.6	403.8	404	465.2	96	497.2	515.4	480	480	517
82	436.8	463.6	408.4	408.8	467.4	97	505.2	521.2	489.8	489.6	522.6
83	440	466.4	412.8	413	470.2	98	514.6	527.8	501.6	501.4	528.6
84	443	469	416.8	417.2	473	99	526.8	535.4	517.6	517.4	535.8
85	446.2	472	421.4	421.6	475.8	100	534.6	539.8	528.6	528.4	540
86	449.2	474.8	425.6	426	478.8						

(a) Particular nodal points. Densities of probability ( $\theta_i$ ) expressed for normalized temperatures (between 0 and 1)						
i	Run:	26	27	28	29	30
0	$T_0$ (°C)	-4.4	12.4	-3.2	-3.2	24.4
	$T_{0,norm}$	0.0423	0.0719	0.0445	0.0445	0.0930
	$\theta_0$	0.0000	0.0000	0.0000	0.0000	0.0000
1	$T_1$ (°C)	156.05	156.05	156.05	156.05	156.05
	$T_{1,norm}$	0.3243	0.3243	0.3243	0.3243	0.3243
	$\theta_1$	0.9254	0.5440	1.2835	1.2762	0.5749
2	$T_2$ (°C)	272.1	272.1	272.1	272.1	272.1
	$T_{2,norm}$	0.5282	0.5282	0.5282	0.5282	0.5282
	$\theta_2$	1.1522	0.8391	1.2452	1.2374	0.7887
3	$T_3$ (°C)	388.15	388.15	388.15	388.15	388.15
	$T_{3,norm}$	0.7321	0.7321	0.7321	0.7321	0.7321
	$\theta_3$	1.5948	1.9337	1.2715	1.2832	1.9147
4	$T_4$ (°C)	534.6	539.8	528.6	528.4	540
	$T_{4,norm}$	0.9895	0.9986	0.9789	0.9786	0.9989
	$\theta_4$	0.2196	0.3818	0.1025	0.0716	0.5230

Source: The author, 2023

(b) Common nodal points. Densities of probability ( $\theta_i$ ) expressed for normalized temperatures (between 0 and 1)						
i	Run:	26	27	28	29	30
0	$T_0$ (°C)	40.0	40.0	40.0	40.0	40.0
	$T_{0,norm}$	0.1204	0.1204	0.1204	0.1204	0.1204
	$\theta_0$	0.5555	0.3650	0.7358	0.7415	0.2489
1	$T_1$ (°C)	156.05	156.05	156.05	156.05	156.05
	$T_{1,norm}$	0.3243	0.3243	0.3243	0.3243	0.3243
	$\theta_1$	0.9254	0.5440	1.2835	1.2762	0.5749
2	$T_2$ (°C)	272.1	272.1	272.1	272.1	272.1
	$T_{2,norm}$	0.5282	0.5282	0.5282	0.5282	0.5282
	$\theta_2$	1.1522	0.8391	1.2452	1.2374	0.7887
3	$T_3$ (°C)	388.15	388.15	388.15	388.15	388.15
	$T_{3,norm}$	0.7321	0.7321	0.7321	0.7321	0.7321
	$\theta_3$	1.5948	1.9337	1.2715	1.2832	1.9147
4	$T_4$ (°C)	504.2	504.2	504.2	504.2	504.2
	$T_{4,norm}$	0.9360	0.9360	0.9360	0.9360	0.9360
	$\theta_4$	0.9195	1.5355	0.5404	0.5274	1.6614
Coefficient of determination ( $R^2$ ) of the Lagrange polynomial regression						
	Run:	26	27	28	29	30
		0.9994	0.9990	0.9996	0.9996	0.9991
Density ( $d_{20}$ ) of the liquid product						
	Run:	26	27	28	29	30
		0.8728	0.8871	0.8589	0.8586	0.8969

Source: The author, 2023

wt.% vap.	Run					wt.% vap.	Run				
	31	32	33	34	35		31	32	33	34	35
0	-5.4	2	2	4.5	3.8	36	185.2	164.6	182.9	221.2	246.9
1	6.4	4.9	5.6	14.2	10.6	37	188.6	167.5	187.1	226	250.6
2	34	23.5	24.5	36.8	36.8	38	194.4	168.5	193	228.9	255.9
3	41.2	34.9	36.8	41	41.4	39	199	173.4	197.7	234.4	263.4
4	51	39.4	40.2	55.8	57.7	40	201.8	179.4	200.9	241.9	269
5	59.8	41.1	47.9	69	70	41	205.8	183.1	205	247.1	274.4
6	69.8	54.3	58	71.3	73.3	42	209.2	187.1	209	250.4	280.2
7	71.4	61.7	69.1	74.9	80.4	43	212.6	192.1	215.4	255	286.7
8	74.6	69.5	70.8	81.1	87.6	44	219	196.8	221.1	262.2	293.9
9	80.6	70.7	73.5	88.2	96.5	45	223.8	200.2	225.8	268	298.9
10	82.6	72.8	78.4	96.3	99.8	46	228	204	227.9	272.9	304.1
11	88.6	75.2	81.3	99.2	109.6	47	229.8	207.7	232	278.4	310.5
12	94	80.4	87.7	104.7	111.2	48	233.4	211.8	238.8	284.6	316
13	98.2	83.3	94.1	110.6	115.8	49	239.2	219	245.4	291.8	321
14	100.6	88.5	97.9	111.7	124.2	50	245.6	223.6	249	296.9	326.2
15	106.2	94.4	100.1	116.7	129	51	249.4	226.7	251.8	302.2	332.1
16	112	97.8	105.7	124.2	136.7	52	252.2	228.9	257.2	308.2	337.5
17	112.6	99.6	110.6	127.9	138.7	53	255.2	234	264.2	314	341.4
18	115.4	103.3	111.4	135.5	142.9	54	260.8	241.8	269.1	319.3	346.2
19	119.6	110.1	113.9	138.2	148.4	55	266.4	246.8	273.9	323.8	351.3
20	125.2	111	119.3	139.5	157	56	270.8	249.6	279.2	329.9	355.4
21	128	111.6	125	143.5	161.3	57	274.8	252.6	285.3	335.8	359.4
22	134.8	113.9	128.2	148.8	166.7	58	279.4	258.5	292.8	339.8	363.6
23	138.8	118.5	135.2	156.2	169.8	59	284	264.9	297.4	344.4	367.6
24	140	124.4	138	160.8	175.5	60	289	269.7	302.6	349.9	371.6
25	141.2	127.2	138.8	164.5	183.1	61	295.4	274.4	309.1	354.3	375.4
26	144.8	134	140.9	167.7	188.2	62	299.4	279.4	314.8	358.6	378.9
27	148	137.2	143.8	172.5	195.6	63	303.4	285.7	320	363	382.1
28	153.8	138.5	148.6	178.1	200.7	64	308.4	293.3	324.9	367.1	385.8
29	160.6	139.1	155.1	183.9	206	65	313.8	297.8	331.3	371.6	389.4
30	162.6	141.4	160.4	188.1	211	66	318.6	303.1	337.2	375.7	392.5
31	165.8	143.8	162.5	195	218.7	67	323	310.1	341.2	379.3	395.9
32	168.8	147.7	166.8	199.8	224.7	68	327	316	346.6	383.1	399.2
33	170.2	154	168.1	204.2	228.1	69	332.4	320.9	352.4	387.1	402.1
34	175	160.1	172.9	208.6	233.6	70	338.2	326.5	356.7	390.8	405.1
35	181.4	161.5	177.8	214.9	241.2	71	341.8	333.7	361.8	394.4	408.4

Source: The author, 2023

wt.% vap.	Run					wt.% vap.	Run				
	31	32	33	34	35		31	32	33	34	35
72	345.6	338.7	366.3	398.2	411.6	87	418.4	415.3	431.1	447.6	454.2
73	351.2	343.1	371.4	401.5	414.2	88	423.6	420.6	435.1	451.1	457.5
74	356	349.5	376.2	404.9	417.2	89	428.8	425.6	439.5	454.7	461.1
75	360	354.7	380.2	408.6	420.3	90	433.8	430.7	443.9	458.7	464.9
76	365	359.8	384.8	412.1	422.9	91	439.2	435.8	448.3	463.1	468.9
77	369.2	364.8	389.5	415.2	425.9	92	445	441.5	453.3	467.7	473.3
78	374.6	370.5	393.5	418.5	428.8	93	450.6	447.2	458.5	472.7	478.1
79	379.4	376	398.1	421.9	431.4	94	457.2	453.7	464.6	478.3	483.4
80	383.6	380.4	401.9	425.2	434	95	464.8	460.9	471.3	484.5	489.3
81	389	385.8	406.3	428.4	436.8	96	473	469.2	479.1	491.7	496.1
82	393.6	390.9	410.8	431.6	439.7	97	483.2	479.2	488.5	500	503.6
83	398.6	396	414.4	434.6	442.4	98	496	492.1	500.2	509.8	512.9
84	403	400.7	418.7	437.8	445.4	99	513	509.9	516	523.2	525.3
85	408.4	405.6	422.8	441.1	448.1	100	525.4	523.2	527.4	532.2	533.6
86	413.6	411	427	444.4	451						

(a) Particular nodal points. Densities of probability ( $\theta_i$ ) expressed for normalized temperatures (between 0 and 1)						
i	Run:	31	32	33	34	35
0	$T_0$ (°C)	-5.4	2	2	4.5	3.8
	$T_{0,norm}$	0.0406	0.0536	0.0536	0.0580	0.0568
	$\theta_0$	0.0000	0.0000	0.0000	0.0000	0.0000
1	$T_1$ (°C)	156.05	156.05	156.05	156.05	156.05
	$T_{1,norm}$	0.3243	0.3243	0.3243	0.3243	0.3243
	$\theta_1$	1.4148	1.5427	1.3633	1.1089	0.9347
2	$T_2$ (°C)	272.1	272.1	272.1	272.1	272.1
	$T_{2,norm}$	0.5282	0.5282	0.5282	0.5282	0.5282
	$\theta_2$	1.3070	1.1080	1.0965	1.0578	0.9991
3	$T_3$ (°C)	388.15	388.15	388.15	388.15	388.15
	$T_{3,norm}$	0.7321	0.7321	0.7321	0.7321	0.7321
	$\theta_3$	1.1143	1.0542	1.2223	1.4627	1.6328
4	$T_4$ (°C)	525.4	523.2	527.4	532.2	533.6
	$T_{4,norm}$	0.9733	0.9694	0.9768	0.9852	0.9877
	$\theta_4$	0.2638	-0.0014	0.0574	0.1699	0.1453

Source: The author, 2023

(b) Common nodal points. Densities of probability ( $\theta_i$ ) expressed for normalized temperatures (between 0 and 1)						
i	Run:	31	32	33	34	35
0	$T_0$ (°C)	40.0	40.0	40.0	40.0	40.0
	$T_{0,norm}$	0.1204	0.1204	0.1204	0.1204	0.1204
	$\theta_0$	0.7774	0.9738	0.8587	0.6779	0.6238
1	$T_1$ (°C)	156.05	156.05	156.05	156.05	156.05
	$T_{1,norm}$	0.3243	0.3243	0.3243	0.3243	0.3243
	$\theta_1$	1.4148	1.5427	1.3633	1.1089	0.9347
2	$T_2$ (°C)	272.1	272.1	272.1	272.1	272.1
	$T_{2,norm}$	0.5282	0.5282	0.5282	0.5282	0.5282
	$\theta_2$	1.3070	1.1080	1.0965	1.0578	0.9991
3	$T_3$ (°C)	388.15	388.15	388.15	388.15	388.15
	$T_{3,norm}$	0.7321	0.7321	0.7321	0.7321	0.7321
	$\theta_3$	1.1143	1.0542	1.2223	1.4627	1.6328
4	$T_4$ (°C)	504.2	504.2	504.2	504.2	504.2
	$T_{4,norm}$	0.9360	0.9360	0.9360	0.9360	0.9360
	$\theta_4$	0.5073	0.3702	0.5554	0.8523	0.9895
Coefficient of determination ( $R^2$ ) of the Lagrange polynomial regression						
	Run:	31	32	33	34	35
		0.9994	0.9996	0.9996	0.9992	0.9990
Density ( $d_{20}$ ) of the liquid product						
	Run:	31	32	33	34	35
		0.8638	0.8413	0.8472	0.8649	0.8700

Source: The author, 2023

wt.% vap.	Run					wt.% vap.	Run				
	36	37	38	39	40		36	37	38	39	40
0	2	1.7	2	2.4	3.8	36	188.4	161.5	200.5	187.9	236.7
1	5.3	4.2	5.6	6.3	11.3	37	195	164.7	204.7	194.5	244.6
2	24.2	21.7	25.6	25.6	36.1	38	199.5	167.5	208.9	199	249
3	36.5	32.8	37.5	37.4	41	39	203.5	168.8	214.9	202.7	252.9
4	40	38	40.6	40.6	55.8	40	207.7	173.8	220.8	207.1	259.9
5	43.4	40.3	52.9	51	68.7	41	211.8	180	225.6	211	266.5
6	56.8	43.7	63.3	59.5	71.2	42	218.6	183.4	228.1	218.2	271.8
7	67.4	55.8	70.2	69.2	74.9	43	223.6	187.2	232.7	223.4	277.8
8	70.5	62.8	72.1	70.8	81.2	44	226.8	192.3	239.1	226.7	284.2
9	72.4	69.5	76.5	73.4	89.7	45	229.6	197	245.4	229.5	291.8
10	75.5	70.6	81.2	77.6	97.2	46	235.7	200.2	249.2	235.6	297.2
11	80.8	72.2	87.8	81.3	100.5	47	242.9	204	252.6	243.2	302.7
12	87	74.5	95.6	87.8	110.1	48	247.3	207.7	258.3	247.5	309.2
13	92.8	80	98.6	94.3	111.3	49	250.3	211.2	264.5	250.4	315.1
14	97.7	81.5	101.3	98.3	115.8	50	254.5	217.9	269.5	254.7	320.3
15	100	87.4	110.1	100.7	124.2	51	261.2	222.6	274.4	261.9	325.5
16	106	91.8	111.1	109.3	128.9	52	266.9	226.4	279.5	267.6	331.5
17	110.7	96.9	113.6	110.9	136.6	53	271.6	228.5	285.7	272.2	337.3
18	111.6	99.1	119.7	111.8	138.5	54	276.9	232.6	292.7	277.7	341.3
19	115.6	101.2	125.3	116.2	142.2	55	282.2	239.3	297.2	283.4	346.3
20	122.3	108.8	129.2	123.1	146.2	56	288.3	245.4	302.3	290.4	351.6
21	126.2	110.8	135.9	126.6	154.3	57	294.9	248.7	308.2	296.1	355.9
22	131.6	111.4	138.2	133.5	160.5	58	299.4	251	313.7	301.2	360.1
23	136.9	113.5	139.6	137.4	164.6	59	304.4	255.6	318.9	307	364.3
24	138.5	117.7	143.4	138.6	167.8	60	310.9	262.8	323.4	313.1	368.4
25	139.9	123.7	148	139.8	173.2	61	316.3	267.9	329.3	318.8	372.7
26	143.5	126.6	154.7	143.5	180.8	62	321.1	272.2	335.2	323.2	376.6
27	148.3	132.2	160.4	147.8	186.3	63	326.3	277.3	339.4	329.5	380
28	154.9	136.5	163.2	154.9	192.7	64	332.4	282.5	343.8	335.8	383.6
29	160.4	138.2	167.2	160.4	198.5	65	337.8	288.9	349.2	339.8	387.4
30	162.9	139	169.7	162.7	203.2	66	341.8	295.2	353.9	344.8	390.9
31	167.1	141.4	174.6	166.9	208.2	67	347	299.7	358	350.6	394.1
32	168.6	143.7	181.4	168.3	214.7	68	352.5	304.8	362.7	355.3	397.8
33	173.9	147.8	186.3	173.3	221.6	69	356.6	311.6	366.9	360	400.9
34	180.6	153.9	190.8	179.8	226.3	70	361.5	317.2	371.4	364.6	403.8
35	185.5	160	196.4	184.4	229.5	71	365.8	322	375.8	369.3	407.2

Source: The author, 2023

wt.% vap.	Run					wt.% vap.	Run				
	36	37	38	39	40		36	37	38	39	40
72	370.5	327.7	379.5	374.3	410.7	87	431.6	407.3	436	434.9	454.5
73	375.3	334.8	383.4	378.5	413.3	88	435.5	412.4	439.8	439	457.8
74	379.3	339.2	387.7	382.4	416.4	89	439.7	417.5	443.7	443.1	461.6
75	383.3	343.9	391.5	387.2	419.6	90	444	423.1	447.6	447.2	465.4
76	387.9	350.3	395.4	391.3	422.4	91	448.2	428.5	451.8	451.7	469.5
77	391.8	355.3	399.3	395.5	425.4	92	453	434.1	456.4	456.5	474
78	396	360.4	402.7	399.6	428.3	93	458	440.2	461.7	462	478.9
79	400.1	365.3	406.7	403.3	431.1	94	464.1	446.6	467.2	467.8	484.3
80	403.7	371.2	410.8	407.7	433.7	95	470.6	453.9	473.7	474.5	490.2
81	408.2	376.6	414	411.8	436.6	96	478.3	462.4	481.1	482.2	497
82	412.1	381	417.8	415.3	439.6	97	487.6	472.4	490.1	491.5	504.6
83	415.7	386.8	421.5	419.5	442.3	98	499.2	485.4	501.3	502.7	513.9
84	419.9	391.7	425.1	423.4	445.4	99	515.3	504.4	516.6	517.9	526.1
85	423.7	397.2	428.8	427.3	448.2	100	527.1	519.1	527.8	528.7	534.1
86	427.8	401.8	432.3	431.1	451.2						

(a) Particular nodal points. Densities of probability ( $\theta_i$ ) expressed for normalized temperatures (between 0 and 1)						
i	Run:	36	37	38	39	40
0	$T_0$ (°C)	2	1.7	2	2.4	3.8
	$T_{0,norm}$	0.0536	0.0531	0.0536	0.0543	0.0568
	$\theta_0$	0.0000	0.0000	0.0000	0.0000	0.0000
1	$T_1$ (°C)	156.05	156.05	156.05	156.05	156.05
	$T_{1,norm}$	0.3243	0.3243	0.3243	0.3243	0.3243
	$\theta_1$	1.3100	1.5737	1.2338	1.3120	0.9793
2	$T_2$ (°C)	272.1	272.1	272.1	272.1	272.1
	$T_{2,norm}$	0.5282	0.5282	0.5282	0.5282	0.5282
	$\theta_2$	1.0941	1.1148	1.1030	1.0734	0.9756
3	$T_3$ (°C)	388.15	388.15	388.15	388.15	388.15
	$T_{3,norm}$	0.7321	0.7321	0.7321	0.7321	0.7321
	$\theta_3$	1.3007	1.0557	1.3700	1.2760	1.5766
4	$T_4$ (°C)	527.1	519.1	527.8	528.7	534.1
	$T_{4,norm}$	0.9763	0.9622	0.9775	0.9791	0.9886
	$\theta_4$	-0.0950	-0.1958	-0.0070	0.0168	0.1610

Source: The author, 2023

(b) Common nodal points. Densities of probability ( $\theta_i$ ) expressed for normalized temperatures (between 0 and 1)						
i	Run:	36	37	38	39	40
0	$T_0$ (°C)	40.0	40.0	40.0	40.0	40.0
	$T_{0,norm}$	0.1204	0.1204	0.1204	0.1204	0.1204
	$\theta_0$	0.8441	1.0215	0.7812	0.8398	0.6638
1	$T_1$ (°C)	156.05	156.05	156.05	156.05	156.05
	$T_{1,norm}$	0.3243	0.3243	0.3243	0.3243	0.3243
	$\theta_1$	1.3100	1.5737	1.2338	1.3120	0.9793
2	$T_2$ (°C)	272.1	272.1	272.1	272.1	272.1
	$T_{2,norm}$	0.5282	0.5282	0.5282	0.5282	0.5282
	$\theta_2$	1.0941	1.1148	1.1030	1.0734	0.9756
3	$T_3$ (°C)	388.15	388.15	388.15	388.15	388.15
	$T_{3,norm}$	0.7321	0.7321	0.7321	0.7321	0.7321
	$\theta_3$	1.3007	1.0557	1.3700	1.2760	1.5766
4	$T_4$ (°C)	504.2	504.2	504.2	504.2	504.2
	$T_{4,norm}$	0.9360	0.9360	0.9360	0.9360	0.9360
	$\theta_4$	0.4871	0.1521	0.5861	0.5889	0.9917
Coefficient of determination ( $R^2$ ) of the Lagrange polynomial regression						
	Run:	36	37	38	39	40
		0.9997	0.9997	0.9996	0.9996	0.9991
Density ( $d_{20}$ ) of the liquid product						
	Run:	36	37	38	39	40
		0.8628	0.7975	0.8580	0.8529	0.8708

Source: The author, 2023

wt.% vap.	Run					wt.% vap.	Run				
	41	42	43	44	45		41	42	43	44	45
0	5.6	4.9	37.8	27.6	16.2	36	287	227.3	276.6	255.4	247.6
1	24.2	18.1	45	40.6	38.4	37	294.5	230.6	280.6	260.8	249.8
2	40.2	37.9	70.2	60.6	55.2	38	300.2	237.3	285.6	264.6	251.2
3	56.1	41.7	80.2	71.4	69.6	39	306	244.6	291.8	268.2	253.8
4	70	57.2	90.4	81	73.2	40	312.5	248.8	295.6	271.4	257
5	73.9	69.5	99	91	81	41	318.3	252.5	300	275.6	262.4
6	81.2	71.5	110.4	98.6	88.6	42	323.3	258.1	304	279.2	266
7	92.3	74.9	114.2	107.6	97.2	43	329.4	264.8	309.6	284	269.6
8	99.1	81.3	124.8	111.4	100.8	44	335.3	269.9	314.2	289.2	272.8
9	109.7	88.3	135	118.8	110.8	45	339.7	275.1	318.6	294	276.8
10	111.6	96.8	138.6	126	112.2	46	344.2	280.4	322.4	297.6	280.4
11	120.5	99.8	144.6	135.2	119	47	349.3	286.7	327	301.8	285
12	127.3	106.6	156.2	138.4	126.2	48	353.7	293.7	331.8	306.6	290
13	136.6	111.3	162.4	143	134.2	49	357.6	298.3	336.4	311.4	295
14	139	113.5	167.6	150.2	138.6	50	361.8	303.4	339.6	315.6	298.6
15	144.1	120.8	177	159.6	141.4	51	365.5	309.5	343.4	319.6	302.8
16	153.5	126.2	185.8	164.2	146	52	369.3	314.9	348	323.4	307.4
17	161	132.9	194	167.8	154	53	373.2	320	352.2	328.4	312.2
18	166.9	137.9	200.2	175	160.8	54	376.7	324.6	355.4	333.4	316.8
19	172.3	139.2	206.6	183.2	165.6	55	379.9	330.3	359.2	337.2	321
20	180.7	143.3	213.4	189	168.6	56	383	336.1	362.8	340.4	324.6
21	187.1	148	220.6	196.8	175.2	57	386.5	340.1	366.4	344.4	329.4
22	195.1	155.6	225.2	201.4	182.8	58	389.7	344.5	369.8	349.2	334.4
23	201.1	161	226.8	206.8	188.2	59	392.5	349.6	373.6	353	338.6
24	207.7	165	229.2	212.4	195.6	60	395.6	354	377	356.2	341.8
25	215	168.2	235	219	200.8	61	398.8	357.9	379.8	360.4	345.6
26	222.5	173.4	241.2	224.4	205.4	62	401.4	362.4	383.2	364	350.6
27	227.3	180.3	245.2	226	209.8	63	404	366.2	386.6	367.4	354.6
28	233.6	186	247.6	228.2	216.6	64	407	370.2	389.8	371.6	358
29	242.1	190.4	249.6	232.2	222.4	65	409.9	374.5	392.6	375.2	362.2
30	248.1	196.8	252	237.2	226.4	66	412.4	378.1	396	378.4	365.8
31	252.9	201.2	255.4	243	227.8	67	414.8	381.5	399	381.6	369.6
32	260.4	206.1	261	245.8	230	68	417.5	385.3	401.6	385.4	373.8
33	267.5	210.5	265	248	234.6	69	420.2	389	404.8	389	377.8
34	273.4	217.5	268.6	249.6	239.8	70	422.6	392.3	407.8	391.8	380.8
35	279.8	223.3	272.2	252.2	245	71	425	395.8	410.8	395.4	384.6

Source: The author, 2023

wt.% vap.	Run					wt.% vap.	Run				
	41	42	43	44	45		41	42	43	44	45
72	427.6	399.4	413.2	398.8	388.8	87	465.1	447.3	453.4	444.6	440
73	429.9	402.4	416	401.6	392	88	468.3	450.6	456.4	447.6	443.4
74	432.2	405.8	419	405	395.8	89	471.6	454.2	459.6	451	447
75	434.4	409.4	421.4	408.6	399.6	90	475.3	458	463.2	454.6	450.6
76	436.7	412.6	424	411.2	402.6	91	479.2	462.4	466.6	458.2	454.6
77	439.3	415.6	426.8	414.2	406.2	92	483.4	466.9	470.4	462.6	458.8
78	441.5	418.9	429.6	417.6	410	93	488	471.8	474.6	466.8	463.8
79	443.9	422.2	431.8	420.4	413	94	493	477.3	479.2	471.6	468.6
80	446.3	425.3	434.4	423.4	416.4	95	498.3	483.5	484.2	477	474.2
81	448.6	428.4	437.2	426.6	420	96	504.3	490.6	490	483.2	480.8
82	451	431.5	439.6	429.6	423.2	97	511.1	499	497	490.4	488.6
83	453.6	434.5	442.2	432.2	426.6	98	519.3	509	506	500	498.4
84	456.2	437.6	445	435.2	430	99	529.7	522.6	519.4	514.2	513.4
85	458.9	440.9	447.6	438.4	433	100	536.4	531.8	529.6	525.8	525.4
86	462.1	444.1	450.4	441.4	436.4						

(a) Particular nodal points. Densities of probability ( $\theta_i$ ) expressed for normalized temperatures (between 0 and 1)						
i	Run:	41	42	43	44	45
0	$T_0$ (°C)	5.6	4.9	37.8	27.6	16.2
	$T_{0,norm}$	0.0599	0.0587	0.1165	0.0986	0.0785
	$\theta_0$	0.0000	0.0000	0.0000	0.0000	0.0000
1	$T_1$ (°C)	156.05	156.05	156.05	156.05	156.05
	$T_{1,norm}$	0.3243	0.3243	0.3243	0.3243	0.3243
	$\theta_1$	0.7256	1.0638	0.8839	1.0102	1.0895
2	$T_2$ (°C)	272.1	272.1	272.1	272.1	272.1
	$T_{2,norm}$	0.5282	0.5282	0.5282	0.5282	0.5282
	$\theta_2$	0.8733	1.0634	1.2207	1.3359	1.3715
3	$T_3$ (°C)	388.15	388.15	388.15	388.15	388.15
	$T_{3,norm}$	0.7321	0.7321	0.7321	0.7321	0.7321
	$\theta_3$	1.8136	1.5325	1.8396	1.6881	1.5604
4	$T_4$ (°C)	536.4	531.8	529.6	525.8	525.4
	$T_{4,norm}$	0.9926	0.9845	0.9807	0.9740	0.9733
	$\theta_4$	0.2064	0.0431	0.1593	0.2275	0.2553

Source: The author, 2023

(b) Common nodal points. Densities of probability ( $\theta_i$ ) expressed for normalized temperatures (between 0 and 1)						
i	Run:	41	42	43	44	45
0	$T_0$ (°C)	40.0	40.0	40.0	40.0	40.0
	$T_{0,norm}$	0.1204	0.1204	0.1204	0.1204	0.1204
	$\theta_0$	0.5521	0.6550	0.0388	0.1960	0.3421
1	$T_1$ (°C)	156.05	156.05	156.05	156.05	156.05
	$T_{1,norm}$	0.3243	0.3243	0.3243	0.3243	0.3243
	$\theta_1$	0.7256	1.0638	0.8839	1.0102	1.0895
2	$T_2$ (°C)	272.1	272.1	272.1	272.1	272.1
	$T_{2,norm}$	0.5282	0.5282	0.5282	0.5282	0.5282
	$\theta_2$	0.8733	1.0634	1.2207	1.3359	1.3715
3	$T_3$ (°C)	388.15	388.15	388.15	388.15	388.15
	$T_{3,norm}$	0.7321	0.7321	0.7321	0.7321	0.7321
	$\theta_3$	1.8136	1.5325	1.8396	1.6881	1.5604
4	$T_4$ (°C)	504.2	504.2	504.2	504.2	504.2
	$T_{4,norm}$	0.9360	0.9360	0.9360	0.9360	0.9360
	$\theta_4$	1.2687	0.8027	0.9414	0.7624	0.6889
Coefficient of determination ( $R^2$ ) of the Lagrange polynomial regression						
Run:	41	42	43	44	45	
	0.9985	0.9994	0.9988	0.9991	0.9992	
Density ( $d_{20}$ ) of the liquid product						
Run:	41	42	43	44	45	
	0.8783	0.8679	0.8919	0.8858	0.8759	

Source: The author, 2023

wt.% vap.	Run					wt.% vap.	Run				
	46	47	48	49	50		46	47	48	49	50
0	-1.2	-4.2	40	27.8	-7.8	36	197.6	168.4	300.8	265	266.4
1	18.6	2.8	51.2	43.2	42	37	201	172.8	307.2	270	268.6
2	38.8	36	76	63	54	38	205	176.4	311.8	274.8	272.2
3	42	40.2	87.4	76.6	75.6	39	208.4	182.4	315.8	278.4	277.4
4	56.8	41.8	103.8	82	83.4	40	212.6	186.8	320.4	281.6	281.2
5	64.4	55.8	113.2	95	94	41	219.2	189.4	326.4	285.4	284.6
6	70.8	61.2	125	104.4	103.2	42	223.2	195.8	331.4	289.6	288.2
7	72.2	69	132	108.8	111	43	226.8	200	336.4	293.8	292.6
8	75.2	70.8	142	119	118.2	44	227.8	203	340.2	298.6	296.2
9	81.4	72	152	122.4	125.2	45	229.8	206	344.6	304.8	301
10	87.6	74.6	157	131.6	129.6	46	232.6	209.4	349.6	308.4	307
11	91.6	80	166.6	137.4	137.8	47	237.6	215.8	354	312.4	311.4
12	97.2	81.8	175.6	146.2	143.8	48	243.2	220.8	357.2	316.8	315.2
13	99.6	88	182	148.2	151.6	49	246.6	225.6	360.6	322.8	319.6
14	102.4	91.4	191.8	153.4	153.4	50	248.6	227.2	365.2	327.6	325.2
15	111	96.6	200.8	162.4	158.4	51	250.6	228	369.4	332.4	330.2
16	112	99	209	169.4	166.6	52	251.8	230	372.6	336	335
17	114.6	101.2	216	175.6	174.2	53	254.2	233.6	376.4	340.6	338.8
18	119	107.4	222.8	180.4	179.8	54	257.6	239.2	380.2	345.4	343
19	125	111.4	231.8	188.4	183.8	55	263	245	383.4	350	347.8
20	128.6	112	238.6	195.6	191	56	266.4	247.6	387	353	352.8
21	136	114	242.2	202	198.8	57	269.8	249	390.8	356.4	356
22	138.8	118	244.6	208.6	204.6	58	272.8	251	394	361.4	359.2
23	139.6	123.8	248.6	213.8	211.8	59	276.2	251.8	396.6	365.6	364
24	143.2	127	254.4	218.4	216.6	60	279.8	254.4	400	368.8	368.4
25	145.4	134.2	260.2	226.2	222.2	61	284	259.2	403.4	372.8	371.6
26	151.4	137.8	263	232.6	228.6	62	288.2	264.6	406.2	376.8	375.6
27	159.4	139	265.6	237	235.4	63	294.4	267.8	409	380.2	379.8
28	161.6	139.6	266.8	238.2	241	64	297.8	270.4	412.4	384.4	383
29	165.4	142.8	269.8	240.8	242.6	65	301.6	273.6	415.4	388.2	387
30	168.2	144.6	275.2	245.6	244.8	66	305.6	277.4	417.6	391.4	391
31	172.2	149.8	280	251.6	248.8	67	311.2	280.8	420.6	394.6	394.4
32	176.4	158.4	283.8	256.4	254	68	315.8	285.4	423.6	398.4	397.6
33	182.6	161.2	287.2	258.8	259.6	69	320.6	291.4	426.4	402	401.4
34	187.2	163	291.8	261.2	262.6	70	324	296	428.8	405	405
35	192	167.2	295.8	262.4	264.8	71	328.6	299.4	431.6	408.6	408

Source: The author, 2023

wt.% vap.	Run					wt.% vap.	Run				
	46	47	48	49	50		46	47	48	49	50
72	334.4	303.8	434.2	412	411.6	87	404.6	381.6	472	457.8	459
73	339	309.6	436.8	414.6	415.2	88	410.4	388.6	474.4	461	462.4
74	342	314.6	439.2	418	417.8	89	415	394.4	477.6	464	465.6
75	346.8	320	442	421.6	421.4	90	420.6	400.6	480.8	467.6	469.2
76	352.2	323.4	444.6	424.4	425	91	425.8	407	484	471	472.6
77	356.6	328.4	446.8	427.4	427.8	92	431.4	413.6	487.6	475	476.6
78	361	335.2	449.2	430.6	431	93	437.2	420.6	491.4	479	480.8
79	365.6	339.6	451.6	433.6	434.2	94	443.6	428	495.6	483.8	485.6
80	370.4	342.8	454.2	436.6	437.2	95	450.2	436	500	488.8	490.6
81	376	349	456.4	439.8	440.4	96	458.2	445.2	505	494.6	496.6
82	380.2	354.6	459	442.8	443.8	97	467.4	455.6	510.8	501.2	503.2
83	385	359.2	461.6	445.4	446.6	98	479.2	469	518.2	509.4	511.6
84	390.4	364.8	464	448.6	449.6	99	496.6	488	528.4	521.4	523.4
85	395	370.4	466.4	451.6	452.8	100	511.2	504.2	535.6	530.8	532.2
86	400.2	376.8	469.2	454.4	455.8						

(a) Particular nodal points. Densities of probability ( $\theta_i$ ) expressed for normalized temperatures (between 0 and 1)						
i	Run:	46	47	48	49	50
0	$T_0$ (°C)	-1.2	-4.2	40	27.8	-7.8
	$T_{0,norm}$	0.0480	0.0427	0.1204	0.0989	0.0364
	$\theta_0$	0.0000	0.0000	0.0000	0.0000	0.0000
1	$T_1$ (°C)	156.05	156.05	156.05	156.05	156.05
	$T_{1,norm}$	0.3243	0.3243	0.3243	0.3243	0.3243
	$\theta_1$	1.4562	1.6321	0.7382	0.9526	0.8740
2	$T_2$ (°C)	272.1	272.1	272.1	272.1	272.1
	$T_{2,norm}$	0.5282	0.5282	0.5282	0.5282	0.5282
	$\theta_2$	1.4699	1.4360	1.0912	1.2580	1.3128
3	$T_3$ (°C)	388.15	388.15	388.15	388.15	388.15
	$T_{3,norm}$	0.7321	0.7321	0.7321	0.7321	0.7321
	$\theta_3$	1.1437	0.9450	1.8069	1.6454	1.5847
4	$T_4$ (°C)	511.2	504.2	535.6	530.8	532.2
	$T_{4,norm}$	0.9483	0.9360	0.9912	0.9828	0.9852
	$\theta_4$	0.1604	0.0486	0.8893	0.6253	0.9790

Source: The author, 2023

(b) Common nodal points. Densities of probability ( $\theta_i$ ) expressed for normalized temperatures (between 0 and 1)						
i	Run:	46	47	48	49	50
0	$T_0$ (°C)	40.0	40.0	40.0	40.0	40.0
	$T_{0,norm}$	0.1204	0.1204	0.1204	0.1204	0.1204
	$\theta_0$	0.6604	0.8440	0.0000	0.1799	0.3241
1	$T_1$ (°C)	156.05	156.05	156.05	156.05	156.05
	$T_{1,norm}$	0.3243	0.3243	0.3243	0.3243	0.3243
	$\theta_1$	1.4562	1.6321	0.7382	0.9526	0.8740
2	$T_2$ (°C)	272.1	272.1	272.1	272.1	272.1
	$T_{2,norm}$	0.5282	0.5282	0.5282	0.5282	0.5282
	$\theta_2$	1.4699	1.4360	1.0912	1.2580	1.3128
3	$T_3$ (°C)	388.15	388.15	388.15	388.15	388.15
	$T_{3,norm}$	0.7321	0.7321	0.7321	0.7321	0.7321
	$\theta_3$	1.1437	0.9450	1.8069	1.6454	1.5847
4	$T_4$ (°C)	504.2	504.2	504.2	504.2	504.2
	$T_{4,norm}$	0.9360	0.9360	0.9360	0.9360	0.9360
	$\theta_4$	0.2488	0.0486	1.5329	1.1129	1.2403
Coefficient of determination ( $R^2$ ) of the Lagrange polynomial regression						
Run:	46	47	48	49	50	
	0.9994	0.9993	0.9986	0.9990	0.9989	
Density ( $d_{20}$ ) of the liquid product						
Run:	46	47	48	49	50	
	0.8581	0.8524	0.8924	0.8834	0.8811	

Source: The author, 2023

wt.% vap.	Run					wt.% vap.	Run				
	51	52	53	54	55		51	52	53	54	55
0	-0.6	-7	39	20.2	0.4	36	204	181.8	295.6	258.6	219.2
1	24.4	23.2	55.2	39.4	28.6	37	207.6	186.2	300.2	263.8	223.6
2	40	39	72.8	57.8	40.6	38	211.2	190.2	304.8	267.4	226.6
3	48.8	41.4	88.4	70.8	55.8	39	217.6	195.4	310.2	270.8	227.8
4	60	55.6	99.4	80.4	65.4	40	222.2	199.2	315	274.4	229.8
5	70	62.6	110.8	89.8	71	41	226.2	202.8	319.4	278.6	234
6	71.6	70	120.6	98	74.6	42	227.4	206	323.4	283	239
7	75.2	71.4	130.2	104.6	81.4	43	229.2	209	328.6	287.6	244.4
8	81.6	74.2	138.2	111.4	88.2	44	231.4	215.4	333.8	293.8	247.2
9	88.4	80.4	145.2	117.2	94.6	45	236.6	220.4	337.8	297.4	249
10	94.2	84.4	158	125.4	98.6	46	242.2	224.8	341.2	302	250.8
11	98.4	89	165	133.4	101.4	47	246	226	345.4	306.4	252.4
12	101	93.8	172.2	138.6	110.6	48	248.2	227	350	311.8	255.2
13	108.6	97.8	182	142.8	111.8	49	250.2	228.8	353.8	316.4	260
14	111.4	99.6	191	148.8	115.2	50	251.4	233.4	357	320.8	264.8
15	112.8	104.4	199	158.4	121.4	51	253.8	239	361	324.6	268
16	117.4	110.4	205.8	163	126	52	256.8	244	364.6	329.6	271
17	123.6	111	213.2	167.8	131.2	53	262.2	246.4	368	334.6	274.2
18	126.8	112.4	220.6	174	137.4	54	265.8	248	371.8	338.8	278.2
19	133.6	116.6	225.2	182.4	139	55	269.2	249.6	375.2	342	281.6
20	138	122.4	227.4	188.2	142.2	56	272.2	250.8	378.4	346.2	286.2
21	139.2	125.6	231	196.4	144.8	57	275.6	253.4	381.2	351	292.2
22	141.6	131.2	237	201.8	151	58	279.4	258.4	384.8	355	296.4
23	144.4	136.2	243.2	207.6	159	59	283.4	263.4	388.2	358.4	299.8
24	149.6	138.2	246.2	213.2	161.8	60	287.8	266.4	390.8	362.6	304
25	156.8	138.8	248.6	220.2	166.4	61	294	269.2	394	366.2	309.6
26	161	141.8	250.2	225.6	168.4	62	297.2	272.4	397.2	369.8	314.2
27	163.8	143.8	253.4	227.2	173.6	63	301.2	276.2	400	374	318.8
28	167.6	149	258.8	229.4	180.6	64	305	279.4	402.4	377.6	322.6
29	169.8	157	263.8	234	185.8	65	311	284	405.6	380.8	327
30	175	160.2	267.6	239.4	189	66	315.4	289.6	408.6	384.4	332.2
31	181.6	162.2	271	245	195.8	67	320.2	294.2	411	388.2	337.4
32	186.4	166.4	275.6	247.6	200.4	68	323.6	297.4	413.6	391.6	340.8
33	189.4	167.6	279.6	249.8	204.4	69	328.2	301.8	416.2	394.6	344.8
34	195.8	172.2	285	251.2	208.2	70	333.8	307.2	418.8	398.4	350
35	200.2	176.8	291.4	254	212.8	71	338.6	312.2	421.2	401.4	354.4

Source: The author, 2023

wt.% vap.	Run					wt.% vap.	Run				
	51	52	53	54	55		51	52	53	54	55
72	341.6	317	423.8	404.4	358.2	87	411.2	391.8	460.8	449.4	422.6
73	346.2	320.6	426.2	407.8	363	88	415.2	397.8	463.8	452.8	426.8
74	351.6	325.2	428.8	411.2	367	89	420.2	403	467	456.2	431
75	355.8	331.2	431	413.8	371.6	90	425	409.6	470.2	459.6	435.2
76	360	336.4	433.2	416.8	376.4	91	430	414.8	473.6	463.6	440
77	364.6	339.6	435.6	420.2	380	92	435	421.2	477.4	467.6	444.6
78	369	344.4	438	423	384.2	93	440.4	427.8	481.4	472	449.4
79	374.2	350.4	440.4	426	389	94	446.2	434.6	486	476.8	454.8
80	378.6	354.8	442.8	429	393	95	452.2	442	490.8	482	460.8
81	382.4	359.8	445.2	431.8	397.4	96	459.4	450.2	496.6	488	467.6
82	387.8	364.6	447.6	434.4	401.6	97	468	460.2	503.4	495.2	475.8
83	392	370.6	449.8	437.6	405.6	98	478.6	472.4	512.2	504.2	485.8
84	397	376	452.6	440.4	410.4	99	494.2	490.2	524.8	518	500.6
85	401.4	380.4	455.2	443.4	414	100	507	505	533.6	528.6	513
86	405.8	386.8	457.8	446.6	418.2						
(a) Particular nodal points. Densities of probability ( $\theta_i$ ) expressed for normalized temperatures (between 0 and 1)											
i	Run:	51	52	53	54	55					
0	$T_0$ (°C)	-0.6	-7	39	20.2	0.4					
	$T_{0,norm}$	0.0490	0.0378	0.1186	0.0856	0.0508					
	$\theta_0$	0.0000	0.0000	0.0000	0.0000	0.0000					
1	$T_1$ (°C)	156.05	156.05	156.05	156.05	156.05					
	$T_{1,norm}$	0.3243	0.3243	0.3243	0.3243	0.3243					
	$\theta_1$	1.4109	1.5682	0.7623	0.9632	1.3051					
2	$T_2$ (°C)	272.1	272.1	272.1	272.1	272.1					
	$T_{2,norm}$	0.5282	0.5282	0.5282	0.5282	0.5282					
	$\theta_2$	1.4830	1.4988	1.1391	1.2844	1.4531					
3	$T_3$ (°C)	388.15	388.15	388.15	388.15	388.15					
	$T_{3,norm}$	0.7321	0.7321	0.7321	0.7321	0.7321					
	$\theta_3$	1.1872	0.9787	1.9132	1.6696	1.2855					
4	$T_4$ (°C)	507	505	533.6	528.6	513					
	$T_{4,norm}$	0.9410	0.9374	0.9877	0.9789	0.9515					
	$\theta_4$	0.4314	0.3816	0.2630	0.4024	0.5197					

Source: The author, 2023

(b) Common nodal points. Densities of probability ( $\theta_i$ ) expressed for normalized temperatures (between 0 and 1)						
i	Run:	51	52	53	54	55
0	$T_0$ (°C)	40.0	40.0	40.0	40.0	40.0
	$T_{0,norm}$	0.1204	0.1204	0.1204	0.1204	0.1204
	$\theta_0$	0.5971	0.7240	0.0161	0.2770	0.5347
1	$T_1$ (°C)	156.05	156.05	156.05	156.05	156.05
	$T_{1,norm}$	0.3243	0.3243	0.3243	0.3243	0.3243
	$\theta_1$	1.4109	1.5682	0.7623	0.9632	1.3051
2	$T_2$ (°C)	272.1	272.1	272.1	272.1	272.1
	$T_{2,norm}$	0.5282	0.5282	0.5282	0.5282	0.5282
	$\theta_2$	1.4830	1.4988	1.1391	1.2844	1.4531
3	$T_3$ (°C)	388.15	388.15	388.15	388.15	388.15
	$T_{3,norm}$	0.7321	0.7321	0.7321	0.7321	0.7321
	$\theta_3$	1.1872	0.9787	1.9132	1.6696	1.2855
4	$T_4$ (°C)	504.2	504.2	504.2	504.2	504.2
	$T_{4,norm}$	0.9360	0.9360	0.9360	0.9360	0.9360
	$\theta_4$	0.4577	0.3853	1.1764	0.9327	0.6082
Coefficient of determination ( $R^2$ ) of the Lagrange polynomial regression						
	Run:	51	52	53	54	55
		0.9995	0.9993	0.9984	0.9990	0.9994
Density ( $d_{20}$ ) of the liquid product						
	Run:	51	52	53	54	55
		0.8634	0.8571	0.8952	0.8839	0.8669

Source: The author, 2023

wt.% vap.	Run					wt.% vap.	Run				
	56	57	58	59	60		56	57	58	59	60
0	27.8	2.8	39.6	19.4	39	36	259.8	214	307.2	293.8	284.6
1	40.4	31.2	57	41	54.8	37	264.8	219.8	312.8	298.2	290.8
2	59	40.4	75.2	62.8	71.8	38	268.6	224.4	317.8	303	295.4
3	71.8	55	93.4	74.8	86	39	271.8	226.6	322.2	308.2	299.8
4	81.2	64.6	104.8	88	97.4	40	275.4	228	326.8	313.6	304.2
5	90.2	70.8	113.8	98.8	106.8	41	279.8	230	331.8	318.4	310
6	98.8	74	126	110.2	112.2	42	284.2	234.8	337.2	323	315
7	104.8	80.8	137.8	115.2	123.4	43	289.2	240.6	340.6	328	319.4
8	112	86.8	143.2	125.2	133.4	44	295	245.2	344.6	333	323.4
9	117.6	91.8	154.6	135.2	138.6	45	298.8	247.6	349.2	338	328.6
10	125.8	97.4	163.6	140	143.6	46	303.4	249.6	353.6	341.8	334
11	132.8	99.8	171.6	146.8	154.6	47	308.4	251	357	346	338
12	139	105.4	182.4	158	162	48	313.4	253.2	360.6	350.8	341.4
13	143.2	111	192.6	165	167.6	49	318	256.2	364.4	355	345.6
14	149	112.2	200.8	172	175.8	50	322.2	261.8	368	358.6	350.4
15	158.4	117	208.2	181.6	185.6	51	326.4	265.6	371.4	362.8	354.2
16	163.4	123.6	217	189.8	194.2	52	331.4	269	375.2	366.4	357.6
17	168.4	126.6	224.6	199.4	200.6	53	336.6	272.2	378.4	370.2	361.8
18	174.4	133.8	227	206.4	207.2	54	340.2	275.8	381.2	374	365.2
19	182.8	138	229.6	214	215.2	55	343.8	279.4	384.6	377.6	368.8
20	188.8	139	235.2	222	222	56	348.2	284	388	380.8	372.8
21	196.8	143	242	226.6	226	57	352.8	288.6	391	384.4	376.2
22	202.2	146.2	246.4	229.4	228	58	356.6	294.4	393.6	388	379.2
23	208	152.2	248.8	235	231.8	59	360.2	298	396.8	391.2	382.6
24	213.8	159.8	250.8	241.4	237.6	60	364.2	302.2	399.8	394.4	386
25	220.8	162.4	253.6	246.2	243.8	61	368	307	402.4	397.6	389.4
26	226.2	167	258.2	249.2	246.8	62	371.8	312.2	404.8	400.8	392.2
27	227.8	168.8	264	251.2	249	63	375.8	317	407.8	403.4	395.6
28	230.2	174.4	268.2	254.8	250.4	64	379.4	321.2	410.8	406.6	398.8
29	234.8	181.2	271.8	260.2	253.4	65	382.4	325	413	409.6	401.4
30	240.4	186.4	276.2	265.2	258.6	66	386.2	330.4	415.4	412.4	404.2
31	245.6	190.6	280.4	269.2	263.8	67	389.8	336.2	418	415	407.4
32	248.2	196.6	286	273.2	267.6	68	392.8	339.8	420.6	417.8	410.4
33	250.6	200.6	292.8	277.8	271	69	396.4	343.4	422.8	420.6	412.8
34	252	204.6	297.2	282.4	275.2	70	399.8	348.6	425.2	423	415.4
35	254.8	208.4	302	287.6	279.4	71	402.6	353.6	427.6	425.8	418.4

Source: The author, 2023

wt.% vap.	Run					wt.% vap.	Run				
	56	57	58	59	60		56	57	58	59	60
72	405.8	357.2	430	428.4	421	87	450.4	422.6	465.2	468	459.2
73	409.4	362	432	430.8	423.4	88	453.6	427	468	471.2	462.4
74	412.4	366	434	433.2	426.2	89	457	431.2	471	474.6	465.6
75	415.2	370.6	436.4	435.6	428.6	90	460.4	435.6	474.2	478.2	469
76	418.2	375.6	438.8	438.4	431	91	464.4	440.2	477.4	482	472.6
77	421.4	379.6	441	440.8	433.4	92	468.4	445	481	486	476.4
78	424.2	383.6	443	443.2	435.8	93	472.6	450	484.8	490.4	480.4
79	427.2	388.6	445.4	445.8	438.4	94	477.4	455.6	489.2	495.4	485
80	430.2	392.6	447.8	448.2	440.8	95	482.6	461.8	493.8	500.6	489.8
81	432.8	397.2	449.8	450.6	443.2	96	488.6	468.8	499.2	506.6	495.8
82	435.6	401.2	452.2	453.4	445.8	97	495.8	477.2	505.6	513.8	502.6
83	438.6	405.4	454.6	456.2	448.2	98	504.8	487.6	514	522.2	511.4
84	441.4	410.2	457.2	458.8	450.8	99	518.4	503.2	525.8	532.6	524.4
85	444.4	414	459.6	461.8	453.6	100	529	516.2	534.2	538.4	533.2
86	447.4	418.2	462.4	464.8	456.4						

(a) Particular nodal points. Densities of probability ( $\theta_i$ ) expressed for normalized temperatures (between 0 and 1)						
i	Run:	56	57	58	59	60
0	$T_0$ (°C)	27.8	2.8	39.6	19.4	39
	$T_{0,norm}$	0.0989	0.0550	0.1197	0.0842	0.1186
	$\theta_0$	0.0000	0.0000	0.0000	0.0000	0.0000
1	$T_1$ (°C)	156.05	156.05	156.05	156.05	156.05
	$T_{1,norm}$	0.3243	0.3243	0.3243	0.3243	0.3243
	$\theta_1$	0.9875	1.3289	0.6997	0.7333	0.8358
2	$T_2$ (°C)	272.1	272.1	272.1	272.1	272.1
	$T_{2,norm}$	0.5282	0.5282	0.5282	0.5282	0.5282
	$\theta_2$	1.2544	1.4222	1.0564	1.0794	1.1549
3	$T_3$ (°C)	388.15	388.15	388.15	388.15	388.15
	$T_{3,norm}$	0.7321	0.7321	0.7321	0.7321	0.7321
	$\theta_3$	1.6842	1.2694	1.9577	1.7984	1.8460
4	$T_4$ (°C)	529	516.2	534.2	538.4	533.2
	$T_{4,norm}$	0.9796	0.9571	0.9888	0.9961	0.9870
	$\theta_4$	0.3070	0.4068	0.3865	0.4504	0.2702

Source: The author, 2023

(b) Common nodal points. Densities of probability ( $\theta_i$ ) expressed for normalized temperatures (between 0 and 1)						
i	Run:	56	57	58	59	60
0	$T_0$ (°C)	40.0	40.0	40.0	40.0	40.0
	$T_{0,norm}$	0.1204	0.1204	0.1204	0.1204	0.1204
	$\theta_0$	0.2046	0.5609	0.0065	0.2606	0.0176
1	$T_1$ (°C)	156.05	156.05	156.05	156.05	156.05
	$T_{1,norm}$	0.3243	0.3243	0.3243	0.3243	0.3243
	$\theta_1$	0.9875	1.3289	0.6997	0.7333	0.8358
2	$T_2$ (°C)	272.1	272.1	272.1	272.1	272.1
	$T_{2,norm}$	0.5282	0.5282	0.5282	0.5282	0.5282
	$\theta_2$	1.2544	1.4222	1.0564	1.0794	1.1549
3	$T_3$ (°C)	388.15	388.15	388.15	388.15	388.15
	$T_{3,norm}$	0.7321	0.7321	0.7321	0.7321	0.7321
	$\theta_3$	1.6842	1.2694	1.9577	1.7984	1.8460
4	$T_4$ (°C)	504.2	504.2	504.2	504.2	504.2
	$T_{4,norm}$	0.9360	0.9360	0.9360	0.9360	0.9360
	$\theta_4$	0.9144	0.5497	1.3399	1.3073	1.1297
Coefficient of determination ( $R^2$ ) of the Lagrange polynomial regression						
	Run:	56	57	58	59	60
		0.9990	0.9994	0.9981	0.9987	0.9986
Density ( $d_{20}$ ) of the liquid product						
	Run:	56	57	58	59	60
		0.8823	0.8670	0.8839	0.8996	0.8914

Source: The author, 2023

wt.% vap.	Run					wt.% vap.	Run				
	61	62	63	64	65		61	62	63	64	65
0	37.6	6.2	24.4	22.2	17.8	36	272.6	252.6	251.2	244	244.8
1	47.2	37.6	39.8	39.4	38.4	37	277	256	254.4	246.6	247
2	70.2	47.6	57.6	56.2	54.8	38	281.2	260.6	259.8	248.6	249.2
3	80.6	64.8	70.6	69.6	68.8	39	286.2	265	264.2	250	250.4
4	91	72.8	77.2	73.8	72.6	40	292.6	269	267.8	252.6	253.2
5	99	80.6	87.2	81.2	80.8	41	296.4	272.8	271	256	258.2
6	110.2	88.4	95.8	89.4	88.2	42	300.8	276.8	275.2	261.6	263.2
7	113.6	96.8	99.6	96.6	96.2	43	305.6	281	279	265.2	266.8
8	123.6	101.2	110	100	99.6	44	311	285.4	284	268.6	270
9	132.2	109	111.4	110	109.4	45	315.8	290.2	289.8	272	273.4
10	138	112.8	118.2	111.2	111	46	320	295	294.6	276	277.6
11	142.6	117.6	125.6	116.4	115.8	47	324.2	299.4	298.6	279.6	282
12	150	124.8	134.4	123.8	123.4	48	329.2	303.8	302.8	284.6	286.8
13	160	129.8	138	128.8	128.2	49	334.6	308.6	308.6	290.4	292.8
14	165.8	137.2	141.6	136.6	136.2	50	338.4	313.4	313.4	294.8	296.6
15	171	140	146.4	138.4	138.4	51	341.8	318	318.2	298.6	301
16	180	144.4	156.4	142.6	142.4	52	346.4	322.8	321.8	302.8	306
17	186.6	150.2	161	147.2	146.8	53	351	327.6	326.6	308.4	311.2
18	195	157.6	166.6	156.4	155.8	54	354.8	332.4	332	313.2	315.8
19	201.2	162.8	171.4	160.8	160.6	55	358.4	337.2	336.6	317.8	320
20	207.2	168	179.4	166	165.8	56	362.4	341.6	339.8	321.6	324.2
21	214.6	173.2	185.6	168.2	168.2	57	366	346	344	326	329.6
22	221.2	180.4	192.8	174.6	174.8	58	369.6	350.6	349	331.2	335.2
23	225.4	187	198.8	182	182.2	59	373.6	355	353.2	336.2	338.6
24	227.2	193.8	203.8	187	187.4	60	377.2	359	356.6	339.4	342.4
25	229.6	200.2	208.6	194.6	195	61	380	363.4	361	343.4	347.4
26	235.8	205.8	216	199.6	200	62	383.8	367.6	364.8	348.6	352
27	242	211.4	221.8	204.2	204.6	63	387.4	371.6	368.6	352.8	355.6
28	245.8	218.6	225.4	208.6	209.4	64	390.4	375.8	372.8	356.2	360
29	247.8	225	227	215.6	216.8	65	393.8	379.8	376.6	360.8	363.8
30	249.8	228.2	229.2	221.2	222.2	66	397.2	383.6	379.6	364.6	367.8
31	252.2	231.6	235.2	225.2	225.6	67	400.2	387.8	383.6	368.4	372.4
32	255.6	236.8	241.2	226.6	227	68	402.8	391.6	387.6	373	376.4
33	261.4	242.2	245.2	228.6	229	69	406.2	395.4	390.8	376.8	379.6
34	265.2	246.8	247.4	233.4	234.4	70	409.4	399.2	394.4	380.2	383.8
35	269	250	249.4	239	240.6	71	411.8	402.8	398	384.4	388

Source: The author, 2023

wt.% vap.	Run					wt.% vap.	Run				
	61	62	63	64	65		61	62	63	64	65
72	414.8	406.4	401	388.4	391.2	87	455.6	459	448	440.8	442.8
73	417.8	410.2	404.6	391.8	395.2	88	458.6	463	451.6	444.4	446.4
74	420.6	413.6	408.2	395.8	399	89	462.2	467	455	447.8	449.8
75	423.2	417.2	411.2	399.4	402	90	465.4	471.2	458.6	451.8	453.6
76	426	420.8	414.2	402.6	406	91	469.2	475.8	462.6	455.8	457.6
77	428.8	424	417.6	406.6	409.8	92	473	480.6	466.8	460.2	462.2
78	431	427.6	420.8	410.2	412.8	93	477.2	485.8	471.2	464.8	466.6
79	433.6	431	423.8	413.4	416.2	94	481.8	491.4	476.2	470	471.8
80	436.4	434.2	427	417	419.8	95	487	497.6	481.4	475.6	477.4
81	439	437.8	429.8	420.4	423	96	492.8	504.4	487.8	482	483.8
82	441.6	441	432.6	423.8	426.4	97	500	512.2	495.2	489.8	491.4
83	444.4	444.6	435.8	427.4	429.6	98	509	521.2	504.6	499.6	501
84	447	448	438.8	430.4	432.8	99	522.4	532	518.8	514.4	515.6
85	449.6	451.6	441.8	433.8	436.2	100	532	538.2	529.4	526.2	527.2
86	452.6	455.2	445	437.4	439.4						
(a) Particular nodal points. Densities of probability ( $\theta_i$ ) expressed for normalized temperatures (between 0 and 1)											
i	Run:	61	62	63	64	65					
0	$T_0$ (°C)	37.6	6.2	24.4	22.2	17.8					
	$T_{0,norm}$	0.1161	0.0610	0.0930	0.0891	0.0814					
	$\theta_0$	0.0000	0.0000	0.0000	0.0000	0.0000					
1	$T_1$ (°C)	156.05	156.05	156.05	156.05	156.05					
	$T_{1,norm}$	0.3243	0.3243	0.3243	0.3243	0.3243					
	$\theta_1$	0.9182	0.9981	1.0424	1.1556	1.1237					
2	$T_2$ (°C)	272.1	272.1	272.1	272.1	272.1					
	$T_{2,norm}$	0.5282	0.5282	0.5282	0.5282	0.5282					
	$\theta_2$	1.2041	1.2247	1.2727	1.3355	1.3140					
3	$T_3$ (°C)	388.15	388.15	388.15	388.15	388.15					
	$T_{3,norm}$	0.7321	0.7321	0.7321	0.7321	0.7321					
	$\theta_3$	1.7738	1.4916	1.6152	1.5132	1.5121					
4	$T_4$ (°C)	532	538.2	529.4	526.2	527.2					
	$T_{4,norm}$	0.9849	0.9958	0.9803	0.9747	0.9765					
	$\theta_4$	0.2523	0.4600	0.2929	0.2566	0.3540					

Source: The author, 2023

(b) Common nodal points. Densities of probability ( $\theta_i$ ) expressed for normalized temperatures (between 0 and 1)						
i	Run:	61	62	63	64	65
0	$T_0$ (°C)	40.0	40.0	40.0	40.0	40.0
	$T_{0,norm}$	0.1204	0.1204	0.1204	0.1204	0.1204
	$\theta_0$	0.0438	0.4264	0.2621	0.3122	0.3599
1	$T_1$ (°C)	156.05	156.05	156.05	156.05	156.05
	$T_{1,norm}$	0.3243	0.3243	0.3243	0.3243	0.3243
	$\theta_1$	0.9182	0.9981	1.0424	1.1556	1.1237
2	$T_2$ (°C)	272.1	272.1	272.1	272.1	272.1
	$T_{2,norm}$	0.5282	0.5282	0.5282	0.5282	0.5282
	$\theta_2$	1.2041	1.2247	1.2727	1.3355	1.3140
3	$T_3$ (°C)	388.15	388.15	388.15	388.15	388.15
	$T_{3,norm}$	0.7321	0.7321	0.7321	0.7321	0.7321
	$\theta_3$	1.7738	1.4916	1.6152	1.5132	1.5121
4	$T_4$ (°C)	504.2	504.2	504.2	504.2	504.2
	$T_{4,norm}$	0.9360	0.9360	0.9360	0.9360	0.9360
	$\theta_4$	1.0263	1.0026	0.8646	0.7083	0.7914
Coefficient of determination ( $R^2$ ) of the Lagrange polynomial regression						
Run:	61	62	63	64	65	
	0.9987	0.9996	0.9991	0.9992	0.9992	
Density ( $d_{20}$ ) of the liquid product						
Run:	61	62	63	64	65	
	0.8917	0.8936	0.8804	0.8739	0.8776	

Source: The author, 2023

wt.% vap.	Run					wt.% vap.	Run				
	66	67	68	69	--		66	67	68	69	--
0	25.2	8.6	10.4	20		36	272.2	262.6	226	236	
1	40.4	36.6	37.6	38.2		37	276.6	266.8	228	242	
2	61.4	51.8	42.8	46		38	280.6	270.8	230.6	245.8	
3	72.4	66.2	61	63.6		39	286	275.2	236.4	247.6	
4	82.2	72.6	70.2	71		40	292.4	279.8	242.4	249.8	
5	95.4	81.4	73.8	75		41	296.8	284.6	245.6	251.4	
6	100.8	90.4	80.6	82.4		42	301.4	290.2	247.6	254.4	
7	111.2	96	87.2	90.8		43	305.8	294.8	249.4	259.8	
8	115.6	103.4	92	97.4		44	311.8	299.4	250.8	264.2	
9	125.4	108.4	97.8	100.4		45	316.6	304.2	253.6	268	
10	134.2	114	100.8	110		46	321.2	309.4	258.8	271.2	
11	138.8	121.6	110	111.4		47	325.4	314.4	263.6	275	
12	143.8	128	111	115.8		48	330.6	319	267.2	278.8	
13	151.2	134.8	114.2	123.2		49	336	323.6	270.2	283.6	
14	160.8	138.8	121	127.2		50	340	328.6	273.4	289	
15	167	143.8	125.8	135.6		51	343.4	334	277.6	294.2	
16	172.6	151.4	133.6	138.4		52	348	338.2	281.8	298	
17	181.4	158.4	137.8	141		53	352.6	342.6	286.6	302.4	
18	188	164.2	138.6	144.6		54	356.4	347.2	292.8	308	
19	197	170	142.6	151.6		55	360.2	351.8	296.4	313	
20	203.2	178	146.2	160		56	364.2	355.8	300.6	317.8	
21	208.8	184.8	154.2	163.2		57	368	360	305.4	321.6	
22	216.6	192.8	160.2	167.2		58	371.6	364.2	310.8	326.2	
23	223.2	199.4	163.4	172.2		59	375.6	368.2	315.6	331.8	
24	226.8	205.6	167	179.6		60	379.2	372.6	319.8	336.8	
25	229	213	171.6	185.4		61	382	376.6	323.8	340	
26	232.8	219.6	177.8	190.8		62	385.8	380.2	329.2	344.4	
27	238.6	223.8	183.4	197.4		63	389.6	384.2	335	349.6	
28	244.8	227	187.4	201.4		64	392.4	388.2	338.4	353.8	
29	247.6	232.6	194.6	206.6		65	395.8	391.8	342.2	357.6	
30	250	238.6	199.2	211.4		66	399.4	395.6	347.4	362.2	
31	251.4	243.4	203.6	218.6		67	402.2	399.2	352.2	366.2	
32	254.6	246.4	207.6	223.8		68	405	402.6	355.8	370.6	
33	259.8	249	214.2	226		69	408.4	406.2	360.6	375	
34	265	252.8	220	227.8		70	411.6	409.8	364.6	378.6	
35	268.8	257.8	224.8	230		71	414	412.8	369	382.4	

Source: The author, 2023

wt.% vap.	Run					wt.% vap.	Run				
	66	67	68	69	--		66	67	68	69	--
72	417	416.2	373.8	386.8		87	458	463.6	433.6	441	
73	420	419.6	377.8	390.4		88	461.2	467.2	437.6	444.6	
74	422.6	422.6	381.6	394.4		89	464.6	471	441.6	448.2	
75	425.4	425.8	386.2	398.4		90	468	475	445.6	452.2	
76	428.2	429	390.2	401.6		91	471.6	479.2	449.8	456.2	
77	430.8	432	394.4	405.6		92	475.6	483.8	454.4	460.8	
78	433.2	435	398.6	409.8		93	479.8	488.6	459.4	465.6	
79	435.8	438	402.2	412.8		94	484.4	494	464.8	470.8	
80	438.6	441	406.6	416.4		95	489.4	499.8	470.8	476.6	
81	441.2	444	410.6	420.2		96	495.4	506.2	477.6	483.2	
82	443.8	447.2	414.2	423.6		97	502.4	513.6	485.8	491.2	
83	446.6	450.2	418.4	427.2		98	511.2	522.4	496	501	
84	449.2	453.4	422	430.4		99	524.2	532.8	511.2	516	
85	452	456.8	426	434		100	533.2	538.6	523.8	527.6	
86	455	460	429.8	437.6							

(a) Particular nodal points. Densities of probability ( $\theta_i$ ) expressed for normalized temperatures (between 0 and 1)

i	Run:	66	67	68	69
0	$T_0$ (°C)	25.2	8.6	10.4	20
	$T_{0,norm}$	0.0944	0.0652	0.0684	0.0852
	$\theta_0$	0.0000	0.0000	0.0000	0.0000
1	$T_1$ (°C)	156.05	156.05	156.05	156.05
	$T_{1,norm}$	0.3243	0.3243	0.3243	0.3243
	$\theta_1$	0.8758	0.9196	1.2526	1.1907
2	$T_2$ (°C)	272.1	272.1	272.1	272.1
	$T_{2,norm}$	0.5282	0.5282	0.5282	0.5282
	$\theta_2$	1.1701	1.1452	1.3671	1.3003
3	$T_3$ (°C)	388.15	388.15	388.15	388.15
	$T_{3,norm}$	0.7321	0.7321	0.7321	0.7321
	$\theta_3$	1.7441	1.5700	1.3592	1.4674
4	$T_4$ (°C)	533.2	538.6	523.8	527.6
	$T_{4,norm}$	0.9870	0.9965	0.9705	0.9772
	$\theta_4$	0.3940	0.4800	0.3692	0.2193

Source: The author, 2023

(b) Common nodal points. Densities of probability ( $\theta_i$ ) expressed for normalized temperatures (between 0 and 1)					
i	Run:	66	67	68	69
0	$T_0$ (°C)	40.0	40.0	40.0	40.0
	$T_{0,norm}$	0.1204	0.1204	0.1204	0.1204
	$\theta_0$	0.2255	0.4128	0.4770	0.3712
1	$T_1$ (°C)	156.05	156.05	156.05	156.05
	$T_{1,norm}$	0.3243	0.3243	0.3243	0.3243
	$\theta_1$	0.8758	0.9196	1.2526	1.1907
2	$T_2$ (°C)	272.1	272.1	272.1	272.1
	$T_{2,norm}$	0.5282	0.5282	0.5282	0.5282
	$\theta_2$	1.1701	1.1452	1.3671	1.3003
3	$T_3$ (°C)	388.15	388.15	388.15	388.15
	$T_{3,norm}$	0.7321	0.7321	0.7321	0.7321
	$\theta_3$	1.7441	1.5700	1.3592	1.4674
4	$T_4$ (°C)	504.2	504.2	504.2	504.2
	$T_{4,norm}$	0.9360	0.9360	0.9360	0.9360
	$\theta_4$	1.1146	1.1245	0.6591	0.7005
Coefficient of determination ( $R^2$ ) of the Lagrange polynomial regression					
	Run:	66	67	68	69
		0.9988	0.9994	0.9993	0.9993
Density ( $d_{20}$ ) of the liquid product					
	Run:	66	67	68	69
		0.8894	0.8939	0.8688	0.8751

Source: The author, 2023